THE INFLUENCE OF SEASONAL DISTRIBUTION PATTERNS, ECOLOGICAL PREFERENCES AND CALCIFICATION PROCESSES ON THE INCORPORATION OF STABLE OXYGEN AND CARBON ISOTOPES IN PLANKTIC FORAMINIFERAL CALCITE SHELLS

Dissertation zur Erlangung
des Doktorgrades am
Fachbereich Geowissenschaften
der Universität Bremen

vorgelegt von
Iris Wilke
Bremen, März 2005

"Dem Anwenden muss das Erkennen vorausgehen"

(Max Planck)

TABLE OF CONTENTS

Danksagung iii
Abstract v
Zusammenfassung ix

CHAPTER 1 **1**
INTRODUCTION 1
1.1 Motivation and main objectives 1
1.2 A brief overview of planktic foraminiferal ecology 3
1.3 Stable isotopes 5
1.3.1 Principles of isotopic fractionation 5
1.3.2 Oxygen isotopes 6
1.3.3 Carbon isotopes 11
1.4 Outline of this thesis 15
1.5 References Chapter 1 18

CHAPTER 2 **23**
SEASONAL DISTRIBUTION AND STABLE OXYGEN ISOTOPE COMPOSITION OF PLANKTIC FORAMINIFERA OFF NW AFRICA (29°N)
[Iris Wilke, Helge Meggers, Torsten Bickert]

CHAPTER 3 **57**
PLANKTIC FORAMINIFERAL FLUXES ASSOCIATED WITH AGULHAS RINGS
[Iris Wilke, Frank J.C. Peeters and Geert-Jan A. Brummer]

CHAPTER 4 **89**
DEPTH INTEGRATED GROWTH OF PLANKTIC FORAMINIFERAL SHELLS PART 1. THE THEORY OF AN OXYGEN ISOTOPE MASS BALANCE MODEL
[Frank J.C. Peeters and Iris Wilke]

CHAPTER 5 **107**
DEPTH INTEGRATED GROWTH OF PLANKTIC FORAMINIFERAL SHELLS PART 2. MODEL FITS TO FIELD OBSERVATIONS
[*Iris Wilke and Frank J.C. Peeters]*

CHAPTER 6 **129**

THE INFLUENCE OF SEAWATER CARBONATE ION CONCENTRTATION [CO_3^{2-}] ON THE STABLE CARBON ISOTOPE COMPOSITION OF PLANKTIC FORAMINIFERA SPECIES *GLOBOROTALIA INFLATA*

[Iris Wilke and Torsten Bickert]

CONCLUSION AND OUTLOOK **149**

APPENDIX **I**

CHAPTER 2 II

CHAPTER 3 VI

CHAPTER 5 VIII

DANKSAGUNG

Für die Vergabe der Arbeit und die Begutachtung bedanke ich mich bei Prof. Dr. Gerold Wefer. Gleichfalls geht mein besonderer Dank an Dr. Torsten Bickert, durch dessen Unterstützung, Ideen und Engagement die Arbeit entscheidend profitierte. Für die freundliche Übernahme des zweiten Gutachtens danke ich Prof. Dr. Andreas Mackensen.

A special word of thanks to Dr. Frank Peeters for being my most important contact person during my stay at the Vrije Universiteit in Amsterdam and for introducing me into the fascinating world of planktic foraminifera. I am very grateful for your support, enthusiasm and many fertile never ending discussions which greatly improved this piece of work in different ways.

Ohne die Hilfe und Unterstützung im Labor, sowie für die vielen guten Ratschläge in analytischen Angelegenheiten danke ich Dr. Monika Segl und Birgit Meyer-Schack. Für die stete Diskussionsbereitschaft und für die konstruktive Kritik bedanke ich mich bei allen Mitarbeitern der AG Wefer, insbesondere bei Dr. Stefan Mulitza und Dr. Helge Meggers.

I thank all members from my Dutch working group at the Vrije Universiteit in Amsterdam, especially Dr. Katharina Kreissig, Dr. Geert-Jan Brummer, Els Ufkes, Jop Briker, Margot Saher, Dr. Gerald Ganssen and Prof. Dr. Dick Kroon for their hospitality during my visit.

Söhnke Rathmann sorgte immer für eine angenehme Arbeitsatmosphäre in unserem Büro, und dafür, dass Computerprobleme stets beseitigt wurden. Danke!

Dr. Helena Filipson und Dr. Mayar Mothadi sei gedankt für die monatliche Organisation des „Europrox Coffee and Science Meeting“. Ein ständiger Informationsfluss und der Austausch und Kontakt aller „Europroxler“ wurde somit ermöglicht und aufrechterhalten.

Ralph, nun haben wir schon so viele verschieden Phasen zusammen durchlebt. Ich danke dir für deine Freundschaft, Liebe und Unterstützung in all den Jahren. Und für dein Vertrauen in mich.

Tausend Dank meinen wunderbaren Eltern, Manfred und Brigitte, dass ihr mich immer „habt machen lassen“.

Die Deutsche Forschungsgemeinschaft hat die vorliegende Arbeit im Rahmen des Internationalen Graduiertenkollegs „Proxies in Earth History“ finanziell gefördert.

ABSTRACT

The presented thesis focuses on the shell isotope-geochemistry and faunal assemblage of living planktic foraminifers in the eastern North (Canary Islands region) and South (Cape Basin) Atlantic. The aim of this work was to better understand the incorporation of stable oxygen and carbon isotopes into the foraminiferal calcite shells and to identify and quantify the most important factors controlling this process. For this purpose, a combination of plankton tow collected species, sediment trap material and surface sediments sampled offered an ideal opportunity to construct the complex life habitat of foraminifers in different hydrographic regions. This thesis includes five manuscripts, each of which takes steps towards a better understanding of the use of planktic foraminifers in paleo-climate research. One important aspect deals with the ecological preferences of these organisms, concentrating on the seasonal distribution patterns and depth habitats of individual species in relation to the hydrographic situation. Furthermore, the species-specific depth integrated shell growth process was modelled to infer where and in which proportion foraminifers take up their isotope signal in the water column. A third field of study within this thesis concerned the role of the seawater carbonate chemistry on the incorporation of stable carbon isotopes.

Foraminiferal absolute abundances in the upper water column and shell fluxes along a productivity gradient from the productive NW-African coast to the oligotrophic gyre in the Canary Islands region show a high correlation to the biological productivity in surface water, coupled to the seasonal hydrographic conditions of the region. Highest concentrations and flux rates were associated with deep-mixing during the winter-bloom along the entire transect, while the nearcoast station exhibited an additional maximum in summer/fall presumably in response to coastal filament production. Beside temperature, nutrient availability appeared to be a main controlling factor for the planktic foraminiferal seasonal distribution in surface waters as well as deeper in the water column, and as such a major control for the species depth habitat and shell growth process. Foraminiferal $\delta^{18}O$ values showed a general increase with increasing depth in the water column. The species-specific and size class-dependent offsets from predicted oxygen isotope equilibrium values are due to kinetic and metabolic fractionation processes. While larger non-symbiotic species showed in general higher $\delta^{18}O$ values compared to smaller specimens, symbiotic species showed a reversed pattern, probably due to the capability to self-control the *p*H in their vicinity during main life processes, such as photosynthesis, which would change the carbonate chemistry in the foraminiferal microenvironment. Seasonal variations in the oxygen isotope ratio of *Globigerinoides ruber* white and pink are a direct function of surface water temperature, rather than due to seasonal variations of the carbonate ion concentration, which were too small to explain the observed seasonal isotopic differences.

In order to improve interpretations from sedimentary records of the variability of Indian Ocean advection into the South Atlantic via Agulhas rings or direct Agulhas leakage, deposition fluxes of planktic foraminifers were monitored in the southeastern Cape Basin. The investigations indicate that highest foraminiferal shell production is coupled to the highly dynamic mixing conditions near the ring frontal zones rather than in the centre of a ring. The following species: *G. ruber, Globigerinoides sacculifer, Globigerinella aequilateralis, Orbulina universa Globorotalia menardii, Neogloboquadrina dutertrei* and *Globorotalia theyeri/G. scitula*

cpx. have been identified to be typical Agulhas ring species. Indian-Atlantic water mass communication have not only influence on the planktic foraminiferal species composition and abundance, but also on the stable isotopic composition of their calcite shells. We found a relationship between temperature data and the oxygen isotopic composition of South Atlantic species *Globigerinita glutinata, Globigerina bulloides, Globorotalia inflata* and *Neogloboquadrina pachyderma* (dex.). The oxygen isotopic composition of *G. glutinata* accurately recorded the SST of the different water masses, *i.e.* the Indian, Atlantic or mixed waters. Highest $\delta^{18}O$ values were recorded during times of highest shell flux associated with the ring frontal zones, *i.e.* where Atlantic and Agulhas waters mix and upwelling of deeper waters may occur (low temperature). In contrast, lowest $\delta^{18}O$ values are associated with lowest shell flux in the ring centre (high temperature). The Agulhas species, which are transported into the South Atlantic Ocean via Agulhas leakage, showed less isotopic variability and did not reflect the lower sea surface temperatures of the South Atlantic Ocean in their oxygen isotope composition. This indicates that they predominantly calcify within water associated with the Indian Ocean. The carbon isotopic composition of *N. dutertrei* may reflect the higher carbon isotopic composition ($\delta^{13}C_{DIC}$) of nutrient-poor Agulhas waters as well as the lower $\delta^{13}C_{DIC}$ values of the upwelled waters at the frontal zones. The modern observations enable to distinguish between species properties associated with Agulhas leakage on the one hand, and Atlantic water masses on the other hand.

To quantify foraminiferal calcification depth habitat, its variability and the depth at which shell growth ceases, an oxygen isotope mass balance model has been developed that may describe the oxygen isotope composition of a foraminifer shell as a function of depth in the water column. The results indicate that shell growth, *i.e.* the increase of shell mass can be described by a cumulative mass development function. The model appears well suited to determine the depth range of calcification for different planktic foraminiferal species, by providing information on the rate of shell growth and the depth at which shell growth is completed. To test the model utility different planktic foraminiferal species from different hydrographic locations were selected. The shell growth pattern of each species is characterized by only two species-specific parameters of our model. The observed variability of these two model parameters suggests that the calcification pattern of a given species may depend on the vertical hydrographic structure and level of food availability.

The carbon isotope composition of surface water is usually not recorded in equilibrium by planktic foraminifers. The $\delta^{13}C$ values of living *G. inflata* were determined to evaluate the effect of seawater carbonate ion concentration ($[CO_3^{2-}]$) on shell $\delta^{13}C$. First of all, the oxygen isotope mass balance model was used to quantify in which proportions *G. inflata* takes up its isotopic signal along the SW-African continental margin. The derived weighted $\delta^{13}C$ differences ($\Delta\delta^{13}C_{shell\text{-}DIC}$) between shell and the seawater changes as a function of seawater $[CO_3^{2-}]$ with increasing depth in the water column. The $\Delta\delta^{13}C_{shell\text{-}DIC}/[CO_3^{2-}]$ slopes for *G. inflata* were -0.012 to –0.014‰ and -0.012 to –0.015‰ $(\mu mol*kg^{-1})^{-1}$ for specimens in the 150-250 and 250-355 μm size fraction, respectively, which are close to slopes found for other non-symbiotic species during experimental culture experiment. If $\delta^{13}C$ of *G. inflata* is corrected for this effect, estimates of the $\delta^{13}C$ of the seawater can be derived with an average

offset of 1.55‰. Hence, it can be concluded that the CO_3^{2-}-effect was successfully identified under natural environmental conditions, which has important implications for the interpretation of stable carbon isotope data in the fossil record.

ZUSAMMENFASSUNG

Die vorliegende Arbeit befasst sich mit der isotopen-geochemischen Zusammensetzung und der Faunenvergesellschaftung lebender planktischer Foraminiferen im östlichen Nord- (Kanarische Inseln) und Südatlantik (Kap Becken). Ziel dieser Arbeit war es, den Einbau stabiler Sauerstoff- und Kohlenstoffisotope in die Kalkschalen planktischer Foraminiferen und die diesen Prozess bestimmenden Faktoren besser zu verstehen und zu quantifizieren. Die in dieser Arbeit ermittelten Daten über Foraminiferen, welche aus einer Kombination aus Planktonfängen, Sedimentfallen und Oberflächensedimenten stammen, boten optimale Bedingungen die komplexen Lebensabläufe in Beziehung zur hydrographischen Situation besser zu verstehen. Die vorliegende Arbeit umfasst fünf Manuskripte, von denen jedes einen Beitrag zum besseren Verständnis für die Anwendung von Isotopen und Faunenvergesellschaftungen planktischer Foraminiferen in der Paläo-Klimaforschung leisten soll. Ein Schwerpunkt lag auf den ökologischen Präferenzen dieser Organismen, insbesondere auf den saisonalen Verteilungsmustern und Tiefenhabitate einzelner Arten in Abhängigkeit von der hydrographischen Situation. Darüber hinaus wurden die artenspezifischen Kalzifizierungsprozesse in der Wassersäule modelliert. Hieraus sollten Rückschlüsse darüber gezogen werden, wo und in welchen Proportionen der Einbau stabiler Isotope erfolgt. Weiter sollte untersucht werden, welche Rolle die Karbonatchemie des umgebenden Meerwassers beim Einbau stabiler Kohlenstoffisotope spielt.

Die absoluten Häufigkeiten der planktischen Foraminiferen in der obersten Wassersäule und die Foraminiferenflüsse entlang eines Gradienten von der hochproduktiven NW-afrikanischen Küstenregion zur oligotrophen subtropischen Gyre in der Kanarenregion zeigten einen engen Zusammenhang mit den biologischen Produktivitätszyklen im Oberflächenwasser, welche an die saisonalen hydrographischen Bedingungen der Region gekoppelt sind. Entlang des gesamten Transekts waren die höchsten Konzentrationen und Flussraten mit der tiefen Durchmischung während der Winterplanktonblüte assoziiert. Hingegen wies die auftriebsbeeinflusste küstennahe Station ein zusätzliches Maximum im Sommer und Herbst auf. Neben der Temperatur scheint die Nährstoffkonzentration im Oberflächenwasser sowie in tieferen Stockwerken bei der saisonalen Verteilung planktischer Foraminiferen eine wichtige Rolle zu spielen und somit die Wahl des Tiefenhabitats und den Schalenwachstumsprozess zu beeinflussen. Die Sauerstoffisotopenwerte der ausgewählten planktischen Foraminiferenarten zeigen einen generellen Trend zu schwereren Werten mit zunehmender Wassertiefe. Kinetische und metabolische Fraktionierungseffekte können für die beobachteten artenspezifischen und größenklassenabhängigen Abweichungen vom sauerstoffisotopischen Gleichgewicht verantwortlich gemacht werden. Während bei nicht-symbiotischen Arten größere Individuen schwerere $\delta^{18}O$-Werte als kleinere aufwiesen, zeigten symbiotische Arten ein entgegengesetztes Verhaltensmuster. Dies ist vermutlich darauf zurückzuführen, dass die Foraminiferen in der Lage sind, den pH-Wert in ihrer unmittelbaren Umgebung selbst zu steuern, beispielsweise durch die photosynthetische Aktivität ihrer Symbionten. Die beobachteten saisonalen Schwankungen der Sauerstoffisotopenverhältnisse in *Globigerinoides ruber* (weiß und rosa) sind eine Funktion der Oberflächenwassertemperatur, da die saisonalen Unterschiede in der Karbonationenkonzentration des umgebenden Meerwassers zu gering waren, um die beobachteten Schwankungen zu erklären.

Zur besseren Interpretation von Sedimentdaten bezüglich des variablen Eintrags von Wassermassen aus dem Indischen Ozean in den Südatlantik, direkt über den Agulhas-Strom oder durch so genannte Agulhas-Ringe, wurden Exportflüsse planktischer Foraminiferen im südöstlichen Kap Becken aufgezeichnet. Die Untersuchungen deuten darauf hin, dass die höchste Produktionsrate planktischer Foraminiferen nicht im Ringinneren vorkommt, sondern an die Randbereiche der Ringstrukturen gekoppelt ist, die durch hochdynamische Mischungsprozesse gekennzeichnet sind. Diese Frontenbereiche sind durch die Mischung Indischer und Atlantischer Wassermassen, sowie durch den Auftrieb tieferer nährstoffreicher Wassermassen gekennzeichnet. Die Arten *G. ruber, Globigerinoides sacculifer, Globigerinella aequilateralis, Orbulina universa, Globorotalia menardii, Neogloboquadrina dutertrei* und *Globorotalia theyeri*/*G. scitula* cpx. konnten als charakteristische Agulhas-Fauna identifiziert werden. Die Kommunikation zwischen Indischen und Atlantischen Wassermassen nimmt sowohl auf die Artenverteilung und Häufigkeiten planktischer Foraminiferen als auch auf die stabile Isotopenzusammensetzung des Kalzitgehäuses Einfluss. Die Sauerstoffisotopen-zusammensetzung der Südatlantik-Foraminiferenarten *Globorotalia inflata, Globigerina bulloides, Globigerinita glutinata* und *Neogloboquadrina pachyderma* (dex.) zeigten eine deutliche Beziehung zur Temperatur. Die Art *G. glutinata* spiegelte dabei sehr deutlich die Oberflächenwassertemperatur der verschiedenen Wassermassen wieder, d.h. Indische, Atlantische und Atlantisch/Indische. Die schwersten $\delta^{18}O$-Werte dieser Arten wurden zeitgleich mit dem maximalen Schalenfluss beobachtet (kalte Temperaturen). Im Gegensatz dazu zeigen diese Arten die leichtesten $\delta^{18}O$-Werte, wenn der Schalenfluss am geringsten war, also genau dann, wenn ein Agulhas-Ring direkt über der Sedimentfalle positioniert war (warme Temperaturen). Die mit dem Agulhas-Strom in den Südatlantik transportierten Arten, wie beispielsweise *G. ruber* und *G. aequilateralis*, zeigten dagegen keine ausgeprägte Isotopenvariabilität und ihr Sauerstoffisotopensignal zeichnete auch nicht die geringen Temperaturen des Südatlantiks auf. Diese Beobachtung verdeutlichte, dass die Kalzifizierung dieser Arten vorzugsweise auf Indische Wassermassen beschränkt ist. Die Kohlenstoffisotopen-untersuchungen zeigten, dass die Art *N. dutertrei* sowohl die hohen $\delta^{13}C_{DIC}$-Werte von nährstoffarmen Agulhas Wassers, als auch die niedrigen $\delta^{13}C_{DIC}$-Werte von nährstoffreichem Auftriebswasser in den Frontenbereichen wiederspiegelt. Dagegen scheint der Einbau stabiler Kohlenstoffisotopen in die Schalen von *G. inflata, G. bulloides, G. glutinata* und *N. pachyderma* (dex.) von der Temperatur beeinflusst zu sein, was sich durch einen vermehrten Einbau von leichtem metabolischen $^{12}CO_2$ bei hohen Temperaturen ausdrückt. Diese modernen Beobachtungen erlauben es zwischen dem Einfluss des Agulhas-Stromes und der atlantischen Wassermassen auf die Foraminiferenfauna zu unterscheiden.

Für eine präzise Quantifizierung der Kalzifizierungsprozesse planktischer Foraminiferen und ihrer Variabilität wurde im Rahmen dieser Arbeit ein Massen-bilanzierungsmodell entwickelt, welches die stabile Sauerstoffisotopenzusammensetzung als Funktion der Wassertiefe beschreibt und vorhersagt. Das Schalenwachstum planktischer Foraminiferen, oder genauer, die Zunahme der Schalenmasse, zeigt keinen linearen Zusammenhang mit zunehmender Wassertiefe, sondern kann mit Hilfe einen kumulativen Massenzunahme-Funktion beschrieben werden. Dieses Modell erlaubt eine genaue Charakterisierung der artenspezifischen Tiefenbereiche, indem es Informationen über die

genaue Schalenwachstumsrate und über die Wassertiefe liefert, in der das Schalenwachstum abgeschlossen ist. Zusätzlich ist es dazu geeignet, die vertikale Temperaturverteilung in der Wassersäule zu entschlüsseln, indem gleichzeitig die $\delta^{18}O$-Werte unterschiedlicher Arten betrachtet werden. Um die Anwendbarkeit des Modells zu veranschaulichen, wurde es an verschiedenen Foraminiferenarten in unterschiedlichen hydrographischen Regionen getestet. Das Schalenwachstumsmuster jeder einzelnen Art lässt sich mit Hilfe von nur zwei Modelparametern beschreiben. Die beobachtete Variabilität dieser Parameter zeigt, dass das Kalzifizierungsmuster einer Art von der hydrographischen Situation gesteuert wird.

Die $\delta^{13}C$-Werte lebender *G. inflata* wurden bestimmt, um den Einfluss der Meerwasser-Karbonationenkonzentration ($[CO_3^{2-}]$) unter natürlichen Bedingungen besser abschätzen zu können. Dafür wurden zunächst die stabilen Sauerstoffisotopenwerte und das Wachstumsmodell genutzt, um zu ermitteln, in welchen Proportionen *G. inflata* ihr stabiles Isotopensignal entlang des SW-afrikanischen Kontinentalhanges in die Schale einbaut. Die berechneten gewichteten Unterschiede zwischen dem $\delta^{13}C$ der Schale und dem des Meerwassers ($\Delta\delta^{13}C_{shell\text{-}DIC}$) variieren als Funktion der $[CO_3^{2-}]$ mit zunehmender Wassertiefe. Die ermittelten $\Delta\delta^{13}C_{shell\text{-}DIC}/[CO_3^{2-}]$-Regressionssteigungen für *G. inflata* betragen -0.012 bis -0.014‰ für die Größenklasse 150-250 μm, beziehungsweise -0.012 bis –0.015‰ $(\mu mol*kg^{-1})^{-1}$ für Individuen von 250-355 μm Größe. Diese Steigungen entsprechen Werten anderer nicht-symbiotischer Arten, die in Kulturexperimenten ermittelt wurden. Nach der Korrektur der $\delta^{13}C$-Werte von *G. inflata* lassen sich die $\delta^{13}C$-Werte des Meerwassers mit einer Abweichung von 1.55‰ abschätzen. Für die Interpretation von $\delta^{13}C$ in der Paläozeanographie bedeutet diese Beobachtung, dass der $[CO_3^{2-}]$-Effekt eine entscheidende Rolle spielt und $\delta^{13}C$ nicht ohne Korrektur auf den Zielparameter übertragen werden kann.

CHAPTER 1

INTRODUCTION

1.1 Motivation and main objectives

Climate prediction requires a precise understanding of past oceanographic and climatic record. Planktic foraminifers, a major protistid group, are particularly suitable for studying past climatic and ocean changes. Their faunal assemblages and shell stable oxygen and carbon isotope composition are powerful tools for paleoceanographic reconstructions (Fischer and Wefer, 1999, and references therein). However, for an accurate and reliable interpretation of information conveyed by species distribution and isotopic signature in the sedimentary record, a detailed knowledge of the behavior of modern species with regard to given environmental variables is needed prior to proxy application. This comprises the identification and quantification of the controlling factors affecting the incorporation of stable isotopes and knowledge on a given species' geographic and seasonal distribution as well as on its calcification depth range.

Ecological aspects, faunal distributions, and stable isotope compositions have been investigated in various studies performed on plankton tow collected foraminifers or sediment trap material in the north Atlantic (e.g. Cifelli, 1965; Bé and Tolderlund, 1971; Tolderlund and Bé, 1971; Deuser et al., 1981; Erez and Honjo, 1981; Williams et al., 1981; Ottens, 1992), in the equatorial Atlantic upwelling regions (e.g. Thiede, 1975), in the South Atlantic (e.g. Boltovskoy, 1962; Kemle-von Mücke, 1994), in the Indian Ocean (e.g. Bé and Hutson, 1977; Peeters, 2000; Peeters and Brummer, 2002), and in the Pacific Ocean (e.g. Fairbanks and Wiebe, 1980; Kahn and Williams, 1981; Fairbanks et al., 1982; Curry et al., 1983; Thunell and Reynolds, 1984; Russell and Spero, 2000). Researchers succeeded to culture planktic foraminifers and, thus, were able to study the organism under controlled environmental

conditions (e.g. Erez and Luz, 1983; Bouvier-Soumagnac and Duplessy, 1985; Spero and Lea, 1996; Spero et al., 1997; Bijma et al., 1998; Bemis et al., 2000).

However, little is known about the exact depth habitat and termination of shell growth of planktic foraminifers. Observations on field collected species show that the specimens do not calcify exclusively at a single depth as often assumed, but the calcification process is more complex and seems to occur at various depths in the water column. Foraminifers further may modify their habitat depth depending on hydrographic conditions and food supply (Fairbanks et al., 1982; Field, 2004). The vertical range of depth habitat and calcification for individually species is wide and varies both regionally and seasonally. Understanding the vertical distribution patterns of different species and their ecological preferences allow reconstruction of the vertical structure of the water column by using differences in a geochemical proxies, e.g. for temperature ($\delta^{18}O$ or Mg/Ca), between species with different preferred depth habitats (Emiliani, 1954; Mulitza et al., 1997). Therefore, a detailed reconstruction of the species-specific calcification process in the water column in response to environmental conditions and the influence on the geochemical signature , i.e. the uptake of the stable isotopic signal, has to be quantified.

Another feature which has to be considered is the significant seasonal and interannual variability observed in planktic foraminifers with respect to species and isotopic composition, and fluxes, shown by many authors (Deuser and Ross, 1989; Thunell and Sautter, 1992). In some extreme environments, for instance, only a short time period of the year will be represented in the fossil record. To make optimal use of the sediment derived information it is necessary to unravel the mixed sediment record by using modern information of sediment trap experiments and/or seasonal plankton tow investigations. Since planktic foraminifers respond quickly to sudden changes in hydrography (e.g. Sautter and Thunell, 1991a; Ottens, 1992), the investigation of the modern faunal assemblages and stable isotope composition of shells, in particular in so-called key locations is of great interest for climate research. For instance, the Indian-Atlantic water mass exchange in the Agulhas Retroflection area south of South Africa plays a crucial role in the termination of glacial conditions and resulting resumption of the Atlantic meridional overturning circulation (Knorr and Lohmann, 2003; Peeters et al., 2004). Hence, information of the present relationship between foraminiferal assemblages and hydrography in such regions helps to understand the past and allows predictions for the future.

Compared to oxygen isotopes the incorporation of carbon isotopes into the calcite shells is less understood. For the application of the carbon isotopic composition of planktic

foraminiferal shells as an indicator for the carbon isotopic ratios of ancient water masses, which provide information about the past oceanic carbon system and its role in climate change, the incorporation of carbon isotopes has to be investigated in more detail. Since the higher *p*H and higher carbonate ion concentration in the glacial ocean has been proposed as a cause of the lower atmospheric CO_2 (Archer and Maier-Reimer, 1994; Sanyal et al., 1995), an important aspect in this context is the investigation of the so-called "carbonate ion effect" under natural conditions. This effect, demonstrated in culturing experiments by Spero et al. (1997), indicates that the shell carbon isotopic composition of planktic foraminifers varies inversely with the carbonate ion concentration of the seawater. This effect might provide an alternate hypothesis (Lea et al., 1999) to the terrestrial biosphere-to-ocean transfer of carbon that is generally accepted as an explanation for lower glacial carbon isotope ratios in foraminiferal shells (Shackleton, 1977). Thus, the investigation of this effect in the field, i.e. under natural environmental conditions, is inevitable.

In this context, the goal of this thesis is to further improve the calibration of planktic foraminifer faunal assemblage and stable carbon and oxygen isotopes as paleoceanographic proxies, studying samples from plankton tows and sediment traps in the eastern North and South Atlantic Oceans.

1.2 A brief overview of planktic foraminiferal ecology

Planktic foraminifers are unicellular marine organisms (Protozoa) which are distributed throughout the entire world oceans, living in the upper water column. Different species favor different environmental preferences resulting in a characteristic biogeographic species distribution (e.g. Bé and Tolderlund, 1971). The biogeographic provinciality in modern planktic foraminifers is restricted to global climate belts and five major faunal provinces were recognized: polar, subpolar, transitional, subtropic and tropic (e.g. Bé, 1977). Since the provinces are symmetrical about the equator the distribution appears to be clearly related to water mass temperature. However, the factors governing abundance and range are certainly more complex (e.g. Boltovskoy, 1971).

Besides a well defined spatial distribution, planktic foraminiferal species show a clear temporal (seasonal) distribution pattern and occur usually in highest abundances during their most preferred thermal and food source conditions, as well as light availability (e.g. Bé, 1960; Parker, 1960; Cifelli, 1962; Tolderlund and Bé, 1971; Fairbanks and Wiebe, 1980; Deuser and Ross, 1989; Field, 2004). Such conditions may exist in a specific hydrographic regime for only

a short period of the year. Consequently, the shells which are found in modern sediments are expected to reflect almost exclusively the hydrographic and biological changes during those periods of the year.

The modern taxonomy classification is based on the shell morphology and the geometric arrangement of the chambers. A total of forty-four recent planktic foraminiferal species are known, which can be divided into non-spinose and spinose species (Murray, 1897a). Thereby, the species diversity is decreasing from the tropical region to the polar regions, where only two to three different species are found. In general, non-spinose species are herbivore, while the spinose species are carnivorous and harbor large numbers of actively photosynthesizing symbiotic algae between their spines (Hemleben et al., 1989). Food usually consists of bacteria, phytoplankton (e.g. diatoms) or small zooplankton (e.g. copepods). The food is generally detected and captured by their rhizopodia, which are long cytoplasmic thread-like extrusions from the shell. The non-spinose species usually do not accept living prey because of their rhizopodial net is incapable of holding them (Hemleben et al., 1989).

Living planktic foraminifers inhabit mainly the photic zone of the upper water column of the ocean (mixed layer and thermocline), and shell concentrations are usually decreasing with increasing depth in the water column. Based on plankton tow investigation it is evident that foraminifers are vertically distributed by showing a distinct depth stratification and inhabiting characteristic ecological niches (e.g. Emiliani, 1954; Fairbanks and Wiebe, 1980; Vincent and Berger, 1981). However, some species descend as deep as 1000 m in their late ontogenetic stages (Erez and Honjo, 1981; Lohmann, 1995). To counter gravitational settling, a foraminifer may adjust its buoyancy by manufacturing low-density lipids or gases (Furbish and Arnold, 1997). In contrast, foraminifers are not able to regulate their horizontal movement, because they do not possess locomotory organelles (Hemleben et al., 1989). Consequently, the horizontal distribution is mainly controlled by the surface water hydrography.

The life span of a planktic foraminifer can vary between three days to up to one year (Hemleben et al., 1989). There is evidence that some species show a reproduction cycle which has a lunar or semi-lunar periodicity (Spindler et al., 1979; Bijma et al., 1990a). In general, foraminifers show a vegetative reproduction through cell division. Hundred thousands of gametes (3-5 μm) are produced within the parent shell and released through the shell aperture(s). After a successful division the shell will be rebuild by each daughter cell and calcification of initial chambers begins shortly after fission.

One important feature of planktic foraminifers is the secretion of a calcite shell ($CaCO_3$) that includes a series of chambers around a coiling axis (Berger, 1969). The calcareous shells show diameters ranging approximately from 0.1 to 1 mm (Hemleben et al., 1989; Wefer and Berger, 1991). Shell growth is characterized by intermittently adding new chambers. Each new chamber is thicker walled and has a larger volume than the preceding one (Hemleben et al., 1989). With the formation of each new chamber, a new layer is also secreted over the outer surface of previous chambers of the test. Bé at al. (1977) reported that foraminifers add a new chamber in a matter of hours. While primary calcification, i.e. the formation of chambers, seems to occur mainly in the upper water column, some species precipitate further calcite, e.g. in form of a crust or a "kummerkammer", while sinking in deeper waters (secondary or gametogenic calcification) (Orr, 1967; Duplessy and Be, 1981).

The usefulness of planktic foraminifers as ocean climate indicators was realized by Murray (1897). Because of their wide distribution in the word oceans, the good fossilization potential of their calcitic shells and their long geological record, planktic foraminifers are particularly suitable for the decrypting of the sedimentary record.

1.3 Stable isotopes

1.3.1 Principles of isotopic fractionation

'A German Professor, who has been working on geochemistry for decades, illustrated the phenomenon of isotopic fractionation by a person eating beans and peas. For some reason the person might have a slightly higher affinity for beans. Thus, almost equal portions of beans and peas would be removed from the plate, however, since beans are slightly preferred, they would accumulate within the stomach of the person, leaving a slight deficit of beans on the plate (compared to the initial mixture)' (Zeebe and Wolf-Gladrow, 2001).

The partitioning of isotopes between two substances or two phases of the same substance with different isotope ratios is called isotopic fractionation. In general, one can distinguish between equilibrium isotope fractionation and non-equilibrium fractionation. Equilibrium isotope fractionation occurs usually during isotopic exchange reactions, e.g. during air-sea gas exchange (Charles and Fairbanks, 1990; Broecker and Maier-Reimer, 1992; Lynch-Stieglitz et al., 1995). In contrast, non-equilibrium effects are associated with incomplete processes such as evaporation, photosynthesis, kinetic isotope effects in chemical reactions or metabolic effects. A normal kinetic isotope effect can be observed by a greater

reaction rate of the lighter isotope compared to the heavier isotope, since light isotopes have a higher mobility.

1.3.2 Oxygen isotopes

During calcite precipitation in seawater, i.e. during planktic foraminiferal shell growth, a temperature dependent fractionation occurs between the oxygen isotopes ^{18}O and ^{16}O (McCrea, 1950). At higher temperature a relatively smaller amount of the heavier isotope ^{18}O is incorporated in the calcareous shell, while at lower temperatures the opposite is true (Erez and Luz, 1983; Bouvier-Soumagnac and Duplessy, 1985). Beside temperature, the oxygen isotope composition of carbonate is controlled by the oxygen isotope composition of the seawater itself. The $^{18}O/^{16}O$ ratio in seawater is primarily controlled by fractionation processes due to evaporation and precipitation at the sea surface, and river discharge. Due to the isotopic fractionation during evaporation the oxygen isotope composition in seawater shows a positive correlation with salinity which is affected by similar processes (Craig and Gordon, 1965). Since during glacial periods large amounts of ocean water were deposited as ice on the continents, the ocean was characterized by higher ^{18}O and salinity values (Mook et al., 1974). The so-called ice volume effect includes the variations of the oceanic oxygen isotopic composition during glacial-interglacial times in the Pleistocene, which were estimated to be 0.4 to 1.1‰ (Emiliani and Shackleton, 1974).

In this context, the oxygen isotope composition of foraminiferal calcite shells can be used to estimate the water temperature in which they calcified by using empirically derived paleotemperature equations (Bemis et al., 1998, and references therein). Since the pioneer work of Urey (1947) the use of stable oxygen isotope ratios, particularly that of foraminiferal calcite ($CaCO_3$), has become a standard tool in paleoceanography as a paleo-thermometer (e.g. Shackleton and Opdyke, 1973; Emiliani and Shackleton, 1974; Miller et al., 1987; Wefer and Berger, 1991). The numerous equations published are either based on laboratory experiments with planktic foraminifers (Erez and Luz, 1983; Bouvier-Soumagnac and Duplessy, 1985) or mollusks (Epstein et al., 1953), and therefore include species-specific effects, or they are derived from inorganically precipitated calcite (e.g. Kim and O`Neil, 1997) and are free of any biological effects (Fig. 1.1). Most of these temperature equations are comparable but often yield calcification temperatures for living plankton which are 1-2 °C too high with respect to the ambient seawater temperature (e.g. Williams et al., 1981; Bemis et al., 1998).

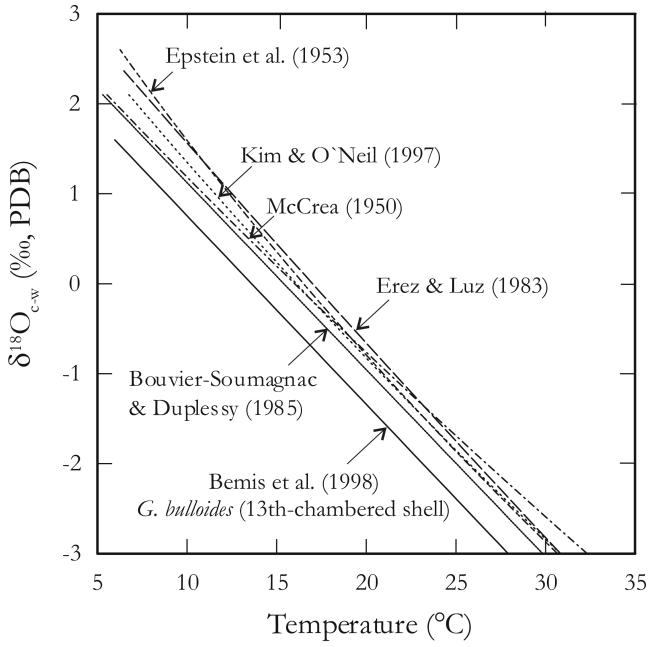

Figure 1.1. Examples of paleotemperature equations as given by various authors (after Bemis et al. (1998)).

In the present study we will refer to the inorganic calcite equation of Kim and O`Neil (1997):

$$T(°C) = 16.1 - 4.64 * (\delta^{18}O_{calcite} - \delta^{18}O_w) + 0.09 * (\delta^{18}O_{calcite} - \delta^{18}O_w)^2 \qquad [1]$$

where T is standing for the *in-situ* temperature during calcite precipitation (°C), $\delta^{18}O_{calcite}$ is representing the oxygen isotopic composition of the calcite (‰, PDB), and $\delta^{18}O_w$ is the oxygen isotopic composition (‰, PDB) of the seawater from which the calcite has been precipitated. Since oxygen isotope analysis of waters are commonly reported relatively to SMOW (Standard Mean Ocean Water), the conversion factor between $\delta^{18}O_w$ from the SMOW to the PDB (Pee Dee Belemnite) scale can be calculated after Hut (1987):

$$\delta^{18}O_w(‰, PDB) = 0.99973 * \delta^{18}O_w(SMOW) - 0.27‰ \qquad [2]$$

However, the current state of research is that ideally temperature equations for different species and for different size classes are necessary. Recently, field-based temperature equations for different species have been established using field collected planktic foraminifers in surface waters (Spero and Lea, 1996; Peeters et al., 2002; Mulitza et al., 2003). For instance, Mulitza et al. (2003) tested paleotemperature equations with $\delta^{18}O$ measurements on the four

species (*Globigerinoides ruber* (white), *Globigerinoides sacculifer, Globigerina bulloides* and *Neogloboquadrina pachyderma*) collected in surface water over a broad range of hydrographic conditions. These authors illustrate that the species show significantly lower $\delta^{18}O$ values than suggested by well established paleotemperature equations. Their resulting temperature-$\delta^{18}O$ relationship produces 2-4°C colder temperatures compared to equations derived from inorganic precipitates or cultured mollusk or foraminifers (Fig. 1.2).

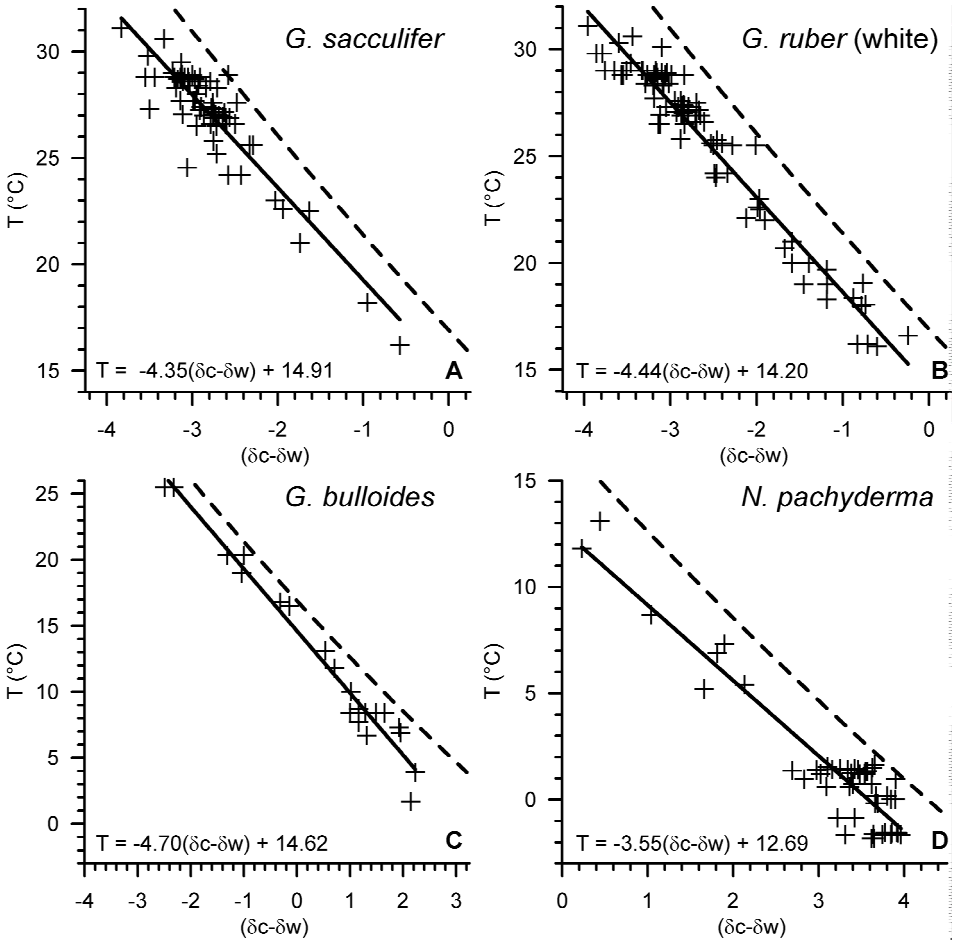

Figure 1.2. Temperature-$\delta^{18}O$ relationship of *Globigerinoides sacculifer* (A), *Globigerinoides ruber* (white) (B), *Globigerina bulloides* (C) and *Neogloboquadrina pachyderma* (D) compared to the paleotemperature equations of Shackleton (1974) based on inorganic precipitates of O'Neil et al. (1969) (dashed line). The bold line represents the calculated regression for each species (data from Mulitza et al. (2003).

Generally, paleotemperature equations are used to calculate the predicted theoretical inorganic calcite values ($\delta^{18}O_{eq}$) which are precipitated in isotopic equilibrium with the ambient temperature and $\delta^{18}O$ of the seawater. Comparisons of measured foraminiferal $\delta^{18}O$ values with predicted $\delta^{18}O_{eq}$ precipitated in isotopic equilibrium often revealed distinct deviations (e.g. Shackleton and Vincent, 1978; Kahn, 1979; Mortyn and Charles, 2003). This

implies that the oxygen isotope composition of a planktic foraminifer may be determined by other factors, in addition to *in-situ* temperature and $\delta^{18}O_w$, including biological effects and carbonate system effects.

It has recently been shown that the foraminiferal stable oxygen isotope composition is influenced by the carbonate ion concentration ($[CO_3^{2-}]$) of the ambient seawater (Spero et al., 1997; Bijma et al., 1998). During laboratory experiments with different species these authors indicate that the shell $\delta^{18}O$ varies inversely with the $[CO_3^{2-}]$ of seawater. Spero et al. (1997) cultured for instance the species *Orbulina universa* and *Globigerina bulloides* across a wide $[CO_3^{2-}]$ range. The $\delta^{18}O$ of the shells decreased as the $[CO_3^{2-}]$ increased, for instance with a regression slope for *O. universa* of -0.0015± 0.0008‰ $(\mu mol*kg^{-1})^{-1}$ under high light laboratory conditions (HL), while *G. bulloides* (13th chamber) yields a slope of –0.005 for $\delta^{18}O/[CO_3^{2-}]$ (Fig. 1.3).

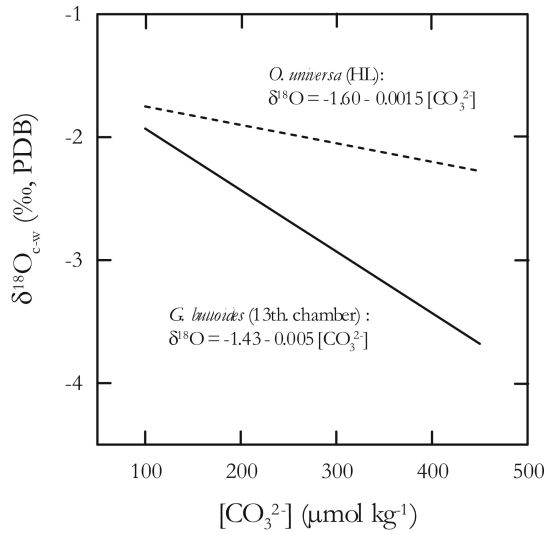

Figure 1.3. Mean $\delta^{18}O/[CO_3^{2-}]$ slopes given by Spero et al. (1997) for *Orbulina universa* (HL = high light conditions) and *Globigerina bulloides,* identified during laboratory culture experiments (under constant ΣCO_2). Note that the slope observed for *G. bulloides* is twice as high as the one of *O. universa*, which indicates that the CIE is species-specific.

The fact that *G. bulloides* shows a regression slope that is twice as high as the one of *O. universa* proves that the so-called carbonate ion effect is species-specific. Model results by Zeebe (1999) suggest that this effect is due to increased incorporation of isotopically depleted CO_2 under higher *p*H, and thus $[CO_3^{2-}]$, probably combined with systematically higher respiration rates or increased kinetic fractionation at higher $[CO_3^{2-}]$. Since HCO_3^- is isotopically heavier compared to the CO_3^{2-}, the oxygen isotopic composition of the total dissolved carbonate species ($S = [H_2CO_3] + [HCO_3^-] + [CO_3^{2-}]$) decreases with increasing *p*H. These authors further suggest that foraminiferal species use obviously a mixture of

bicarbonate and carbonate for calcite formation such that the oxygen isotope composition of the calcite (solid) and of S (dissolved) are equally decreasing with increasing [CO_3^{2-}] (Zeebe, 1999; Zeebe and Wolf-Gladrow, 2001).

Since the carbonate ion effect is probably inherent to all foraminiferal species, only with species-specific magnitudes, these results emphasized that the oxygen isotope fractionation between calcium carbonate and water does not longer only depend on the temperature but also on the *p*H of the solution from which it is formed. This has important consequences for paleo-reconstructions. For instance, a higher seawater *p*H during the last glacial maximum, as indicated by foraminiferal boron isotope (Sanyal et al., 1995), would result in lower foraminiferal $\delta^{18}O$ values, which would in turn be interpreted as sea surface temperatures (SST) that might be up to 1°C too high. A correction for this effect would bring tropical SST closer to estimates based on other marine temperature proxies, such as Sr/Ca ratios in corals.

Further, foraminiferal shell size must be regarded as an important criterion when quantifying disequilibrium effects. It has been shown that due to an ontogenetic effect small shells are depleted in ^{18}O compared to larger ones (Spero and Lea, 1996; Bemis et al., 1998). Juvenile foraminifers calcify faster and respire at higher rates (Berger et al., 1978; Hemleben et al., 1989). During a rapid calcification a discrimination of the heavier isotope ^{18}O occurs due to kinetic fractionation (McConnaughey, 1989).

Laboratory experiments demonstrated that the deviations from isotopic equilibrium may also be due to symbiont activity during photosynthesis (Spero and Lea, 1993b). For example, $\delta^{18}O$ of species grown under high light conditions, i.e. increased symbiont photosynthetic activity, show lighter oxygen isotope values compared to shells who were grown under dark conditions (Spero et al., 1997). The responsible mechanisms for this effect are not well understood, but appear to be linked to the carbonate system. Physiological processes, such as photosynthesis, control the *p*H of the foraminiferal microenvironment in addition to seawater *p*H (Jørgensen et al., 1985; Wolf-Gladrow et al., 1999) (Fig. 1.4). Consequently, the carbonate chemistry in the near vicinity of the foraminifer can be quite different from that of the bulk seawater. An increase of the symbiont photosynthetic activity leads to higher *p*H in the vicinity of a foraminifer. Model results show that both, the CO_2 and HCO_3^{2-} concentration decrease towards the shell, which is an enormous perturbation of seawater carbonate chemistry in the microenvironment of the host-symbiont system, and leads to an increase in pH (and [CO_3^{2-}]). This effect might be associated with either higher light intensity, but can also be related to a higher number of symbionts in a larger foraminifer. It

seems quite possible that for foraminifers containing symbionts the ontogenetic effect may be superimposed by the photosynthetic activity of their symbiotic algae.

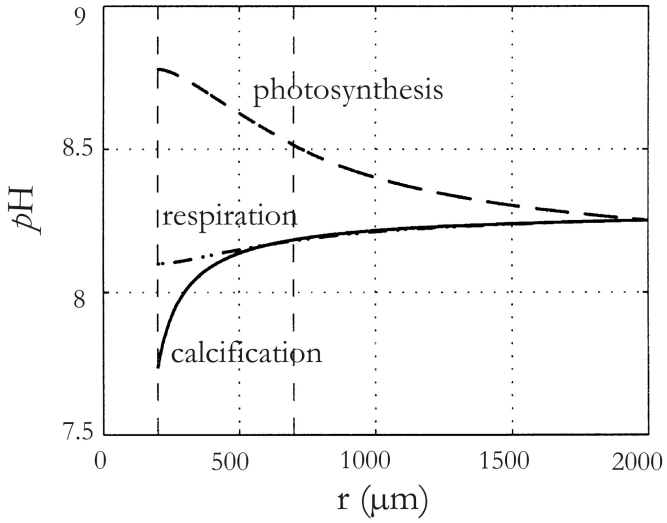

Figure 1.4. Modeled profile of *p*H for different life processes (photosynthesis, respiration and calcification) as a function of the distance from the centre of the shell r. Whereas calcification and respiration produce CO_2 and thereby lower the *p*H at the site of calcification, symbiont photosynthetic activity sequesters CO_2 and thereby increases *p*H in the foraminiferal microenvironment (after Wolf-Gladrow, 1999).

1.3.3 Carbon isotopes

Planktic foraminifers use the marine total dissolved inorganic carbon (ΣCO_2) to build their calcite shells and, hence, record the $\delta^{13}C$ of seawater ΣCO_2 during calcification. The ΣCO_2 itself comprises the sum of the concentrations of CO_2 (= aqueous carbon dioxide), HCO_3 (= bicarbonate), and CO_3^{2-} (= carbonate ion). The relative proportion of these components is controlled by the seawater *p*H (Fig. 1.5). Thereby, the ΣCO_2 is mainly in the form of CO_3^{2-} at high *p*H and mainly in the form of HCO_3 at intermediate *p*H. The $\delta^{13}C$ of the total dissolved inorganic carbon in modern oceans shows usually a natural range of about -1 to +3‰.

Changes in seawater $\delta^{13}C_{\Sigma CO2}$ are mainly controlled by balances between water column photosynthesis and respiration cycle and the degree of air-sea isotopic equilibrium (Charles et al., 1993; Lynch-Stieglitz et al., 1995).

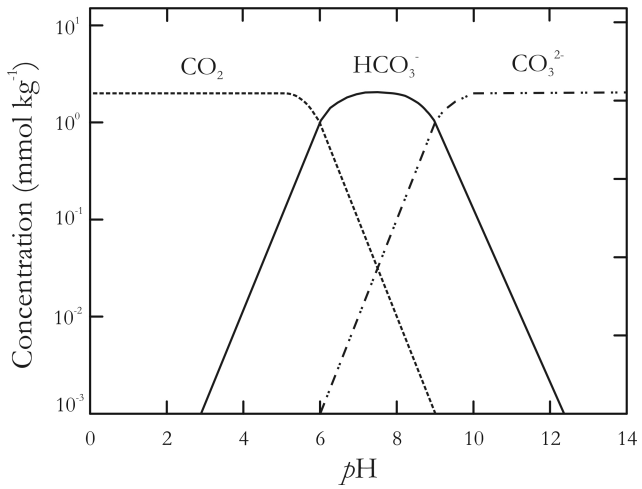

Figure 1.5. The concentration of the dissolved carbonate species as a function of *p*H. (T = 19°C, S = 35 psu, $\Sigma CO_2 \approx 2$ mmol kg^{-1}).

During biological production in the euphotic zone organisms preferentially remove the light isotope ^{12}C which is concentrated in organic matter. Since nearly all of the organic matter that is produced by photosynthesis is subsequently remineralized in the water column, the surface ocean becomes usually enriched in the heavier isotope ^{13}C while the deep water masses have lower $\delta^{13}C$ values. The thermodynamic fractionation during gas exchange at the air-sea boundary between the atmospheric CO_2 and the dissolved CO_2 in surface ocean is rather small, whereas the stronger fractionation occurs during the hydration process between the dissolved CO_2 and HCO_3^-. The thermodynamic fractionation shows a clear temperature dependence (Mook et al., 1974; Siegenthaler and Münnich, 1981), with ΣCO_2 becoming more enriched relative to the atmospheric value by about 1‰ per 10°C cooling. The extend of this fractionation further depends on the exchange rate and surface water residence times. Due to the burning of fossil fuels and the release of isotopically light CO_2 into the atmosphere the $\delta^{13}C$ of atmospheric CO_2 has decreased from approximately –7.4‰ to -7.8‰ between 1978 and 1997 ("Suess-effect"), and in response, the $\delta^{13}C_{\Sigma CO2}$ has also decreased (Broecker and Peng, 1993; Keeling et al., 1995; Gruber et al., 1999).

The carbon isotopic composition of marine carbonates, such as planktic foraminiferal shells, is usually close to the isotopic composition of ΣCO_2 in the ocean. In general the $\delta^{13}C$ values of $CaCO_3$ fall within the range from -2‰ to +2‰ (Wefer and Berger, 1991). Because of this tracking, foraminifers have the potential to preserve the $\delta^{13}C_{\Sigma CO2}$ and thus are generally used as a proxy for past ocean circulation, biological productivity in surface waters, and variation of the global carbon cycle (e.g. Broecker and Peng, 1982; Ganssen and Sarnthein, 1983; Kroon and Ganssen, 1988; Mortlock et al., 1991). However, a requirement for the

application is that the signal stored in the planktic foraminiferal shells mirrors the properties of the bulk water mass, i.e. calcify in equilibrium with the ambient seawater or have predictable offsets. Many studies have shown that most foraminiferal species exhibit $\delta^{13}C$ values which deviate from the seawater $\delta^{13}C_{\Sigma CO2}$ (e.g. Shackleton and Vincent, 1978; Kahn and Williams, 1981; Kroon and Ganssen, 1989; Wefer and Berger, 1991; Mulitza et al., 1999). As discussed for the influence on the oxygen isotopic composition of carbonates, there are several factors responsible for the observed deviations between shell $\delta^{13}C$ and $\delta^{13}C_{\Sigma CO2}$ which are known to be species-specific and which limits our ability to understand carbon cycling in past oceans.

For instance, as a result of ontogenetic/metabolic effects, larger shells show higher $\delta^{13}C$ values compared to smaller shells. This size-dependence is due to considerable amounts of respired light carbon in the carbon pool that is used for calcite precipitation during the juvenile phase (Berger et al., 1978; Spero and Lea, 1996). Since temperature does not influence the $\delta^{13}C$ of inorganic calcite (Romanek et al., 1992), it may affect foraminiferal shell $\delta^{13}C$ through its effect on metabolic rate and on symbiont photosynthesis (Ravelo and Fairbanks, 1995; Ortiz et al., 1996; Bemis et al., 2000). For example, Ortiz et al. (1996) pointed out the temperature and food effects on $\delta^{13}C$ disequilibria and showed that the shells of four planktic foraminiferal species were ^{13}C depleted by 1 to2.4‰ relative to the isotopic equilibrium with ambient seawater.

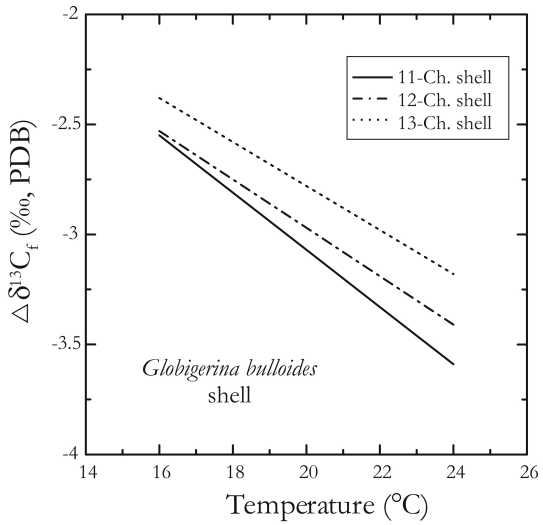

Figure 1.6. Laboratory experiment with *G. bulloides* demonstrate the influence of ambient temperature and specimen size, where $\Delta\delta^{13}C_f = \delta^{13}C_{foram} - \delta^{13}C_{\Sigma CO2}$. Larger shells are less depleted in ^{13}C relative to ΣCO_2. The slope of these linear equations appear to decrease slightly with increasing shell size ($[CO_3^{2-}]$ = 171 μmol*kg $^{-1}$). The $\delta^{13}C$ of *G. bulloides* shells decreases with a common slope of –0.11 ‰ °C^{-1} (modified after Bemis et al. (2000).

The decreased $\delta^{13}C$ values at higher temperatures are a function of greater metabolic modification of $\delta^{13}C_{\Sigma CO2}$ near the shell (Bijma et al., 1990b; Ortiz et al., 1996). Laboratory experiments with the species *G. bulloides* follow a slope of –0.11‰ $°C^{-1}$ (Bemis et al., 2000), the strongest temperature/$\delta^{13}C$ relationship yet identified, probably due to temperature-dependent respiratory effects (Fig. 1.6). These authors further show the correlation between shell size and $\delta^{13}C$ due to ontogenetic changes in metabolic rates, i.e. smaller chambers and shells exhibit a greater disequilibrium than larger specimens at all experimental temperatures (Bemis et al., 2000).

In contrast, laboratory cultural experiments reveal that the symbiont photosynthetic effect leads to enriched shell $\delta^{13}C$ values due to the preferential removal of ^{12}C from the foraminiferal microenvironment by symbiontic algae (Spero and DeNiro, 1987; Spero and Lea, 1993b). Higher light conditions, higher temperatures and a higher symbiont density may increase this effect. However, the effect of symbionts on foraminiferal $\delta^{13}C$ is difficult to quantify.

Figure 1.7 shows a schematic illustration of the origin of metabolic and kinetic isotope effects in biological carbonates after McConnaughey et al.(1997):

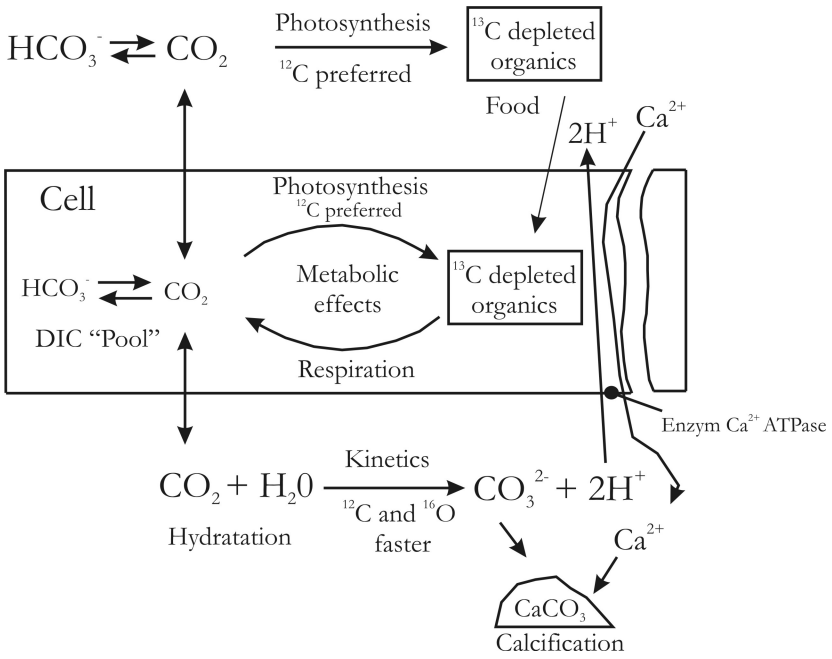

Figure 1.7. Schematic illustration of the basic mechanism of most biological calcification. The cell DIC "Pool" is controlled by main life processes, such as respiration and photosynthetic, which are responsible for the origin of metabolic effects. In contrast, during faster calcification and respiration in early ontogenetic life stages, the rapid HCO_3^- precipitation to $CaCO_3$ is associated with a kinetic fractionation and a discrimination of the heavier isotope ^{13}C. The disequilibrium may result from precipitation before isotopical equilibrium is reached with cell DIC. Calcification appears to be driven by proton removal from the calcifying fluid, catalyzed by the enzyme Ca^{2+} ATPase (black dot on membrane) (after McConnaughey, 1994; McConnaughey et al., 1997).

Analogous to oxygen isotopes, the incorporation of $\delta^{13}C$ into foraminiferal shells is controlled by the carbonate chemistry in the ocean (Spero et al., 1997; Bijma et al., 1998). The laboratory results show that the seawater carbonate ion concentration ($[CO_3^{2-}]$) affects the $\delta^{13}C$ of foraminiferal shells to a much greater extend compared to $\delta^{18}O$. An increase in the $[CO_3^{2-}]$, at constant $\delta^{13}C_{\Sigma CO2}$, results in lower $\delta^{13}C$ of foraminiferal shells, whereas the $\delta^{13}C/[CO_3^{2}]$ slopes, are species-specific, as a result of species-specific fractionation. *G. bulloides* shells show decreased $\delta^{13}C$ values at higher seawater $[CO_3^{2-}]$ (–0.012 ‰ µmol*kg^{-1}). The carbonate ion effect effect shows a proportional decrease in $\delta^{13}C$ and $\delta^{18}O$ and suggests therefore a kinetic discrimination against the heavier isotopes ^{13}C and ^{18}O during the slow isotopic equilibration between CO_2 and HCO_3^- during the calcification process (hydration and hydroxylation) (McConnaughey et al., 1997) (Fig. 1.7).

Recently, studies were carried out to investigate the carbonate ion effect under natural environmental conditions (Russell and Spero, 2000; Itou et al., 2001; Bauch et al., 2002; Peeters et al., 2002). For example, Peeters et al. (2002) demonstrated for the Indian Ocean that the $\Delta\delta^{13}C_{shell\text{-}DIC}$ changes as a function of seawater $[CO_3^{2-}]$. Thereby, the established slopes for *G. bulloides* (-0.013‰ (µmol*kg^{-1}) and *G. ruber* (-0.0098‰ (µmol*kg^{-1}) were close to those found during laboratory culture experiments (Spero et al., 1997; Bijma et al., 1998). The carbonate ion effect acts, more strongly, in an opposite sense than the effect of $\delta^{13}C_{DIC}$. This effect explains why the $\delta^{13}C$ of *G. bulloides* was higher during the SW monsoon upwelling period than during NE monsoon non-upwelling conditions.

1.4 Outline of this thesis

The presented thesis contributes to a better knowledge of planktic foraminiferal ecology as a prerequisite to understand the incorporation of stable carbon and oxygen isotopes into their calcite shells. This in turn provides the opportunity of improved proxy development and/or proxy calibration. The following manuscripts focus on different aspects of foraminiferal ecology and shell isotope-geochemistry in different hydrographic oceanic regions.

The first manuscript *"Seasonal distribution and stable oxygen isotope composition of planktic foraminifera off NW-Africa (29°N)"* (Iris Wilke, Helge Meggers and Torsten Bickert, submitted to Deep Sea Research) investigates the seasonal distribution and stable oxygen isotope composition of selected species of planktic foraminifers along a productivity gradient in the

Canary Island regions off NW Africa. This study aims to provide a clear assignment of different species to specific seasons, which is made possible by the combination of seasonal plankton tow observations and time-series sediment trap investigations. The relationship between the shell concentrations in the upper water column and shell fluxes of planktic foraminifers and the seasonal hydrographic situation is investigated. Stable oxygen isotope compositions of planktic foraminifers species are compared to predicted oxygen isotope values. Different mechanisms responsible for the observed species and size dependent disequilibrium fractionation are discussed.

The second manuscript *"Planktic foraminiferal fluxes associated with Agulhas rings"* (Iris Wilke, Frank J.C. Peeters and Geert-Jan A. Brummer, submitted to Marine Micropaleontology) presents results from a sediment trap study (MST-15) which monitored deposition fluxes of planktic foraminifers in the southeastern Cape Basin to improve interpretations from sedimentary records of the variability of Indian Ocean advection into the South Atlantic via Agulhas leakage. We report on the changing species, oxygen and carbon isotopic composition of planktic foraminifers as a results of Agulhas rings that moved over our trap site. The main aim of this work is to assess the changes in the faunal assemblage as a result of the inflow of warm Indian Ocean water into the Cape Basin. In order to develop robust proxies that trace Indian Ocean advection into the Atlantic we 1) identify the faunal assemblage associated with Indian/Atlantic Ocean, 2) quantify the shell flux of different species, and 3) understand the changes in the stable isotope composition.

In the third manuscript *"Depth integrated growth of planktic foraminiferal shells Part 1. The theory of an oxygen isotope mass balance model"* (Frank J.C. Peeters and Iris Wilke, to be submitted for publication) a model based on field observations is introduced, that successfully describes and quantifies the change in shell mass and $\delta^{18}O$ of different species of planktic foraminifers as a function of depth in the water column. The shell growth of foraminiferal species can be describe by only two parameters of a function known as the cumulative Weibull distribution function. This model appears well suited to exactly determine the depth habitat and calcification depth of different species. It further allows to quantify the amount of calcite precipitated with increasing depth in the water column and provides information on the rate of shell growth and the depth at which shell growth is completed. Thus, the derivation of the isotope signal found in the sedimentary record is deducible. The model may be used ultimately to unravel the vertical thermal structure of the upper water column by using the $\delta^{18}O$ of different species simultaneously.

The fourth manuscript *"Depth integrated growth of planktic foraminiferal shells Part 2. Model fits to field observations"* (Iris Wilke and Frank J.C. Peeters, to be submitted for publication) examines the application of the oxygen isotope mass balance model to field observations. Planktic foraminiferal species, symbiotic and non-symbiotic, with different ecological preferences from different regions were chosen to illustrate our approach. A major result of this manuscript is that shell growth is strongly controlled by the vertical structure of the water column (mixed layer depth and on the depth of the thermocline in the photic zone), as well as on food supply. The model application allows a more accurate assignment in terms of species depth habitat compared to the simplified classification in mixed layer-, thermocline- or deep-dwellers.

The fifth manuscript *"The influence of seawater carbonate ion concentration [CO_3^{2-}] on the stable carbon isotope composition of planktic foraminifera species Globorotalia inflata"* (Iris Wilke and Torsten Bickert, submitted to Marine Micropaleontology) investigates the influence of the seawater carbonate ion concentration ([CO_3^{2-}]) on the incorporation of planktic foraminiferal stable carbon isotopes ($\delta^{13}C$) under natural conditions. We determine the stable oxygen and carbon isotopic composition of *Globorotalia inflata*, collected by plankton tows in the southeastern Atlantic Ocean (Cape Basin). The oxygen isotope mass balance model is applied to quantify the exact calcification range of *G. inflata*. The calculated weighted $\Delta\delta^{13}C_{shell\text{-}DIC}$ are correlated to the [CO_3^{2-}] in seawater. The resulted slopes from our field data are compared to slopes found for other non-symbiotic species (e.g. *Globigerina bulloides*) from laboratory culture experiment.

References

Archer, D. and Maier-Reimer, E., 1994. Effect of deep-sea sedimentary calcite preservation on atmospheric CO_2 concentration. Nature 367, 260-263.

Bauch, D., Erlenkeuser, H., Winckler, C., Pavlova, G. and Thiede, J., 2002. Carbon isotopes and habitat of polar planktic foraminifera in the Okhotsk Sea: the "carbonate ion effect" under natural conditions. Mar. Micropaleontol. 871, 1-17.

Bé, A.W.H., 1960. Ecology of recent planktonic foraminifera: Part 2-Bathymetric and seasonal distribution in the Sargasso Sea off Bermuda. Micropaleontology 6, 373-392.

Bé, A.W.H., 1977. An ecological, zoogeographic and taxonomic review of recent planktonic foraminifera. In: Ramsay, A.T.S. (Editor), Oceanic Micropaleontology, Vol. 1, London, pp. 1-100.

Bé, A.W.H. and Hutson, W.H., 1977. Ecology of planktonic foraminifera and biogeographic patterns of life and fossil assemblages in the Indian ocean. Micropaleontology 23, 369-414.

Bé, A.W.H. and Tolderlund, D.S., 1971. Distribution and ecology of living planktonic foraminifera in surface waters of the Atlantic and Indian Ocean. In: Funnel, B.M. and Riedel, W.R. (Eds.), Micropaleontology of the Oceans. Cambridge University Press, London, pp. 105-149.

Bemis, B., Spero, H.J., Lea, D.W. and Bijma, J., 2000. Temperature influence on the carbon isotopic composition of *Orbulina universa* and *Globigerina bulloides* (planktic foraminifera). Mar. Micropalentol. 38, 213-228.

Bemis, B.E., Spero, H.J., Bijma, J. and Lea, D.W., 1998. Reevaluation of the oxygen isotopic composition of planktonic foraminifera. Paleoceanography 13, 150-160.

Berger, W.H., 1969. Planktonic foraminifer: basic morphology and ecological implications. J. Paleontology 43(6), 1369-1384.

Berger, W.H., Killingley, J.S. and Vincent, E., 1978. Stable isotopes in deep-sea carbonates: Box Core ERDS-92 west equatorial Pacific. Oceanol. Acta 1, 203-216.

Bijma, J., Erez, J. and Hemleben, C., 1990a. Lunar and semi-lunar reproductive cycle in some spinose planktonic foraminifers. Journal of Foraminiferal Research 20, 117-127.

Bijma, J., Faber, W.W. and Hemleben, C., 1990b. Temperature and salinity limits for growth and survival of some planktonic foraminifers in laboratory cultures. Journal of Foraminiferal Research 20, 95-116.

Bijma, J., Spero, H.J. and Lea, D.W., 1998. Oceanic carbonate chemistry and foraminiferal isotopes: new laboratory results paper presented at the Sixth International Conference on Paleoceanography, Lisbon, 1998.

Boltovskoy, D., 1962. Planktonic foraminifera as indicators of different water masses in the South Atlantic. Micropaleontology 8(3), 403-408.

Boltovskoy, E., 1971. Patchiness in the distribution of planktonic foraminifera. In: Farinacci, A. (Editor), Proc. II Planktonic Conf., Roma, Rome, pp. 107-155.

Bouvier-Soumagnac, Y. and Duplessy, J.-C., 1985. Carbon and oxygen isotopic composition of planktonic foraminifera from laboratory culture, plankton tows and recent sediment: implication for the reconstruction of paleoclimatic conditions and of the global carbon cycle. Journal of Foraminiferal Research 15, 302-320.

Broecker, W.S. and Maier-Reimer, E., 1992. The influence of air and sea exchange on the carbon isotope distribution in the sea. Global Biogeochemical Cycles 6, 315-320.

Broecker, W.S. and Peng, T.-H., 1982. Tracers in the sea. Lamont-Doherty geological observatory. University of Columbia, Palisades, New York 10964, 690 pp.

Broecker, W.S. and Peng, T.-H., 1993. Evaluation of the ^{13}C constraint on the uptake of fossil fuel CO_2 by the ocean. Global Biogeochemical Cycles 7(3), 619-626.

Charles, C.D. and Fairbanks, R.G., 1990. Glacial to interglacial changes in the isotopic gradients of the Southern Ocean surface water. In: Bleil, U. and Thiede, J. (Eds.), Geological history of the Polar Oceans: Arctic versus Antarctic. Kluwer, Dordrecht, pp. 519-538.

Charles, C.D., Wright, J.D. and Fairbanks, R.G., 1993. Thermodynamic influences on the marine carbon isotope record. Paleoceanography 8, 691-697.

Cifelli, R., 1962. Some dynamic aspects of the distribution of planktonic foraminifera in the western North Atlantic. J. Mar. Res 20, 201-213.

Cifelli, R., 1965. Planktonic foraminifera from the western North Atlantic. Smithson. Misc. Collect. 148, 1-35.

Conan, S.M.H. and Brummer, G.J.A., 2000. Fluxes of planktic foraminifera in response to monsoonal upwelling on the Somalia Basin margin. Deep Sea Research II 47, 2207-2227.

Craig, H. and Gordon, L.I., 1965. Deuterium and oxygen 18 variations in the ocean and the marine atmosphere. Symposium on Marine Geochemistry. University of Rhode Island Publication Vol. 3, 277-374.

Curry, W.B., Thunell, R.C. and Honjo, S., 1983. Seasonal changes in the isotopic composition of planktonic foraminifera collected in Panama Basin sediment traps. Earth and Planetary Science Letters 64, 33-43.

Deuser, W.G., Hemleben, C. and Spindler, M., 1981. Seasonal changes in species composition, numbers, mass, size, and isotopic composition of planktonic foraminifera settling into the deep Sargasso Sea. Palaeogeogr., Palaeoclim., Palaeoecol. 33, 103-127.

Deuser, W.G. and Ross, E.H., 1989. Seasonally abundant planktonic foraminifera of the Sargasso Sea: Succession, deep-water fluxes, isotopic composition, and paleoceanographic implications. Journal of Foraminiferal Research 19(4), 268-293.

Duplessy, J.C. and Be, A.W.H., 1981. Oxygen-18 enrichment of planktonic foraminifera due to gametogenic calcification below the euphotic zone. Science 213, 1247-1250.

Emiliani, C., 1954. Depth habitats of some species of pelagic foraminifera as indicated by oxygen isotope ratios. Am. J. Sci. 252, 149-158.

Emiliani, C. and Shackleton, N.J., 1974. The Brunhes epoch: Isotopic paleotemperatures and geochronology. Science 183, 511-514.

Epstein, S.R., Buchsbaum, R., Lowenstam, H.A. and Urey, H.C., 1953. Revised carbonate-water isotopic temperature scale. Geol. Soc. Am. Bull 64, 1315-1325.

Erez, J. and Honjo, S., 1981. Comparison of isotopic composition of planktonic foraminifera in plankton tows, sediment traps and surface sediments. Palaeogeogr., Palaeoclim., Palaeoecol. 33, 129-156.

Erez, J. and Luz, B., 1983. Experimental paleotemperature equation for planktonic foraminifera. Geochimica et Cosmochimica Acta 47, 1025-1031.

Fairbanks, R.G., Sverdlove, M., Free, R., Wiebe, P.H. and Be, A.W.H., 1982. Vertical distribution and isotopic fractionation of living planktonic foraminifera from the Panama Basin. Nature 298, 841-844.

Fairbanks, R.G. and Wiebe, P.H., 1980. Foraminifera and chlorophyll maximum: vertical distribution, seasonal succession, and paleoceanographic significance. Science 209, 1524-1526.

Field, D.B., 2004. Variability in vertical distribution of planktonic foraminifera in the California Current: Relationships to vertical ocean structure. Paleoceanography 19.

Fischer, G. and Wefer, G., 1999. Use of proxies in paleoceanography: Examples from the South Atlantic. Springer-Verlag, Berlin Heidelberg, 735 pp.

Furbish, D.J. and Arnold, A.J., 1997. Hydrodynamic strategies in the morphological evolution of spinose planktonic foraminifera. Geol. Soc. Am. Bull 109(8), 1055-1072.

Ganssen, G. and Sarnthein, M., 1983. Stable-isotopes compositions of foraminifers: The surface and bottom record of coastal upwelling. In: Suess, E. and Thiede, J. (Eds.), Coastal upwelling : Its Sediment Record (Part A). Plenum Press, New York, pp. 99-121.

Gruber, N., Keeling, C.D., Bacastow, R.B., Guenther, P.R., Lueker, T.J., Wahlen, M., Meijer, H.A.J., Mook, W.G. and Stocker, T.F., 1999. Spatiotemporal patterns of carbon-13 in the global surface oceans and the oceanic Suess effect. Global Biogeochemical Cycles 13(2), 307-335.

Hemleben, C., Spindler, M. and Anderson, O.R., 1989. Modern Planktonic Foraminifera. Springer Verlag, New York, 363 pp.

Hut, G., 1987. Stable isotope reference samples for geochemical and hydrological investigations, Consultants Group meeting 16-18.09.1985. International Atomic Energy Agency (I.A.E.A.), Vienna, Austria, pp. 42.

Itou, M., Ono, T., Oba, T. and Noriki, S., 2001. Isotopic composition and morphology of living *Globorotalia scitula*: a new peoxy of sub-intermediate ocean carbonate chemistry? Mar. Micropalentol. 42, 189-210.

Jørgensen, B.B., Erez, J., Revsbech, N.P. and Cohen, Y., 1985. Symbiotic photosynthesis in a planktonic froaminifer, *Globigerinoides sacculifer* (Brady), studied with microelectrodes. Limnol. Oceanogr. 30(6), 1253-1267.

Kahn, M.I. and Williams, D.F., 1981. Oxygen and carbon isotopic composition of living planktonic foraminifera from the northeast Pacific Ocean. Palaeogeogr., Palaeoclim., Palaeoecol. 33, 47-69.

Kahn, M.J., 1979. Non-equilibrium oxygen and carbon isotope fractionation in tests of living planktonic foraminifera. Oceanologica Acta 2, 195-208.

Keeling, C.D., Whorf, T.P., Wahlen, M. and v. d. Plicht, J., 1995. Interannual extremes in the rate of atmospheric carbon dioxide since 1980. Nature 381, 666-670.

Kemle-von Mücke, S., 1994. Oberflächenwasserstruktur und - zirkulation des Südostatlantiks im Spätquartär. Berichte aus dem Fachbereich Geowissenschaften, 55. Universität Bremen.

Kim, S.-T. and O`Neil, J.R., 1997. Equilibrium and non-equilibrium oxygen isotope effects in synthetic carbonates. Geochimica et Cosmochimica Acta 61, 3461-3475.

Knorr, G. and Lohmann, G., 2003. Southern Ocean origin for the resumption of Atlantic thermohaline circulation during deglaciation. Nature 424, 532-536.

Kroon, D. and Ganssen, G., 1988. The planktic $d^{13}C$ record, upwelling and climate. In: Brummer, G.J.A. and Kroon, D. (Eds.), Planktonic foraminifera as Tracers of Ocean-Climate History. Free University Press, Amsterdam, pp. 335-346.

Kroon, D. and Ganssen, G., 1989. Northern Indian Ocean upwelling cells and the stable isotope composition of living planktonic foraminifers. Deep Sea Research 36, 1219-1236.

Lea, D.W., Bijma, J., Spero, H.J. and Archer, D., 1999. Implications of a carbonate ion effect on shell carbon and oxygen isotopes for glacial ocean conditions. In: Fischer, G. and Wefer, G. (Eds.), Use of proxies in paleoceanography: Examples from the South Atlantic. Springer, Berlin, pp. 513-522.

Lohmann, G.P., 1995. A model for variation in the chemistry of planktonic foraminifera due to secondary calcification and selective dissolution. Paleoceanography 10, 445-457.

Lynch-Stieglitz, J., Stocker, T.F., Broecker, W.S. and Fairbanks, R.G., 1995. The influence of air-sea gas exchange on the isotopic composition of oceanic carbon: observations and modelling. Global Biogeochemical Cycles 9, 653-665.

McConnaughey, T., 1989. ^{13}C and ^{18}O isotopic disequilibrium in biological carbonates: II. In vitro simulation of kinetic isotope effects. Geochimica et Cosmochimica Acta 53, 163-171.

McConnaughey, T., 1994. Calcification, photosynthesis, and global carbon cycle. Bull. de l'Institut Oceanographique, Monaco No special 13, 137-161.

McConnaughey, T., Burdett, J., Whelan, J.F. and Paull, C.K., 1997. Carbon isotopes in biological carbonates: Respiration and photosynthesis. Geochim. Cosmochim. Acta 61, 611-622.

McCrea, 1950. On the isotopic chemistry of carbonates and a paleotemperature scale. The Journal of Chemical Physics 18, 849-857.

Miller, K.G., Fairbanks, R.G. and Mountain, G.S., 1987. Tertiary oxygen isotope synthesis, sea level history, and continental margin erosion. Paleoceanography 2, 1-19.

Mook, W.G., Bommerson, J.C. and Staverman, W.H., 1974. Carbon isotope fractionation between dissolved bicarbonate and gaseous carbon dioxide. Earth and Planetary Science Letters 22, 169-176.

Mortlock, R.A., Charles, C.D., Froelich, P.N., Zibello, M.A., Salzmann, J., Hayes, J.D. and Burckle, L.H., 1991. Evidence for lower productivity in the Antarctic Ocean during the last glaciation. Nature 351, 220-223.

Mortyn, G.P. and Charles, C.D., 2003. Planktonic foraminiferal depth habitat and delta ^{18}O calibrations: Plankton tow results from the Atlantic sector of the Southern Ocean. Paleoceanography 18.

Mulitza, S., Arz, H., Kemle-von Mücke, S., Moos, C., Niebler, H.S., Pätzold, J. and Segl, M., 1999. The South Atlantic carbon isotope record of planktic foraminifera. In: Fischer, G. and Wefer, G. (Eds.), Use of proxies in paleoceanography: Examples from the South Atlantic. Springer, Berlin, pp. 427-445.

Mulitza, S., Boltovskoy, D., Donner, B., Meggers, H., Paul, A. and Wefer, G., 2003. Temperature: delta 18O relationships of planktonic foraminifera collected from surface waters. Palaeogeogr., Palaeoclim., Palaeoecol. 202, 143-152.

Mulitza, S., Dürkoop, A., Hale, W., Wefer, G. and Niebler, H.S., 1997. Planktonic foraminifera as recorders of past surface-water stratification. Geology 25(4), 335-338.

Murray, J., 1897a. On the distribution of pelagic foraminifera at the surface and on the floor of the ocean. Nat. Sci. 11, 17-27.

Murray, J., 1897b. On the distribution of the pelagic Foraminifera at the surface and on the floor of the ocean. Nat. Sci. (Ecology) 11, 17-27.

Orr, W.N., 1967. Secondary calcification in the foraminiferal genus *Globorotalia*. Science 157, 1554-1555.

Ortiz, J.D., Mix, A.C., Rugh, W., Watkins, J.M. and Collier, R.W., 1996. Deep-dwelling planktonic foraminifera of the northeastern Pacific Ocean reveal environmental control of oxygen and carbon isotope disequilibria. Geochim. Cosmochim. Acta 60(22), 4509-4523.

Ottens, J.J., 1992. Planktic Foraminifera as indicators of ocean environments in the Northeast Atlantic. Ph.D.-thesis, 189 pp.

Parker, F.L., 1960. Living planktonic foraminifera from the equatorial and southeast Pacific: Tohoku Univ. Sci. Repts., Ser. 2 (Geol.) Spec., v. 4,. 71-82.

Peeters, F.J.C., 2000. The distribution and stable isotope composition of living planktic foraminifera in relation to seasonal changes in the Arabian Sea. Ph.D. Thesis. Free University, Amsterdam, The Netherlands, 184 pp.

Peeters, F.J.C., Acheson, R., Brummer, G.J.A., de Ruijter, W.P.M., Schneider, R., Ganssen, G., Ufkes, E. and Kroon, D., 2004. Vigorous exchange between the Indian and Atlantic oceans at the end of the past five glacial periods. Nature, 661-665.

Peeters, F.J.C., Brummer, G.-J. and Ganssen, G., 2002. The effect of upwelling on the distribution and stable isotope composition of *Globigerina bulloides* and *Globigerinoides ruber* (planktic foraminifera) in modern surface waters of the NW Arabian Sea. Global and Planetary Change 34, 269-291.

Peeters, F.J.C. and Brummer, G.J.A., 2002. The seasonal and vertical distribution of living planktic foraminifera in the NW Arabian Sea. In: Clift, P.D., Kroon, D., Gaedicke, C. and Craig, J. (Eds.), The Tectonic and Climatic Evolution of the Arabian Sea Region. Geological Society, London, pp. 463-497.

Ravelo, A.C. and Fairbanks, R.G., 1995. Carbon isotopic fractionation in multiple species of planktonic foraminifera from core-tops in the tropical Atlantic. Journal of Foraminiferal Research 25, 53-74.

Romanek, C.S., Grossmann, E.L. and Morse, J.W., 1992. Carbon isotope fractionation in synthetic aragonite and calcite: effects of temperature and precipitation rate. Geochim. Cosmochim. Acta 56, 419-430.

Russell, A.D. and Spero, H.J., 2000. Field examination of the oceanic carbonate ion effect on stable isotopes in planktonic foraminifera. Paleoceanography 15, 43-52.

Sanyal, A., Hemming, N.G., Hanson, G.N. and Broecker, W.S., 1995. Evidence for a higher pH in the glacial ocean from boron isotopes in foraminifera. Nature 373, 234-236.

Sautter, L.R. and Thunell, R.C., 1991a. Planktonic foraminiferal response to upwelling and seasonal hydrographic conditions: Sediment trap results from San Pedro Basin, Southern California Bight. Journal of Foraminiferal Research 21(4), 347-363.

Shackleton, N.J., 1977. ^{13}C in *Uvigerina*: Tropical rainforest history and the equatorial Pacific carbonate dissolution cycles. In: Anderson, N. and Malahof, A. (Eds.), Fate of Fossil Fuel CO_2 in the Oceans. Plenum, New York, pp. 401-427.

Shackleton, N.J. and Opdyke, N.D., 1973. Oxygen isotope and paleomagnetic stratigraphy of equatorial Pacific core V 28-238: Oxygen isotope temperatures and ice volume on a 10^5 year scale. Quaternary Research 3, 39-55.

Shackleton, N.J. and Vincent, E., 1978. Oxygen and carbon isotope studies in recent foraminifera from the southwest Indian Ocean. Mar. Micropalentol. 19, 275-285.

Siegenthaler, U. and Münnich, K.O., 1981. $^{13}C/^{12}C$ fractionation during CO_2 transfer from air to sea. In: Bolin, B. (Editor), Carbon Cycle Modelling, SCOPE. J. Wiley & Sons, Chichester, pp. 249-258.

Spero, H.J., Bijma, J., Lea, D.W. and Bemis, B., 1997. Effect of seawater carbonate concentration on foraminiferal carbon and oxygen isotopes. Nature 390, 497-500.

Spero, H.J. and DeNiro, M.J., 1987. The influence of symbiont photosynthesis on the $d^{18}O$ and $d^{13}C$ values of planktonic foraminiferal shell calcite. Symbiosis 4, 218-228.

Spero, H.J. and Lea, D.W., 1993b. Intraspecific stable isotope variability in the planktic foraminifera *Globigerinoides sacculifer*: Results from laboratory experiments. Mar. Micropalentol. 22, 221-234.

Spero, H.J. and Lea, D.W., 1996. Experimental determination of stable isotope variability in *Globigerina bulloides*: Implications for paleoceanographic reconstruction. Mar. Micropalentol. 28, 231-246.

Spindler, M., Hembleben, C., Bayer, U., Bé, A.W.H. and Anderson, D.M., 1979. Lunar periodicity of reproduction in the planktonic foraminifer *Hastigerina pelagica*. Mar. Eco., Prog. Ser. 1, 61-64.

Thiede, J., 1975. Distribution of foraminifera in surface waters of a coastal upwelling area. Nature 253, 712-714.

Thunell, R. and Sautter, L.R., 1992. Planktonic foraminiferal faunal and stable isotopic indices of upwelling: a sediment trap study in the San Pedro basin, Southern California Bight. In: Summerhayes, C.P., Prell, W.L. and Emeis, K.C. (Eds.), Upwelling systems: Evolution since the early Miocene. Geological Society Special Publication, pp. 77-91.

Thunell, R.C. and Reynolds, L.A., 1984. Sedimentation of planktonic foraminifera: Seasonal changes in species flux in the Panama Basin. Micropaleontology 30, 243-262.

Tolderlund, D.S. and Bé, A.W.H., 1971. Seasonal distribution of planktonic foraminifera in the western North Atlantic. Micropaleontology 17, 297-329.

Vincent, E. and Berger, W.H., 1981. Planktonic Foraminifera and their use in paleoceanography. In: Emiliani, C. (Editor), *The Oceanic Lithosphere*. Wiley, New York.

Wefer, G. and Berger, W.H., 1991. Isotope paleontology: growth and composition of extant calcareous species. Marine Geology 100, 207-248.

Williams, D.F., Bé, A.W.H. and Fairbanks, R.G., 1981. Seasonal stable isotope variations in living planktonic foraminifera from Bermuda plankton tows. Paleogeor. Paleoclim. Paleoecol. 33, 71-102.

Wolf-Gladrow, D.A., Bijma, J. and Zeebe, R.E., 1999. Model simulation on the carbonate chemistry in the microenvironment of symbiont bearing foraminifera. Marine Chemistry 64, 181-198.

Zeebe, R.E., 1999. An explanation of the effect of seawater carbonate concentration on foraminiferal oxygen isotopes. Geochimica et Cosmochimica Acta 63, 2001-2007.

Zeebe, R.E. and Wolf-Gladrow, D.A., 2001. CO_2 In Seawater: Equilibrium, Kinetics, Isotopes. Elsevier Sciences B.V., Amsterdam, The Netherlands, 346 pp.

CHAPTER 2*

SEASONAL DISTRIBUTION AND STABLE OXYGEN ISOTOPE COMPOSITION OF PLANKTIC FORAMINIFERA OFF NW AFRICA (29°N)

Iris Wilke, Helge Meggers, Torsten Bickert

Fachbereich Geowissenschaften/MARUM, Universität Bremen, Leobenerstrasse, 28359 Bremen, Germany

*This chapter is submitted for publication
to *Deep Sea Research*

2.1 Abstract

Planktic foraminiferal species from plankton tows, sediment traps and surface sediments at three stations along a productivity gradient off NW Africa at 29°N were investigated in order to unravel their seasonal and vertical distribution and their oxygen isotopic composition in relation to seasonal hydrographic conditions north of the Canary Islands. Two main production periods could be distinguished regarding seasonal surface water properties: a deeply stratified ocean during winter mixing associated with a phytoplankton bloom visible at all three stations, and a coastal upwelling situation influencing the nearshore station mainly during summer and fall.

Absolute abundances in the upper water column and shell fluxes show a distinctive response to seasonal hydrographic conditions. Highest concentrations and flux rates were observed during the winter-bloom at all three stations. *Turborotalita humilis*, *Globorotalia truncatulinoides* and *Pulleniatina obliquiloculata* show highest affinity to winter mixed layer conditions. *Globigerina bulloides* exhibits maximal standing stock and fluxes in summer/fall at the nearshore station presumably in response to coastal upwelling. In contrast, *Globigerinoides ruber* white and pink behave in general more like perennial species in ocean surface water, with maxima during winter and fall, respectively. While the depth of maximal concentrations of non-symbiotic species is clearly associated with the chlorophyll maximum, the symbiotic species are not inevitably coupled to the chlorophyll maximum but seem to be more connected to the photic zone, and especially for *G. ruber* pink to warmer temperatures.

The $\delta^{18}O$ values of foraminiferal shells from plankton tows, sediment traps and surface sediments show a general increase in $\delta^{18}O_{shell}$ with increasing depth in the water column. Thereby the deviation from the predicted $\delta^{18}O_{calcite}$ profile becomes larger with increasing depth, which clearly indicates integrated shell growth over a certain depth range. This further suggest that calcite precipitation is not restricted to the depth range where highest standing stock values occurs.

In the surface mixed layer we observe species-specific deviations from the predicted $\delta^{18}O_{calcite}$ profile, which are strongly size-dependent. Since planktic foraminifer have the capability to self-control the *p*H in their vicinity during main life processes, we suppose differences in the carbonate chemistry between the experiment and the foraminiferal microenvironment. While larger non-symbiotic species show in general higher $\delta^{18}O$ values compared to smaller specimens, symbiotic species show a reversed pattern. For instance, smaller shells of symbiotic species *G. ruber* white were unexpectedly enriched in $\delta^{18}O$ compared to larger shells, which is most likely due to a higher symbiont photosynthetic activity of larger species, due to a higher symbiont density, and its integrated effect on the *p*H of the foraminiferal microenvironment. Since the seasonal variations of seawater $[CO_3^{2-}]$ are small, seasonal variations in the oxygen isotope ratio of *G. ruber* white and pink seems to be a direct function of surface water temperature and light level.

2.2 Introduction

The relationship between planktic foraminifer shell stable oxygen isotopes and surface water hydrography is an important tool for understanding and interpreting environmental signals preserved within the sedimentary record. Unfortunately, planktic foraminifera do not precipitate their calcite in equilibrium with the ambient sea water. The deviations in the oxygen isotope content is attributed to several biological and chemical processes that may cause a disequilibrium (e.g. ontogeny/metabolism, photosynthesis, $[CO_3^{2-}]$ and/or *p*H of the seawater) (Fairbanks et al., 1982; Spero et al., 1997; Mulitza et al., 1999; Zeebe, 1999; Peeters et al., 2002). It has been shown that small shells are depleted in ^{18}O compared to larger specimens due to an ontogenetic effect (Spero and Lea, 1996). Further, it is evident that the oxygen isotope fractionation between water and the dissolved carbonate species $S = [H_2CO_3] + [HCO_3^-] + [CO_3^{2-}]$ decreases with increasing seawater *p*H (and thus $[CO_3^{2-}]$), e.g. with a slope of shell $\delta^{18}O$ vs. seawater $[CO_3^{2-}]$ of –0.0022‰(µmol $kg^{-1})^{-1}$ for *Globigerinoides ruber* (Bijma et al., 1998). Because the slopes found for different species are species-specific, additional mechanism such as an internal pool or kinetic isotope effects are assumed (Zeebe, 1999). Model results show that foraminifera species are able to control the *p*H of their microenvironment during main life processes, such as calcification and photosynthesis (Wolf-Gladrow et al., 1999). Since most of the existing knowledge is based on laboratory culture experiments, studies under natural conditions are necessary.

In this field study we present results on the seasonal and vertical distribution and stable oxygen isotopic composition of seven planktic foraminifer species. Samples were collected with plankton tows, sediment traps and the surface sediment at three stations along a transect from the eutrophic, upwelling influenced locality (EBC = Eastern Boundary Current) to the oligothrophic area of the North Atlantic gyre (ESTOC = European Station for Time-series in the Ocean, Canary Islands and LP = La Palma) (Fig. 2.1).

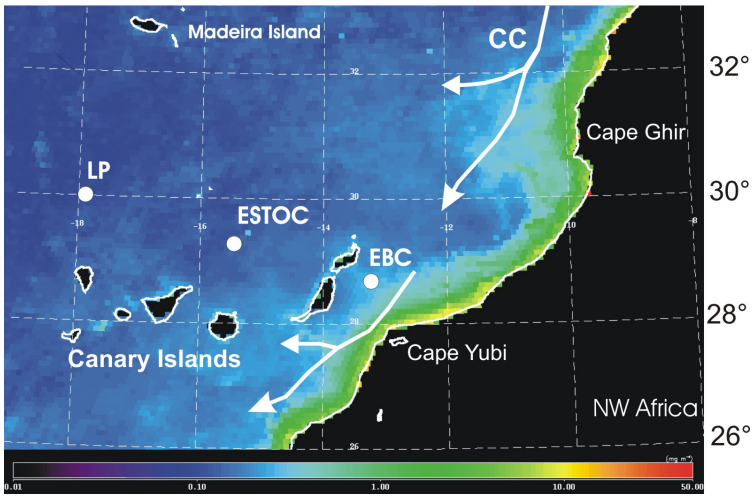

Figure 2.1. Map of annual mean chlorophyll concentration (mg m^{-3}) off NW Africa in 1997 as observed by SeaWIFS (NASA/ Goddard Space Flight Center). Dots show position of stations (EBC, ESTOC and LP) where plankton tows, sediment traps and surface sediment samples were collected. CC=Canary Current, an essential part of the Eastern Boundary Current System.

Main objectives of the present study are 1) to compare the seasonal fluxes and species distribution in surface waters with the seasonal hydrographical changes and 2) to investigate the oxygen isotopic composition in relation to species distribution and abundances, shell sizes and seasonality to unravel mechanisms responsible for the observed deviations between the oxygen isotope composition of the shells ($\delta^{18}O_{shell}$) and predicted equilibrium values ($\delta^{18}O_{calcite}$).

2.3 Hydrography

The hydrographic situation of the investigated region is controlled by the subtropical gyre recirculation system and coastal upwelling processes along the northwest African margin. The Azores Current which originates from a southern branch of the Gulf Stream passes just south of the Azores and splits into a northern and a southern branch at 35°N. The latter joins the Canary Current, which moves southeastward towards the Canary Islands as part of the eastern boundary current system along the African coast (Stramma and Siedler, 1988; Mittelstaedt, 1991) (Fig. 2.1). The strength and persistence of upwelling is coupled to the trade winds, which are subject to seasonal variations of the position of the Inter Tropical Convergence Zone (ITCZ). The main upwelling occurs during summer, and an associated filament situation occurs during fall north of 25°N (van Camp et al., 1991; Barton et al., 1998). Upwelling is usually restricted to the shelf area and the upper slope region in a distance of 50-70 km (Mittelstaedt, 1991; Nykjaer and van Camp, 1994). The upwelling water mass is the

North Atlantic Central Water (NACW), which usually extends between 100 and 600 m water depth and has its origin at 40°N at the Subtropical Convergence Zone (STCZ) (Mittelstaedt, 1972; Tomczak and Hughes, 1980).

An important feature of coastal upwelling in the Canary Islands region is the creation of filament structures at specific coastal positions such as Cape Ghir and Cape Yubi mainly during summer and fall (Nykjaer and van Camp, 1994; Barton et al., 1998; Davenport et al., 2002). Thus, the front between the eutrophic and oligotrophic waters itself depends on the filament production, which are injected into the open ocean due to turbulent flow. According to Sea-WiFS derived chlorophyll concentrations (Davenport et al. 2002) and to primary productivity data calculated following Antoine and Morel (1996) it can be recognized that LP and ESTOC lie well outside of the upwelling and filament-influenced area. In contrast, EBC lies outside the primary upwelling zone but is periodically affected by Cape Yubi filaments (Neuer et al., 2002).

2.4 Material and Methods

2.4.1 Plankton samples

Sample material was obtained during several research cruises between 1995 and 1998 as part of the CANIGO (Canary Islands Azores Gibraltar Observatory) project. For faunal and stable isotope investigations, planktic foraminifer samples from all seasons were collected with a Multiple Opening-Closing Net (multinet). Plankton samples were recovered in 1995 (fall season) during RV Poseidon cruise POS212/1 at five depth intervals (0-50, 50-150, 150-300, 300-500, and 500-800 m). Winter samples were collected during RV Victor Hensen VH96/2 in 1996 (0-25, 25-50, 50-150,150-300, and 300-440 m). Additionally, material was sampled in 1998 during RV Poseidon cruise POS 237 to cover the spring season, and during RV Meteor M42/1b for the summer period (0-25, 25-50,50-150, 150-300, and 300-500 m), respectively. All samples were conserved with a saturated $HgCl_2$ solution. The foraminifera were picked out by pipette and counted (>125 μm) from wet samples. Additionally, sediment-trap samples were collected using cone-shaped particle traps of the Kiel-type (Aquatec) with 20 cups and a collection area of 0.5 m^2. The sediment traps were moored at 13°09.34'W/ 28°24.49'N (EBC 2-1 (700 m depth)), at 15°27.00'W/29°11.00'N (ESTOC CI7 (500 and 3000 m)) and at 17°57.26'W/ 29°45.73'N (LP 1 (900 and 3700 m)) from January to September in 1997, with bi-weekly sample intervals (see Table 2.1a for details).

Table 2.1. General information of sampling location (EBC, ESTOC and LP), a) sediment trap samples and b) surface sediment samples (Meggers et al. 2002, Wefer et al. 1997).

a)

Station	Longitude (W)	Latitude (N)	Water depth (m)	Trap depth (m)	Collection period	Distance from coast (m)
EBC	13°09.34	28°42.49	996	700	02/01/97 – 15/09/97	180
ESTOC	15°27.00	29°11.00	3610	500 3000	23/12/96 – 15/09/96	387
LP	17°57.26	29°45.73	4327	900 3700	06/01/97 – 15/09/97	630

b)

Station	GeoB-Nr.	Longitude (W)	Latitude (N)	Water depth (m)	Device	Distance from coast (m)
EBC (M37/1)	4234-1	13°13.6	28°53.4	1360	multicore	180
ESTOC (M38/1)	4301-1	15°30.0	29°09.0	3614	multicore	387
LP (M42/4)	5529-1	17°41.9	29°41.4	4166	multicore	630

Surface-sediment samples (0-1 cm) were analyzed from multicorers sampled during RV Meteor cruises M37/1 (EBC), 38/1 (ESTOC), and during 42/2 (LP). The samples were freeze-dried, wet-sieved over a 63-µm mesh, and split into smaller subfractions. The >125-µm fraction was split into aliquots of 300-500 specimen. All species were identified using the taxonomy of Bé (1977) and Hemleben et al. (1989).

Oxygen isotope ratios of planktic foraminifera were measured using a Finnigan Mat 252 mass spectrometer equipped with an automatic carbonate preparation device (University Bremen). Depending on species and sizes, 3 to 50 specimens were picked for stable isotope analysis. Isotope composition is given in the usual δ-notation and is calibrated to Vienna Pee Dee Belemnite (V-PDB) standard. Precision based on replicates of an internal standard (Solnhofen limestone) was better than 0.07‰ for $\delta^{18}O$.

2.4.2 Water samples

For a direct comparison of the stable isotope values between water and calcareous plankton, water samples were collected using a rosette equipped with 18 water samplers (each 10 liters volume). Water from each sampler was filled into glass bottles. Oxygen isotope measurements of the water samples were carried out at the University of Bremen. We used a fully automatic CO_2/H_2O equilibration device. The equilibrated CO_2 gas was transferred to an on-line-connected Finnigan MAT Delta-Plus mass spectrometer. The external reproducibility was better than 0.07‰ for $\delta^{18}O$.

Each station was accompanied by a CTD cast providing information on the vertical structure of the water column including temperature, salinity and fluorescence and chlorophyll a (see Appendix A for detailed information).

2.4.3 Paleotemperature and oxygen isotope equilibrium calculations

The oxygen isotope equilibrium calcite values ($\delta^{18}O_{calcite}$), are calculated using the actual oxygen isotope composition of seawater ($\delta^{18}O_w$) and the measured *in situ* temperature (T). We chose the equation of Kim and O`Neil (1997) because it is based on inorganic calcite precipitation without any species-specific biological influence. They found out that the oxygen isotope equilibrium value for inorganic (synthetic) calcium carbonate precipitated at low temperatures (10-40°C) follows the relationship:

$$T = 16.1\text{-}4.64\ (\delta^{18}O_{calcite}\text{-}\delta^{18}O_w) + 0.09\ (\delta^{18}O_{calcite}\text{-}\delta^{18}O_w)^2 \qquad (1)$$

The conversion factor between $\delta^{18}O_w$ from the V-SMOW to the V-PDB scale is after Hut (1987):

$$\delta^{18}O_w\ (VPDB) = 0.99973*\delta^{18}O_w\ (V\text{-}SMOW) - 0.27‰ \qquad (2).$$

2.5 Results

2.5.1 Seasonal variability of surface water conditions

Figure 2.2 describes the variability of temperature, salinity, chlorophyll a and stable isotope composition ($\delta^{18}O_w$) as a function of depth during four different seasons (Table 2.3). All three stations are characterized by deep seasonal mixing during winter. The time of deep

mixing coincides with the highest surface chlorophyll a concentrations observed during the year. During summer/fall the three station differ significantly. For instance water temperatures show a decrease with increasing distance from the coast beginning in spring. This difference becomes more pronounced in summer and fall due to the influence of nearby coastal upwelling. In general, all parameters mirror the seasonal changes of the upper water column by reflecting a deeply stratified ocean during winter as a consequence of deep mixing and a less stratified ocean during summer and fall (Fig. 2.2). The spring season can be regarded as a state of transition between the winter-bloom and the upwelling situation in summer/fall.

2.5.2 Seasonal distribution pattern of planktic foraminifera

Plankton-tows of all seasons and sediment traps over a 9-months period were used to document planktic foraminifer species seasonal distribution along a transect in the subtropical region of NW Africa. A list of all species identified in the plankton tows, upper sediment traps and surface sediment samples is published by Abrantes et al., 2002. Here, we will concentrate on the seasonal distribution pattern of the following species: *Globigerinoides ruber* white, *Globigerinoides ruber* pink, and *Turborotalia humilis* (all symbiotic), and *Globigerina bulloides, Pulleniatina obliquiloculata* and *Globorotalia truncatulinoides* (all non-symbiotic). These species were chosen because they cover different seasons and depth habitats and occurred in adequate numbers for isotope measurements.

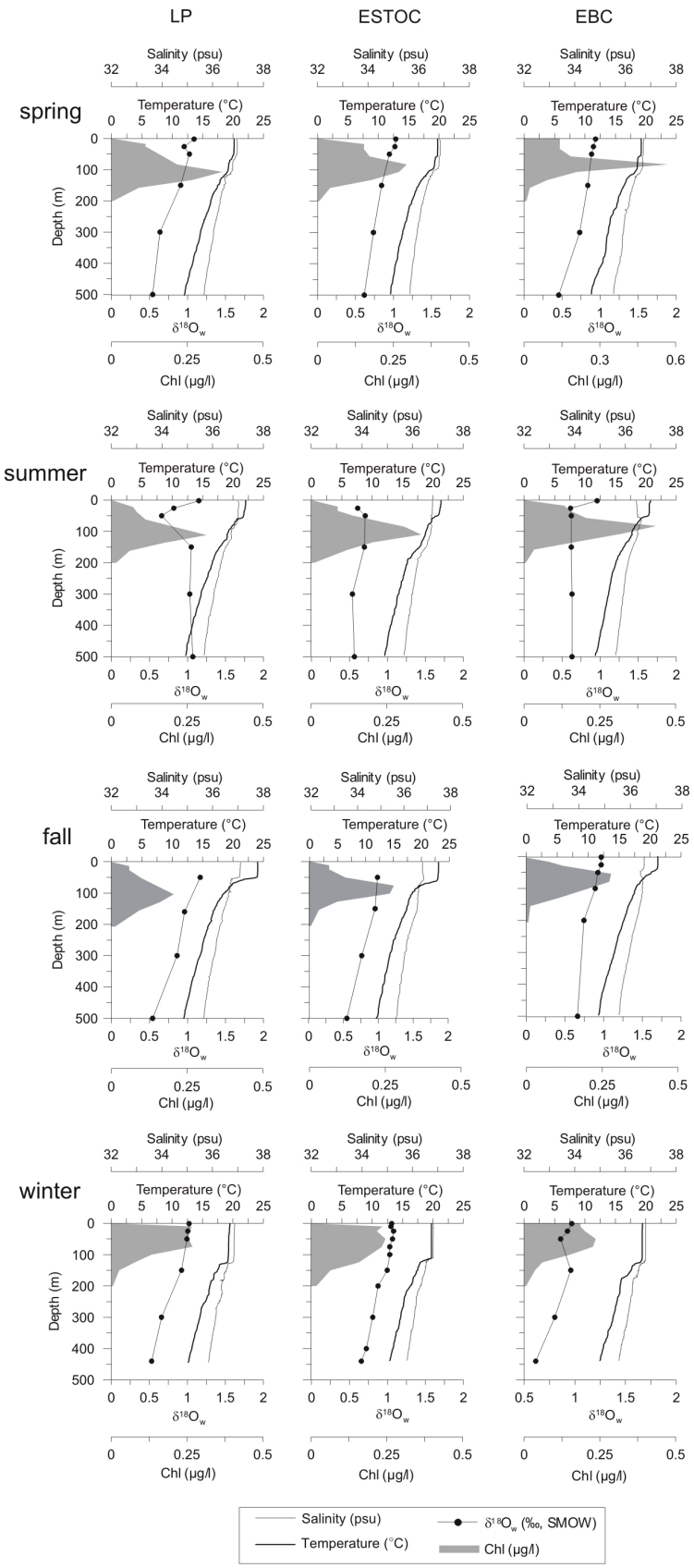

Figure 2.2. Temperature (solid line), salinity (thin line), chlorophyll a (gray shaded area) and stable oxygen isotopic composition (filled dots) in the upper water column at stations EBC, ESTOC and LP during four different seasons.

2.5.2.1 Plankton tows

Figure 2.3 gives an overview of the average seasonal depth distribution of planktic foraminifers in the upper water column at the nearshore site EBC and the two offshore sites ESTOC and LP. Counts are given in absolute abundance (ind. m^{-3}) and in relative abundance (%) of total living planktic foraminifera assemblage in the >125 μm size class.

During winter, highest relative abundance of living planktic foraminifera are mainly found in the upper mixed layer 150 m (upper three sampling intervals) at all three stations. In contrast, maximum concentrations during spring were related to deeper waters (50-300 m). While during winter and spring the three stations show a similar pattern with respect to the vertical distribution of planktic foraminifera, differences between the nearshore site and the two offshore sites are evident during summer and fall. Nearshore station EBC shows two maxima during summer, one between 0-25 m and a second between 50-150 m, while in fall a single maximum exists between 25-50 m. In fall the distribution at the two offshore sites show highest concentrations in the upper 25 m. During summer, planktic foraminifera are most abundant not at the sea surface but slightly deeper between 25-50 m at ESTOC and between 50-150 m at LP.

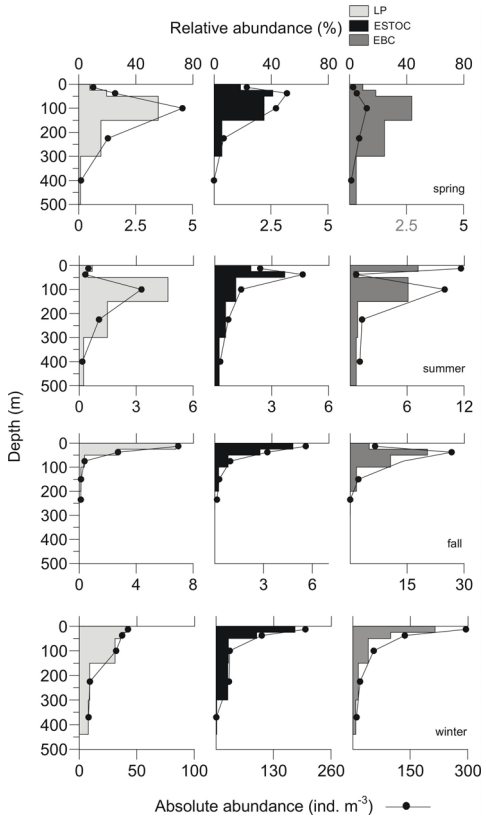

Figure 2.3. Absolute abundance (ind. m^{-3}; shaded bars) and relative abundance (%; black dots) of living planktic foraminifera in the upper water column at stations EBC, ESTOC, and LP during four different seasons. Note different scaling for absolute abundance (ind. m^{-3}).

Regarding the absolute abundance of living foraminifera in the >125 µm size class, highest concentrations occur in general during winter. EBC shows maximum concentrations of ~520 ind./m^3 in winter, while lowest numbers of species occurred in spring at EBC with ~2 ind./m^3. In general, the absolute abundance is decreasing with increasing distance from the coast.

Figure 2.4 shows the seasonal vertical distribution of the six selected species in the upper water column. A distinctive seasonal pattern is observable at all three stations. Each species shows a period of preferred production and a distinct depth interval where highest shell concentration occurs.

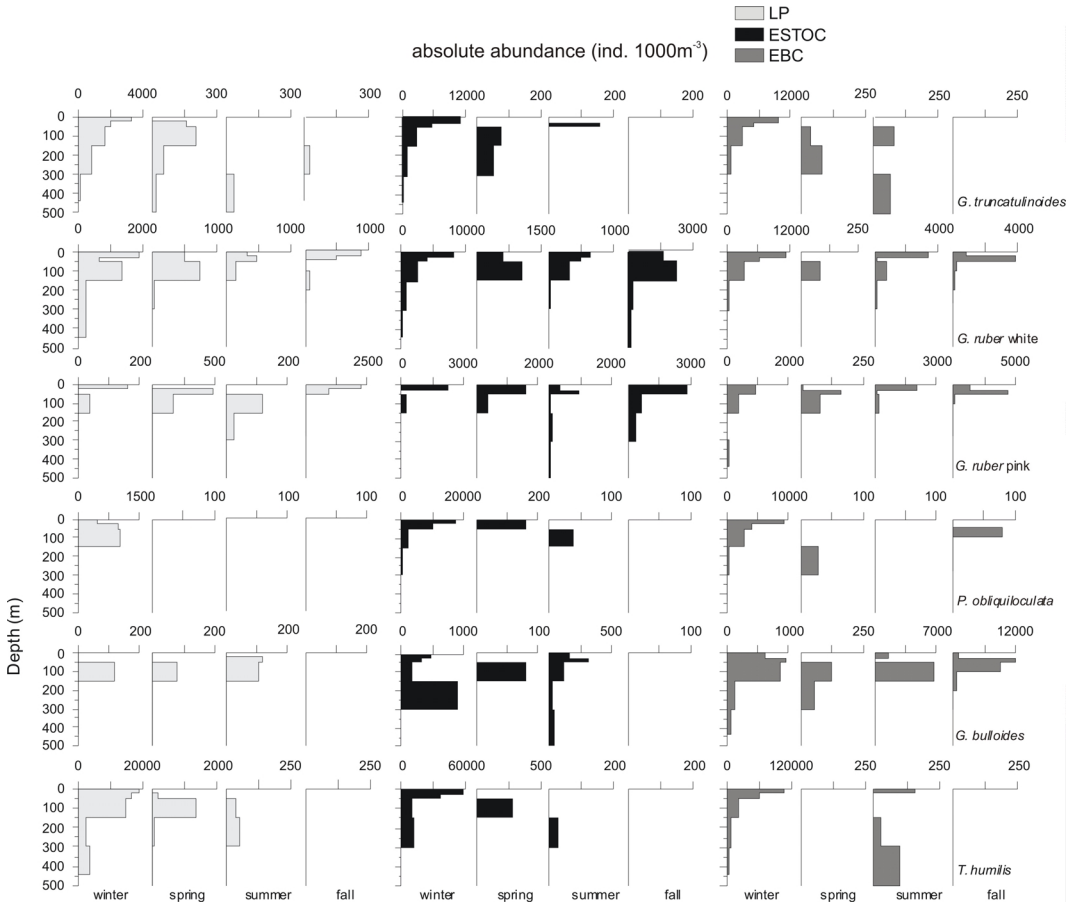

Figure 2.4. Absolute abundance (ind. 1000m^{-3}) of six selected species in the upper water column at stations EBC, ESTOC and LP. Note different scales.

The species *T. humilis* was the most abundant species in the upper mixed layer (0-115 m) during winter at all three sites (Fig. 2.4). Other species showing a similar abundance pattern were *P. obliquiloculata, G. truncatulinoides* and *G. ruber* white. Concentrations are usually decreasing with distance from the coast. During other seasons all species, except *G. ruber* white, were either totally absent or occur in lower numbers in deeper water depths. The

species *G. ruber* white behaves in general more as a perennial species in terms of absolute abundance at EBC as well as at ESTOC and LP.

The species *G. bulloides* is clearly dominant in summer (50–150 m) and fall (25-100 m), but does not play any significant role in the offshore region at ESTOC and LP at any time. Its shell concentration is two times higher in fall compared to summer. An additionally smaller peak in abundance of *G. bulloides* are related to the winter bloom. Another species showing its highest concentration during summer and fall is *G. ruber* pink. At all three stations it is most abundant in the upper 50 m in fall. Similar to the white variety *G. ruber* pink also occurs more or less year-round in the upper surface waters.

2.5.2.2 Total planktic foraminiferal flux

Comparing the three sites, EBC has the highest total planktic foraminiferal flux (>125 μm) considering the total record of upper traps (Fig. 2.5). The average flux at this site is 277 shells m^{-2} day^{-1}, decreasing to 166 and 121 shells m^{-2} day^{-1} at ESTOC and LP, respectively. In the upper sediment trap studies at EBC, ESTOC and LP, a total of 24 different species could be distinguished during the 9-months record (Abrantes et al., 2002). The total planktic foraminiferal shell flux >125 μm shows a bimodal distribution at EBC (750 m) with a clear maximum in winter and a second maximum beginning in late spring and continuing during summer (Fig. 2.5). Because the fall season was sampled insufficiently only, the fall maximum, which is obvious within the plankton tow samples, cannot be observed here. However, a better resolution of the sediment trap time series indicate a second maximum occurred in late spring. More offshore, only a single winter maximum occurs in the shallower traps at ESTOC and LP (Fig. 2.5). During the remaining year total shell flux was generally low at both stations.

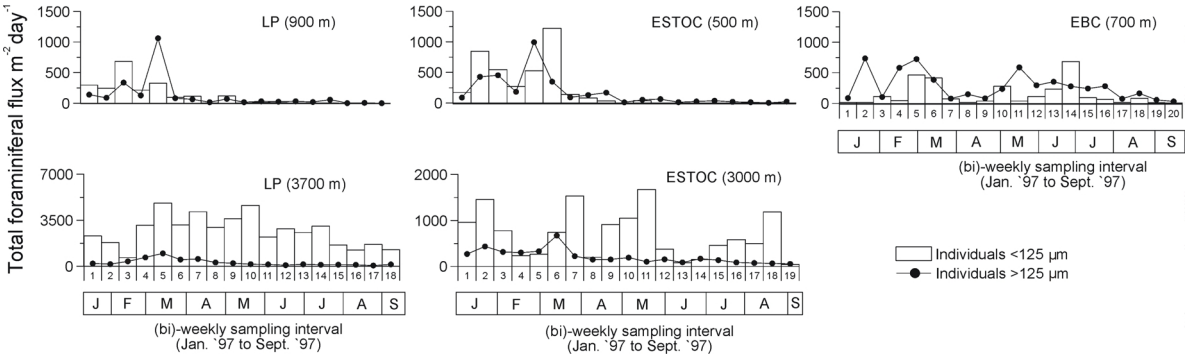

Figure 2.5. Total planktic foraminiferal flux m^{-2} day^{-1} (>125 μm open dots, <125 μm black dots) at EBC (700 m), ESTOC (500 and 3000 m) and LP (900 and 3000 m). The deeper traps at ESTOC and LP are characterized by a significant increase in shell flux in the size fraction <125 μm.

Regarding the deeper sediment traps at ESTOC and LP (Fig. 2.5), at both stations total planktic foraminifera shell flux increases towards deeper traps with average fluxes of 209 and 278 shells m^{-2} day^{-1} at ESTOC and LP, respectively. We also identified a considerable difference in the magnitude of total foraminiferal fluxes of species >125 μm and <125 μm between the upper and lower traps. While species flux <125 μm was similar to the larger fraction in the shallower traps, flux values of the smaller fraction were significantly higher in the deeper traps.

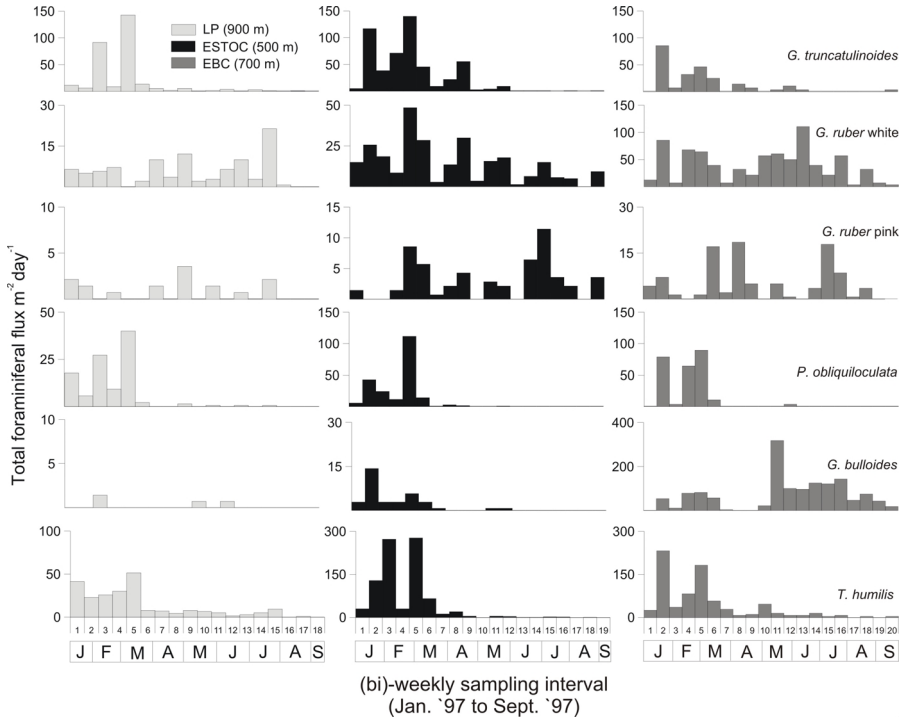

Figure 2.6a. Seasonal variations of planktic foraminiferal shell flux record (forams m^{-2} day^{-1}; >125 μm) of six selected species collected in the upper sediment traps at stations EBC (700 m), ESTOC (500 m) and LP (900 m) between January 1997 and September 1997.

Hence, the seasonal occurrence of species identified in the plankton tows were significant (Fig. 2.4) and are in general supported by flux results from bi-weekly sediment trap samples (Fig. 2.6a). The planktic foraminifera species *T. humilis*, *P. obliquiloculata* and *G. truncatulinoides* showed highest fluxes between January and March and therefore indicate that they favored ecological conditions during winter. Although our plankton tow observations suggest that *G. ruber* white is associated to winter- bloom conditions this is not supported by a distinct flux peak during winter at EBC and LP, whereby at ESTOC the seasonal standing stock in the upper water column and the flux of *G. ruber* white are in good agreement.

The upwelling maximum in late spring/early summer is associated with the highest abundance of *G. bulloides* (Fig. 2.6b). Also *G. ruber* pink produces peak shell fluxes during the

summer months. However, the flux record of *G. ruber* pink suggests that this species is as well as the white variety not restricted to only one season.

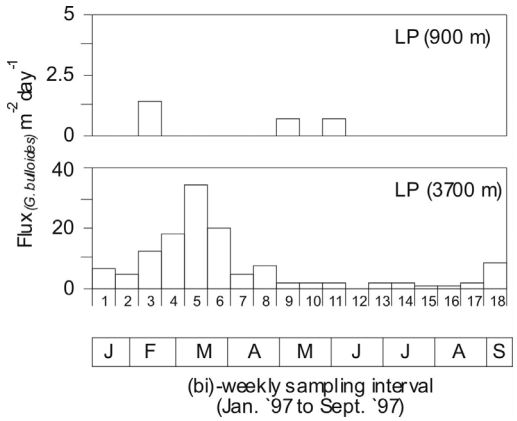

Figure 2.6b. Differences in the flux record of *G. bulloides* between the shallow (900 m) and deep (3700 m) sediment trap at the offshore station LP.

2.5.2.3 Surface sediment assemblage

According to ^{14}C analysis, the surface sediment samples (0-1 cm) represent an ^{14}C-age over about 500 years for the open ocean (ESTOC and LP) and 100 years or less in the upwelling-influenced area (EBC) (Freudenthal et al., 2001; Meggers et al., 2002). The sediment plankton assemblages reveal therefore a yearly and seasonally mix-signal. In total 31 different taxa of planktic foraminifera >125 μm could be identified in the surface sediment samples (Abrantes et al., 2002). Figure 2.7 shows the relative frequencies of the ten most abundant species in the surface sediments in comparison to the net results. The planktic foraminifera *G. bulloides* dominates the surface sediment assemblages in the >125 μm size class at EBC. Here, *G. bulloides* represents ~30 % of the total distribution. At ESTOC and LP, *G. ruber* white comprises ~25 % of the total assemblages and is therefore the most abundant species in the surface sediments at the two oligotrophic sites (Meggers et al., 2002).

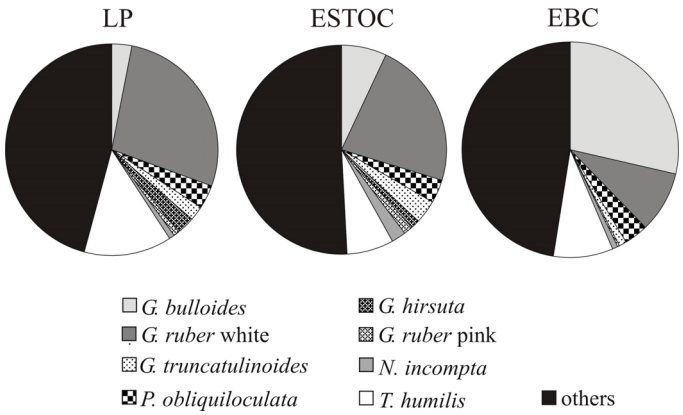

Figure 2.7. Relative abundance of planktic foraminifers in sediment surface samples at EBC, ESTOC and LP.

2.5.3 Stable oxygen isotopic composition

Predicted equilibrium $\delta^{18}O_{calcite}$ values calculated from measured water temperatures and $\delta^{18}O_w$-values after Kim and O`Neil (1997) are compared to $\delta^{18}O_{shell}$ values in the upper water column (Fig. 2.8a-b, Appendix B and C). Data from plankton tows, sediment traps and the surface sediments demonstrate the development of the $\delta^{18}O_{shell}$ signature in the water column during winter and fall. The calculated $\delta^{18}O_{calcite}$-profiles show a general increase with increasing water depth. Relative to the equilibrium calcite values, the $\delta^{18}O$ of the species in the upper mixed layer show species-specific deviation (Fig. 2.8a-b). Below the mixed layer the deviations from the equilibrium profile are usually negative for all species. For instance, deviations from $\delta^{18}O_{calcite}$ range from –0.68 to -0.82‰ for *G. bulloides* (250-355 μm) to –0.37 to +0.15‰ for *P. obliquiloculata* (280-380 μm) in the upper most tow interval.

Along the transect no significant differences in $\delta^{18}O$ shell calcite values can be observed between the nearshore site EBC and the two offshore sites ESTOC and LP. Different $\delta^{18}O_{shell}$ profiles in the water column can be observed for different species. For instance, *G. ruber* white (150-250 μm) shows an average deviation of -0.23‰ from the equilibrium profile in the mixed layer. Below the thermocline, *G. ruber* white shows a slight increase in its $\delta^{18}O$ value, and then remains constant until it reaches the sea floor. In contrast, *G. truncatulinoides* shows relatively small average deviation from equilibrium in the mixed layer s(-0.09‰) in the 280-440 μm size fraction. Below the mixed layer, $\delta^{18}O$ values are continuously getting heavier, mirroring the equilibrium profile down to a depth of ~500 m, with an average off-set of ~0.33 ‰ from the equilibrium profile.

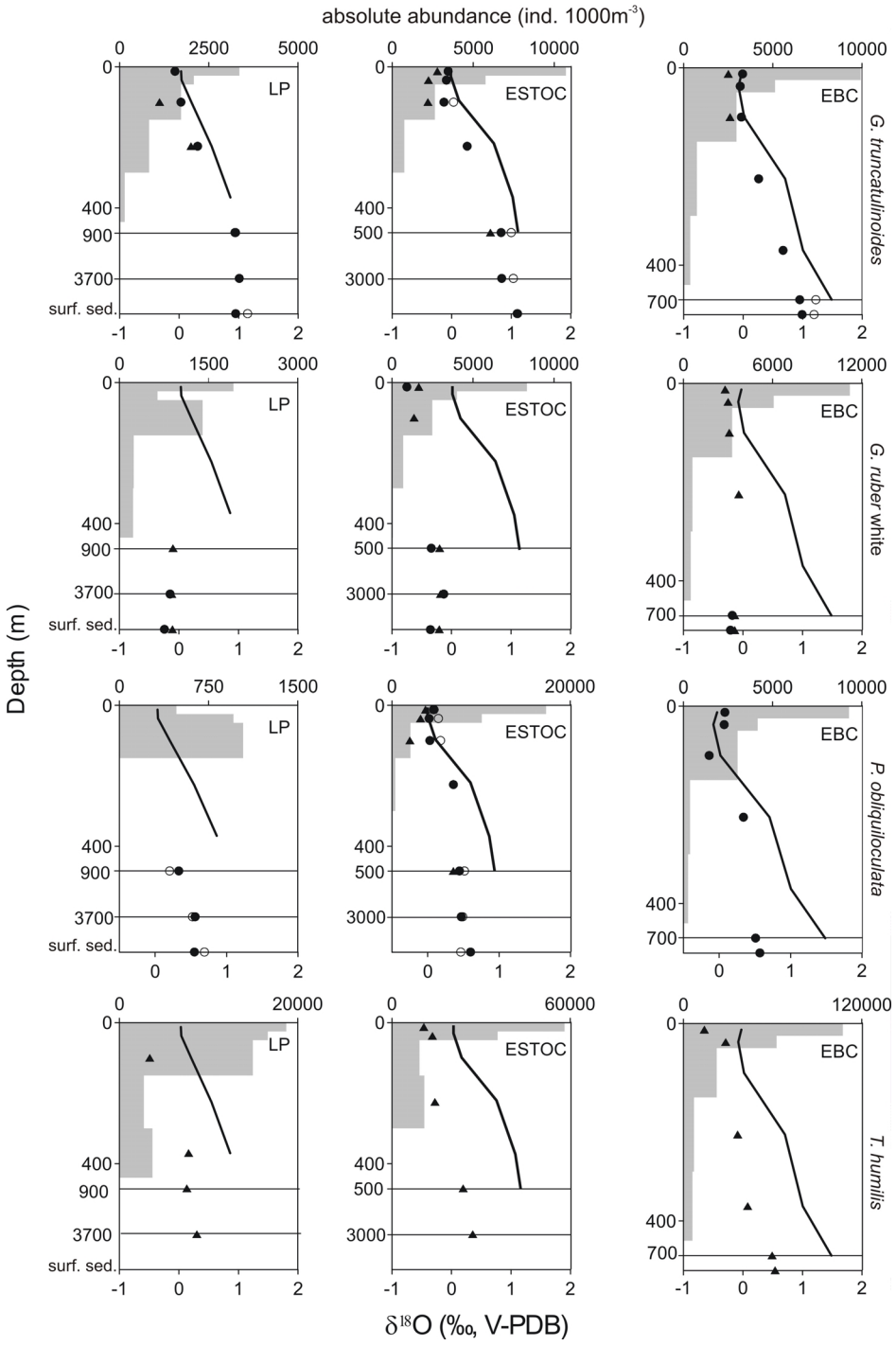

Figure 2.8a. The $\delta^{18}O$ composition of *G. truncatulinoides, G. ruber* white, *P. obliquiloculata* and *T. humilis* (from plankton tows, sediment traps and surface sediment samples) collected during winter at EBC, ESTOC and LP is shown. The predicted $\delta^{18}O_{calcite}$ shown were calculated from measured temperature and the oxygen isotope values of the seawater using the regression equation after Kim and O`Neil (1997). Gray bars indicate the species absolute abundance (ind. 1000 m^{-3}). Please see Figure 2.8b for legend.

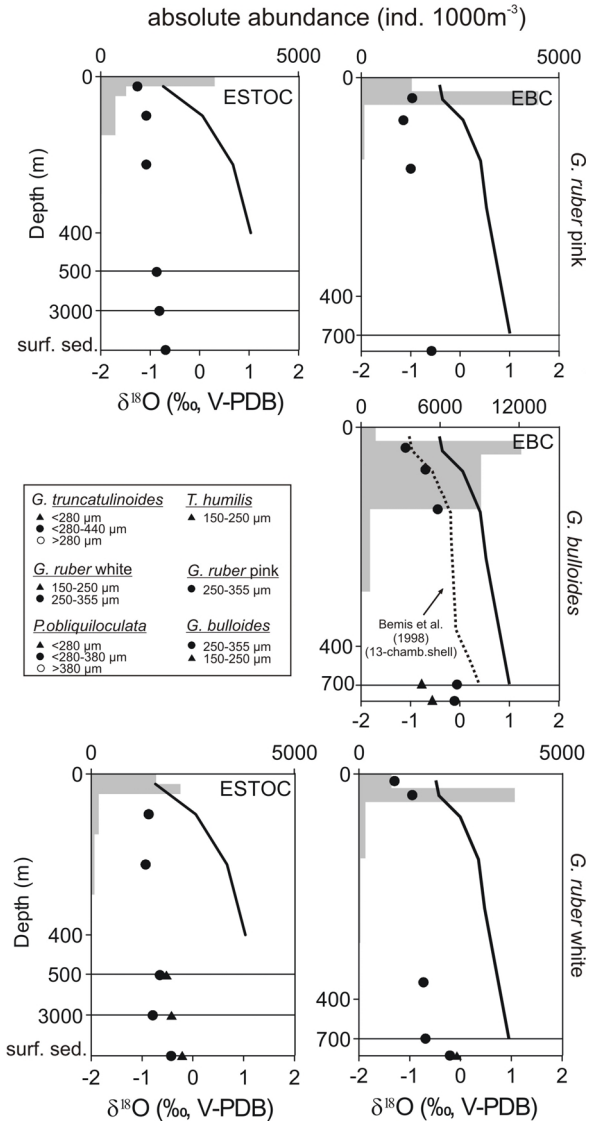

Figure 2.8b. The $\delta^{18}O$ composition of *G. ruber* white and pink and *G. bulloides* (from plankton tows, sediment traps and surface sediment samples) collected during fall at EBC, ESTOC and LP are shown. The predicted $\delta^{18}O_{calcite}$ shown were calculated from measured temperature and the oxygen isotope values of the seawater using the regression equation after Kim and O`Neil (1997). For comparison reason the predicted $\delta^{18}O_{calcite}$ profile calculated after the specific culture-derived regression for *G. bulloides* is shown (Bemis et al. 19998).

For symbiont-barren species *G. truncatulinoides* and *P. obliquiloculata* an increase of $\delta^{18}O$ with shell size is evident. *G. truncatulinoides* (280-440 µm) $\delta^{18}O$ values are on average 0.24‰ (+/-0.08‰) higher compared to those of smaller ones (<280 µm) and on average 0.16‰ lower than those of species >440 µm. $\delta^{18}O$ values of larger shells of *P. obliquiloculata* (>380 µm) are on average 0.10‰ (+/-0.07‰) higher compared to those of species in the size class (280-380 µm). These are again on average 0.25‰ higher than of smaller ones (<280 µm). Symbiont-bearing species *G. ruber* white shows an opposite trend. Larger shells (250-350 µm) of this species are slightly lower in $\delta^{18}O$ by ~0.20‰.

2.6 Discussion

2.6.1 Lateral advection

As has been shown in Figures 2.4 and 2.6a, a good correlation was found for the seasonal variation of planktic foraminifera species between our vertically integrated standing stock in the upper water column and the shell flux rates of the upper sediment traps. By contrast, the deeper traps at ESTOC (3000 m) and LP (3700 m) show drastically enhanced fluxes of planktic foraminifera <125 μm (Fig. 2.5) and unexpected high concentrations of the species *G. bulloides* in the 3700 m trap at LP (Fig. 2.6b). In the oligotrophic waters above (shallower sediment trap and plankton tows), the abundance of *G. bulloides* was low. The general seasonal flux pattern with distinct sedimentation events during winter is not transmitted in the smaller size fraction towards the deeper traps at ESTOC and LP. Thus, the deeper traps at ESTOC and LP appear not to represent the hydrological processes in the upper water column directly above the trap site. Measured increased flux rates towards deeper traps observed within this study may be the result of lateral advective transport of material to the mooring sites or it might be due to a different trapping efficiency between the shallow and deep traps. Freudenthal et al. (2001) assumed an input of lateral advected material to the deeper traps at ESTOC and LP by showing an increase of the total organic carbon/total nitrogen ratio with depth, while the flux of organic carbon between the shallow and deep traps remain relatively constant. Further Sprengel et al. (2002) describes a significant increase of total coccolith and carbonate fluxes at LP and ESTOC towards the deeper traps. These authors suggest that, based on the mean south-westward geostrophic flow of the Canary Current (Stramma and Siedler, 1988) and associated features such as cyclonic eddies and meanders as reported from a fine resolution model of Johnson and Stevens (2000), surface waters located to the north-east of the mooring stations ESTOC and LP must be the source location of particles intercepted by the different traps. Near Cape Ghir (~ 31°N), a recurrent, quasi-permanent large upwelling filament often extends several hundreds of meters off the NW African coast (Davenport et al., 1999). Hence, advection of particles from higher productivity shelf waters might be associated by a high number of juveniles and thus small (<125 μm) planktic foraminifera and further by species which are considered to be indicators for upwelling regions (such as *G. bulloides*), as observed in our samples. Neuer et al. (2002) put forward that LP may be stronger influenced by the Cape Ghir filament than ESTOC. These authors argued that model results by Johnson and Stevens (2000) reveal that particles within the Cape Ghir filament trace an arced trajectory from the Cape to the LP station. This could explain the higher fluxes recorded in the deeper trap at LP (3700 m) compared to the fluxes

observed in the deep ESTOC trap (3000 m). Due to its closeness to the NW African coast, ESTOC receives mainly material advected in so-called intermediate nepheloid layers, which derived from the primary upwelling, in addition to filament related particulates (Neuer et al., 2002). Deuser et al. (1981) explained the process of lateral particle input by the concept of the 'statistical funnel'. It has been considered that deeper traps probably sample material of a large area, due to a larger catchment area, compared to shallower traps. Since the ESTOC mooring is located in the proximity to a high productive domain, the increased flux with depth at this site due to this reason is quite possible. Thus, our study confirms what has been found in other studies of this area and therefore supports the idea that the oligotrophic subtropical gyre region is strongly influenced by the NW African coastal upwelling margin.

Nevertheless, despite the described influences there seems to be no significant influence of this process on the sediment (Meggers et al., 2002). These authors demonstrated by a multiproxy approach that the distribution of geochemical proxies (e.g. $\delta^{13}C_{org}$, TOC) and micropaleontological parameters (e.g. foraminifera, diatoms) in surface sediment samples mirror the E-W productivity gradient. These authors suggested that the surface sediment results are a good average of the modern oceanic situation.

For the reasons discussed above we did not consider the modern species fluxes in the deeper traps because they do not adequately reflect the seasonal succession of the species fluxes at ESTOC and LP.

2.6.2 Planktic foraminifera in relation to seasonal hydrography

One aim of this study was to examine how the distribution of planktic foraminifera is influenced by the seasonal changes of surface water hydrography. Seasonal fluctuations of foraminiferal fluxes reported in this study can generally be regarded as a reflection of seasonal foraminiferal production changes in surface waters. Our data show that in this part of the subtropical North Atlantic the planktic foraminifers assemblages along the Canary Islands transect is controlled mainly by winter cooling with deep mixing and a simultaneous phytoplankton bloom, and in addition at the nearshore site EBC, by nearby upwelling and filament production during summer and fall (Fig. 2.5). This may be caused by the highest chlorophyll a concentrations from January to March observed by long-term satellite measurements, indicating a relatively short period of high biological production and nearly nutrient depleted offshore surface waters during the rest of the year (Barton et al., 1998; Davenport et al., 1999). The deep vertical mixing during winter leads to a supply of nutrients

from subsurface waters to the euphotic zone, making new biological production possible, as described by Arístegui et al. (1997) for the Canary Islands regions. Thus, while coastal upwelling at nearshore station EBC determines the seasonal planktic foraminifera standing stock and flux, the winter-bloom at ESTOC and LP is rather related to local increased production. The decrease in the magnitude of foraminiferal standing stock and flux with increasing distance from the coast indicates variations in surface productivity. The foraminiferal absolute abundance at near-coast station EBC was significantly higher compared to the two oligotrophic stations. Our results corroborate previous findings about seasonal distribution pattern of other micro-organisms and total particle fluxes described for instance in Sprengel et al. (2002) and Neuer et al. (2002). Total coccolith fluxes along the studied transect were highly seasonal, with pronounced sedimentation events occurring in winter/spring, related to the winter phytoplankton bloom in surface waters. Total coccolith flux rates and fluxes of different species fluxes were comparable at the offshore sites ESTOC and LP. Increased flux rates and changes in the assemblages were observed towards the nearcoast station EBC indicating increased productivity due to the influence of upwelling filaments (Sprengel et al., 2002). The seasonality of particle flux at all three stations was mainly related to the winter bloom, and in addition at EBC, by nearby upwelling. Highest particle flux, during all seasons, was observed at EBC containing highest input of biogenic opal and lithogenic components, and the lowest $\delta^{15}N$ compared to the offshore sites (Neuer et al., 2002). Davenport et al. (2002) further observed a steep decrease in westwards mean annual production along the transect by estimating primary productivity, computed from SeaWiFS near-surface chlorophyll concentrations, using the method of Antoine and Morel (1996). Freudenthal et al. (2001) interpreted the decrease of total biogenic mass flux (carbonate, TOC) along the transect as an indicator for the productivity gradient.

Going into more detail, our winter plankton tows showed a strong correspondence of all foraminifer species to chlorophyll a maxima, which was associated with the mixed layer during winter season (Fig. 2.2). This observation is consistent with the idea that the availability of food is of particular importance for planktic foraminifera species shell growth (Fairbanks and Wiebe, 1980) and as such a major control for the depth habitat. In our case this seems to apply not only for symbiotic species but also for the non-symbiotic species. This suggests that even deep-dwelling species such as *G. truncatulinoides* dwell a certain time of their life in the mixed layer, probably with respect to primary shell growth.

The possession of photosynthetic algal symbionts require usually a life in the photic zone for symbiotic species. Opposite to this, non-symbiotic species usually inhabit deeper

water masses (Hemleben et al., 1989). However, the deep mixing and low-density stratification of the water column during winter in the subtropics give especially deep dwelling species like *G. truncatulinoides* the possibility to introduce juveniles from deeper depths into surface waters (Lohmann and Schweitzer, 1990). *G. truncatulinoides* is well known as a species, which is affected by the stratification of the water column (Mulitza et al., 1997). Our standing stock and flux data of *G. truncatulinoides* show that the production is related to the ecological conditions during winter (Fig. 2.4). The seasonal pattern is in agreement with earlier plankton tow investigations considering the ecology and distribution of this species, e.g. by Cifelli (1965) in the Western North Atlantic or by Hemleben et al. (1985) from Bermuda. At the end of the winter-bloom *G. truncatulinoides* disappears from the plankton zone where its primary shell was build. Based on our seasonal observations we suggest that *G. truncatulinoides* reappears in the surface mixed layer the following winter. This suggests that it reproduces once a year in late fall/early winter in deeper water depth, probably below 500 m, from where the juveniles starts to migrate upwards into the surface waters.

The symbiotic species *T. humilis* showed a similar seasonal distribution pattern like *G. truncatulinoides*. It was the dominant species from the nearshore to the offshore in surface waters during winter. Comparable high concentrations during winter were found also by Schiebel et al. (2002) in the water column in the Azores Front-Current System. These authors concluded that *T. humilis* and *G. truncatulinoides* may probably use the same ecological niche because they showed the same changes in abundance during winter. During other seasons *T. humilis* descend as well to deeper waters before in the following winter juvenile of these species reoccur in surface waters. Therefore an annual reproduction cycle for this species is very plausible. We further notice that both, *G. truncatulinoides* and *T. humilis*, are influenced by strong secondary thickening of its calcite tests, in general happening during later life cycles while species descend to deeper and colder water depths (Orr, 1967; Duplessy and Be, 1981). Our data further suggest a comparable seasonal distribution pattern for non-symbiotic species *P. obliquiloculata*, which is known to inhabit tropical to subtropical water masses during winter times (Bé and Tolderlund, 1971; Deuser et al., 1981).

Although station EBC is not located in the area influenced by primary upwelling, it is periodically influenced by cooler and nutrient-rich upwelling waters via filaments, which mainly arise at Cape Yubi during summer and fall, migrating offshore and lead to an enhanced primary productivity at station EBC (Davenport et al., 1999; Johnson and Stevens, 2000). This is also in accordance with CZCS (Coastal Zone Color Scanner) pigment data, which indicates that enhanced pigment concentrations at EBC during summer and fall could be the result of

both in situ growth of phytoplankton in nutrient-rich offshore waters and advective transport of phytoplankton biomass from the primary coastal upwelling regime (Barton et al., 1998; Davenport et al., 1999). Hence, this explains the additional maximum in planktic foraminifera absolute abundance in surface waters and the peak in foraminiferal flux during summer and fall at the nearshore site for which mainly *G. bulloides* is responsible (Fig. 2.5). The standing stock and the flux record show that *G. bulloides* abundance increases in late spring and further grow during the summer/fall upwelling season at EBC. This observation confirms the general assumption of *G. bulloides* to be an upwelling indicator (Kroon and Ganssen, 1988; Thunell and Sautter, 1992). Abrantes et al. (2002) who investigated the fluxes of micro-organism along the transect observed that the highest fluxes of *G. bulloides* occurs contrary to the diatom genus *Chaetoceros* whose major peak occurs in winter. These authors assumes that since this diatom genus is not easy to handle for spinose *G. bulloides* because of long setae, this can be seen as a reflection of *G. bulloides* preferences for less spinose species occurring during summer and fall. A strong positive correlation exists between *G. bulloides* abundance and chlorophyll concentration during each season (Fig. 2.9).

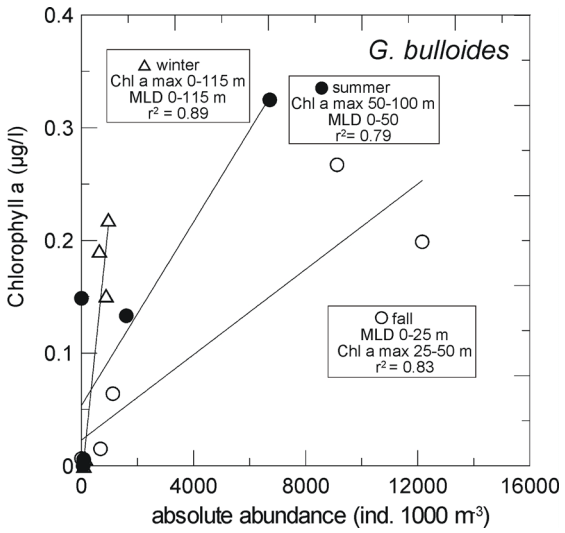

Figure 2.9. The absolute abundance of *G. bulloides* (ind. 1000 m^{-3}) as a function of the chlorophyll a concentration (µg/l) in the upper water column during different seasons (winter, summer and fall). Highest concentration of non-spinose species *G. bulloides* are constantly associated with highest chlorophyll a concentrations. This indicates clearly the importance of the chlorophyll maximum as a food source for planktic foraminifera and as such the major control for the depth habitat of *G. bulloides*.

While in summer and fall the chlorophyll maximum was located below the mixed layer, between 50 and 150 m and slightly shallower in fall (25 and 50 m), during winter it was associated with the mixed layer depth. This suggests that *G. bulloides* strongly follows the chlorophyll maximum during all seasons. Thus, the availability of food (chlorophyll maximum

zone) controls the vertical distribution of planktic foraminifera in the water column to a great extent during the winter-bloom as well during upwelling in summer/fall (Fairbanks and Wiebe, 1980). The occurrence of *G. bulloides* ends abruptly outside the influence of coastal upwelling.

Compared to other species, the two non-symbiotic species *G. ruber* white and pink behave more or less as perennial species along the transect. However, the plankton tow observations show a clear affinity to a specific season. Thus, the pink variety seems to prefer warmer temperatures and is therefore most abundant during summer/fall when SST are usually higher than 20°C. In contrast, *G. ruber* white seems to be more tolerant against colder temperatures (Hilbrecht, 1996), which is visible by its highest concentration during the winter-bloom where the mixed layer temperature is usually below 20°C. The two symbiotic species are not clearly coupled to the chlorophyll a maximum (Fig. 2.10), but rely probably more on the temperature and light conditions of the upper surface water.

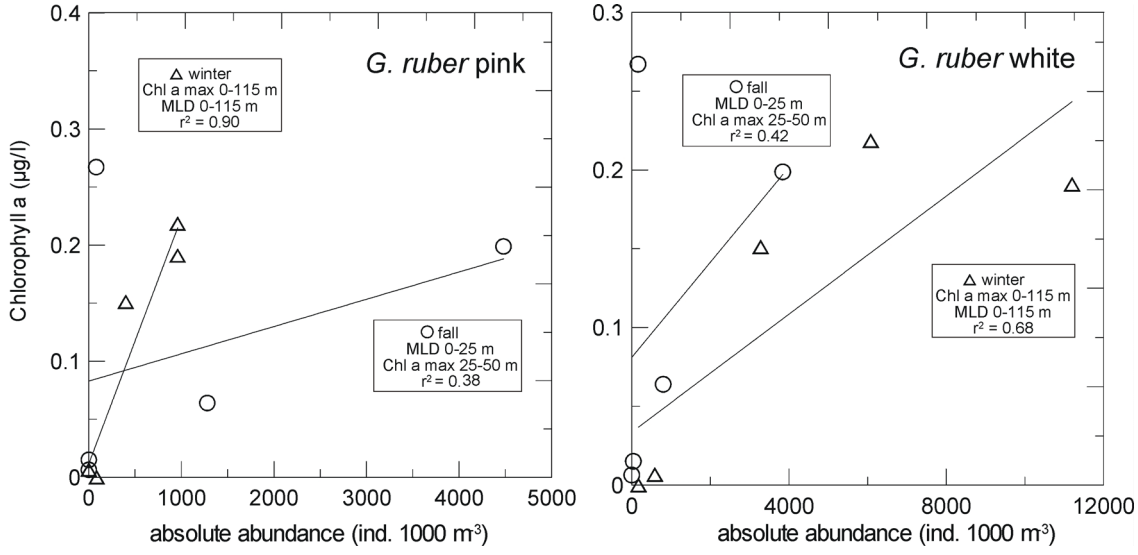

Figure 2.10. The absolute abundance of *G. ruber* white and pink (ind. 1000 m^{-3}) as a function of the chlorophyll a concentration (µg l^{-1}) in the upper water column during different season (winter and fall). In contrast to *G. bulloides*, the two symbiotic species are not inevitably coupled to maximum chlorophyll a concentrations but seems to rely more on the temperature and light conditions in surface water; unless, the chlorophyll a maximum is located at the sea surface as in winter anyway.

When the chlorophyll a maximum is located at the sea surface, such as in winter, a high correlation exists between the absolute abundance and the chlorophyll a concentration in the upper water column. Instead, in fall when the chlorophyll a maximum is found below the mixed layer maximum concentrations of *G. ruber* white and pink were not found at the sea surface but in the lower mixed layer/upper thermocline, thus slightly above the chlorophyll a maximum layer. We assume that these symbiotic species have to remain in a sufficient light

level because they may obtain nutrition from their symbionts and proliferate therefore as well in oligotrophic regions. Thus, even the shallow-living symbiotic species reflect not a pure surface water signal but build rather a mixture of mixed layer/upper thermocline calcite.

Hence, it has been shown that foraminiferal production, flux rates, faunal composition and vertical distribution in the upper water column are strongly coupled to seasonal changes in surface water hydrography, and therefore reflect biological production cycle in the surface waters of NW Africa. Based on our foraminiferal study we conclude that near-surface waters at LP and ESTOC are oligotroph while the EBC station region is a coastal upwelling zone.

2.6.3 The $\delta^{18}O$ signal

2.6.3.1 Comparison of $\delta^{18}O_{shell}$ and predicted $\delta^{18}O_{calcite}$

Our plankton-tow collected living foraminifera show that the oxygen isotope composition of those foraminifers collected close to the sea surface, *i.e.* within the mixed layer, is depleted in ^{18}O compared to specimens that dwell at greater depth. This has been observed by many other studies (e.g. Erez and Honjo, 1981; Kahn and Williams, 1981; Peeters et al., 2002), and suggests that planktic foraminifer shells gain calcite with increasing water depth. The offset between the predicted $\delta^{18}O_{calcite}$ and the $\delta^{18}O_{shell}$ becomes greater with increasing depth in the water column down to a depth level where shell growth ceases. The increase of $\delta^{18}O_{shell}$ with depth in the water column is lower than that of $\delta^{18}O_{eq}$ because the foraminifera must have built a part of its shell in shallower warmer waters. This clearly indicates depth-integrated shell growth. Planktic foraminifera found in the sediment record have a cumulative oxygen isotopic signal which comprises calcification at various depths in the water column. The calcification pattern in the water column is a species-specific process. For instance, species, such as *G. ruber* white, does not show an increase in $\delta^{18}O$ below the thermocline, and therefore can be generally regarded as a species calcifying mainly within the surface mixed layer and the upper thermocline waters. In contrast, *G. truncatulinoides* seems to calcify also in deeper waters and continues calcification down to approximately 700 m.

The stable oxygen isotopic composition of planktic foraminifer shells is assumed to be mainly controlled by the temperature and the $\delta^{18}O$ of the ambient seawater. However, recent culture experiments with living foraminifera have shown that the carbonate ion concentration $[CO_3^{2-}]$ of ambient seawater controls the incorporation of stable oxygen isotopes (Spero et al., 1997). These authors demonstrated that a decrease in the $[CO_3^{2-}]$ results in an increase of the $\delta^{18}O$ values of foraminiferal calcite.

Since both, seawater temperature and pH usually decrease with depth in the water column, the observed increase of the $\delta^{18}O$ value for species with depth, might be attributed to decreasing temperature and/or [CO_3^{2-}] with depth. Thus, during calcite precipitation in the water column, a depth-dependent fractionation can be expected.

Relative to the predicted $\delta^{18}O_{calcite}$ by Kim and O`Neil (1997), the $\delta^{18}O_{shell}$ of the plankton tow collected species show species-specific and size–dependent deviations. Since the temperature equation based on Kim and O`Neil (1997) is based on inorganically precipitated calcite and thus free of any biological effects, deviations from the predicted $\delta^{18}O_{calcite}$ must be attributed to biological factors and carbonate system effects. In the surface mixed layer it becomes obvious that species, such as *G. ruber* white and *T. humilis*, as well as *G. bulloides*, show oxygen isotopic values which are in general considerably lower compared to the synthetic carbonate equation after Kim and O`Neil (1997). Only $\delta^{18}O$ values of the species *G. truncatulinoides* in the 280-440 μm size class are in a good agreement with the equilibrium values, whereby smaller specimens of *G. truncatulinoides* show also negative deviations from $\delta^{18}O_{calcite}$.

Mulitza et al.(2004) assumed that the offsets between the predicted $\delta^{18}O_{calcite}$ and $\delta^{18}O_{shell}$ in the surface mixed layer may be due to different carbon chemistries in the culture experiment and the present-day open oceans. The *p*H in the experiment of the Kim and O`Neil (1997) was probably significantly lower compared to the modern open ocean surface water *p*H of ~8.2 (estimated as ~7.8, (Zeebe, 1999)). Thus, we have to consider that the experimental situation must be referred to a different contribution of the carbonate system components. Hence, if we proceed from this assumption that our foraminifera have calcified under higher *p*H, i.e. higher [CO_3^{2-}], in the open ocean, this would result in lower $\delta^{18}O$ values compared to Kim and O`Neil. (1997). Assuming a decrease of 1.1‰ per unit *p*H increase (Zeebe, 1999), it seems reasonable that the lower $\delta^{18}O$ values shown by planktic foraminifera in our field data (mainly symbiotic species, or small non-symbiotic species) may be partly explained by different carbonate system conditions between the experiment and the open ocean. If we use for instance a specific culture-derived regression for *G. bulloides* (Bemis et al., 1998) ($T = 13.6 – 4.77*(\delta^{18}O_{G.\ bulloides} - \delta^{18}O_{water})$, during which the *p*H in the experiment was controlled to be close to the oceanic *p*H, the deviation becomes noticeable smaller. However, if different *p*H conditions are the reason for the deviations from the Kim and O`Neil (1997) equation, one could assume that at least all species must show the same deviation, because they all grew under same conditions. Since this is not the case, because the observed deviations are both, species-specific and size-dependent, we assume that rather the *p*H in the

microenvironment of the shell has to be taken into account because it can deviate considerably from the oceanic *p*H (Wolf-Gladrow et al., 1999).

2.6.3.2 Size effect

We observed that the deviation from the synthetic carbonate equation after Kim and O`Neil (1997) seems to depend strongly on foraminiferal shell size. Assuming small and larger species calcify under equal temperature condition, e.g. in the winter mixed layer, they show different deviations from predicted $\delta^{18}O_{calcite}$.

If we consider non-symbiotic species, such as *G. truncatulinoides* and *P. obliquiloculata,* the stable oxygen isotope values of smaller specimens are depleted in ^{18}O compared to larger ones. It is evident that, due to an ontogenetic effect, small shells are depleted in ^{18}O (Spero and Lea, 1996; Bemis et al., 1998), because for juvenile foraminifera a larger amount of metabolic $^{12}CO_2$ is available due to a higher respiration rate. Respired CO_2 has a lower $\delta^{18}O$ value relative to the ambient seawater (McConnaughey, 1989). Hence, the metabolic activity rate of non-symbiotic species might be an important factor controlling the incorporation of stable oxygen isotopes, assuming that ontogeny is size correlated.

Another relevant feature is the interaction of metabolic effects of foraminifera and the chemical conditions in their microenvironment (Wolf-Gladrow et al., 1999; Zeebe, 1999). Planktic foraminifera are able to produce a specific *p*H in their microenvironment, which can differ from the ambient oceanic *p*H (Wolf-Gladrow et al., 1999). The carbon fluxes occurring during the main life processes, like calcification, respiration and symbiont photosynthesis, control the *p*H and thus the concentrations of the carbonate system components (CO_2, HCO_3^- and CO_3^{2-}) in the foraminiferal microenvironment. For instance calcification produces CO_2 and thereby lower the *p*H in the microenvironment of a planktic foraminifer. Hence, the positive deviation from the synthetic carbonate equation observed for large non-symbiotic species could be explained by a process that would shift the *p*H to values lower than the experimental *p*H of ~7.8. If the calcification rate of larger specimens were higher this could result in a strengthening of these effect, and thus might explain the higher $\delta^{18}O$ values observed in larger non-symbiotic species. We therefore assume that it seems reasonable that the observed differences in $\delta^{18}O$ between different size classes found in the mixed layer are the result of different *p*H values in the foraminiferal microenvironment, produced by the species itself. This suggests that very large species of *G. truncatulinoides* (>440 μm) and *P. obliquiloculata* (>380 μm) must produce a *p*H in their micro-environment that is even smaller

than the one during the Kim and O`Neil (1997) experiment (*p*H 7.8). Such a low *p*H (e.g. low $[CO_3^{2-}]$) may effect the $\delta^{18}O_{shell}$ and thus could explain the positive deviation observed in our data for large non-symbiotic species. We do not support the idea of upward migration as pointed out by Erez and Honjo (1981). These authors suggest that the positive deviation of *G. truncatulinoides* can be explained by the deposition of calcite in deeper colder waters and an upwards migration of the species in shallower warmer water depth. In our data species from the same size fraction found in deeper water depth were even heavier in $\delta^{18}O$ compared to species dwelling at shallower depth.

Symbiotic species *G. ruber* white shows an opposite size trend in this study. Larger specimens of *G. ruber* white were slightly depleted in $\delta^{18}O$ compared to smaller individuals. This suggests that the ontogenetic effect can not be applied for symbiotic-bearing *G. ruber* white. For symbiotic species like *G. ruber* the photosynthesis process have to be taken into account. The photosynthetic uptake of carbon by symbionts significantly influences the chemical microenvironment of the foraminifer as well (Wolf-Gladrow et al., 1999). In contrast to calcification this process sequester CO_2 and thereby increases the *p*H in the foraminiferal microenvironment (Wolf-Gladrow et al., 1999). Hemleben and Bijma (1994) suggest that the number of symbionts significantly increases with shell size. Hence, we can expect a higher photosynthetic rate in larger specimens which leads to a stronger *p*H increase and which could explain the lower $\delta^{18}O$ values observed in larger specimens of *G. ruber* white in this study. Higher $\delta^{18}O$ values in smaller species of *G. ruber* white has also been shown by Kemle von Mücke et.al. (1994) in the southeast Atlantic Ocean and by Wefer et al. (1983) for the upwelling region off Peru. They assume that a rapid growth and an early reproduction of smaller individuals of *G. ruber* white in nutrient rich cold surface waters results in higher $\delta^{18}O$ with decreasing shell size.

It seems that the oxygen isotope fractionation between foraminiferal $CaCO_3$ and water might be controlled to a great extend by the self-controlled *p*H in the micro-environment from which it is formed. Therefore, a match between the $\delta^{18}O_{shell}$ and the predicted $\delta^{18}O_{calcite}$ in the surface mixed layer depends on the species shell size and the microenvironment *p*H.

2.6.3.3 Seasonality

As we have shown in chapter 4.2. the vertical distribution and abundance of planktic foraminifera vary seasonally. Several studies have shown that a significant seasonal variability is evident in the isotopic composition of planktic foraminifera species (e.g. Williams et al.,

1979; Deuser et al., 1981). We tested this hypothesis with the species *G. ruber* white and pink of the 250-355 μm size class collected by sediment traps at EBC and ESTOC (Fig. 2.11). The $\delta^{18}O$ of *G. ruber* white varies seasonally from –0.18‰ in winter to –0.69‰ in fall at EBC, and from –0.33‰ in winter to –0.65‰ in fall at ESTOC. *G. ruber* pink shows a comparable seasonal range in $\delta^{18}O$ at ESTOC from –0.18‰ in winter to –0.87‰ in fall. The difference of approximately 0.5‰ at EBC corresponds to ~3°C which is close to the SST temperature difference between winter and fall. Based on the information from our plankton tow observation we suggest that *G. ruber* white and pink usually inhabit the upper ocean environment, down to higher chlorophyll a concentration in fall, but without leaving the photic zone. Hence, we assume that the $\delta^{18}O$ composition of living foraminifera is mainly a function of surface water temperature. It is possible that higher SST during fall might accelerate the metabolic activity of planktic foraminifera which results in higher amounts of respired $^{12}CO_2$ which leads to lower $\delta^{18}O$ values.

Another aspect is that the lower $\delta^{18}O$ values during fall could be caused by a higher photosynthetic rate of *G. ruber* due to higher temperatures and higher light levels during fall (Spero and Lea, 1993b). Enhanced symbiont photosynthetic activity in fall increases the *p*H (and therefore the $[CO_3^{2-}]$) in the foraminiferal microenvironment (Wolf-Gladrow et al., 1999). Thus, the $\delta^{18}O$ depletions found in fall might be the result of changing carbonate chemistry in the near vicinity of the foraminifera due to enhanced photosynthetic activity.

A third hypothesis to explain the seasonal isotopic differences arises from the fact that the $[CO_3^{2-}]$ of surface water might vary seasonal between winter and fall (Spero et al., 1997). A higher $[CO_3^{2-}]$ of seawater during fall could explain the lower $\delta^{18}O$ values of *G. ruber* observed during fall. Seasonal studies with regard to the carbonate system have been conducted by González-Dávila et al. (2003) at ESTOC station between 1996 and 2000. These investigations reveal that the seasonal difference of total alkalinity (TA) and total dissolved inorganic carbon (DIC) between winter and fall are rather small. Our calculation of the seawater $[CO_3^{2-}]$, using TA and DIC, show a seasonal difference of ~27 $\mu mol*kg^{-1}$, whereas during fall concentrations are higher. Using the $\delta^{18}O/[CO_3^{2-}]$-slope for *G. ruber* after Bijma (1999) of –0.0022‰ $\mu mol*kg^{-1}$, the difference of ~27 $\mu mol*kg^{-1}$ could only explain 0.06‰ of the observed seasonal difference of 0.32‰ for *G. ruber* white at ESTOC station. We therefore conclude that the seasonal $[CO_3^{2-}]$ variations are not sufficient enough to explain the observed differences in $\delta^{18}O_{shell}$.

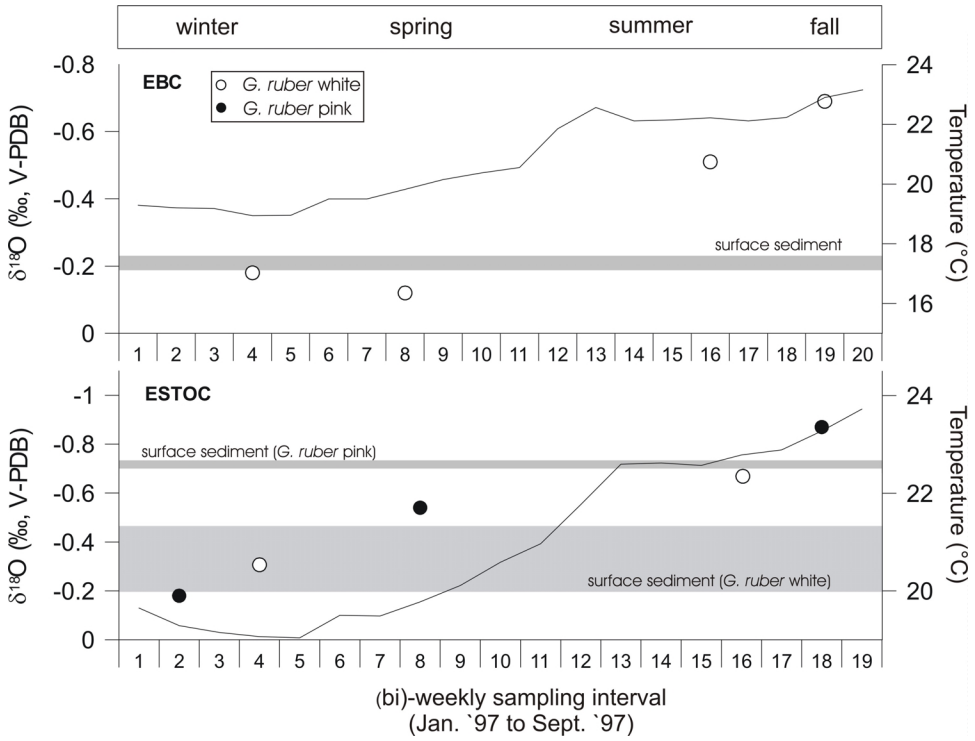

Figure 2.11. Seasonal variation of the $\delta^{18}O$ values of *G. ruber* white (filled dots) and *G. ruber* pink (open dots) in the upper sediment traps at EBC (700 m) and ESTOC (500 m). Sea surface temperature at the trap sites during 1997 is given by the black line. The gray shaded bars indicate the $\delta^{18}O$ range of multiple measurements from the surface sediment.

A comparison of the sediment trap values from the different seasons with the integrated surface sediment $\delta\ ^{18}O$ signal (Fig. 2.11, gray bars) confirms that *G. ruber* white mirrors winter ocean properties. This suggests that the influence of other seasons have only little effect on the $\delta\ ^{18}O$ signal of *G. ruber* white finally preserved in the sedimentary record. The $\delta\ ^{18}O$ sediment signal of *G. ruber* pink can be assigned to warmer conditions suggesting that *G. ruber* pink mirrors the surface temperature during fall. Apparently, *G. ruber* white record a winter signal, while *G. ruber* pink is shifted towards the fall. This evidence suggests that the $\delta\ ^{18}O$ of these two species from surface sediment samples resemble those from sediment traps, if the time of the foraminifera collection is identical with that of the main growing season of the species. Hence, *G. ruber* white and pink might be a useful proxy of the temperature contrast between winter and fall. This is in contrast to Ganssen (1983) who suggested that both species, *G. ruber* white and pink, delineate the temperature of the summer off NW Africa.

2.7 Conclusions

In this study, the seasonal variations of selected species identified in modern vertically stratified plankton tow samples were significant and were supported by bi-weekly sediment trap samples. Concentrations in the upper water column and shell fluxes of planktic foraminifera in the Canary Islands region along an E-W profile show a distinctive response to seasonal hydrographic properties. The seasonality of planktic foraminifera standing stock and flux was mainly related to the winter-bloom at all three stations, and in addition at the nearshore site EBC, by nearby upwelling during summer and fall, associated with upwelling filaments. Based on increased productivity and changes in assemblage composition at the nearcoast station we conclude that the EBC station region is a coastal upwelling zone, while near-surface waters in the ESTOC and LP regions are oligotrophic.

Our observations show that besides temperature the availability of food is of particular importance for planktic foraminifer shell growth and as such a major control for the depth habitat. The absolute abundance and flux of planktic foraminifer species were highest during the winter-bloom. All investigated species show highest concentrations in the upper mixed layer associated with the chlorophyll a maximum. *G. truncatulinoides, P. obliquiloculata, G. humilis* and *G. ruber* white favor winter conditions. *G. bulloides* is an indicator for upwelling season showing maximum concentration in the deep chlorophyll maximum. In contrast to the white species, *G. ruber* pink shows highest affinity to warmer conditions during fall. The symbiotic species *G. ruber* white and pink were not inevitably coupled to the chlorophyll a maximum but seem to be more related to the photic zone.

A strong influence of lateral advected material was demonstrated for the deeper traps at the two offshore sites ESTOC and LP. Seasonality of the yearly production cycle in surface water is more reliable reflected by the shallower traps.

A general increase of the $\delta^{18}O_{shell}$ values from the sea surface to deeper water depths is shown by all species. This indicates depth-integrated shell growth and suggests that the calcite precipitation of individual species is not restricted to the depth interval where highest standing stock values were found.

We show that in the surface mixed layer symbiotic species and mainly small specimens show negative depletions in $\delta^{18}O_{shell}$ relative to the predicted $\delta^{18}O_{calcite}$ values after Kim and O`Neil (1997). The deviations seems to be strongly size dependent. For instance, *G. truncatulinoides* in the size fraction 280-440 μm matches the equilibrium profile, while smaller individuals show negative and larger fraction even positive deviations, respectively. Since the deviations are not equal for all species and sizes we suggest that these differences must be a

consequence of the self-controlled adjustment of the pH in the foraminiferal microenvironment.

As a result of ontogenetic effects, larger shells of non-symbiotic species are enriched in ^{18}O compared to smaller ones. In contrast we found smaller shells of symbiotic species *G. ruber* white to be enriched in $\delta^{18}O$ compared to larger shells. This pattern is most likely due to a higher symbiont photosynthetic activity of larger species (higher symbiont density) and its integrated effect on the *p*H of the foraminiferal microenvironment.

Seasonality is clearly reflected in the isotopic composition of *G. ruber* white and pink. In sediment trap samples collected in winter, when surface temperature is low, both species show higher $\delta^{18}O$. The higher $\delta^{18}O$ values during fall might be due to higher sea surface temperature and higher light levels during fall which leads to enhanced symbiont photosynthetic rates. The observed difference of approximately 0.5‰ between winter and fall corresponds to ~3°C which is close to the SST temperature difference between winter and fall. Hence, *G. ruber* white and pink might be a useful proxy of the temperature contrast between winter and fall.

The $\delta^{18}O$ of planktic foraminifera species from the surface sediment is not significant different compared to species $\delta^{18}O$ from sediment traps from the same location. Thus, planktic foraminifera appear to be less altered by dissolution.

Acknowledgments: We thank captains and crews of RV Victor Hensen VH96/2, RV Poseidon POS212/1, RV POS 237 and RV Meteor M42/1b. We further thank M. Segl and B. Meyer-Schack for help with isotope analysis. Thanks to S. Mulitza for critical discussion which helped to improve the manuscript, and to S. Neuer who provided the chlorophyll a data. This project was funded by the Deutsche Forschungsgemeinschaft (International Graduate College "Proxies in Earth History", University of Bremen).

References

Abrantes, F., Meggers, H., Nave, S., Bollmann, J., Palma, S., Sprengel, C., Henderiks, J., Spies, A., Salgueiro, E., Moita, T. and Neuer, S., 2002. Fluxes of micro-organism along a productivity gradient in the Canary Islands region (29°N): implications of paleoreconstructions. Deep Sea Res. I 49, 3599-3629.

Antoine, M. and Morel, A., 1996. Oceanic primary productivity. 1. Adaption of a spectral light-photosynthesis model in view of application to satellite chlorophyll observations. Global Biogeochemical Cycles 10, 43-55.

Barton, E.D., Aristegui, J., Tett, P., Canton, M., Garcia-Braun, J.A., Hernandez-Leon, S., Nykjaer, L., Almeida, C., Almunia, J., Ballesteros, S., Basterretxea, G., Escanez, J., Garcia-Weill, L., Hernandez-Guerra, A., Lopez-Laatzen, F., Molina, R., Monterro, M.F., Navarro-Perez, E., Rodriguez, J.N., van Lenning, K., Velez, H. and Wild, K., 1998. The transition zone of the Canary Current upwelling region. Progress in Oceanography 41, 455-504.

Bé, A.W.H., Hembleben, C., Anderson, O.R., Spindler, M., Hacunda, J. and Tuntivate-Choy, S., 1977. Laboratory and field observations of living planktonic foraminifera. Micropaleontology 23, 155-179.

Bé, A.W.H. and Tolderlund, D.S., 1971. Distribution and ecology of living planktonic foraminifera in surface waters of the Atlantic and Indian Ocean. In: Funnel, B.M. and Riedel, W.R. (Editors), Micropaleontology of the Oceans. Cambridge University Press, London, pp. 105-149.

Bemis, B.E., Spero, H.J., Bijma, J. and Lea, D.W., 1998. Reevaluation of the oxygen isotopic composition of planktonic foraminifera. Paleoceanography 13, 150-160.

Bijma, J., Spero, H.J. and Lea, D.W., 1998. Oceanic carbonate chemistry and foraminiferal isotopes: new laboratory results paper presented at the Sixth International Conference on Paleoceanography, Lisbon, 1998.

Davenport, R., Neuer, S., Helmke, P., Perez-Marrene, J., Llinas, O. and Wefer, G., 2002. Primary production in the northern Canary Island region as inferred from SeaWiFS imagery. Deep Sea Res. II 49, 3481-3496.

Davenport, R., Neuer, S., Hernandez-Guerra, A., Rueda, M.-J., Llinas, O., Fischer, G. and Wefer, G., 1999. Seasonal and interannual pigment concentrations in the Canary Islands region from CZCS data and comparison with observations from the ESTOC. International Journal of Remote Sensing 20(7), 1419-1433.

Deuser, W.G., Hemleben, C. and Spindler, M., 1981. Seasonal changes in species composition, numbers, mass, size, and isotopic composition of planktonic foraminifera settling into the deep Sargasso Sea. Palaeogeogr., Palaeoclim., Palaeoecol. 33, 103-127.

Duplessy, J.C. and Be, A.W.H., 1981. Oxygen-18 enrichment of planktonic foraminifera due to gametogenic calcification below the euphotic zone. Science 213, 1247-1250.

Erez, J. and Honjo, S., 1981. Comparison of isotopic composition of planktonic foraminifera in plankton tows, sediment traps and surface sediments. Palaeogeogr., Palaeoclim., Palaeoecol. 33, 129-156.

Fairbanks, R.G., Sverdlove, M., Free, R., Wiebe, P.H. and Be, A.W.H., 1982. Vertical distribution and isotopic fractionation of living planktonic foraminifera from the Panama Basin. Nature 298, 841-844.

Fairbanks, R.G. and Wiebe, P.H., 1980. Foraminifera and chlorophyll maximum: vertical distribution, seasonal succession, and paleoceanographic significance. Science 209, 1524-1526.

Freudenthal, T., Neuer, S., Meggers, H., Davenport, R. and Wefer, G., 2001. Influence of lateral particle advection and organic matter degradation on sediment accumulation and stable nitrogen isotope ratios along a productivity gradient in the Canary Islands region. Marine Geology 177, 93-109.

Ganssen, G., 1983. Dokumentation von küstennahem Auftrieb anhand stabiler Isotope in rezenten Foraminiferen vor Nordwest-Afrika, Geologisch-Palaeontologisches Institut der Universität Kiel, Berlin, Stuttgart, 46 pp.

Gonzalez-Davila, M., Santana-Casiano, J.M., Rueda, M.-J., Llinas, O. and FGonzalez-Davila, E.-F., 2003. Seasonal and interannual variability of sea-surface carbon dioxide species at the European Station for Time Series in the Ocean at the Canary Islands (ESTOC) between 1996 and 2000. Global Biogeochemical Cycles 17(3).

Hemleben, C., Spindler, M. and Anderson, O.R., 1989. Modern Planktonic Foraminifera. Springer Verlag, New York, 363 pp.

Hilbrecht, H., 1996. Extant planktic foraminifera and the physical environment in the Atlantic and Indian Oceans. Mitteilungen aus dem Geologischen Institut der Eidgen. Technischen Hochschule und der Universität Zürich. Neue Folge, Zürich, 99 pp.

Hut, G., 1987. Stable isotope reference samples for geochemical and hydrological investigations, Consultants Group meeting 16-18.09.1985. International Atomic Energy Agency (I.A.E.A.), Vienna, Austria, pp. 42.

Johnson, J. and Stevens, I., 2000. A fine resolution model of the eastern North Atlantic between the Azores, the Canary Islands and the Gibraltar Strait. Deep Sea Research Part I 47(5), 875-899.

Kahn, M.I. and Williams, D.F., 1981. Oxygen and carbon isotopic composition of living planktonic foraminifera from the northeast Pacific Ocean. Palaeogeogr., Palaeoclim., Palaeoecol. 33, 47-69.

Kemle-von Mücke, S., 1994. Oberflächenwasserstruktur und - zirkulation des Südostatlantiks im Spätquartär. Berichte aus dem Fachbereich Geowissenschaften, 55. Universität Bremen.

Kim, S.-T. and O`Neil, J.R., 1997. Equilibrium and non-equilibrium oxygen isotope effects in synthetic carbonates. Geochimica et Cosmochimica Acta 61, 3461-3475.

Kroon, D. and Ganssen, G., 1988. Northern Indian Ocean upwelling cells and the stable isotope composition of living planktic foraminifers. In: Brummer, G.J.A. and Kroon, D. (Editors), Planktonic Foraminifers as Tracers of Ocean-Climate History. Free University Press, Amsterdam, pp. 299-317.

Lohmann, G.P. and Schweitzer, P.N., 1990. *Globorotalia truncatulinoides*: Growth and chemistry as probes of the past thermocline: 1. shell size. Paleoceanography 5, 55-75.

McConnaughey, T., 1989. ^{13}C and ^{18}O isotopic disequilibrium in biological carbonates: II. In vitro simulation of kinetic isotope effects. Geochimica et Cosmochimica Acta 53, 163-171.

Meggers, H., Freudenthal, T., Nave, S., Targarona, J., Abrantes, F. and Helmke, P., 2002. Assessment of geochemical and micropaleontological sedimentary parameters as proxies of surface water properties in the Canary Islands region. Deep Sea Res. II 49, 3631-3654.

Mittelstaedt, E., 1972. Der hydrographische Aufbau und die zeitliche Variabilität der Schichtung und Strömung im nordwestafrikanischen Auftriebsgebiet im Frühjahr 1968. Meteor Forsch.-Ergebnisse No. 11, 1-57.

Mittelstaedt, E., 1991. The ocean boundary along the Northwest African coast: Circulation and oceanographic properties at the sea surface. Progress in Oceanography 26, 307-355.

Mulitza, S., Arz, H., Kemle-von Mücke, S., Moos, C., Niebler, H.S., Pätzold, J. and Segl, M., 1999. The South Atlantic carbon isotope record of planktic foraminifera. In: Fischer, G. and Wefer, G. (Editors), Use of proxies in paleoceanography: Examples from the South Atlantic. Springer, Berlin, pp. 427-445.

Mulitza, S., Dürkoop, A., Hale, W., Wefer, G. and Niebler, H.S., 1997. Planktonic foraminifera as recorders of past surface-water stratification. Geology 25(4), 335-338.

Neuer, S., Freudenthal, T., Davenport, R., Llinás, O. and Rueda, M.-J., 2002. Seasonality of surface water properties and particle flux along a productivity gradient off NW Africa. Deep Sea Res. II 49, 3561-3576.

Nykjaer, L. and van Camp, L., 1994. Seasonal and interannual variability of coastal upwelling along northwest Africa and Portugal from 1981 to 1991. J. Geophys. Res. 99, 14,197-14,207.

Orr, W.N., 1967. Secondary calcification in the foraminiferal genus *Globorotalia*. Science 157, 1554-1555.

Peeters, F.J.C., Brummer, G.-J. and Ganssen, G., 2002. The effect of upwelling on the distribution and stable isotope composition of *Globigerina bulloides* and *Globigerinoides ruber* (planktic foraminifera) in modern surface waters of the NW Arabian Sea. Global and Planetary Change 34, 269-291.

Spero, H.J., Bijma, J., Lea, D.W. and Bemis, B., 1997. Effect of seawater carbonate concentration on foraminiferal carbon and oxygen isotopes. Nature 390, 497-500.

Spero, H.J. and Lea, D.W., 1993b. Intraspecific stable isotope variability in the planktic foraminifera *Globigerinoides sacculifer*: Results from laboratory experiments. Mar. Micropalentol. 22, 221-234.

Spero, H.J. and Lea, D.W., 1996. Experimental determination of stable isotope variability in Globigerina bulloides: Implications for paleoceanographic reconstruction. Mar. Micropalentol. 28, 231-246.

Sprengel, C., Baumann, K.-H., Henderiks, J. and Henrich, R., 2002. Modern coccolithophore and carbonate sedimentation along a productivity gradient in the Canary Islands region: seasonal export production and surface accumulation rates. Deep Sea Research II 49.

Stramma, L. and Siedler, G., 1988. Seasonal changes in the North Atlantic subtropical gyre. J. Geophys. Res. 93(C7), 8,111-8,118.

Thunell, R. and Sautter, L.R., 1992. Planktonic foraminiferal faunal and stable isotopic indices of upwelling: a sediment trap study in the San Pedro basin, Southern California Bight. In: Summerhayes, C.P., Prell, W.L. and Emeis, K.C. (Editors), Upwelling systems: Evolution since the early Miocene. Geological Society Special Publication, pp. 77-91.

Tomczak, M. and Hughes, P., 1980. Three dimensional variability of water masses and currents in the Canary current upwelling region. Meteor Forsch.-Ergebnisse A No. 21, 1-24.

van Camp, L., Nykjar, L., Mittelstaedt, E. and Schlittenhardt, P., 1991. Upwelling and boundary circulation off Northwest Africa as depicted by infrared and visible satellite observations. Progress in Oceanography 26, 357-402.

Wefer, G., Dunbar, R.B. and Suess, E., 1983. Stable isotopes of foraminifers off Peru recording high fertility and changes in upwelling history. In: Tiede, J. and Suess, E. (Editors), Coastal upwelling, Part B, pp. 295-308.

Williams, D.F., Bé, A.W.H. and Fairbanks, R.G., 1979. Seasonal oxygen isotopic variations in living planktonic foraminifera of Bermuda. Science 206, 447-449.

Wolf-Gladrow, D.A., Bijma, J. and Zeebe, R.E., 1999. Model simulation on the carbonate chemistry in the microenvironment of symbiont bearing foraminifera. Marine Chemistry 64, 181-198.

Zeebe, R.E., 1999. An explanation of the effect of seawater carbonate concentration on foraminiferal oxygen isotopes. Geochimica et Cosmochimica Acta 63, 2001-2007.

CHAPTER 3*

PLANKTIC FORAMINIFERAL FLUXES ASSOCIATED WITH AGULHAS RINGS

Iris Wilke[a]; Frank J.C. Peeters[b] and Geert-Jan A. Brummer[c]

[a]*Fachbereich Geowissenschaften/MARUM, Universität Bremen, Leobenerstrasse, 28359 Bremen, Germany*

[b]*Afdeling Palaeo-ecologie en Palaeoklimatologie, Faculteit Aard- en Levenswetenschappen, Vrije Universiteit, de Boelelaan 1085, 1081 HV, Amsterdam, The Netherlands*

[c]*Department of Marine Chemistry and Geology (MCG), Netherlands Institute for Sea Research (NIOZ), P.O. Box 59, 1790 AB Den Burg, Texel, The Netherlands*

*This chapter is submitted for publication
to *Marine Micropaleontology*

3.1 Abstract

Deposition fluxes of planktic foraminifera were monitored in the southeastern Cape Basin to improve interpretations from sedimentary records of the variability of Indian Ocean advection into the South Atlantic via Agulhas leakage. We deployed a time-series sediment trap from August 2000 to February 2001 in the area of influence of Agulhas rings, *i.e.* large anti-cyclonic eddies detached from the Agulhas Current, to assess the advection of Indian Ocean plankton by Agulhas leakage. Here, we report on the species fluxes and oxygen and carbon isotopic composition of their shells in response to Agulhas rings that moved over the trap site.

We found a relationship between the shell flux and satellite derived sea surface height and temperature indicating that deposition fluxes originated from distinct hydrographic regimes. Our data indicate that highest foraminiferal shell production, observed in October 2000 and January 2001, occurs during frontal mixing near the boundaries of different water masses of Atlantic and Indian origin, rather than in the centre of an Agulhas ring. Highest amounts of resuspended material were recorded simultaneously with the shell flux maxima and support the dynamic conditions at the frontal zones of the rings. The faunal assemblage at the frontal zones was dominated by *Globorotalia inflata, Globigerina bulloides, Globigerinata glutinata*, and *Neogloboquadrina pachyderma* (dex.). In-between, in November 2000, Agulhas water influenced the planktic foraminiferal fluxes as indicated by warm, tropical-subtropical Indian Ocean species, including *Globigerinoides ruber, Globigerinoides sacculifer, Globigerinella aequilateralis, Neogloboquadrina dutertrei, Orbulina universa, Globorotalia menardii* and *Globorotalia theyeri*/*G. scitula* cpx., and low shell flux, whereas the species *G. glutinata* is characteristic for both, Indian and Atlantic water masses. The species *G. inflata,* however, occurred also in significant fluxes in the intermediate period dominated by Agulhas water, corroborating physical oceanographic evidence for rapid mixing between Agulhas rings and Atlantic water masses.

We found a good relationship between SST data and the oxygen isotopic composition of South Atlantic species *G. glutinata, G. bulloides, G. inflata* and *N. pachyderma* (dex.). The oxygen isotopic composition of *G. glutinata* accurately record the SST of the different water masses, *i.e.* the Indian, Atlantic or mixed waters. The species related to the Agulhas waters, such as *G. ruber, G. aequilateralis* and *N. dutertrei* show relatively constant oxygen isotopic composition throughout the record, indicating that they predominantly calcify within water associated with the Indian Ocean. The carbon isotope values of *G. bulloides, G. glutinata, G. inflata* and *N. pachyderma* (dex.) show a clear temperature influence through its effect on metabolic rate, while the species *N. dutertrei* exhibit no temperature-dependence, but seems to reflect the higher carbon isotopic composition ($\delta^{13}C_{DIC}$) of nutrient-poor Agulhas waters above the trap site

The modern observations enable to distinguish between species associated with Agulhas leakage on one hand and species related to Atlantic water masses on the other.

3.2 Introduction

Inter-ocean exchange of thermocline and intermediate waters between the Indian and Atlantic Ocean occurs south off Africa (Lutjeharms, 1996). This water mass exchange is considered to play an important role in the upper branch of the thermohaline circulation (Gordon, 1996; Weijer et al., 2002). Along with the Agulhas Current living plankton of Indian Ocean origin is transported into the Cape Basin and advected into the Atlantic Ocean via so-called Agulhas rings (Peeters et al., 2004). Sedimentary records located in the southern Cape Basin (Esper et al., 2004; Flores et al., 1999; Peeters et al., 2004; Rau et al., 2002) mirror a high diversity of plankton, reflecting the presence of different water masses in this region. To better understand the variability of past Agulhas leakage into the South Atlantic it is essential to identify those species that are characteristic for Agulhas Current and Agulhas rings. Except for stratigraphic purposes the isotopic composition of planktic foraminiferal shells has not been considered for paleoceanographic reconstructions of this area. Hence, it is important to assess the spatial and temporal distribution of different species in relation to the hydrographic regimes related to the Indian advection.

Here, we present results from a sediment trap deployed in the South Atlantic Ocean directly in the sphere of influence of Agulhas rings, that weekly collected material from August 2000 through February 2001 (MST-15, at 38°46`S, 14°00`E; 3500 m water depth). The main aim of this work is to assess the changes in the faunal assemblage as a result of the inflow of warm Indian Ocean water into the Cape Basin. In order to develop robust proxies that trace Indian Ocean advection into the Atlantic we 1) identify the faunal assemblage associated with Indian/Atlantic Ocean, 2) quantify the shell flux of different species, and 3) understand the changes in the stable isotope composition.

3.3 The Agulhas Retroflection

Indian Ocean waters enter the southeast Atlantic Benguela system through Agulhas rings or direct Agulhas leakage (Gordon, 1996; Gordon, 2003; Lutjeharms, 1996). The Agulhas Current (AC), which flows southwestwards along the continental slope of eastern South Africa transports warm and saline surface water and central water from the Indian into the South Atlantic Ocean (Fig. 3.1). The surface water temperature of Agulhas water is typically ~23°C in autral summer and about 21°C in winter (Shannon, 1985). This water usually penetrates into the southern Benguela system during austral summer when the wind field is conducive to a north-northwesterly advection of warm Agulhas tongues (Garzoli et al.,

1996; Shannon, 1966). At approximately 35°S the AC becomes detached from the coast of the African continent. Further to the south it meets water masses that flow in an eastward direction: the South Atlantic Current (SAC), and the Antarctic Circumpolar Current (ACC). The ACC flows south of the Sub Tropical Convergence (STC) and transports cold and nutrient-rich polar and subpolar water masses into the Cape Basin. North of the STC, the SAC transports cooler, nutrient-poor thermocline water from the oligotrophic areas of the South Atlantic Ocean.

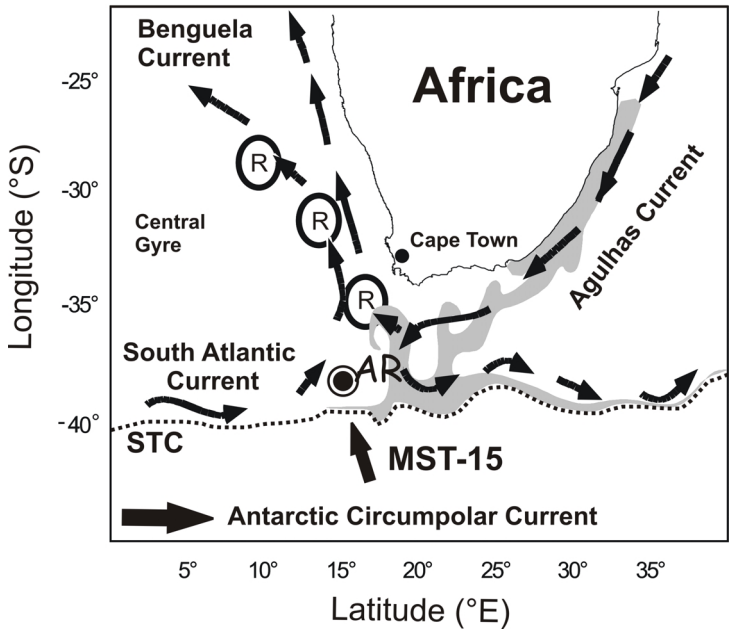

Figure 3.1. Map showing location of sediment trap mooring location MST-15 (black filled dot) and schematic main hydrographic features: The hydrography of the southeastern South Atlantic Ocean is characterized by the interaction of three different currents: 1. the Antarctic Circumpolar Current (ACC), 2. the South Atlantic Current (SAC) and 3. the Agulhas Current (AC). The region where the AC returns back into the Indian Ocean is referred to as the Agulhas Retroflection (AR). During this process Agulhas rings (labelled "R") are shed off from the AC at the AR and move into the South Atlantic Ocean. The position Sub Tropical Convergence is indicated by dotted line labeled STC.

The collision of the westward flowing Agulhas and the eastward flowing Atlantic water masses results in the retroflection of the AC where it almost bends back to itself (Gordon, 1985). Consequently, a part of the Agulhas waters flow back into the Indian Ocean in the form of the Agulhas Return Current (ARC). Interocean exchange takes place through direct leakage and the detachment of rings and filaments from the Agulhas Current at the retroflection (Gordon, 1986; Lutjeharms and van Ballegooyen, 1988). The Agulhas rings shed off irregularly and continue to move into the Atlantic Ocean in a north-westerly direction with a typical speed of 5 to 8 cm s^{-1} (Shannon, 1985). The processes described above is responsible

for the transport of heat and salt from the Indian Ocean into the Atlantic Ocean and form an important link between the Indian Ocean and the subtropical gyres of the South Atlantic Ocean (de Ruijter et al., 1999).

A vertical section of potential temperature through the upper 1000 m of an Agulhas ring ("Astrid") is shown in Figure 3.2 (van Aken et al., 2003). Agulhas rings mixed layer and thermocline waters consists of Southern Indian Central Water (SICW), and underlying intermediate water, dominated by Antarctic Intermediate Water (AAIW) (Shannon and Hunter, 1988). At deeper levels, not seen in Figure 3.2, North Atlantic Deep Water (NADW) is observed, overlying Antarctic Bottom Water (AABW).

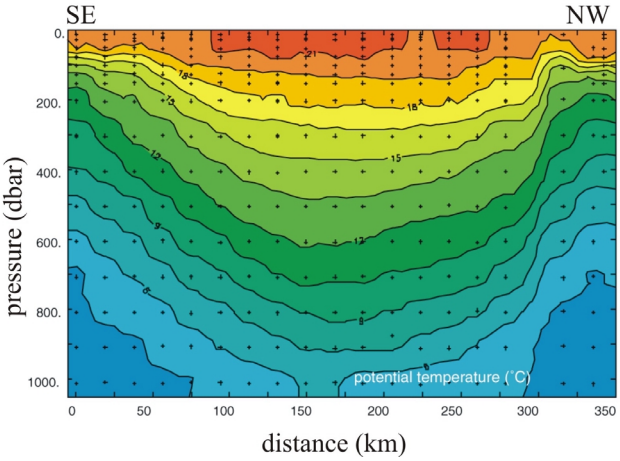

Figure 3.2. An example of a cross section of potential temperature through Agulhas ring "Astrid", as measured during the MARE 1 expedition in March 2001. The bowl-shaped form of the isotherms shows a very homogenous mixed layer in the centre of the ring. This is clearly shown by the 12°C isotherm, which is found at approximately 600 m in the centre, while it is at 180 m near the boundaries of the ring. The angular velocities are highest where the isotherms dip steepest (*i.e.* 70 and 300 km on the horizontal axis).

3.4 Material and methods

As part of the Dutch Mixing of Agulhas Rings Experiment (MARE) program a sediment trap (MST-15) was deployed in the Cape Basin (38°46`S, 14°00`E) at a water depth of 3500 m (Table 3.1). Particle fluxes were intercepted from August 2000 to February 2001 in 1-week intervals. Samples were preserved in a pH-buffered solution of $HgCl_2$ in sea-water added to the trap cups prior to the mooring (Conan and Brummer, 2000). Further samples were wet sieved over a 2 mm mesh to remove the larger marine organisms and split into a number of aliquots using a Folsom-splitter. One quarter of the sample was wet-sieved over a 150 μm mesh sieve and rinsed with buffered demineralized water to remove the poisonous salts.

Table 3.1. General information of sediment trap deployment and plankton tow collected samples

Station code	Cruise	Sample type	Latitude (E)	Longitude (S)	Date	Sampling interval (m)	Remarks
MST-15	MARE 2+4	trap	14°01.09	38°46.02	09.08.00 - 09.02.01	3500	
1153	MARE 2	tow	13°58.25	38°41.11	09.08.00	0-150	start of trap
1151	MARE 2	tow	13°29.54	38°42.61	09.08.00	150-1000	end of trap
21-1	MARE 4	tow	14°01.02	38°46.92	18.02.01	0-150	start of trap
21-3	MARE 4	tow	13°56.76	38°49.32	18.02.01	150-800	end of trap

The residue was frozen, freeze-dried and weighed. After combustion of the organic matter using a Low Temperature Asher (T < 115°C), the samples were wet-sieved into five fractions (125-150, 150-250, 250-355, 355-500, >500 μm). Faunal counts were made for each size fraction >150 μm using the taxonomy of Bé and Hutson (1977) and Hemleben et al. (1989). The samples contain high amounts of fossil foraminifera which were easy to distinguished from the fresh fraction by their heavy crust and/or by being filled with sediment, and which were counted separately. Sample size allowing, at least 200 specimens were identified in each size fraction. Sample cups #4 and #11 were lost during recovery of the trap.

In addition to the trap material, plankton tow samples were collected at the beginning (August 2000) and at the end (February 2001) of the sediment trap time series (Table 3.1). A Hydrobios Multinet system modified for oblique towing with five plankton nets (mesh 100 μm) were consecutively opened and closed during the upcast while towed behind the ship. The upper 150 m of the water column was sampled at five depth intervals (100-150, 100-75, 75-50, 50-25 and 25-0 m), while the deep cast covered the intervals 1000-500 (800-500), 500-300, 300-200 and 200-150 m. For the deep cast 100-1300 m^3 of sea water was filtered per interval, for the shallow casts 50-270 m^3 per interval (flow-meter-control). Samples were frozen at –80°C shipboard, freeze dried and weighed. After combustion of the organic matter in a Low Temperature Asher (T<100°C), samples were wet-sieved into four fractions, *i.e.* <150, 150-250, 250-500 and >500 μm.

Oxygen and carbon isotope ratios of planktic foraminifera were measured at the Vrije Universiteit in Amsterdam on a Finnigan Mat 252 mass spectrometer equipped with an automatic carbonate preparation device. Depending on the expected shell mass, three to twenty specimens were picked from the size fractions 150-250 μm, 250-500 μm. Samples have been dissolved in concentrated orthophosphoric acid at a temperature of 80°C. Isotope composition is reported in the conventional δ-notation versus Vienna Pee Dee Belemnite (V-PDB). The external reproducibility was better than 0.07‰ for $\delta^{18}O$ and 0.04‰ for $\delta^{13}C$ (1s.d.).

We calculated the Shannon-Weaver diversity ($H' = -\Sigma p_i \ln (p_i)$; where p is the number of species i) and equitability ($E' = e^{H'}/s$; in which s is the number of species in the sample). The Shannon information index describes diversity (Shannon and Weaver, 1949), taking into account the relative abundance of each species within the sample. The equitability index is a measure of the evenness of the species distribution within a sample (Buzas and Gibson, 1969). In case all species are present in the same proportion, equitability equals one, and approaches zero if the fauna is dominated by one species only.

The observed changes in species flux during the six-months sediment trap deployment might have an effect on the isotopic composition in the sedimentary record. To determine this effect we calculated the flux weighted average isotopic composition by using the following equation (Curry et al., 1983):

$$\delta^{18}O_{shell} = \frac{\Sigma f_i \times \delta^{18}O_i}{\Sigma f_i}$$

where f_i is the flux of the species in a trap sample, $\delta^{18}O_i$ is the isotopic composition of the species for each sample, and $\delta^{18}O_{shell,\ flux\text{-}weighted\ average}$ is the flux weighted isotopic composition of the species.

3.5 Results

3.5.1 Hydrographic observations

3.5.1.1 Sea Surface Height anomaly images

We used TOPEX/ERS satellite derived Sea Surface Height (SSH) anomaly images to determine the position of Agulhas rings through time present in the surrounding area of our trap site during the time of sample collection (http://www.ccar.colorado.edu). This satellite method records the height of the sea surface, and therefore enables to characterize the approximate location of the warm anti-cyclonic Agulhas rings. The warm water rings are indicated by positive SSH-anomalies relative to the sea surface (Fig. 3.3) (Byrne et al., 1995). The images show the SSH contrast between the warmer Agulhas rings and the colder surrounding waters of the southeast Atlantic Ocean. Between August 2000 and February 2001

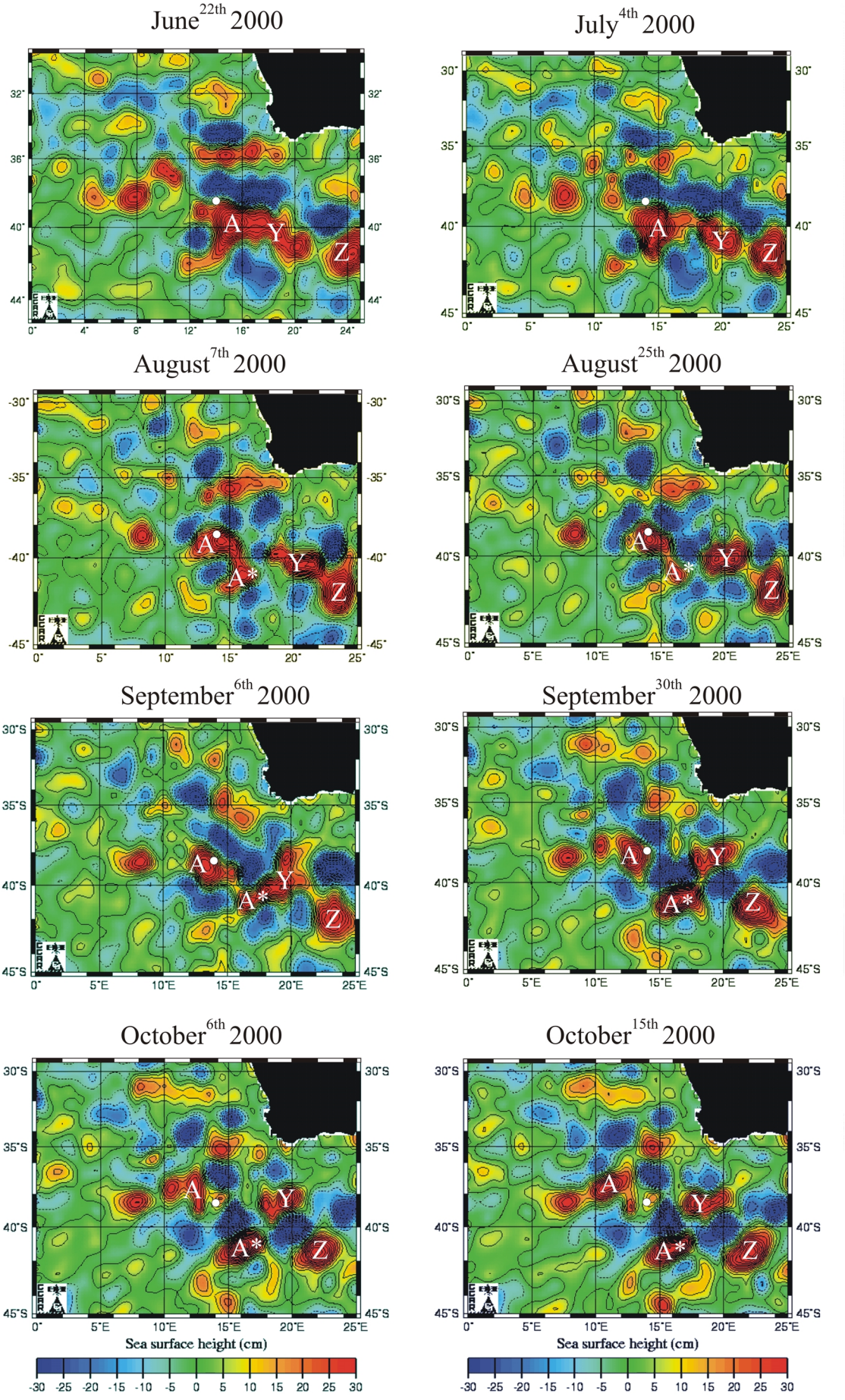
June 22th 2000
July 4th 2000
August 7th 2000
August 25th 2000
September 6th 2000
September 30th 2000
October 6th 2000
October 15th 2000
A
Y
Z
A*
Sea surface height (cm)
-30 -25 -20 -15 -10 -5 0 5 10 15 20 25 30

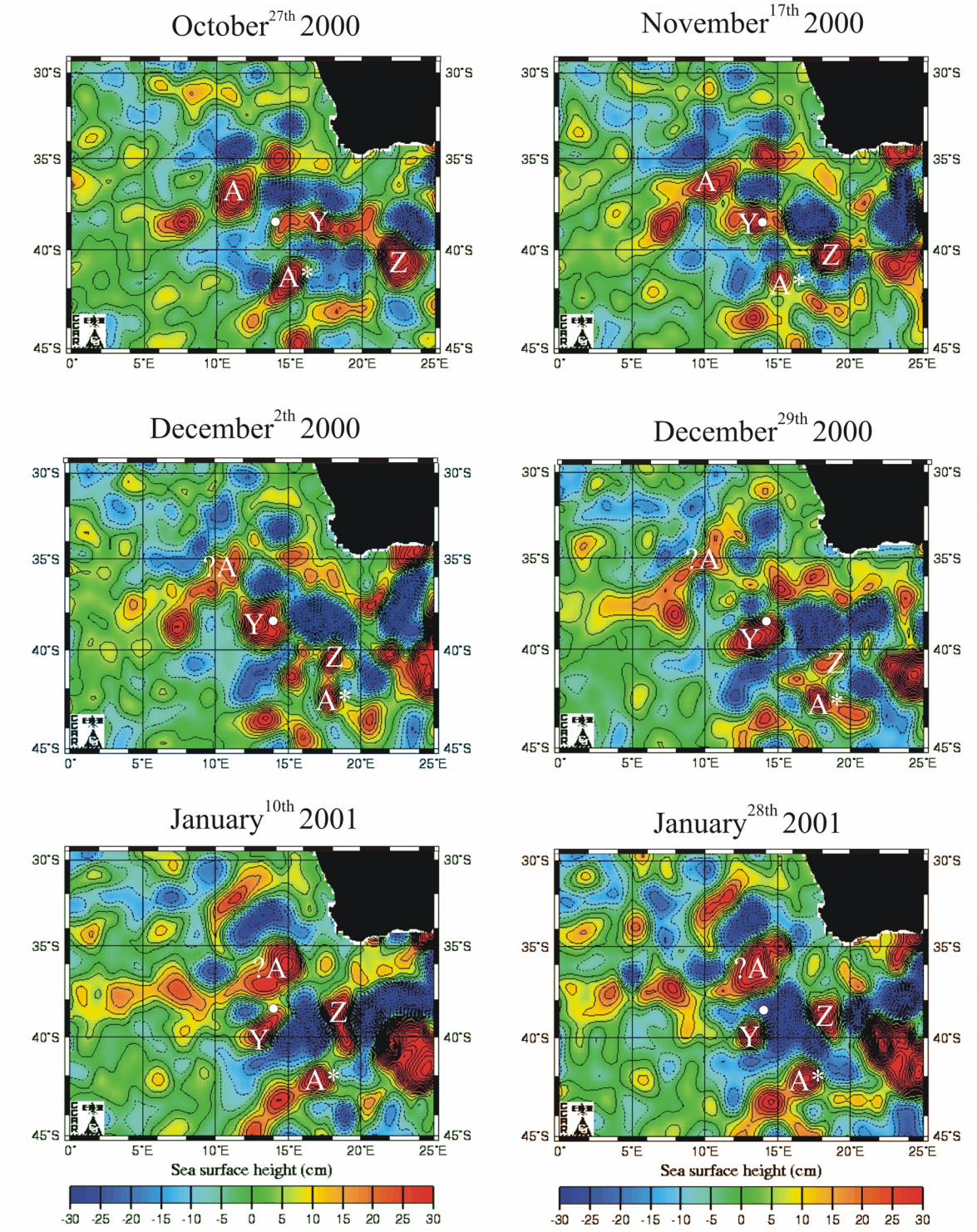

Figure 3.3. TOPEX/ERS Sea Surface Height (SSH) anomaly images for different time slices between June 22nd 2000 and January 28th. 2001. The white dot in each panel indicates the location of trap site MST-15. Letters 'A', 'Y' and 'Z' have been assigned to Agulhas rings, large-scale positive SSH anomalies indicated by red color, which where consistently present in the region throughout the six months sampling period. See text for interpretation.

the hydrographic conditions above the trap site changed with respect to the estimated position and number of Agulhas rings (Fig. 3.3).

About four to five weeks before the trap started its six months time series, there has been a long EW elongated SSH anomaly just south of the trap site, *i.e.* from 12°E to about 22°E (Fig. 3.3, image of June 22nd). Using SST images we identified this elongated SSH anomaly as the Agulhas Current. In the beginning of July 2000 (image of July 4th), the elongated SSH anomaly splits up into anomaly 'A' and 'Y' (Fig. 3.3). Both anomalies were identified as Agulhas rings given their size and consistent presence in the region. To the east a third anomaly named 'Z' can be recognized. Ring 'A' has been just south of the trap site in July 2000.

Following the tracks of the rings it becomes evident that the trap site has been influenced mainly by two rings, namely 'A' and 'Y', between the time of sample collection. Figure 3.4 illustrates the tracks for ring 'A' between August 2000 and December 2000 and for ring 'Y' between September 2000 and January 2001, whereby the location of the SSH maximum is taken as the centre of the Agulhas ring.

The SSH anomaly data indicate that in the beginning of August 2000 (see image August 7th) ring 'A' has become elongated and showed two centres. In mid-August 2000 the ring split into two separate SSH anomalies, a larger ('A') and a smaller ring feature ('A*'). In the following three weeks ring 'A' started to move in a more northwestwards direction while at the same time the smaller ring 'A*' moves southeastwards (see image September 6th). The images suggest that in the end of September (see image September 30th) the eastern boundary of ring 'A' was located above the trap site. At this time, a large negative SSH anomaly (cyclone) was observed area east of the trap site. The track of ring 'A' indicates that ring 'A' had moved quickly to a northwestwards position *i.e.* between September 30th and October 9th 2000 (Fig. 3.4). The October 6th image shows that although the centre of ring 'A' was already located further northwestwards, a small SSH anomaly (filament?) was separated from ring 'A' on the east. This positive anomaly was located directly above the trap site in early and mid-October 2000, while ring 'Y' continued to move westwards towards the trap position (see images October 6th and October 15th). In the last week of October 2000 (see image October 27th), the western boundary of an elongated ring 'Y' arrived at the trap site, and merged with the filament.

To summarize, in October 2000 major hydrographic changes took place above the trap site: *i.e.* Agulhas ring 'A' was present above the trap site in the beginning of October 2000, while at the end of October 2000 the western boundary of Agulhas ring 'Y' has reached

the trap location. Between November 2nd and November 17th ring 'Y' moved over the trap site. In early December 2000 (see image December 2nd) ring 'Y' started to move in a southern direction, while a few weeks later (see image December 29th) the northern boundary of ring 'Y' was still located above the trap site. The images suggest that in mid-January 2001 (see image of January 10th) a large positive SSH anomaly (ring A?), located north of the trap site, moves close to ring 'Y'. The southern boundary of ring 'A(?)' and the northern boundary of ring 'Y' merge until in the end of January 2001 ring 'Y' moved further southwards (see image January 28th) and a large negative SSH anomaly was located above the trap site.

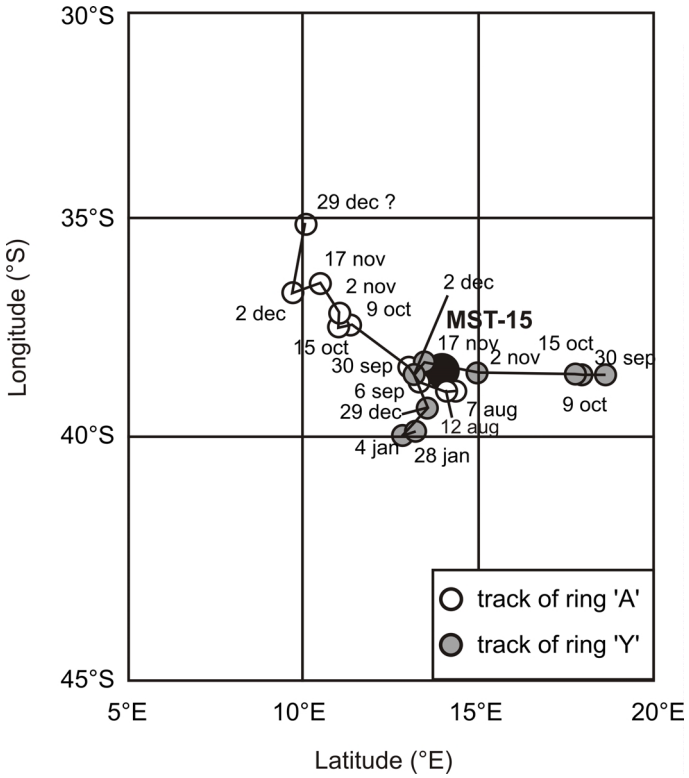

Figure 3.4. Map indicating the spatial and temporal movement of the estimated centre of Agulhas ring 'A' between August and December 2000 (white dots) and track of ring 'Y' between September 2000 and January 2001 (gray dots). The black dot indicates the location of sediment trap MST-15. For further discussion see text.

3.5.1.2 Sea Surface Temperature

In addition to SSH images, MODIS-Terra Sea Surface Temperature (SST) data (Distributed Archive Center (DAAC) of the Goddard Spaceflight Center (USA)) are used as a tool to interpret the hydrographic changes above the trap site (Fig. 3.5). The data show that the SST ranges between 14.5°C and 19.6°C during the time series. In August 2000 the surface waters show temperature between 16 and 17°C, while towards the end of September 2000 SST decrease to a minimum value of 14.5 °C. A sudden SST increase, from 14.5°C to a

maximum of 19.6°C takes place between the end of September 2000 and mid-October 2000. SST's gradually decrease between mid-October and mid-January 2001 down to a value of 15.5°C. At the end of the record SST increase again.

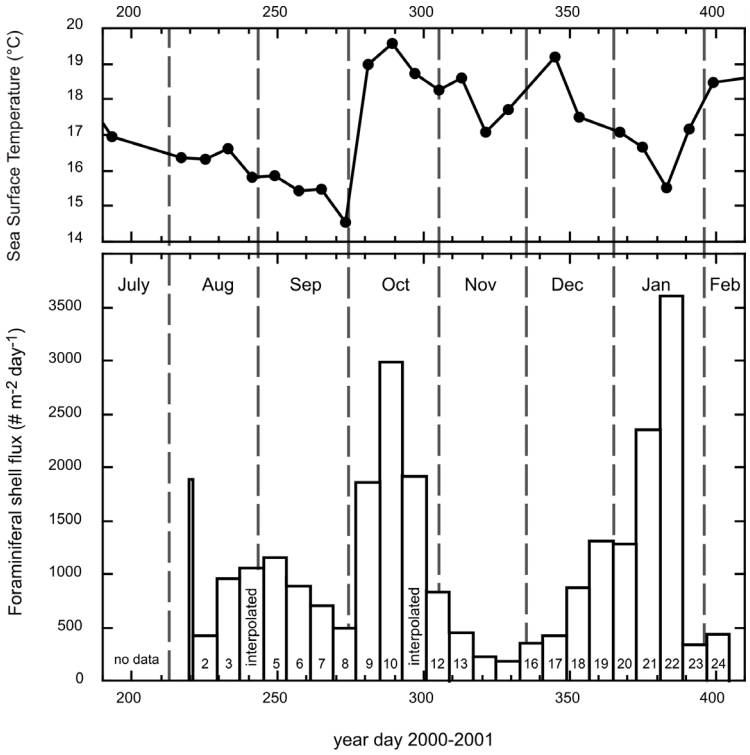

Figure 3.5. Figure showing MST-15 foraminiferal shell fluxes (>150 μm) between August 2000 and February 2001 and the MODIS-Terra Sea Surface Temperature data (provided by the Distributed Archive Center (DAAC) Goddard Spaceflight Center, USA) for the trap location.

3.5.2 Planktic foraminiferal shell flux

The total planktic foraminifera flux shows two distinct maxima during the time series (Fig. 3.5). The first maximum of 3000 shells $m^{-2}day^{-1}$ occurred in mid October 2000. Whereas, the second maximum appears in January 2001 with fluxes of ~3600 shells m^{-2} day^{-1}. Lowest export flux is observed in-between (November 2000). A smaller maximum of ~1200 shells $m^{-2}day^{-1}$ occurred between late August and early September 2000.

Regarding the total planktic foraminiferal shell flux of different size classes (Fig. 3.6a) reveals that the increase in shell flux is mainly composed of specimens in the size fraction 150-250 μm. This size fraction dominates the total foraminiferal shell flux during the whole series by accounting for ~70% in average.

Maxima in the resuspended fossil and benthic foraminifera occur simultaneously with the highest fresh shell flux (Fig. 3.6b). In some cases, the resuspended specimens account for

more than 50% of the total shell flux, especially in the fine size fraction 150-250 μm (cf. Conan and Brummer, 2000).

Of the eleven most abundant species, the species *Globorotalia inflata* dominates the assemblage (Fig. 3.7a). Its high fluxes were recorded in October 2000 (~1900 shells m^{-2} day^{-1}) and January 2001 (~1400 shells m^{-2} day^{-1}), averaging ~500 shells m^{-2} day^{-1} for the entire time series. Other abundant species were *Neogloboquadrina pachyderma* (dex.)*, Globigerinata glutinata* and *Globigerina bulloides,* averaging 70, 111 and 111 shells m^{-2} day^{-1}. All other species show fluxes <50 shells m^{-2} day^{-1} (Appendix A).

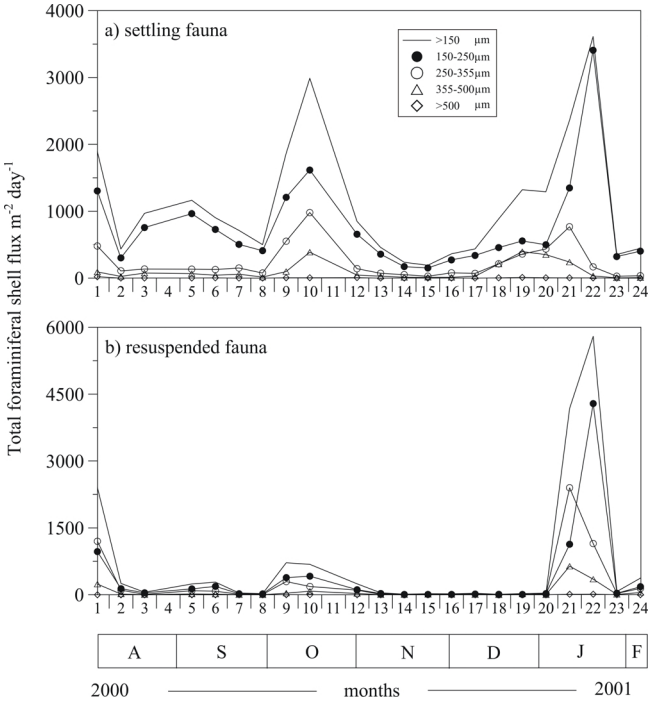

Figure 3.6. Size composition of the MST-15 total foraminiferal shell flux (150-250, 250-355, 355-500, >500 and >150 μm). a) The total foraminiferal shell flux excluding the sea-floor resuspended fauna. b) Resuspended fauna of total foraminiferal shell flux.

3.5.3 Species diversity and composition

3.5.3.1 Sediment trap

In total twenty-nine different species of planktic foraminifera were identified in the sediment trap samples (Appendix A). Shannon diversity (*H`*) and Equitability (*E`*) are low during mid-October 2000 and early January 2001 (Fig. 3.7). These minima in *H`* and *E`* coincide with the maxima in total planktic foraminiferal shell flux. As opposed to this, both faunal indices increase in-between (November 2000) when Agulhas rings "A" and "Y" were in the vicinity of the trap site, indicating a well balanced and rich species assemblage.

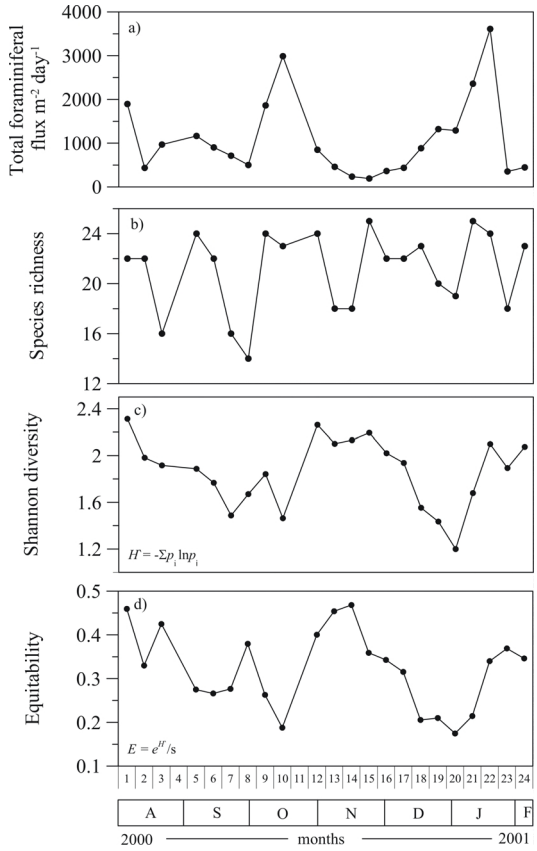

Figure 3.7. Overview of different faunal indices for sediment trap MST-15. a) Total foraminiferal shell flux (excluding the sea-floor resuspended fauna), b) species richness, c) Shannon diversity and d) equitability of planktic foraminifera for specimens >150 μm.

The eleven most abundant species account for approximately 89% of the total foraminiferal shell flux (Fig. 3.8), dominated by *G. inflata*. During October 2000 and January 2001 *G. inflata* accounts for ~64% and ~74% of the shell assemblage settling out during the 6-months record. During November 2000, when the total shell flux was low, the relative abundance indicated that the following species *Globigerinoides ruber, Globigerinoides sacculifer, Globigerinella aequilateralis, Globorotalia menardii*, *Orbulina universa, Neogloboquadrina dutertrei, Globorotalia theyeri*/*G. scitula* cpx. and *G. glutinata* attain their maximum in early November 2000 (Fig. 3.8b). For instance, the relative abundance of *G. ruber* increases to ~10% during this period. The abrupt increase of warm-water species is accompanied by lowest relative abundance of *G. inflata,* which exhibits a clear minimum. A similar situation is observed for early August 2000. The (flux weighted) composition of the faunal assemblage integrated over a period of six months indicate that the most dominant species is *G. inflata* (~46%), followed by *G. bulloides* (10%), *G. glutinata* (10%) and *N. pachyderma* (dex.) (7%). Other species show an average relative abundance of <5% (Appendix A).

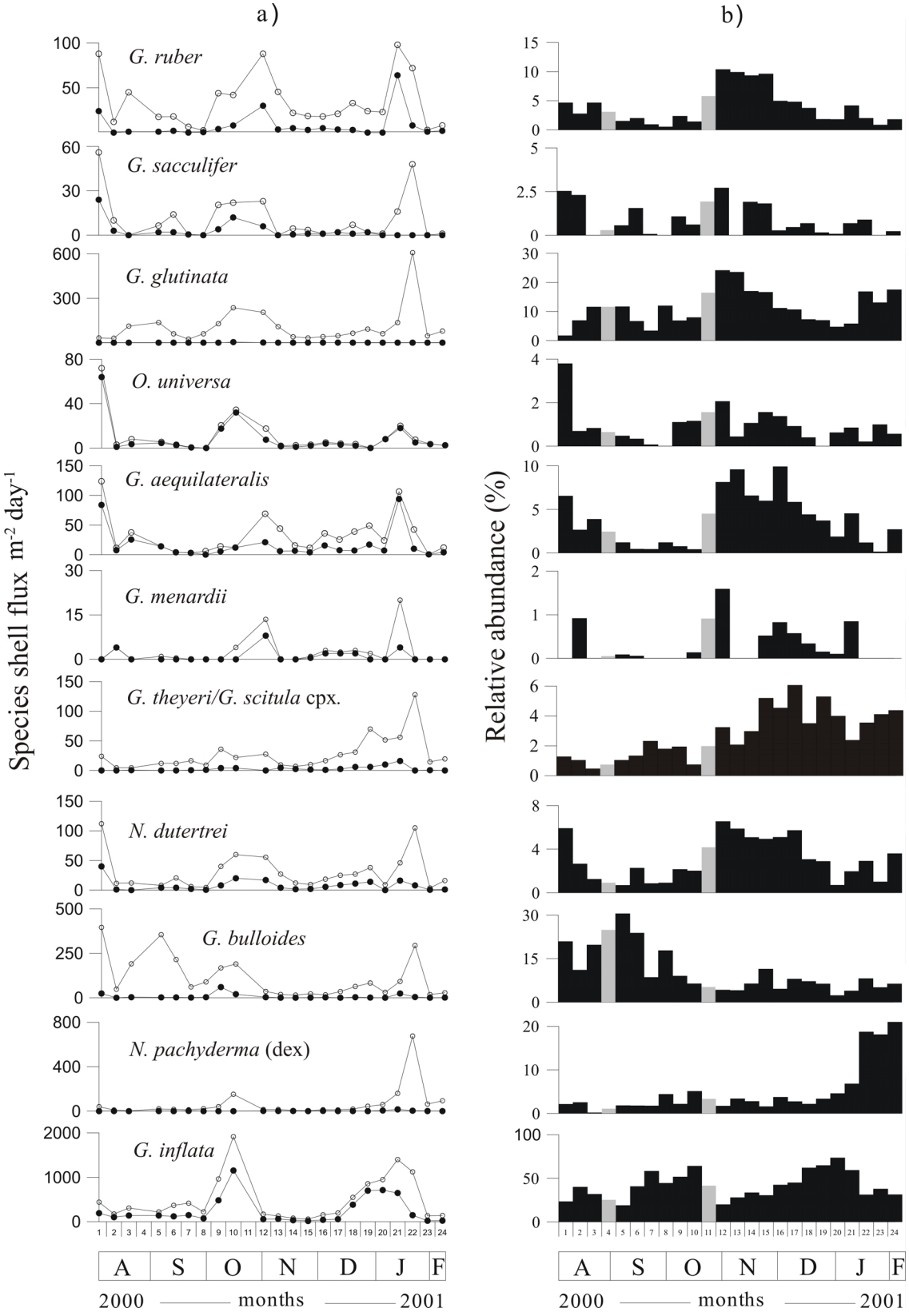

Figure 3.8. Absolute and relative abundance of the eleven most abundant planktic foraminiferal species in sediment trap MST-15 between August 2000 and February 2001. a) The absolute species flux (open dots (> 150 μm) and filled dots (>250 μm), and b) black bars represent relative abundance (%) of species >150 μm. The gray bars represent the estimated fluxes of the neighboring cups.

Figure 3.9 shows the differences in species composition and relative abundance at two characteristic hydrographic situations during the trap period. In sample-cup #12 the flux was only 849 specimen $m^{-2}day^{-1}$, while in sample #10 the flux was three times higher (3000 specimen $m^{-2}day^{-1}$). Because *G. inflata* strongly dominates the assemblage in sample-cup #10 (~65%) the species diversity (*H`*) and equitability (*E`*) were lower compared to sample cup #12. Compared to sample #10, the faunal assemblage in sample #12 is characterized by high relative abundances of tropical-subtropical species.

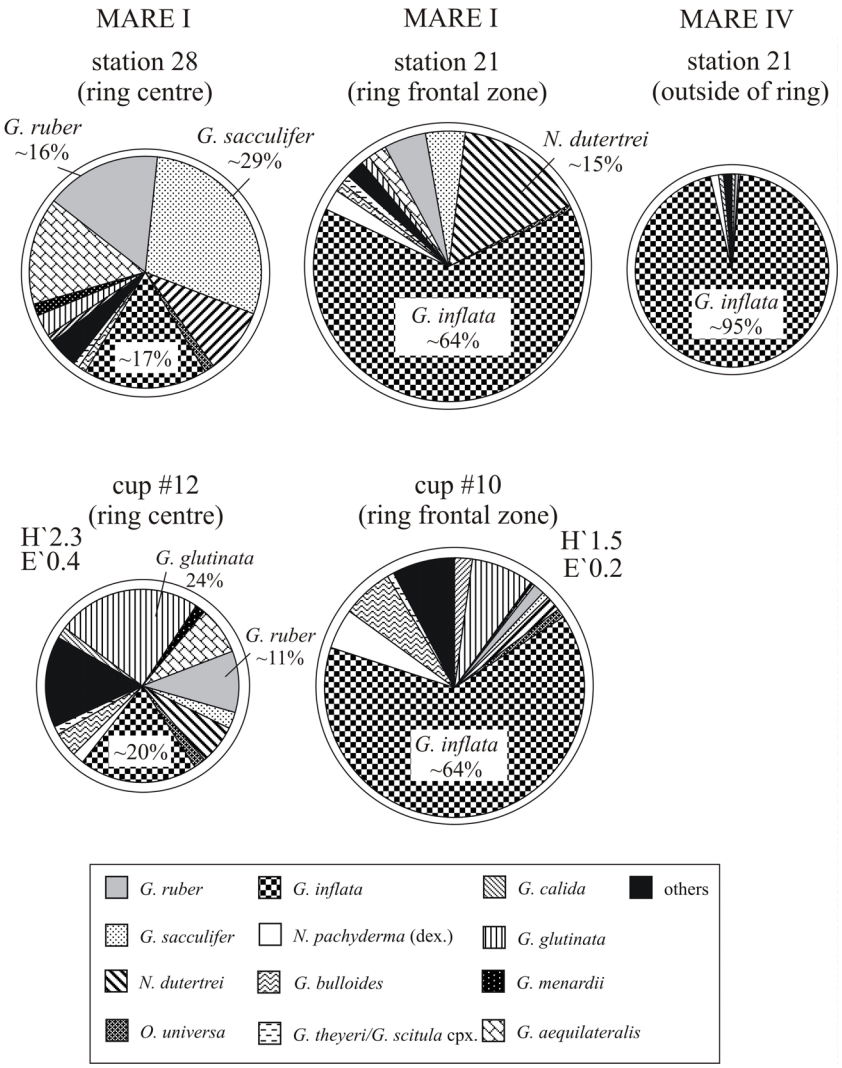

Figure 3.9. The faunal composition in selected plankton tow and sediment trap samples. In the upper row three examples of the faunal composition in plankton tow samples (0-800m integrated) taken at the centre of the ring, station 28 (MARE I), at the ring frontal zone, station 21 (MARE I), and outside of the ring, station 21 (MARE IV) are shown. In the lower row two examples of the faunal composition from sediment trap MST-15, indicative for the centre of an Agulhas ring (cup #12) and its frontal zone (cup #10). Surface area of circles is proportional to integrated standing stock or, for the trap samples the total shell flux (849 specimen m^{-2} day^{-1} in cup #12 and 2989 specimen m^{-2} day^{-1} in cup #10). It appears that the ring frontal zones produce highest standing stocks and shell fluxes.

3.5.3.2 Plankton tows

Based on the altimetry information, the upper water column from different sections of an Agulhas ring "Astrid" and its surrounding area was sampled by using depth-stratified plankton tows during different MARE cruises between February 2000 and March 2001 (Fig. 3.9). Station 28 was located in the centre of the ring (van Aken et al., 2003), while station 21 was located near the ring boundary, *i.e.* at its frontal zone (both February 2000, MARE 1). As opposed to this the third station, 21, sampled during MARE IV in February 2001 represents a station located outside of ring "Astrid". The upper diagrams in Figure 3.8 mirror the differences of planktic foraminifera concentration and species composition between the three stations. The average shell concentrations (0-200 m) are highest at station 21 (MARE I, ring frontal zone), followed by station 28 (MARE I, ring centre) and station 21 (MARE IV, no ring). The faunal composition at plankton tow station 21 (MARE IV), which were not influenced by Agulhas waters, is strongly dominated by *G. inflata* (~96%), and with trace amounts, <2% of *G. bulloides* and *N. pachyderma* (dex.). Warm-water species were virtually absent at this station that is located far from the "area of influence" from waters from the Agulhas Current. This observation is further evidence that tropical and subtropical species in the Cape Basin exclusively reflect the Agulhas waters from the Indian Ocean. As opposed to this tropical-subtropical species were more abundant at station 28 (MARE I) which was located in the centre of Agulhas ring "Astrid" studied in February 2000. However, high amounts of tropical-subtropical species were also found at station 21 (MARE I) located at the ring frontal zone, with *G. inflata* being the dominant species with ~64% (Fig. 3.9).

3.5.4 Stable isotopic composition of foraminiferal shells

3.5.4.1 The oxygen isotope composition

The $\delta^{18}O$ composition of *G. ruber, G. glutinata, N. dutertrei, G. bulloides, N. pachyderma* (dex.), *G. aequilateralis, G. inflata and G. theyeri/G. scitula* cpx. is given in Appendix B and shown in Figure 3.10.

Since the temperature at the sea surface is higher than in deeper waters, the $\delta^{18}O$ of the shallow living species can be expected to be lower than that of deep living species. The $\delta^{18}O$ values thus roughly (not considering vital effects corrections) reflect the depth habitat ranking of species in the water column, with *G. ruber, G. glutinata* and *G. bulloides* being the shallowest dwellers, followed by *G. aequilateralis, N. dutertrei, N. pachyderma* (dex.), *G. inflata and G. theyeri/G. scitula* cpx. (Figs. 10 and 11).

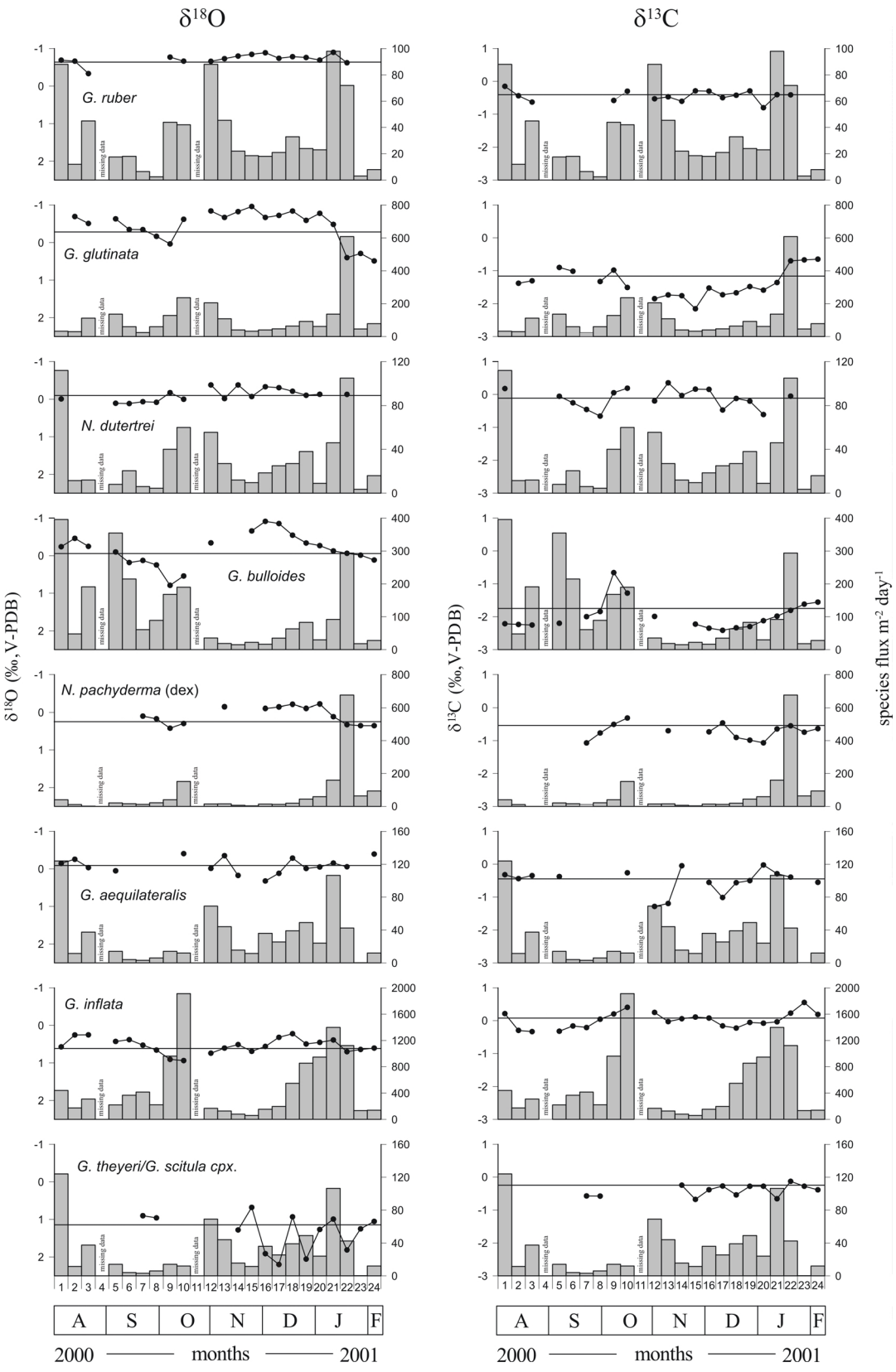

Figure 3.10. The oxygen and carbon isotopic composition of eight species in trap MST-15. The horizontal black lines indicate the flux weighted isotopic composition for the trap (using samples where an isotope measurement was done). Note that the $\delta^{18}O$ axis is reversed.

The observed ranges and flux weighted mean values of the $\delta^{18}O$ values of different species are given in Figure 3.12 and Table 3.2. The $\delta^{18}O$ shows a total range of 3.16‰ corresponding to a temperature range of more than 14°C. A minimum flux weighted mean value of –0.96‰ are shown by *G. glutinata* and a maximum value of +2.20‰ by *G. theyeri/G. scitula* cpx..

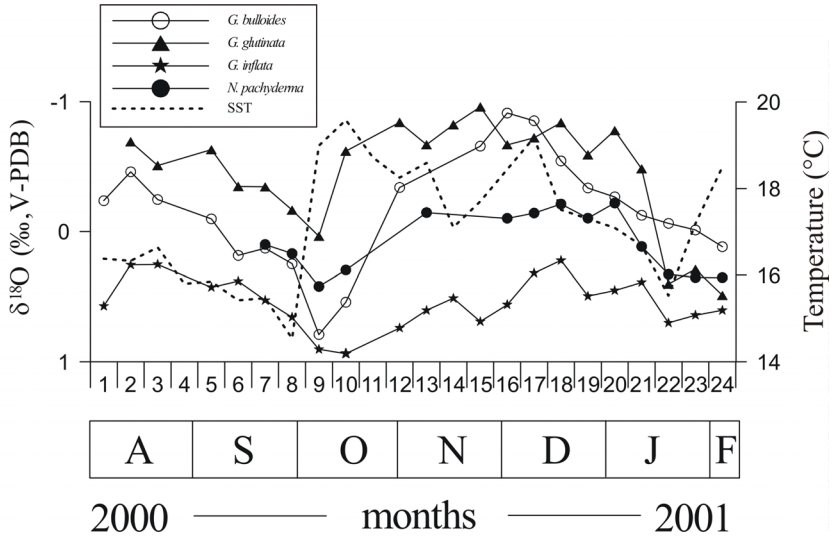

Figure 3.11. A detailed consideration of the oxygen isotopic composition of the four "South Atlantic species" *G. bulloides, G. glutinata, G. inflata* and *N. pachyderma*. The dashed line indicate the SST data at the MST-15 trap site location.

The lowest flux weighted oxygen isotope values are observed for the shallow dwelling species *G. ruber, G. glutinata* and *G. bulloides*. The oxygen isotope range, however, is low for *G. ruber* (0.57‰) and high for *G. glutinata* (1.45‰) and *G. bulloides* (1.70‰). These ranges corresponds to a temperature range of 2.6°C, 6.6°C and 7.7°C, respectively. The temperature range *of G. glutinata* and *G. bulloides* agrees well with the observed sea surface temperature range during the time series (Fig. 3.5). Apparently, the lower sea surface temperatures are not reflected in the oxygen isotope composition of *G. ruber*. Changes in the oxygen isotope composition of both, *G. glutinata* and *G. bulloides*, occur simultaneously. This means highest values are found mid-October 2000 and January 2001, while lowest values are recorded in November 2000 (Figs. 3.10 and 3.11).

Compared to the shallow dwelling species the species *G. aequilateralis, N. dutertrei, G. inflata* and *N. pachyderma* (dex.) show lower flux weighted $\delta^{18}O$ lower isotope variability. The temporal pattern, however, is different. While highest values for *N. pachyderma* (dex.) and *G. inflata* are recorded in October 2000 and January 2001 when shell fluxes are highest, according to *G. glutinata* and *G. bulloides*, these maxima are not recorded in *N. dutertrei* and *G. aequilateralis*.

Lowest oxygen isotope values are observed in the deep dwelling species *G. theyeri/G. scitula* cpx..

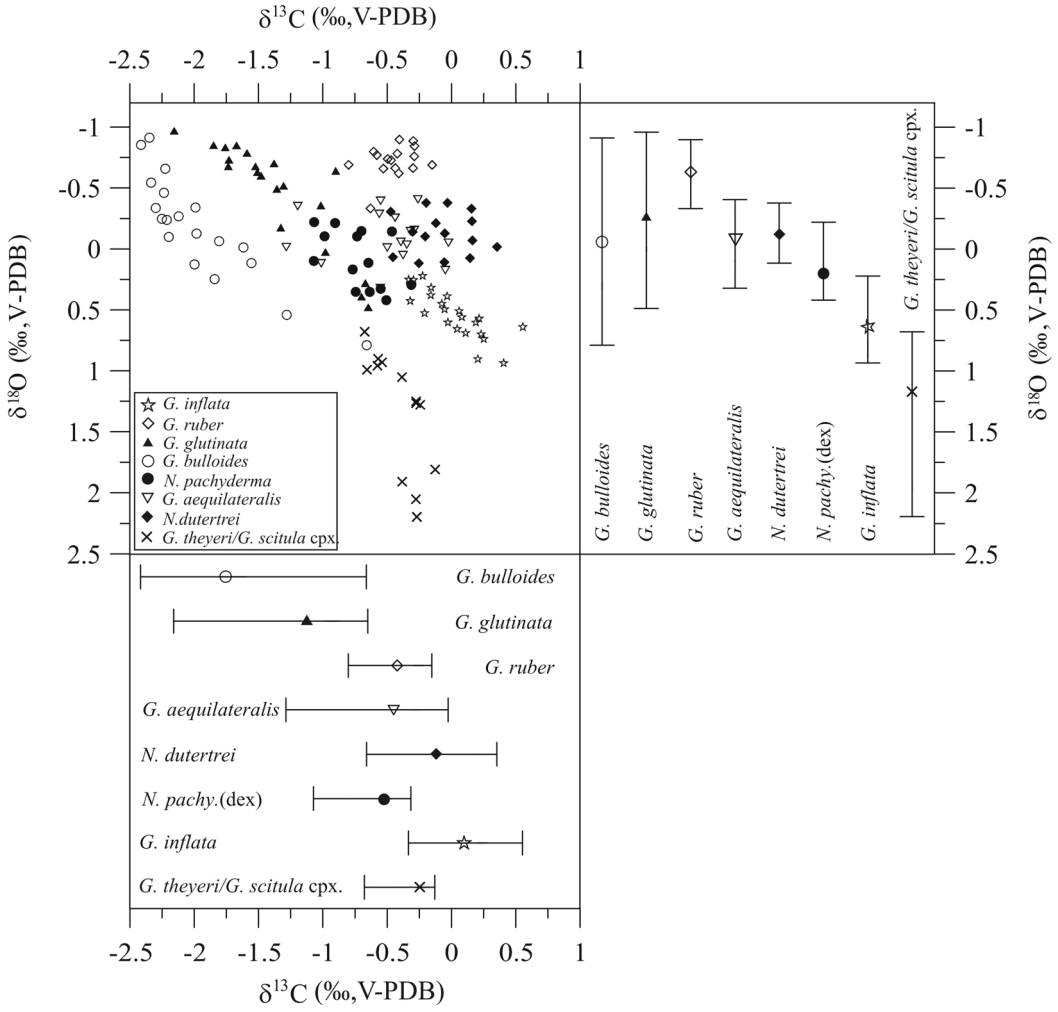

Figure 3.12. A $\delta^{13}C$ vs. $\delta^{18}O$ scatter plot of the isotopic composition of several species in MST-15. On the right hand site of the scatter plot the total range and flux weighted mean of the $\delta^{18}O$ of each species is given. Below the same is done for the $\delta^{13}C$. The $\delta^{18}O$ exhibits a total range of 3.16‰, which corresponds to a temperature range of ~14.3°C. The $\delta^{13}C$ exhibits a total range of 2.96‰. The $\delta^{18}O$ values rank roughly rank the species relatively in depth, shallowest *G. ruber, G. bulloides* and *G. glutinata*, followed by *G. aequilateralis, N. dutertrei, N. pachyderma* (dex.), *G. inflata* and *G. theyeri/G. scitula* cpx..

In general, the weighted $\delta^{18}O$ and $\delta^{13}C$ values of most species fall near the middle of their total range. An exception to this observation are the weighted $\delta^{18}O$ and $\delta^{13}C$ values of *N. pachyderma* (dex.) which are shifted to the maximum isotopic values. The flux of *N. pachyderma* (dex.) is low during intervals when its $\delta^{18}O$ and $\delta^{13}C$ is low, hence its weighted average is slightly shifted to the maximum observed value. The weighted $\delta^{18}O$ of *G. theyeri/G. scitula* cpx. is nearly identical to its minimum observed $\delta^{18}O$ value while its $\delta^{13}C$ is nearly identical to its maximum observed $\delta^{13}C$ value.

3.5.4.2 The carbon isotope composition

Flux weighted average carbon isotope composition are low for the species *G. bulloides* (-1.75‰) and *G. glutinata* (-1.18‰), while the average carbon isotope values of the other species *G. ruber*, *G. aequilateralis*, *N. dutertrei, N. pachyderma* (dex.), *G. inflata* and *G. theyeri/G. scitula* were higher and range between –0.55 and +0.08‰ (Figs. 12, Table 3.2).

Compared to their flux weighted average carbon isotope value, the species *G. bulloides, G. glutinata* and *G. aequilateralis* have relatively low values between October/November 2000 and the second week of January 2001 (samples 12 to 21) (Figs. 10 and 11). A distinct temporal pattern in the carbon isotopic composition in the other species is not observed, except for *G. inflata* which clearly shows maxima in October 2000 and in the end of January (cup 10 and 23) (Figs. 10 and 11), and for *N. dutertrei,* which shows lower carbon isotope values between late October/early December 2000 compared to its flux weighted average carbon isotope value. Surprisingly, the high temporal variability observed in the oxygen isotope composition for *G. theyeri/G. scitula* cpx., is not visible in the carbon isotope record.

The species *G. inflata* (r^2=0.65), *G. glutinata* (r^2=0.78), *G. bulloides* (r^2=0.77) and *G. theyeri/scitula* cpx. (r^2=0.53) show a positive correlation between $\delta^{18}O$ and $\delta^{13}C$, while the species *G. ruber, N. dutertrei, G. aequilateralis* and *N. pachyderma* (dex.) (r^2 <0.3) are only moderate correlated (Fig. 3.12).

Table 3.2. Comparison of weighted average isotopic composition with minimum and maximum observed $\delta^{18}O$ and $\delta^{13}C$ values for different species for the MST-15 sediment trap deployment

Species	$\delta^{18}O$			$\delta^{13}C$		
	minimum	maximum	Flux-weighted	minimum	maximum	Flux-weighted
G. ruber	-0.90	-0.33	-0.63	-0.80	-0.15	-0.40
G. glutinata	-0.96	+0.49	-0.27	-2.16	-0.65	-1.18
G. bulloides	-0.91	+0.79	-0.05	-2.41	-0.66	-1.75
N. dutertrei	-0.38	+0.12	-0.13	-0.47	+0.35	-0.12
G. aequilateralis	-0.41	+0.32	-0.09	-1.28	-0.02	-0.42
N. pachyderma (dex)	-0.22	+0.42	+0.09	-1.07	-0.31	-0.55
G. inflata	+0.22	+0.94	+0.61	-0.33	+0.55	+0.08
G. theyeri/G. scitula cpx	+0.68	+2.20	+0.91	-0.68	-0.13	-0.21

3.6 Discussion

3.6.1 Settling velocities

Along with the transport of warm Indian Ocean water into the South Atlantic Ocean via Agulhas leakage, it can be expected a characteristic Indian Ocean fauna reaches the waters

south of Africa and possibly those of the Southern Benguela System. The foraminifera collected by the sediment trap MST-15 in the Cape Basin may provide information on this process. Obviously, some time is needed for the foraminiferal tests to reach the sediment trap at 3500 m water depth. Estimates of settling velocities of planktic foraminiferal shells in the water column (Takahashi and Bé, 1984) suggest that shells of size >150 μm, depending on the shell weight and presence or absence of spines, sink between 300 to 1000 m day^{-1}. It thus should be taken into account that the flux record lags the hydrographic observation, SSH and SST, roughly by one to two weeks.

3.6.2 Agulhas rings and associated planktic foraminiferal fluxes

A number of positive SSH anomalies are identified that could be traced confidently through time for the entire six month sediment trap sampling period. Obviously, not all SSH anomalies identified contributed to the foraminiferal fluxes intercepted by trap MST-15. As the general flow direction of waters in the upper 1500 m is westwards, it is not likely the trap intercepted material originating from hydrographic conditions west of the trap site. The SSH analysis suggests that the hydrographic features associated with ring "A" and "Y" and their surrounding waters determined the foraminiferal fluxes through the time series (Figs. 3.3 and 3.4). Evidence exists that Agulhas rings may merge and split, which leads to rapid mixing of Agulhas and Southeast Atlantic waters (Arhan et al., 1999; Boebel et al., 2003a; de Steur, 2005; Donners et al., 2004), a process that increases the mixing of faunal assemblages associated with the different water masses. For this reasons it is critical to indicate the exact position of an Agulhas ring with respect to the trap site.

In-between the two shell flux maxima in October 2000 (first maximum) and January 2001 (second maximum) (Fig. 3.5) the SST were relatively high. In the beginning of October 2000, the SST increased from 14.5°C to 19.6°C within one to two weeks. This rapid increase can only be explained by warmer Agulhas water above the trap site, and is unlikely to result from the gradual summer warming. Based on our SSH analysis we found that a filament of Agulhas ring 'A', in early to mid October 2000, followed by Agulhas ring 'Y' from late October until late November 2000, were the dominant hydrographic features above the trap site. Consequently, the relatively high SST's in October and November 2000 are the result of two Agulhas rings above the trap site. Furthermore, our SSH images indicate that ring 'Y' moved over the trap site in a western direction between mid-October and mid-November 2000. During this time the highest relative abundance of tropical-subtropical species were

collected, while shell fluxes were low. These observations indicate that the increase in the relative abundance of tropical–subtropical species must be related to the centre of the warm Agulhas ring 'Y' moving over the trap site. The faunal signal that originated from ring 'Y' was recorded in sample cups #12 to #15, taken into account the lag of one to two weeks for the foraminiferal shells to reach the trap. This means that the species *G. ruber*, *G. sacculifer, G. aequilateralis, O. universa, G. menardii, N. dutertrei* and *G. glutinata* are transported into the South Atlantic Ocean by the Agulhas Current. The increase of tropical-subtropical species, however, is accompanied by lowest absolute and relative abundance of *G. inflata*, *N. pachyderma* (dex.) and *G. bulloides,* which are thus not part of the Agulhas assemblage.

As we have discussed above, the high SST's appeares to be related to the presence of Agulhas rings above the trap site. Obviously, the periods of highest total fluxes in mid-October 2000 and mid-January 2001 are likely related to a different hydrographic situation above the trap site. The most abundant species associated with these maxima are *G. inflata*, *G. bulloides, G. glutinata* and *N. pachyderma* (dex.), although tropical-subtropical species are present as well. The high shell flux in cup #10 must be related to a hydrographic situation that was present above the trap site between end-September and early-October 2000. It is unlikely that ring 'A' and 'Y' have significantly affected the foraminiferal fluxes during this time (ring 'A' is moving west while 'Y' is still at a position of 19°E). Therefore, the SSH images suggest that the waters represented by the negative SSH anomalies and the filament of ring 'A', between ring 'A' and 'Y', predominantly controlled the foraminiferal fluxes. This situation may be described as transitional, *i.e.* mixed waters of Atlantic and Indian origin. The low SST during end-September and early-October 2000 and early to mid-January 2001 are indicative for mixing, as becomes apparent by shallower isotherms near the ring frontal zones (Fig. 3.2). We therefore suggest that the higher shell flux must be due to highly dynamic situations at the ring frontal zones. This causes an entrainment of nutrient-rich deeper waters to the euphotic zone at the ring boundary resulting in an increase in biological production and thus shell fluxes.

Furthermore, highest amounts of resuspended material were recorded simultaneously with the shell flux maxima in mid-October 2000 and mid-January 2001. Obviously an increase of the resuspended fraction is the result from an increase in bottom current velocities. Since there is evidence that Agulhas rings may extend down to a depth of 4500 m (Gordon et al., 1987; van Aken et al., 2003) and that the angular velocities are lowest in the ring centre and increase toward the boundary of the ring, we believe that this is further support that the highest shell fluxes are related to the dynamic conditions at the frontal zones of the rings.

The characteristic increase of the species *G. inflata* in frontal zone conditions is well in line with previous investigations which show that the species are associated with the water masses of the southern subtropical to subantarctic zones and typically proliferates in frontal environments (Schiebel et al., 2001). The species *G. bulloides* and *N. pachyderma* (dex) are also associated with the colder subantarctic and transitional water masses close to the Sub Tropical Convergence (STC) (e.g. Bé and Tolderlund, 1971; Mortyn and Charles, 2003; Niebler et al., 1999). The species *G. glutinata* has a broad latitudinal distribution, *i.e.* from tropical to subpolar regions (Bé and Tolderlund, 1971). Although *G. glutinata* is related to waters from the Indian Ocean, this species proliferates also in waters of the transitional and subtropical zones of the South Atlantic.

The exchange of "end-member" foraminiferal assemblages, *i.e.* of Indian and Atlantic origin, may take place through a process proposed by Donners et al.(2004) in a modeling study. These authors show that the surrounding waters may be drawn into the ring at a depth of roughly 150 m, well-up within the ring and flow back outwards near the surface (overturning cell). This suggests that the South Atlantic species may be transported into the ring and its boundaries, such as *G. inflata*, while Indian Ocean species may be transported to the ring edges. Since it has been detected that a part of the waters from the Cape Basin or from the STC may be included into the ring in a very early stage (Lutjeharms, 1996), we hypothesize that *G. inflata,* and other South Atlantic species may be transported into the ring directly after it is spawned from the retroflection.

Our sediment trap results are supported by a series of plankton tows, which provides the opportunity to relate water column observations to the settling flux for different parts of an Agulhas ring. Hence, based on a six-months time-series sampling of foraminiferal flux combined with a series of plankton tows, we clearly identified the following species to be characteristic for a typical Agulhas fauna (AF): *G. ruber, G. sacculifer, G. aequilateralis, N. dutertrei, O. universa* and *G. menardii.* Their occurrence in the southeastern South Atlantic thus must be explained predominantly by the advection of Indian Ocean water via Agulhas rings or direct Agulhas leakage (Fig. 3.13 and Table 3.3). The species *G. inflata*, *G. bulloides* and *N. pachyderma* (dex.) are not part of the Agulhas fauna, as they are associated with the Atlantic waters. The presence of the species *G. glutinata* in the Cape Basin reflects specimens from two "sources": 1) a fraction of the population is representing the Indian Ocean advection (brought along with the Agulhas water), while 2) another part of the population reflects specimens that are living in the Atlantic waters, and thus are produced locally. (Fig. 3.13). We summarized the characteristic living planktic foraminiferal faunas corresponding to the main Indian-Atlantic

hydrographic features. These results are a composition of our own data based on sediment trap MST-15 and plankton tows, and complemented by previous investigations of other authors (see Table 3.3).

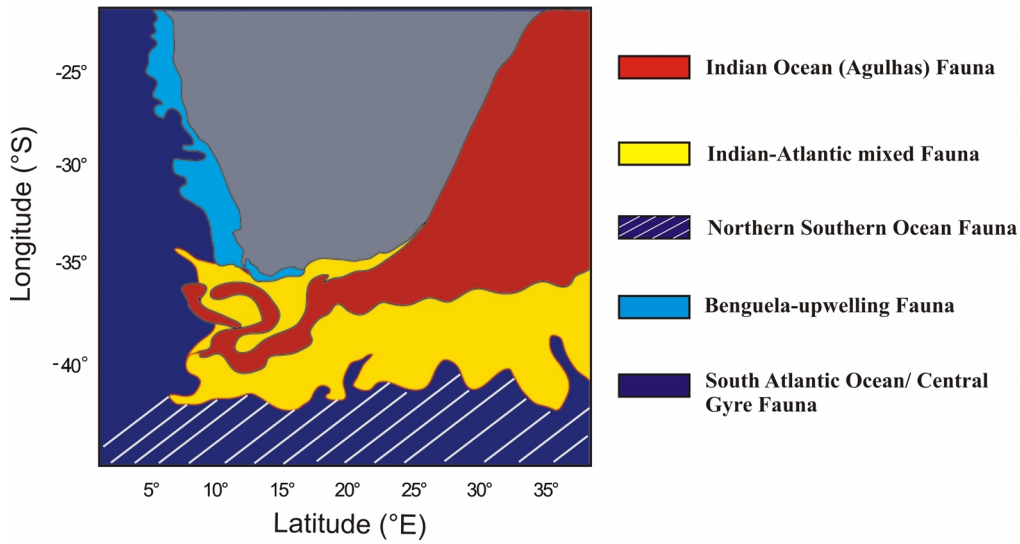

Figure 3.13. Summarized distribution of living planktic faunal assemblages south of Africa in relation to the main Indian-Atlantic hydrographic features.

Table 3.3. Summary of foraminiferal fauna (main species) associated with the main Indian-Atlantic hydrographic features

Fauna	***Main species***	References
Indian Ocean (Agulhas)	*G. ruber, G. sacculifer, G. aequilateralis, N. dutertrei, O. universa, G. menardii, G. glutinata* *G. ruber, G. sacculifer, G. glutinata* *G. hexagona* *G. menardii*	This work (Bé and Hutson, 1977), (Hutson, 1980), (Peeters et al., 2004) (Berger and Wefer, 1996), (Rau et al., 2002)
Indian-Atlantic mixed	*G. inflata, G. bulloides, G. glutinata, N. pachyderma* (dex.), *G. ruber, G. sacculifer, G. aequilateralis, N. dutertrei, O. universa, G. menardii*	This work
Northern South Atlantic Ocean	*N. pachyderma* (sin.), *G. quinqeuloba, G. bulloides, N. pachyderma* (dex.), *G. inflata*	(Bé and Tolderlund, 1971), (Niebler and Gersonde, 1998)
Benguela-upwelling	*N. pachyderma* (dex.), *N. pachyderma* (sin.), *G. bulloides*	(Bé and Tolderlund, 1971), (Oberhänsli et al., 1992), (Giraudeau, 1993), (Ufkes et al., 1998)
Benguela Current/ subtropical Central Gyre	*G. sacculifer, G. bulloides, G. inflata, O. universa, N. dutertrei*	(Bé and Tolderlund 1971), (van Leeuwen, 1989), (Oberhänsli et al., 1992) (Giraudeau, 1993), (Ufkes et al., 1998)

3.6.3 The isotopic composition

3.6.3.1 Oxygen isotopes

The oxygen isotopic composition of different species was measured in order to investigate their potential use as indicators of the process of Indian-Atlantic water exchange south off Africa. We found a remarkable resemblance between the SST data and the oxygen isotopic composition of *G. glutinata*. This indicates that this species accurately records the SST of the different water masses, *i.e.* the Indian, Atlantic or mixed waters. The rapid increase of the SST in end-September and in the beginning of October 2000 (from 14.5 to 19.6°C) is best recorded in the oxygen isotopic composition of *G. glutinata*, and allows to estimate directly the time associated with settling: one to two weeks. This independent observation agrees well with our estimated lag from settling velocities. Furthermore, also the decline in the SST data from mid-December 2000 to mid-January 2001 (sample #22) is well recorded in the oxygen isotopic composition of *G. glutinata*. This observation is further evidence that this species is characteristic for both, Indian and Atlantic water masses. If converted to temperature, the difference of $\delta^{18}O$ between cup #9 and #12 is ~5°C, which is in perfect agreement with the observed SST difference between the two cups. We also found a good relationship between SST data and the oxygen isotopic composition of *G. bulloides*. Although, the fluxes of *G. bulloides* are very low when Agulhas ring 'Y' was above the trap site in November 2000, the lower oxygen isotope values suggest that these specimens of *G. bulloides* recorded the higher temperatures within the Agulhas ring. Its oxygen isotopic composition is therefore considered to well reflect the SST of Atlantic, Indian and mixed Indian-Atlantic waters.

As discussed above the shallow-dwelling species *G. ruber*, *N. dutertrei* and *G. aequilateralis* are associated with the Agulhas waters. This is well reflected in a relatively constant oxygen isotopic composition of these species throughout the record, indicating that the temperature variability of the Agulhas waters was very low. The rapid temperature increase in early October 2000 is not reflected in the species' $\delta^{18}O$ record, providing evidence *G. ruber, G. aequilateralis* and *N. dutertrei* indeed are predominantly calcifying within water associated with the Indian Ocean.

The analysis of the SSH images shows that the flux record of both, *G. inflata* and *N. pachyderma* (dex.), reflect the Atlantic to mixed Indian-Atlantic waters. The flux weighted mean value of both species is higher compared to *G. glutinata, G. ruber* and *G. bulloides*, suggesting a deeper habitat. The trend in the oxygen isotope record of these species mirrors the SST trend with an offset and with lower variability. In the frontal zone, *i.e.* reflected in samples #9 and #22, the difference in the oxygen isotopic composition between *G. bulloides* and *G. inflata* is

small, while this difference increases when both species, although low in abundance, calcified in the ring as in November 2000 (samples #12 to #15). These observations suggest that in the ring frontal zone, *i.e.* where Indian and Atlantic waters mix and isotherms move up (samples #9 and #22), both species calcify in similar water depth and thus temperatures (Fig. 3.11).

Since stronger variations in isotopic composition can be observed for the South Atlantic species *G. bulloides*, *G. glutinata, G. inflata* and *N. pachyderma* (dex.), we suggest that these species must be more tolerant to changing water properties compared to the tropical-subtropical Indian Ocean species, such as *G. ruber* or *G. aequilateralis* and *N. dutertrei*. It is possible that these species, which are transported from the Indian Ocean via Agulhas leakage, stop calcifying when they are drawn into the "new" and colder environment.

3.6.3.2 Carbon isotopes

We observed a positive correlation between $\delta^{13}C$ and $\delta^{18}O$ for *G. glutinata, G. bulloides* and *G. inflata*. Increased $\delta^{13}C$ values of the species *G. bulloides*, *G. glutinata* and *G. inflata* are found simultaneously to increased $\delta^{18}O$ values in October 2000 and January 2001. As discussed above, these periods are characterized by low SST data and highest shell flux associated with ring frontal mixing of Atlantic and Indian Ocean waters. Furthermore, these species record lower $\delta^{13}C$ values when warmer, oligotrophic Indian Ocean waters where located above the trap site and the total shell flux was low (November/early December 2000). This indicates that the carbon isotopic composition of *G. bulloides, G. glutinata* and *G. inflata,* is influenced by the changing temperature (and, potentially the lower carbonate ion concentration ($[CO_3^{2-}]$)) during the time series. This further suggests that they do not record the lower carbon isotope values of the total dissolved inorganic carbon ($\delta^{13}C_{DIC}$), which is expected to well up during mixing at the ring frontal zones. It has been well quantified for the species *G. bulloides* that lower temperature (and lower $[CO_3^{2-}]$) are known to increase the $\delta^{13}C$ of *G. bulloides* (Bemis et al., 2000; Spero et al., 1997). Apparently, the observed variations in $\delta^{13}C$ of *G. glutinata,* and *G. inflata* are inversely related to temperature as well. Higher SST, as in November 2000, may increase the respiration rate and hence the amount of incorporated metabolic CO_2 increases. This effect of low metabolic $^{12}CO_2$ on the $\delta^{13}C$ of foraminiferal carbonate has been documented previously for other species (Ortiz et al., 1996; Ravelo and Fairbanks, 1995; Spero and Lea, 1996).

The flux record and the oxygen isotopic composition showed that *N. pachyderma* (dex.), reflects Atlantic and mixed Indian-Atlantic waters. Although the correlation between the $\delta^{13}C$

and $\delta^{18}O$ for this species were only moderate, the trend in the carbon isotope record of *N. pachyderma* (dex.) mirrors the pattern observed for the three other South Atlantic species *G. inflata, G. bulloides* and *G. glutinata*, however, with lower variability.

The relatively constant oxygen isotopic composition of *N. dutertrei* indicated that this species predominantly calcifies within waters associated with the Indian Ocean, while its carbon isotopic composition is shifted to higher values when warmer Indian Ocean waters moved over the trap site, as observed in November 2000. This indicates that the concept of temperature-dependent "metabolic" fractionation may not be applicable to all species. We therefore suggest that *N. dutertrei's* $\delta^{13}C$ mirror the higher $\delta^{13}C_{DIC}$, and thus possibly reflects the lower nutrient concentrations of Agulhas waters. Its lower $\delta^{13}C$ values in October 2000 and January 2001 mirror the lower $\delta^{13}C_{DIC}$ values (and thus higher nutrients concentrations) at the ring frontal zones, due to mixing and upwelling of deeper, $\delta^{13}C$-depleted, water masses. This indicates that the species *N. dutertrei* seems to be a reliable recorder of the $\delta^{13}C_{DIC.}$ This is in agreement with previous findings (Mulitza et al. (1999), indicating that the carbon isotopic composition of *N. dutertrei* exhibits a constant and temperature-independent off-set from $\delta^{13}C_{DIC}$ of ~0.5‰ over a wide temperature range. The carbon isotopic composition of other Agulhas species, such as *G. ruber* and *G. aequilateralis*, is relatively constant, confirming the observations that these species predominantly calcify within Agulhas water.

3.7 Conclusion

Our results indicate that the Indian-Atlantic water mass communication affect the planktic foraminiferal species composition, abundance, and the stable isotopic composition of their calcite shells. The most important conclusions that can be drawn from this study are:

Agulhas leakage increases the species diversity in the Cape Basin: tropical-subtropical Indian Ocean planktic foraminifera species are transported into the Cape Basin via the Agulhas Current. The species *Globigerinoides ruber, Globigerinoides sacculifer, Globigerinella aequilateralis, Neogloboquadrina dutertrei, Orbulina universa, Globorotalia menardii* and *G. thyeri/G. scitula* cpx. appear characteristic for modern Agulhas rings. The species *Globorotalia inflata, Neogloboquadrina pachyderma* (dex.) and *Globigerina bulloides* are not part of the Agulhas fauna and are considered to reflect predominantly the South Atlantic waters. In the Cape Basin, the species *Globigerinata glutinata* is characteristic for both Indian and Atlantic waters. The most dominant species during the 6-months record is the South Atlantic species *G. inflata*. Although this species dominates the foraminiferal assemblage "inside" and "outside" the ring, the fluxes

associated with the centre of an Agulhas ring are relatively low. We conclude that 'young' Agulhas rings already contain water of Atlantic origin. As such, water exchange must occur between the ring waters and surrounding waters.

We found a relationship between the shell flux record and satellite derived sea surface height and temperature indicating that high shell flux must be due to highly dynamic mixing conditions near the ring frontal zones. This is associated with mixing of waters of Atlantic and Indian origin at the ring boundaries which causes an entrainment of nutrient-rich from deeper waters to the euphotic zone resulting in an increase in biological production and thus shell fluxes. Relatively low fluxes are associated with the oligotrophic waters of the centre of Agulhas rings above the trap site.

The sea-floor resuspended material found in our flux record, implies that the dynamics of the Agulhas hydrography may affect sea-floor processes down to at least 3.5 km. This supports the observations that the highest fresh shell fluxes are related to the dynamic conditions at the frontal zones of the rings, where Atlantic and Indian Ocean waters mix.

We have demonstrated that planktic foraminifera species respond quickly to changes in surface water hydrography. Specifically, the similarity between the oxygen isotopic composition of *G. glutinata* and SST data suggests that this species accurately record the SST of the different water masses, *i.e.* the Indian, Atlantic or mixed waters, above the trap site. We also found a reasonable correlation between SST data and the oxygen isotopic composition of South Atlantic species *G. bulloides, G. inflata* and *N. pachyderma* (dex.). The carbon isotope values of these species may show a temperature influence through its effect on metabolic rate, while the species *N. dutertrei* exhibit no temperature-dependence. Its carbon isotopic composition is considered to reflect the higher carbon isotopic composition of nutrient-poor Agulhas water above the trap site.

Our results yield several opportunities for the development of proxies that may prove useful the reconstruction of the relative position of the Sub Tropical Convergence (STC) and the history of Agulhas leakage. The species diversity could be an excellent proxy for long term changes and/or intensity of Indian Ocean advection. Further, the absence of tropical and subtropical species could also be an indicator for the reduction or shut down of the Agulhas leakage during glacial times as proposed earlier (Peeters et al., 2004).

Acknowledgments: We thank the captain and crew of R/V Pelagia and R/V Agulhas as well as the Royal NIOZ technicians. The research presented here was made possible through sponsoring by the Deutsche Forschungsgemeinschaft (DFG)/Netherlands Foundation for Scientific Research (NWO) EuroProx program.

References

Arhan, M., Mercier, H. and Lutjeharms, J.R.E., 1999. The disparate evolution of three Agulhas rings in the South Atlantic Ocean. Journal of Geophysical Research, 104(C9): 20,987-21,005.

Bé, A.W.H. and Hutson, W.H., 1977. Ecology of planktonic foraminifera and biogeographic patterns of life and fossil assemblages in the Indian ocean. Micropaleontology, 23: 369-414.

Bé, A.W.H. and Tolderlund, D.S., 1971. Distribution and ecology of living planktonic foraminifera in surface waters of the Atlantic and Indian Ocean. In: B.M. Funnel and W.R. Riedel (Editors), Micropaleontology of the Oceans. Cambridge University Press, London, pp. 105-149.

Bemis, B., Spero, H.J., Lea, D.W. and Bijma, J., 2000. Temperature influence on the carbon isotopic composition of *Orbulina universa* and *Globigerina bulloides* (planktic foraminifera). Mar. Micropalentol., 38: 213-228.

Berger, W.H. and Wefer, G., 1996. The South Atlantic: Present and past circulation. In: G. Wefer, W.H. Berger, G. Siedler and D.J. Webb (Editors). Springer Verlag, Berlin Heidelberg, pp. 363-410.

Boebel, B., Lutjeharms, J.R.E., Rossby, H.T. and Zenk, W., 2003a. The Cape Cauldron: an Agulhas mixing and exchange regime. Deep Sea Research II, 50.

Buzas, M.A. and Gibson, T.G., 1969. Species diversity: benthonic foraminifera in Western North Atlantic. Science, 163: 72-75.

Byrne, D.A., Gordon, A.L. and Haxby, W.F., 1995. Agulhas Eddies: a synoptic view using Geosat ERM data. Journal of Physical Oceanography, 25: 902-917.

Conan, S.M.H. and Brummer, G.J.A., 2000. Fluxes of planktic foraminifera in response to monsoonal upwelling on the Somalia Basin margin. Deep Sea Research II, 47: 2207-2227.

Curry, W.B., Thunell, R.C. and Honjo, S., 1983. Seasonal changes in the isotopic composition of planktonic foraminifera collected in Panama Basin sediment traps. Earth and Planetary Science Letters, 64: 33-43.

de Ruijter, W.P.M. et al., 1999. Indian-Atlantic interocean exchange: Dynamics, estimation and impact. J. Geophys. Res., 104: 20,885-20,910.

de Steur, L., 2005. Stirred, not mixed: A study on the decay of Agulhas rings. Ph.D Thesis. Free University, Amsterdam, The Netherlands, 116 pp.

Donners, J., Drijfhout, S.S. and Coward, A.C., 2004. Impact of cooling on the water mass exchange of Agulhas rings in a high resolution model. Geophysical Research Letters, 31.

Esper, O., Versteegh, G.J.M., Zonneveld, K.A.F. and Willems, H., 2004. A palynogical reconstruction of the Agulhas Retroflection (South Atlantic Ocean) during the Late Quaternary. Global and Planetary Change: 31-62.

Flores, J.-A., Gersonde, R. and Sierro, F.J., 1999. Pleistocene fluctuations in the Agulhas current retroflection based on the calcaeous plankton record. Marine Micropaleontology, 37: 1-22.

Garzoli, S.L., A.L. Gordon, V. Kamenkovich, D. Pillsbury and Ducombe-Rae, C., 1996. Variability and sources of the southeastern Atlantic circulation. J. Mar. Res, 54: 1039-1071.

Giraudeau, J., 1993. Planktonic foraminiferal assemblages in surface sediments from the southwest Africancontinental margin. Mar ine Geology, 110: 47-62.

Gordon, A.L., 1985. Indian-Atlantic Transfer of Thermocline Water at the Agulhas Retroflection. Science, 227: 1030-1032.

Gordon, A.L., 1986. Interocean exchange of thermocline water. Journal of Geophysical Research, 91: 5037-5046.

Gordon, A.L., 1996. Communication between oceans. Nature, 382: 399-400.

Gordon, A.L., 2003. The brawniest retroflection. Nature, 421: 904-905.

Gordon, A.L., Lutjeharms, J.R.E. and Gründlingh, M.J., 1987. Stratification and circulation at the Agulhas retroflection. Deep-Sea Research I, 34: 565-599.

Hemleben, C., Spindler, M. and Anderson, O.R., 1989. Modern Planktonic Foraminifera. Springer Verlag, New York, 363 pp.

Hutson, W.H., 1980. The Agulhas Current During the Late Pleistocene: Analysis of Modern Faunal Analogs. Science, 207: 64-66.

Lutjeharms, J.R.E., 1996. The exchange of water between the South Indian and the South Atlantic. In: G. Wefer, W.H. Berger, G. Siedler and D.J. Webb (Editors), The South Atlantic: Present and past circulation. Springer Verlag, Berlin Heidelberg, pp. 125-162.

Lutjeharms, J.R.E. and van Ballegooyen, R.C., 1988. The Retroflection of the Agulhas Current. J. Phys. Oceanogr., 18: 1570-1583.

Mortyn, G.P. and Charles, C.D., 2003. Planktonic foraminiferal depth habitat and delta ^{18}O calibrations: Plankton tow results from the Atlantic sector of the Southern Ocean. Paleoceanography, 18.

Mulitza, S. et al., 1999. The South Atlantic carbon isotope record of planktic foraminifera. In: G. Fischer and G. Wefer (Editors), Use of proxies in paleoceanography: Examples from the South Atlantic. Springer, Berlin, pp. 427-445.

Niebler, H.S. and Gersonde, R., 1998. A planktic foraminiferal transfer function for the southern South Atlantic Ocean. Marine Micropaleontology, 34: 213-234.

Niebler, H.S., Hubberten, H.W. and Gersonde, R., 1999. Oxygen Isotope Values of Planktic Foraminifera. In: G. Fischer and G. Wefer (Editors), Use of proxies in paleoceanography: Examples from the South Atlantic. Springer, Berlin, pp. 165-189.

Oberhänsli, H. et al., 1992. Planktonic foraminifera as tracers of ocean currents in the eastern South Atlantic. Paleoceanography, 5: 607-632.

Ortiz, J.D., Mix, A.C., Rugh, W., Watkins, J.M. and Collier, R.W., 1996. Deep-dwelling planktonic foraminifera of the northeastern Pacific Ocean reveal environmental control of oxygen and carbon isotope disequilibria. Geochim. Cosmochim. Acta, 60(22): 4509-4523.

Peeters, F.J.C. et al., 2004. Vigorous exchange between the Indian and Atlantic oceans at the end of the past five glacial periods. Nature: 661-665.

Rau, A.J. et al., 2002. A 450-kyr record of hydrological conditions on the western Agulhas Bank Slope, south of Africa. Marine Geology, 180: 183-201.

Ravelo, A.C. and Fairbanks, R.G., 1995. Carbon isotopic fractionation in multiple species of planktonic foraminifera from core-tops in the tropical Atlantic. Journal of Foraminiferal Research, 25: 53-74.

Schiebel, R., Waniek, J., Bork, M. and Hemleben, C., 2001. Planktic foraminiferal production stimulated by chlorophyll redistribution and entrainment of nutrients. Deep Sea Research I, 48: 721-740.

Shannon, C. and Weaver, W., 1949. The Mathematical Theory of Communication. University of Illinois Press, Urbana, 125 pp.

Shannon, L.V., 1966. Investl Rep. Div. Sea Fish. S. Africa, 58: 22.

Shannon, L.V., 1985. The Benguela ecosystem. 1. Evolution of the Benguela, physical features and processes. In: M. Barnes (Editor), Oceanography and Marine Biology: An Annual Review. University Press, Aberdeen, pp. 1-85.

Shannon, L.V. and Hunter, D., 1988. Notes on Antarctic Intermediate Water around Southern Africa. S. Afr. J. Mar. Res. Sci., 6: 107-117.

Spero, H.J., Bijma, J., Lea, D.W. and Bemis, B., 1997. Effect of seawater carbonate concentration on foraminiferal carbon and oxygen isotopes. Nature, 390: 497-500.

Spero, H.J. and Lea, D.W., 1996. Experimental determination of stable isotope variability in *Globigerina bulloides*: Implications for paleoceanographic reconstruction. Mar. Micropalentol., 28: 231-246.

Takahashi, K. and Bé, A.W.H., 1984. Planktic foraminifera: factors controlling sinking speeds. Deep Sea Research, 31(12): 1477-1500.

Ufkes, E., Jansen, F.J.H. and Brummer, G.J.A., 1998. Living planktonic foraminifera in the eastern South Atlantic during spring: indicators of water masses, upwelling and the Congo (Zaire) River plume. Marine Micropaleontology, 33: 27-53.

van Aken, H.M. et al., 2003. Observations of a young Agulhas ring Astrid during MARE in March 2000. Deep Sea Research II, 50: 167-195.

van Leeuwen, P.J., 1989. Sea-floor distribution and late Quaternary faunal patterns of planktonic and benthic foraminifers in the Angola Basin. Utrecht Micropaleontol. Bull. 38, 287 pp.

Weijer, W., de Ruijter, W.P.M., Sterl, A. and Drijfhout, S.S., 2002. Response of the Atlantic overturning circulation to South Atlantic sources of buoyancy. Global and Planetary Change, 34: 293-311.

CHAPTER 4*

DEPTH INTEGRATED GROWTH OF PLANKTIC FORAMINIFERAL SHELLS PART 1. THE THEORY OF AN OXYGEN ISOTOPE MASS BALANCE MODEL

Frank J.C. Peeters[1] and Iris Wilke[2]

[1]*Afdeling Palaeo-ecologie en Palaeoklimatologie, Faculteit Aard- en Levenswetenschappen, Vrije Universiteit, de Boelelaan 1085, 1081 HV, Amsterdam, The Netherlands*

[2]*Fachbereich Geowissenschaften/MARUM, Universität Bremen, Leobenerstrasse, 28359 Bremen, Germany*

*This chapter is in preparation for submission

4.1 Abstract

The temperature at which planktic foraminifera live is recorded in the oxygen isotope composition of their calcite shells. Shallow dwelling species generally have a lower oxygen isotope composition compared to species that live deeper, and thus at lower temperatures, in the ocean. A straightforward relationship between foraminiferal oxygen isotope composition and depth habitat is obstructed because foraminifera are observed to migrate vertically through the water column during their life cycle. Although large and small specimens of a given species can be found at any depth in the water column, field observations indicate that, on average, smaller, immature and thin walled specimens preferentially dwell shallower than larger, adult and thicker walled specimens. This indicates that, while shell growth continues, the depth habitat increases during the foraminifer life cycle. As a result, the exported oxygen isotope composition of shells is considered to reflect an integrated, mass weighted, oxygen isotope signal over the upper water column depth interval in which specimens live and secrete their calcite.

We here present and discuss a conceptual oxygen isotope mass balance model for depth integrated shell growth of planktic foraminifera. The model assumes that, within the interval in which foraminifera live and grow (the productive zone), there is an uninterrupted increase of shell mass and increasing oxygen isotope composition of a given species with depth in the water column due to growth and wall thickening of their shells. Below the productive zone, however, shell mass and thus oxygen isotope composition do not change, as the specimens here are considered to be part of the pelagic rain of particulate organic matter that settles to the seafloor. The mass development function (MDF) describes the required increase of shell mass with depth in the water column that would be needed to explain the observed oxygen isotope composition of a given species at different depths in the water column, *i.e.* 1) the increasing oxygen isotope composition within the productive zone and 2) the exported and constant oxygen isotope composition in the export zone. Model fits to field data may be used to find potential species-specific MDF's, *i.e.* characteristic depth integrated growth patterns, which can be used to quantify and unravel the relationship between the oxygen isotope composition of different species and thermal structure of the water column.

4.2. Introduction

The stable isotope composition of planktic foraminiferal shells provides an important source of information for the reconstruction of past surface ocean environments. Observations on field-collected foraminifera show that different species live and grow their calcite shells at different depths in the water column. For example some species grow their shells predominantly in the surface mixed layer, while others may dwell near the thermocline or even below (Kahn and Williams, 1981; Hemleben et al., 1989; Ortiz et al., 1996; Simstich et al., 2002). Although a general assignment or classification in terms of depth habitat ('mixed layer', 'thermocline' or 'deep') appears roughly possible for each species, some variability in the species' depth habitat may be observed depending on environmental and/or hydrographic conditions (Fairbanks and Wiebe, 1980; Fairbanks et al., 1982; Ortiz et al., 1995; Peeters and Brummer, 2002; Field, 2004).

Quantification of the foraminiferal depth habitat, its variability and the depth at which shell growth ceases, however, is still an open question in palaeo-oceanography. Knowledge and quantification of their ecological behavior, however, is very useful in the view of the potential application of the stable isotope measurements of multi-species in reconstructions of past upper ocean climate conditions. In this respect, the oxygen isotope composition of the foraminiferal shell provides an important geochemical fingerprint of the ambient seawater temperature and its oxygen isotope composition at which the shell grew.

Since the oxygen isotope ratio of calcite is known to increase with decreasing temperature (Urey, 1947; Kim and O`Neil, 1997), species that live close to the sea surface, *i.e.* within the 'warm' mixed layer, are depleted in ^{18}O compared to shells of species that dwell at greater depths and lower temperatures (Emiliani, 1954; Deuser et al., 1981; Erez and Honjo, 1981; Kahn and Williams, 1981; Hembleben et al., 1985; Peeters et al., 2002). Conversely, the $\delta^{18}O$ of (fossil) specimens may be used to calculate the temperature of the seawater, *i.e.* the temperature at the depth at which calcification took place. Unfortunately, a number of factors often obstruct this 'inverse' approach and thus hamper the straightforward use of the oxygen isotope composition of shells of different species as a proxy for past surface water conditions. The first complicating factor is that different species may have an oxygen isotope composition that is offset from the expected value, the so-called oxygen isotope disequilibrium or 'vital effect' (Kahn, 1979; Niebler et al., 1999). Not correcting for this offset may result in incorrect estimates of the calcification temperature. Second, vertical migration of foraminifera during their life cycle results in test growth at different depths, and thus different $\delta^{18}O_{eq}$, in the water column. As a consequence the oxygen isotope composition of an exported foraminifer shell

($\delta^{18}O_{shell\text{-}export}$) does not reflect the temperature at a single depth level but rather represents the mass weighted equilibrium value over the depth interval of calcification.

Field collected planktic foraminifera provide the unique opportunity to study the isotope composition of the shells in the natural environment. By using depth stratified plankton tows, it is possible to study the pattern of shell densities and change in the species' oxygen isotope composition as a function of depth and temperature in the water column. Comparing the oxygen isotope composition to the expected equilibrium in the surface mixed layer allows precise quantification of 'the vital effect'. Once this is known, the change of the oxygen isotope composition with depth in the water column allows quantification of the depth integrated test growth and definition of the base of the productive zone: *i.e.* the depth at which shell growth ceases.

The main aim of this study is to unravel the depth integrated growth pattern of planktic foraminifera, *i.e.* to detect where foraminiferal calcite is formed and, as a result, how the temperature of the upper water column is reflected in the oxygen isotope composition of different species. We here follow an ecological approach, which means that we take into account the effect of growth during vertical migration of planktic foraminifera that is often observed in the natural environment to take place during the foraminiferal life cycle (Hemleben and Bjima, 1994; Bauch et al., 2002b; Peeters et al., 2002; Peeters and Brummer, 2002; Simstich et al., 2002; Mortyn and Charles, 2003; LeGrande et al., 2004). Here, we discuss and propose a conceptual oxygen isotope mass balance model for depth integrated shell growth of planktic foraminifera. When applied to depth stratified plankton tow field data, by using the oxygen isotope composition of a given species at different depth levels in the water column, the model fits may be used to estimate, or potentially quantify, the growth patterns and calcification ranges of different species. The application of this model proposed here to field data is discussed in a subsequent manuscript (Wilke and Peeters, in prep.).

4.3. Model theory

4.3.1 The productive zone

The productive zone (PZ) for a planktic foraminifer species is defined as that part of the upper water column in which a given species lives and builds its shell (Fig. 4.1). Formerly, the productive zone was defined using shell concentration profiles in the water column (for discussion see Peeters et al., 2002). The method was based on the observation that shell densities are often high in the upper part of the water column, reflecting specimens that are

alive and capable of adjusting their buoyancy (Furbish and Arnold, 1997), and low/lower at greater depths in the ocean, reflecting the pelagic rain of exported dead specimens to the seafloor. The transition between the productive and export zone (EZ), *i.e.* the zone below the PZ, is characterized by the decline in the shell concentration profile and mirrors the base of the productive zone (BPZ). The BPZ is thus considered to reflect, approximately, the depth at which shell growth ceases. As a result, it can be expected that the oxygen isotope composition of a foraminiferal shell increases with depth within the PZ. In the EZ, however, the oxygen isotope composition of exported specimens is expected to be approximately constant since no additional calcite is formed here. It should be noted, however, that non-biotic processes, such as secondary calcification or carbonate dissolution, might affect the isotopic composition of shells within the EZ.

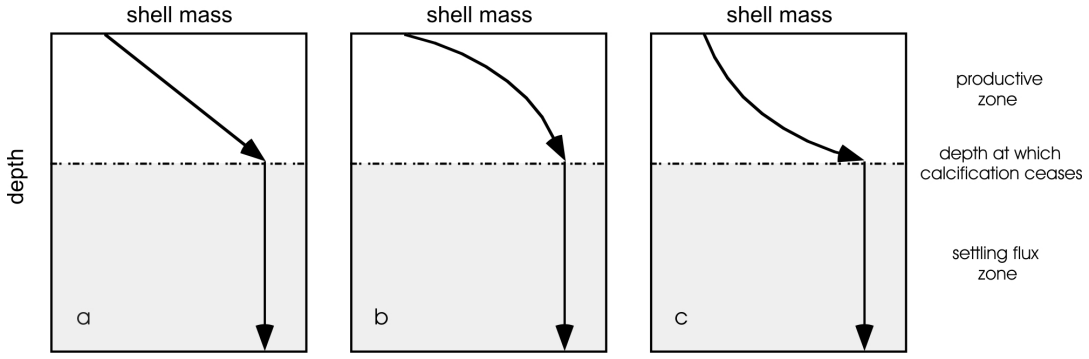

Figure 4.1. Shell mass as a function of depth in the water column. For a given specimen, the shell mass may change with depth in the water column due to growth within the productive zone. The change of the shell mass with depth in the productive zone (dM/dZ), may be a) constant, b) decrease or, c) increase with depth depending on the species' growth and subsidence rate. Whatever the pattern of shell growth within the productive zone, it can be expected that shell growth ceases at some depth in the water column.

4.3.2 Depth integrated shell growth

As the seawater temperature decreases with depth, the expected oxygen isotope composition of calcite, known as the equilibrium value ($\delta^{18}O_{eq}$), increases with depth in the water column (assuming the changes of the oxygen isotope composition of the seawater with depth are small). At a given location in the ocean different species might reach a different 'final' (read $\delta^{18}O_{shell\text{-}export}$) isotopic composition. Three main reasons can be given that explain differences in the $\delta^{18}O_{shell\text{-}export}$ for different species under similar hydrographic conditions: 1) different species might have a different base of the productive zone, 2) the species might have different vital effects, or 3) the species might exhibit a different shell mass development or 'growth' pattern over the PZ. For example, a specimen that predominantly precipitates its

calcite in the upper part of the PZ (Fig. 4.1b) will have a lower (warmer) $\delta^{18}O_{shell}$ compared to a specimen that adds most calcite to its shell in the lower part of its productive zone (Fig. 4.1c). The concept of depth-integrated shell growth thus explains the $\delta^{18}O_{shell, export}$ as the mass weighted sum of isotopic equilibrium values at different depths in the PZ. Thus, in order to understand the $\delta^{18}O_{shell, export}$ of a given species it is essential to quantify the value of the vital effect, estimate the maximum depth of calcification (BPZ) and determine its cumulative mass development function (CMDF).

4.3.3 The cumulative mass development function

A general pattern observed in field collected planktic foraminifera is that, within the PZ, the test size of a foraminiferal population increases with depth in the water column (Hemleben and Bjima, 1994; Peeters and Brummer, 2002). Since test size and mass are well correlated, it can be expected that also the shell mass must increase with depth down to the base of the productive zone. During the foraminiferal life cycle, migration between the reproductive depth, thermocline and/or the chlorophyll maximum, and the upper part of the photic zone occurs (Hemleben and Bjima, 1994). If indeed deepening occurs during growth, it can be expected that the oxygen isotope composition of a shell must increase with mass and size. The isotopic composition of a shell thus may be seen as the mass weighted sum of equilibrium calcite precipitated over the range of the productive zone. Given the $\delta^{18}O_{eq}$ profile in the water column and observations on the $\delta^{18}O_{shell}$ at different depths in the water column (within PZ and EZ), it will be possible to find the CMDF that can be used to accurately predict the oxygen isotope composition of a shell at any depth in the water column. Once known, the CMDF may be used to calculate the mass development density function (MDDF) for different species, providing direct information on the process of calcification for different species.

4.3.4 Modelling the shell mass increase as a function of depth in the productive zone

The shell mass of a given specimen may increase because of 1) growth, *i.e.* the formation of new chambers, or because of 2) wall thickening, including the growth of secondary calcite (Bé, 1980; Duplessy and Bé, 1981; Lohmann, 1995). Separating both components is difficult, as the relationship between shell size and mass may depend on the environmental growth conditions. Previous studies indicate that the relationship between shell

size and shell mass may be approximated by an exponential growth function (Bijma et al., 1998) or by a log-linear relationship (Lohmann, 1995). The fact that two components, growth (*i.e.* test size) and test wall thickening contribute to the total mass of the shell, suggests that a more sophisticated approach, *i.e.* including quantification of the contribution of each component to the total shell mass, is considered necessary for each species to accurately describe the relationship between shell size and mass. For the present purpose however, a simple relationship between shell mass and size (Fig. 4.2) is sufficient and we will proceed using the log-linear approach:

$$M = a \cdot L^b \qquad [1]$$

in which M represents the mass of the shell and L represents some measure of the foraminiferal test size, whereas *a* and *b* are species specific constants.

The main aim of this study is to find a realistic CMDF that explains the observed increase of the oxygen isotopic composition of a given species within the PZ as well as the approximately constant isotopic composition of shells within the EZ. Consequently, a realistic CMDF should 1) increase within the PZ reflecting the increase of shell mass due to growth and wall thickening, and 2) should remain constant below the BPZ. A number of mathematical functions describing such patterns often contain an exponential term and are named "exponential rise to maximum functions'. The simplest function that would meet these requirements would look like:

$$M(z) = 1 - \exp(-az) \qquad [2]$$

Unfortunately, this function is quite inflexible and has a rather 'frozen' shape. It is only possible to change its curvature and does not allow to model the wide range of mass development shapes that might be expected for our practical application. It will not be possible, for example, to model a sigmoidal-shaped increase of shell mass with depth as might be required for some deep dwelling species such as *Globorotalia truncatulinoides*, who are known to preferentially precipitate a large fraction of their shell mass hundreds of meters below the surface mixed layer (e.g. Mulitza et al., 1997; LeGrande et al., 2004). It thus seems reasonable to expand the simple exponential function to accommodate a wider range of possible CMDF-shapes. We have chosen to add an extra parameter to the function described above, which allows changing the shape of the MDF into a more sigmoidal form:

$$M(z) = 1 - \exp(-az)^b \quad [3]$$

It should be noted that this function, by replacing $a = 1/\beta$ and $b = \alpha$, is known as the cumulative form of the Weibull function (Weibull, 1939), that can be written:

$$M(z) = 1 - \exp(-z/\beta)^\alpha \quad [4]$$

For practical reasons we prefer to use equation 4. Obviously this function is more flexible and may accommodate a wide range of different mass development shapes that might be expected to occur in nature (Fig. 4.3). For the purpose of calculating a mass balance, equation 3 is sufficient, as the shell mass is normalized between 0 near the sea surface and 1 near the base of the productive zone, where calcification ceases. Equation 4, however, might be extended even further to accommodate the initial and final shell mass:

$$\mathrm{M(z)} = \mathrm{M_0} + (\mathrm{M_{final}} - \mathrm{M_0}) \cdot \left(1 - \exp(-\mathrm{z}/\beta)^\alpha\right). \quad [5]$$

In this equation, M_0 and M_{final} represent the initial and final shell mass respectively, whereas the parameters α and β determine the shape of the distribution. In Figure 4.3, we show how the cumulative function changes for different parameters of α and β. Although we will not use shell size further in this manuscript, it is noted that the shell size as a function of depth might obtained by combining equation 1 and 2, which then results in:

$$\mathrm{L(z)} = \left[\frac{\mathrm{M_0} + (\mathrm{M_{final}} - \mathrm{M_0}) \cdot \left(1 - \exp(-\mathrm{z}/\beta)^\alpha\right)}{\mathrm{a}}\right]^{1/\mathrm{b}} \quad [6]$$

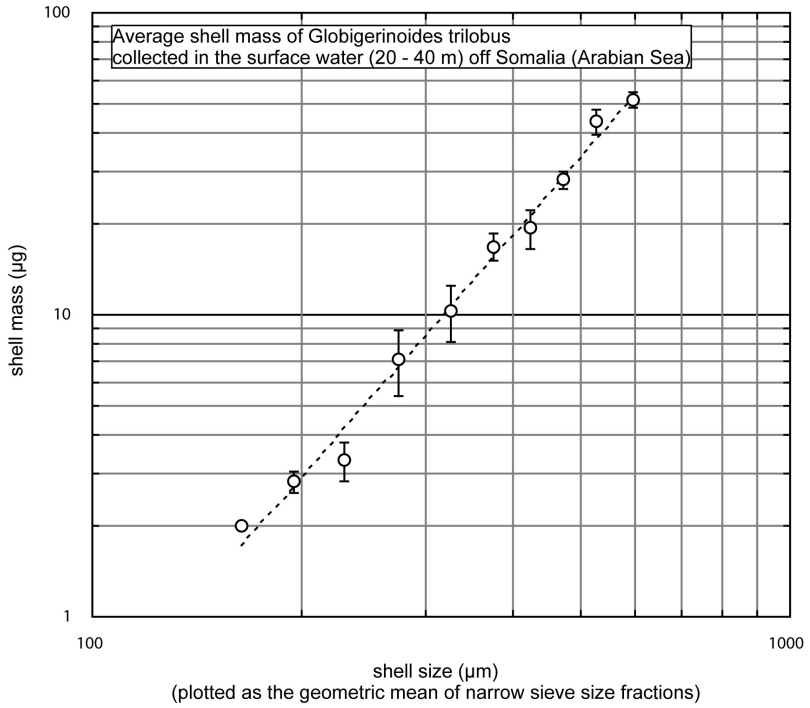

Figure 4.2. The relationship between shell size and shell mass of a living planktic foraminifer species (*Globigerinoides trilobus*), collected with a plankton tow in surface water off Somalia (Arabian Sea), is described well using a log-linear relationship. Shell mass = $2.4061\ 10^{-6}\ S^{2.6446}$.

4.3.5 Required field observations

A number of field observations are considered crucial in order to understand the modern calcification patterns of the pelagic foraminifera. First of all, the foraminifera should be collected with depth stratified plankton tows in order to quantify the change in the oxygen isotope composition of the foraminiferal shells with depth in the water column. This means that the $\delta^{18}O_{shell}$ both within the PZ and the EZ ($\delta^{18}O_{shell,\ export}$) should be determined. Second, *in situ* measurements of seawater temperature as well as its oxygen isotope composition ($\delta^{18}O_w$) are required in order to calculate the equilibrium profile with depth ($\delta^{18}O_{eq}$). Once a sufficient number of $\delta^{18}O_w$ measurements are available, a regression of $\delta^{18}O_w$ vs. salinity may be used to calculate the profile of $\delta^{18}O_{eq}$ with depth.

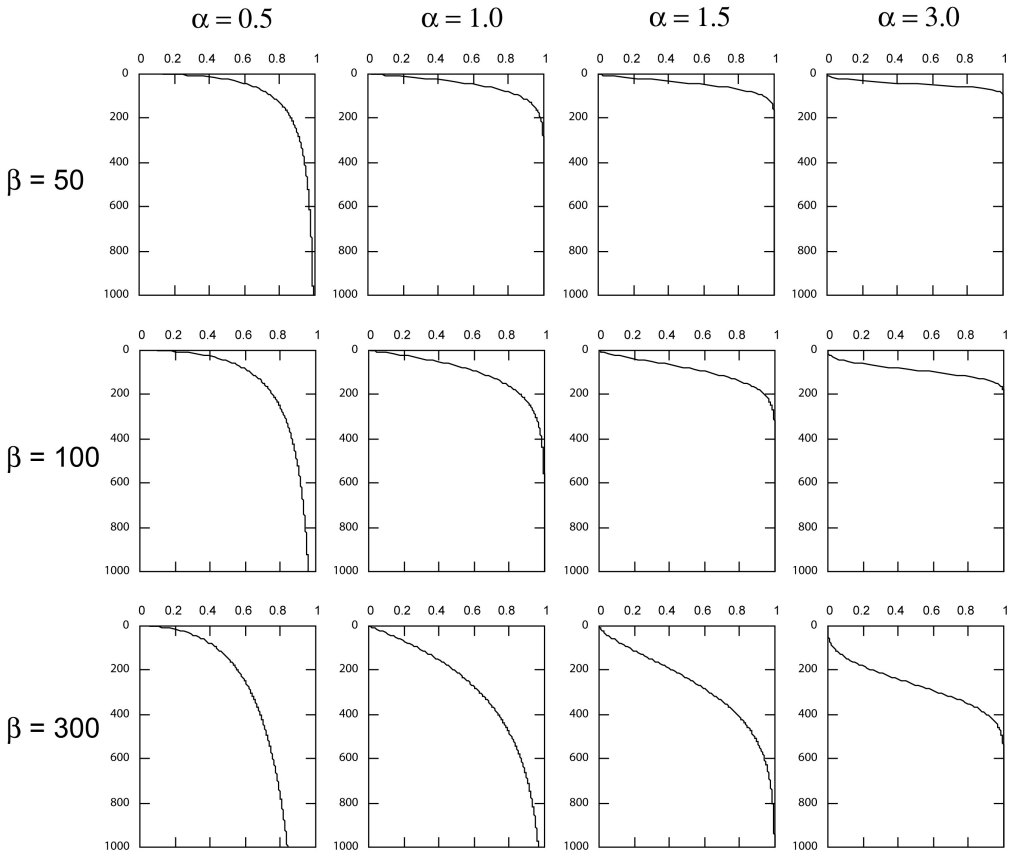

Figure 4.3. Some examples of the shape of the cumulative Weibull distribution for normalised shell mass for different α and β parameters. In these examples of the cumulative Weibull distribution, it is assumed that shell mass near the sea surface is 0 and the final mass is equal to 1. For $\alpha = 1$ the cumulative distribution equals a simple exponential rise to maximum function. Increasing the α value, forces the curve to a more 'horizontal position', thus narrowing the calcification interval. Increasing the β parameter results in 'deepening' of the calcification curve. Consequently it largely determines the position of the base of the productive zone, *i.e.* where the shell mass approaches the value of 1. The base of the productive zone, may be defined at a depth level where 95% of the shell mass has been formed.

4.3.6 Temperature equations

A temperature equation relates $\delta^{18}O$ of carbonates to temperature and $\delta^{18}O_w$. Two kinds of temperature equations can be found in literature: 1) those for inorganic precipitated calcite (McCrea, 1950; Kim and O`Neil, 1997) and 2) those determined on biogenic carbonates in the laboratory or using field data (Epstein et al., 1953; Erez and Luz, 1983; Bouvier-Soumagnac and Duplessy, 1985; Bemis et al., 1998). Most of these equations appear to have a slope of approx. –0.22‰°C^{-1} (if approximated by a linear equation over the temperature rage of seawater *i.e.* 0 - 30°C). In this paper we use the temperature equation of Kim and O'Neil (1997) that was obtained from inorganic precipitates. We here assume that the species $\delta^{18}O_{shell\text{-}w}$ offsets from the expected equilibrium, known as 'the vital effect', is constant over the temperature range of seawater for a given species. We note, however, that it might be necessary to modify this temperature equation, to include for example 'ontogenetic

effects' or the effect of the carbonate ion on the $\delta^{18}O_{shell}$ in order to predict the expected $\delta^{18}O_{eq}$ very accurately for different species or shell sizes (Spero et al., 1997; Bijma et al., 1999; Itou et al., 2001; Peeters et al., 2002).

4.3.7 Using the model

In our model we presume that the value of $\delta^{18}O_{shell,\ export}$ encloses the history of depth integrated calcification that took place within the PZ. In other words, the $\delta^{18}O_{shell,\ export}$ value is considered to mirror the entire process of depth-integrated growth for a specimen that started growing near the sea-surface, with mass M_0, down to the base of the productive zone where it reached its 'final mass' M_∞. Assuming that the shell mass near the sea surface is very small compared to its final mass we start illustrating our method using $M_0(0m) = 0$. Similarly, the shell mass at the base of the productive zone is set to the value of 1, $M_\infty(BPZ) = 1$. Consequently, as a first order approximation, the shell mass as a function of depth in the water column is described using equation [4]. As a result, the modelled oxygen isotope composition of a specimen, which is referred to as $\delta^{18}O^*_{shell}$ (MDF), can be calculated given the CMDF. For discrete depth intervals, as obtained using depth stratified plankton tows, the expected oxygen isotope composition of a specimen within a given interval i may be calculated following:

$$\delta^{18}O^*_{shell,i} = \frac{\sum_{i=1}^{n}(M_i - M_{i-1}) \cdot \delta^{18}O_{eq,i}}{M_i} \qquad [7]$$

In this equation i represents the plankton tow number starting with 1 for the surface net *etc.* Note that for $i = 1$, the shallowest net, it is necessary to use $M_{i-1} = 0$. Furthermore, $\delta^{18}O_{eq,i}$, represents the interval averaged oxygen isotope composition of equilibrium calcite for plankton tow interval *i*. When using field data, equation 7 should be used to estimate the CMDF for a species at a given location. The CMDF, characterized by α and β, might thus be obtained from field data by minimizing the sum of the squared differences, for a number (N) of plankton tow depth interval observations. In practice, our method thus aims to find those values for α and β that produce the sum of the smallest squared differences between predicted, $\delta^{18}O^*_{shell}$, and observed $\delta^{18}O_{shell}$ values for specimens collected at different depths in the water column.

4.3.8 Calcification patterns in relation to the α and β parameters

The two parameters of the calcification function, α and β, fully describe the CMDF (and MDDF) of a given species. In this paragraph we illustrate how the oxygen isotope composition of a hypothetical species changes when these parameters vary. In order to illustrate the depth integrated calcification we will make use of a synthetic temperature and $\delta^{18}O_{eq}$ profile given in Figure 4.4.

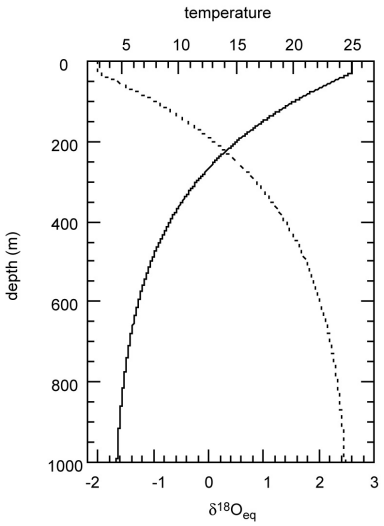

Figure 4.4. A synthetic temperature and $\delta^{18}O_{eq}$ profile (dashed line). A synthetic temperature and $\delta^{18}O_{eq}$ profile is used to illustrate our method. The surface mixed layer is 30m deep and has a constant temperature of 25.0ºC. At 100 m the temperature has decreased down to 20ºC. At 200 m the temperature is 15ºC. The surface water $\delta^{18}O_{eq}$ is set to –2.0‰.

We will use α and β combinations given in Figure 4.3 to calculate the expected $\delta^{18}O_{shell}$ values at selected depth intervals (10, 20, 40, 80 100, 150, 200, 300, 500, 700 and 900 m). The base of the productive zone is defined at an arbitrary depth at which 95% of the shell mass ($M_{0.95}$) has been formed. This is done because the CMDF is approaching the value of 1 for $Z = \infty$, which would thus yield very large and unrealistic BPZ values if BPZ would be defined at $M_{1.00}$. Figure 4.5 shows the results of our calculations for different MDF scenarios. It is clear form this Figure that an increase of the α value results not only in a shallower BPZ, but also forces the calcification curve to a more horizontal position, thus narrowing the interval in which the shell mass increases quickly. Increasing the β parameter is very efficient in 'deepening' of the MDF. We note that the absolute value of β mirrors the depth at which the function reaches a value of 0.63, independent of the α value.

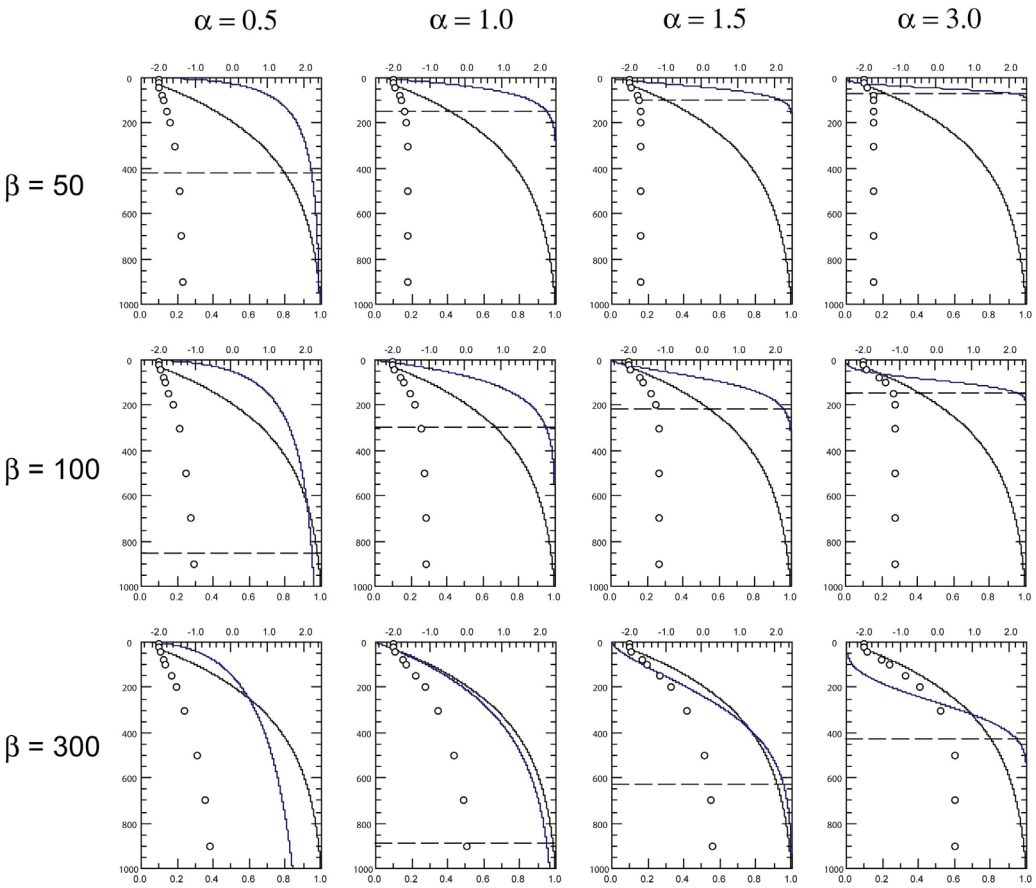

Figure 4.5. Some examples of depth integrated shell growth. The cumulative Weibull distribution is used to model the increase of shell mass as a function of depth in the water column for different values of the parameters α and β (grey lines). The *in situ* $\delta^{18}O_{eq}$ is indicated with a black line using the temperature profile given in Figure 4.4. The expected oxygen isotope composition of a hypothetical species is indicated with dots at selected depth levels to illustrate the increase in $\delta^{18}O_{shell}$ with depth in the water column. The depth of the productive zone is indicated with a horizontal dashed line, corresponding to the depth at which the shell has reached 95% of its final mass ($M_{0.95}$). Below the base of the productive zone, the $\delta^{18}O_{shell}$ does not change since shell growth has ceased. Note that depth integrated shell growth results in an offset between the $\delta^{18}O_{shell}$ and the *in situ* $\delta^{18}O_{eq}$ for specimens caught below the surface mixed layer.

Consequently, species that are considered as 'shallow dwellers', *i.e.* they predominantly calcify within the surface mixed layer, are characterized by relatively high α and low β values (see for example α = 3 and β = 50 in Fig. 4.5). Deep living species, however, are characterized predominantly by high β values. Increasing the α parameter when β is relatively large, results in a larger fraction of shell mass precipitated at deeper levels in the water column. Such species thus mainly build the largest portion of their shell deep in the water column. The depth of the BPZ thus depends on both parameters. In Figure 4.6 we show how the BPZ, defined as that depth level in the water column where 95% of the shell mass has been formed, varies as a function of both α and β. Application of our method to

field data should provide insight in the variability of the α and β parameter for different species in different hydrographic settings. Furthermore, it may be anticipated that, in order to quantify the calcification pattern of a given species in different hydrographic settings, both parameters may be studied as a function of hydrographic characteristics, such as depth or temperature of mixed layer or thermocline.

In a subsequent manuscript we will perform model fits to field data, in order to test and evaluate the practical use of the model proposed here.

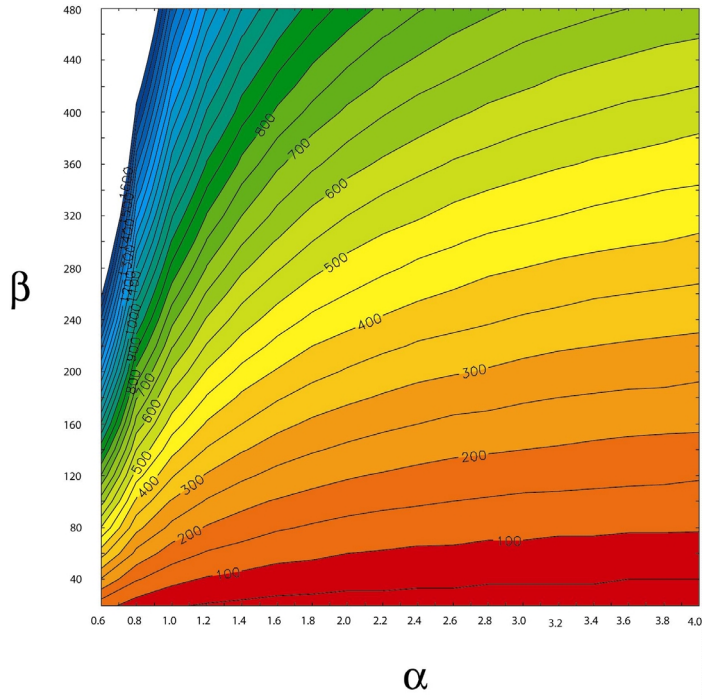

Figure 4.6. The depth of the base of the productive zone is contoured as a function of α and β. The level in the water column at which 95% of the final shell mass has been built is taken as the depth of the productive zone. Note that the base of the productive zone is strongly determined by the value of β-parameter. Deep living species will therefore have a large β-value.

4.4 Discussion and conclusion

In this manuscript we propose a conceptual oxygen isotope mass balance model that may allow to quantify the effect of depth integrated calcification for different species of planktic foraminifera. We note that a similar mass-balance approach has been used earlier to quantify, for example, the effect of secondary calcification and dissolution on the chemistry of foraminiferal shells (Lohmann, 1995; LeGrande et al., 2004). In our approach, however, we propose that depth integrated shell growth, reflected in an increasing the oxygen isotope composition with depth, is a more or less continuous process of growth and wall thickening

that takes place during the downward vertical migration path of foraminiferal life cycle. Our vertical migration path model assumption is based on a number of field observations which indicate that the oxygen isotope composition of plankton tow collected foraminifera increases with depth in the water column and remains constant in deeper parts of the water column (Hemleben and Bjima, 1994; Bauch et al., 2002a; Peeters et al., 2002; Peeters and Brummer, 2002; Simstich et al., 2002; Mortyn and Charles, 2003; LeGrande et al., 2004). The constant oxygen isotope composition of specimens deep in the water column obviously reflects the Base of the Productive Zone for the species considered. In a subsequent manuscript we will test and validate our model to field observations. Model fits to field data might be used to quantify and understand the calcification patterns of different species.

References

Bauch, D., Erlenkeuser, H., Winckler, C., Pavlova, G. and Thiede, J., 2002a. Carbon isotopes and habitat of polar planktic foraminifera in the Okhotsk Sea: the "carbonate ion effect" under natural conditions. Mar. Micropaleontol. 871, 1-17.

Bauch, D., Erlenkeusrer, H., Winckler, G., Pavlova, G. and Thiede, J., 2002b. Carbon isotopes and habitat of polar planktic foraminifera in the Okhotsk Sea: the 'carbonate ion effect' under natural conditions, Marine Micropaleontology, pp. 83-99.

Bé, A.W.H., 1980. Gametogenic calcification in a spinose planktonic foraminifer, *Globigerinoides sacculifer* (Brady). Marine Micropaleontology 5, 283-310.

Bemis, B.E., Spero, H.J., Bijma, J. and Lea, D.W., 1998. Reevaluation of the oxygen isotopic composition of planktonic foraminifera. Paleoceanography 13, 150-160.

Bijma, J., Spero, H.J. and Lea, D.W., 1998. Oceanic carbonate chemistry and foraminiferal isotopes: new laboratory results paper presented at the Sixth International Conference on Paleoceanography, Lisbon, 1998.

Bijma, J., Spero, H.J. and Lea, D.W., 1999. Reassessing foraminiferal stable isotope geochemistry: impact of the oceanic carbonate system (experimental results). In: Fischer, G. and Wefer, G. (Eds.), Use of proxies in paleoceanography: Examples from the South Atlantic. Springer, Berlin, pp. 489-512.

Bouvier-Soumagnac, Y. and Duplessy, J.-C., 1985. Carbon and oxygen isotopic composition of planktonic foraminifera from laboratory culture, plankton tows and recent sediment: implication for the reconstruction of paleoclimatic conditions and of the global carbon cycle. Journal of Foraminiferal Research 15, 302-320.

Deuser, W.G., Hemleben, C. and Spindler, M., 1981. Seasonal changes in species composition, numbers, mass, size, and isotopic composition of planktonic foraminifera settling into the deep Sargasso Sea. Palaeogeogr., Palaeoclim., Palaeoecol. 33, 103-127.

Duplessy, J.C. and Bé, A.W.H., 1981. Oxygen-18 enrichment of planktonic foraminifera due to gametogenic calcification below the euphotic zone. Science 213, 1247-1250.

Emiliani, C., 1954. Depth habitats of some species of pelagic foraminifera as indicated by oxygen isotope ratios. Am. J. Sci. 252, 149-158.

Epstein, S.R., Buchsbaum, R., Lowenstam, H.A. and Urey, H.C., 1953. Revised carbonate-water isotopic temperature scale. Geol. Soc. Am. Bull 64, 1315-1325.

Erez, J. and Honjo, S., 1981. Comparison of isotopic composition of planktonic foraminifera in plankton tows, sediment traps and surface sediments. Palaeogeogr., Palaeoclim., Palaeoecol. 33, 129-156.

Erez, J. and Luz, B., 1983. Experimental paleotemperature equation for planktonic foraminifera. Geochimica et Cosmochimica Acta 47, 1025-1031.

Fairbanks, R.G., Sverdlove, M., Free, R., Wiebe, P.H. and Be, A.W.H., 1982. Vertical distribution and isotopic fractionation of living planktonic foraminifera from the Panama Basin. Nature 298, 841-844.

Fairbanks, R.G. and Wiebe, P.H., 1980. Foraminifera and chlorophyll maximum: vertical distribution, seasonal succession, and paleoceanographic significance. Science 209, 1524-1526.

Field, D.B., 2004. Variability in vertical distribution of planktonic foraminifera in the California Current: Relationships to vertical ocean structure. Paleoceanography 19.

Furbish, D.J. and Arnold, A.J., 1997. Hydrodynamic stratgies in the morphological evolution of spinose planktonic foraminifera. GSA Bulletin 109(8), 1055-1072.

Hembleben, C., Spindler, M., Beitinger, I. and Deuser, W.G., 1985. Field and laboratory studies on the ontogeny and ecology of some globorotaliid species from the Sargasso Sea off Bermuda. Journal of Foraminiferal Research 15(4), 254-272.

Hemleben, C. and Bjima, J., 1994. Foraminiferal population dynamics and stable carbon isotopes. In: Zahn, R. (Editor), Carbon cycling in the glacial ocean: constrains on the ocean´s role in the global change. NATO ASI series I, 17, pp. 146-166.

Hemleben, C., Spindler, M. and Anderson, O.R., 1989. Modern Planktonic Foraminifera. Springer Verlag, New York, 363 pp.

Itou, M., Ono, T., Oba, T. and Noriki, S., 2001. Isotopic composition and morphology of living *Globorotalia scitula*: a new peoxy of sub-intermediate ocean carbonate chemistry? Mar. Micropalentol. 42, 189-210.

Kahn, M.I. and Williams, D.F., 1981. Oxygen and carbon isotopic composition of living planktonic foraminifera from the northeast Pacific Ocean. Palaeogeogr., Palaeoclim., Palaeoecol. 33, 47-69.

Kahn, M.J., 1979. Non-equilibrium oxygen and carbon isotope fractionation in tests of living planktonic foraminifera. Oceanologica Acta 2, 195-208.

Kim, S.-T. and O`Neil, J.R., 1997. Equilibrium and non-equilibrium oxygen isotope effects in synthetic carbonates. Geochimica et Cosmochimica Acta 61, 3461-3475.

LeGrande, A.N., Lynch-Stieglitz, J. and Farmer, E., 2004. Oxygen isotopic composition of *Globorotalia truncatulinoides* as a proxy for intermediate depth density. Paleoceanography 19.

Lohmann, G.P., 1995. A model for variation in the chemistry of planktonic foraminifera due to secondary calcification and selective dissolution. Paleoceanography 10, 445-457.

McCrea, 1950. On the isotopic chemistry of carbonates and a paleotemperature scale. The Journal of Chemical Physics 18, 849-857.

Mortyn, G.P. and Charles, C.D., 2003. Planktonic foraminiferal depth habitat and delta ^{18}O calibrations: Plankton tow results from the Atlantic sector of the Southern Ocean. Paleoceanography 18.

Mulitza, S., Dürkoop, A., Hale, W., Wefer, G. and Niebler, H.S., 1997. Planktonic foraminifera as recorders of past surface-water stratification. Geology 25(4), 335-338.

Niebler, H.S., Hubberten, H.W. and Gersonde, R., 1999. Oxygen Isotope Values of Planktic Foraminifera. In: Fischer, G. and Wefer, G. (Eds.), Use of proxies in paleoceanography: Examples from the South Atlantic. Springer, Berlin, pp. 165-189.

Ortiz, J.D., Mix, A.C. and Collier, R.W., 1995. Environmental control of living symbiotic and asymbiotic foraminifera of California Current. Paleoceanography 10, 987-1009.

Ortiz, J.D., Mix, A.C., Rugh, W., Watkins, J.M. and Collier, R.W., 1996. Deep-dwelling planktonic foraminifera of the northeastern Pacific Ocean reveal environmental control of oxygen and carbon isotope disequilibria. Geochim. Cosmochim. Acta 60(22), 4509-4523.

Peeters, F.J.C., Brummer, G.-J. and Ganssen, G., 2002. The effect of upwelling on the distribution and stable isotope composition of *Globigerina bulloides* and *Globigerinoides ruber* (planktic foraminifera) in modern surface waters of the NW Arabian Sea. Global and Planetary Change 34, 269-291.

Peeters, F.J.C. and Brummer, G.J.A., 2002. The seasonal and vertical distribution of living planktic foraminifera in the NW Arabian Sea. In: Clift, P.D., Kroon, D., Gaedicke, C. and Craig, J. (Eds.), The Tectonic and Climatic Evolution of the Arabian Sea Region. Geological Society, London, pp. 463-497.

Simstich, J., Sarnthein, M. and Erlenkeuser, H., 2002. Paired d18O signals of *Neogloboquadrina pachyderma* (s) and *Turborotalita quinqeuloba* show thermal stratification structure in Nordic Seas. Mar. Micropaleontol. 912, 1-19.

Spero, H.J., Bijma, J., Lea, D.W. and Bemis, B., 1997. Effect of seawater carbonate concentration on foraminiferal carbon and oxygen isotopes. Nature 390, 497-500.

Urey, H.C., 1947. The thermodynamic properties of isotopic substances. J. Chem. Soc., 562-581.

Weibull, W., 1939. A statistical theory of the strength of materials. Ingenioersvetenskapsakad. Handl. 151, 1-45.

Wilke, I. and Peeters, F.J.C., in prep. Depth integrated growth of planktic foraminiferal shells Part 2. Model fits to field observations.

CHAPTER 5*

DEPTH INTEGRATED GROWTH OF PLANKTIC FORAMINIFERAL SHELLS PART 2. MODEL FITS TO FIELD OBSERVATIONS

Iris Wilke[1] and Frank J.C. Peeters[2]

[1]*Fachbereich Geowissenschaften/MARUM, Universität Bremen, Leobenerstrasse, 28359 Bremen, Germany*

[2]*Afdeling Palaeo-ecologie en Palaeoklimatologie, Faculteit Aard- en Levenswetenschappen, Vrije Universiteit, de Boelelaan 1085, 1081 HV, Amsterdam, The Netherlands*

*This chapter is in preparation for submission

5.1 Introduction

Previously, we have proposed a model that may describe the oxygen isotopic composition ($\delta^{18}O$) of a planktic foraminifer shell as a function of depth in the water column (Peeters and Wilke, in prep.). In this model, we propose that foraminiferal shell growth, *i.e.* the increase of the foraminiferal shell mass, is expected to increase with depth in the zone in which specimens live and precipitate their calcite. This shell mass increase during the foraminiferal life cycle may be described by an exponential function similar to the cumulative Weibull distribution function. We expect the model to be well suited to quantify the growth pattern and depth range of calcification of different species of planktic foraminifers. If so, it may adequately provide information on the increase of mass with depth, on the depth at which shell growth ceases as well as on the depth at which calcite precipitation is maximal. In this manuscript, we will test and validate our model to field observations. The model is used to assess which depth range, and as such which temperature gradient is reflected in the $\delta^{18}O$ of shells of different species.

To confidently use the $\delta^{18}O$ of different species in paleoceanographic studies, knowledge on the geographic and seasonal distribution as well as the preferred depth habitat and calcification pattern is essential. Different species are known to favour different environmental conditions with respect to food availability, temperature and light conditions (e.g. Fairbanks et al., 1982; Bijma et al., 1990b; Ortiz et al., 1995; Watkins et al., 1996; Watkins and Mix, 1998; Field, 2004). These environmental factors affect the growth and distribution of planktic foraminifers, which may results in different vertical distribution patterns in the water column. In general, non-spinose species are herbivore, while the spinose species are carnivorous and harbor actively photosynthesizing symbiotic algae (Hemleben et al., 1989). The symbiotic algae, for instance, allow the spinose species to live also in oligotrophic, food-poor waters. As a result these spinose species are found more abundant in the photic zone. Non-spinose species, however, are often associated with deeper water, where they may feed on dead-sinking prey (Hemleben et al., 1989). Such species may grow a considerable fraction of their calcite shell in deeper water. It is evident, that in addition to the physical/chemical vertical structure of the water column, the foraminiferal ecology controls the oxygen isotopic composition of their calcite shells (e.g. Fairbanks and Wiebe, 1980; Sautter and Thunell, 1991a; Ortiz et al., 1996; Peeters et al., 2002). Since the favoured ecological niches are strongly coupled to the hydrographic conditions and/or geographic position in the ocean, species-specific depth habitats and calcification patterns can be expected.

The presented oxygen isotope mass balance model proposed earlier, is used here, to unravel the $\delta^{18}O$ of different species of foraminifers in relation to the vertical thermal structure of the upper water column. Here, plankton tow collected foraminifera from different geographical locations are selected to test our model.

5.2 Material and methods

Plankton samples were selected to test the model utility. These samples were collected during various research cruises. We used foraminiferal shells collected in the subtropical northeastern Atlantic, north of the Canary Islands (29°N), between Lanzarote/Fuerteventura and the African shelf. The station EBC (Eastern Boundary Current) were sampled during winter 1996 (RV Victor Hensen 96/1) as part of the CANIGO-project (Canary Islands Gibraltar and Azores Observations). Furthermore, samples were derived from the transitional southeastern Atlantic Ocean (Cape Basin) at station 21 during the Dutch MARE-1 cruise in spring 2000, and at station 1153/1151 during the Dutch MARE-2 cruise in summer 2000 (Mixing of Agulhas Rings Experiment) (Table 5.1).

Table 5.1. Selected stations and general hydrographic information

Station	Cruise	Longitude	Latitude	SST (°C)	MLD (m)	DCM (m)	Sampling interval (m)
EBC	VH 96/1	28°42.5 N	13°09.3'W	19.75	126	mixed layer	0-440, 700
21-1/21-3	MARE-1	38°82.1'S	19°54.2'E	19.74	53	base of mixed layer	0-150/150-800
1153/1151	MARE-2	38°41.1'S	13°58.3'E	18.05	138	mixed layer	0-150/150-800

SST = sea surface temperature. MLD = mixed layer depth. DCM = deep chlorophyll maximum.

Foraminifers were collected using plankton tows that sampled the water column over discrete depth intervals. Water samples were collected at the same station. The oxygen isotope measurements of the foraminiferal shells and the water samples were carried out at the Universität Bremen and at the Vrije Universiteit Amsterdam. Isotope composition is given using the conventional δ-notation reported versus Vienna Pee Dee Belemnite (V-PDB) and V-SMOW (Appendix 5A).

Each station was accompanied by a CTD cast providing information on sea water temperature, salinity and fluorescence (Fig. 5.1). Station EBC and M1-21 show sea surface temperatures (SST) of ~19.7°C, while SST at station M2-1153/1151 were lower (18.1°C). Station M1-21 is characterized by a low surface water salinity of 35.4 and by a relatively

shallow mixed layer (0-53 m). As opposed to this, a deeper mixed layer was found at the two other stations EBC (0-126 m) and M2-1153/1151 (0-138 m). The depth of the mixed layer is defined at that depth at which the water temperature is 0.5°C less than the sea surface temperature (SST). The fluorescence data at these two stations indicate that chlorophyll was distributed over the entire mixed layer, while at station M1-21 a deep chlorophyll maximum coincides with the base of the mixed layer (Fig. 5.1). The thermocline is determined as the depth (range) where the temperature gradient is highest. At station EBC the thermocline was found approximately between 126 and 180 m. At station M1-21 the temperature gradient was steepest between 53 and ~100 m, while at station M2-1153/1151 the thermocline extended between 138 and ~160 m.

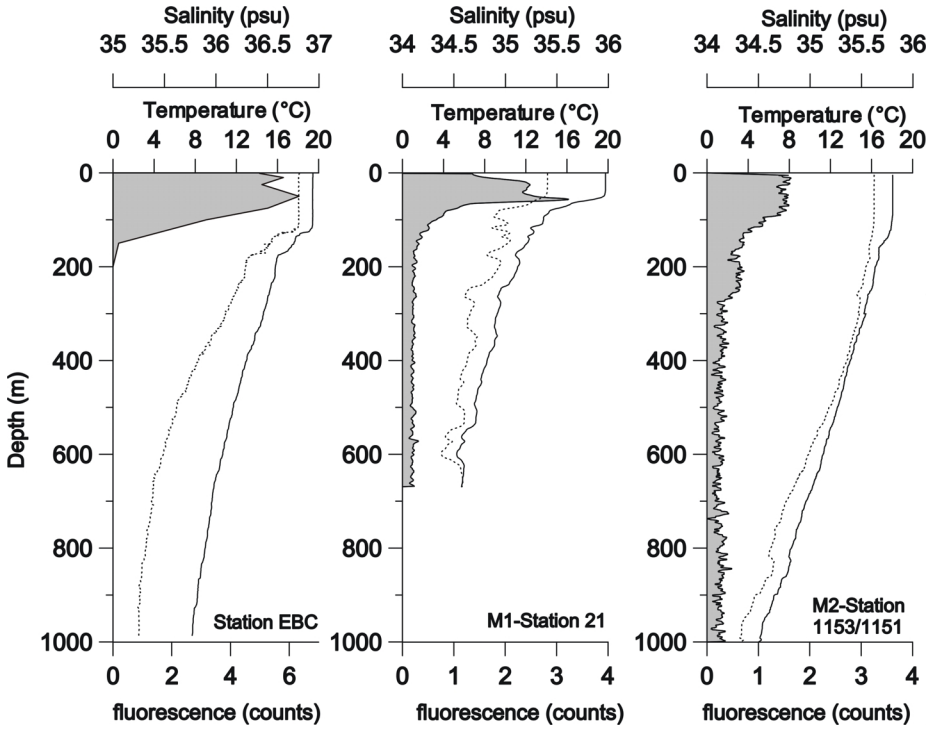

Figure 5.1. Graph showing *in situ* temperature (black line), salinity (dashed line) and fluorescence (gray) profiles at station EBC, M1-21 and M2-1153/1151.

We calculated expected equilibrium profile ($\delta^{18}O_{eq}$) from *in situ* measurements of seawater temperature and the oxygen isotopic composition ($\delta^{18}O_w$) using the equation after Kim and O`Neil (1997):

$$\delta^{18}O_{eq} = 25.778 - 3.333 * (43.704 + T)^{0.5} + \delta^{18}O_w$$

5.3 Data processing

Figure 5.2 shows a Microsoft EXCEL®-work sheet that serves as an example of how we organized the data in order to perform model fits to field data. The $\delta^{18}O_{eq}$ profile in the water column was calculated by using the regression of $\delta^{18}O_w$ vs. salinity (column 'B'). The measured oxygen isotope values of the calcite shell ($\delta^{18}O_{shell}$) are listed in column 'H' (small size fraction) and column 'I' (large size fraction) for the corresponding depth interval midpoint (column 'G'). In column 'J' and 'K' the corresponding foraminiferal shell concentrations for the two size fractions are given. We calculated the concentration weighted average $\delta^{18}O_{shell}$ values ($\delta^{18}O_{shell}$ = (($\delta^{18}O_{small}$*shell conc.$_{small}$) + ($\delta^{18}O_{large}$*shell conc.$_{large}$))/(shell conc.$_{small}$+shell conc.$_{large}$) (column 'L'). The vital effect is estimated for each species at each station by taking the difference between the concentration weighted average $\delta^{18}O_{shell}$ and $\delta^{18}O_{eq}$ in the shallowest plankton tow. This difference is considered to be constant for a given species at a given station, and indicated in cell 'M11', (VE). Consequently, we correct the concentration weighted average $\delta^{18}O_{shell}$ values in all depth intervals for this species-specific 'vital effect' (Table 5.3). Column 'M' shows the corrected $\delta^{18}O_{shell}$ values.

Datei Bearbeiten Ansicht Einfügen Format Extras Daten Fenster ?

	A	B	C	D	E	F	G	H	I	J	K	L	M	N	O
1	Depth	d18Oeq	Density Weibull fct.	Cumulative Weibull fct.	modelled shell value (d18O 'shell)		depth interval (mean)	18O shell (small)	18O shell (large)	shell conc. (small)	shell conc. (large)	18O conc weigh. aver	18O Ve-corrected	modelled shell value (d18O 'shell)	obs. - pred. squared diff.
2	1	-0.54	0.0018	0.00	-0.54		8	-0.76	-0.61	37.82	1.77	-0.76	-0.54	-0.54	0.00
3	2	-0.54	0.0022	0.00	-0.54		20	-0.66	-0.67	20.06	0.61	-0.66	-0.45	-0.54	0.01
4	3	-0.54	0.0025	0.01	-0.54		35		-0.59		0.28	-0.59	-0.37	-0.54	0.03
5	4	-0.54	0.0027	0.01	-0.54		61		-0.68		0.46	-0.68	-0.46	-0.50	0.00
6	5	-0.54	0.0028	0.01	-0.54		94	-0.50	-0.57	5.74	0.65	-0.51	-0.29	-0.21	0.01
7	6	-0.54	0.0030	0.01	-0.54		133	-0.30	-0.27	7.74	3.19	-0.29	-0.08	0.03	0.01
8	7	-0.54	0.0031	0.02	-0.54		234	0.22	0.01	4.76	1.86	0.16	0.38	0.35	0.00
9	8	-0.54	0.0032	0.02	-0.54		408	0.60	0.38	0.67	0.23	0.54	0.76	0.54	0.05
10	9	-0.54	0.0033	0.02	-0.54		656	0.30	-0.06	0.40	0.10	0.22	0.44	0.59	0.02
11	10	-0.54	0.0034	0.03	-0.54							VE	-0.22		0.13
12	11	-0.54	0.0035	0.03	-0.54										
13	12	-0.54	0.0035	0.03	-0.54										
14	13	-0.54	0.0036	0.04	-0.54		alpha	1.28							
15	14	-0.54	0.0037	0.04	-0.54		beta	168.11							
16	15	-0.54	0.0037	0.04	-0.54										
17	16	-0.54	0.0038	0.05	-0.54										
18	17	-0.54	0.0038	0.05	-0.54										
19	18	-0.54	0.0039	0.06	-0.54										
20	19	-0.54	0.0039	0.06	-0.54										
21	20	-0.54	0.0039	0.06	-0.54										

Figure 5.2. Example of an Microsoft EXCEL-worksheet for application of the model to field observation.

In the next step, we calculate the model parameters, alpha and beta, that describe the MDF for the species considered. This is done by the least squares method, *i.e.* minimizing the

sum of the squared differences, between observations ($\delta^{18}O_{shell}$) and model output ($\delta^{18}O^{*}_{shell}$), by solving for the parameters alpha and beta. In this context we use the calcification function given in the companion of this paper (Peeters and Wilke, in prep.) (equation [7]). As a result, we calculate a $\delta^{18}O^{*}_{shell}$ value for every meter in the water column (column 'E') by using the cumulative Weibull function (column 'D') that depends on two parameters, alpha and beta given in cells 'H14' and 'H15', respectively. In order to optimize the fit between the predicted and observed oxygen isotope values measured at different depths in the water column, we use the least squares method. The squared difference between the predicted (column 'N', taken from column 'E' at corresponding depth interval mean) and the observed (column 'M') oxygen isotope values are given in column 'O'. The cell 'O11' sums all squared differences and needs to be minimized for finding the best curve fit. For this purpose we use the EXCEL SOLVER-function with alpha and beta as the variable parameters. In addition to the cumulative Weibull function the density Weibull function is given in column 'C' (Fig. 5.2). In the following we will refer to the cumulative Weibull function as the cumulative mass development function (CMDF) and to the density Weibull function as the mass development density function (MDDF). The CMDF describes the increase of shell mass with increasing depth due to shell growth and wall thickening, while the MDDF provides information on the 'growth pattern', e.g. the rate of change of shell mass versus depth.

Table 5.3. Compilation of the oxygen isotope disequilibrium (Vital effects, ($\delta^{18}O_{VE}$ (‰-PDB)= $\delta^{18}O_{shell;conc.-weighted}$ - $\delta^{18}O_{eq}$)) for selected planktic foraminiferal species at a) EBC, b) M1-21 and c) M2-1153/1151

a) Station EBC

Species	VE EBC (‰, PDB)
G. ruber	-0.26
T. humilis	-0.61
P. obliquiloculata	+0.12
G. truncatulinoides (dex.)	+0.03

b) Station M1-21

Species	VE M1-21 (‰, PDB)
G. ruber	-0.61
G. inflata	-0.22
G. trilobus	-0.43
N. dutertrei	-0.16

c) Station M2-1153/1151

Species	VE M2-1153/1151 (‰, PDB)
G. ruber	-0.49
G. aequilateralis	-0.34
G. truncatulinoides (sin.)	-0.25
G. glutinata	-0.58
G. calida	-0.54

5.4 Results and Discussion

5.4.1 Model Application To Field Observations

To test our model we selected ten different species of planktic foraminifers from three different stations. From station EBC the species *Globigerinoides ruber*, *Pulleniatina obliquiloculata, Turborotalita humilis* and *Globorotalia truncatulinoides* (dex.) were chosen. From station M1-21 the species *G. ruber, Globigerinoides trilobus, Neogloboquadrina dutertrei* and *Globorotalia inflata*, while from station M2-1153/1151 *G. ruber, Globigerinita glutinata, Globigerinella aequilateralis, G. inflata* and *G. truncatulinoides* (sin.) were selected.

As the temperature decreases with increasing depth in the water column, the expected oxygen isotopic composition of calcite ($\delta^{18}O_{eq}$), calculated after Kim and O`Neil (1997), shows an increase with depth in the water column (Fig. 5.3 a-c). An increase of the foraminiferal $\delta^{18}O_{shell}$ values from the sea surface to deeper water is shown by all species (Fig. 5.3 a-c). The oxygen isotopic composition of foraminifers depends also on the seawater carbonate ion concentration (Spero et al., 1997), which is usually decreasing with water depth. Thus, the incorporation of oxygen isotopes in planktic foraminiferal calcite may be influenced by the decreasing concentration of this ion with increasing water depth. We observe that the difference between $\delta^{18}O_{shell,}$ corrected for the vital effect, and *in situ* $\delta^{18}O_{eq}$ increases until a certain depth level in the water column (BPZ = base of the productive zone). This implies that the precipitation of calcite, while descending to deeper and colder waters, contributes to the foraminiferal $\delta^{18}O_{shell}$, thus reflecting depth integrated shell growth. Below the BPZ, the $\delta^{18}O_{shell\text{-}export}$ do not show further increase, indicating that no further calcite is precipitated (export zone). The BPZ is thus a transition zone between the production and export zone and reflects approximately the depth at which shell growth ceases (95% growth level) (for discussion see Peeters et al., 2002; Peeters and Wilke, in prep.).

In Figure 5.3 a-c, the modelled shell mass profiles well describe the increase of the $\delta^{18}O_{shell}$ for a particular species at a given station. The calcification pattern of a given species is characterized by species-specific alpha and beta parameter of our model, although some variability in both parameters is observed for a given species at different stations. The model obtained alpha and beta values for all investigated species are listed in Table 5.4 a-c.

5.4.2 Species-Specific Calcification Pattern

5.4.2.1 Globigerinita glutinata

The species *Globigerinita glutinata* is characterized by an α value of 3.1 and a β value of 50, which is typical for a shallow dwelling species (Station M2-1153/1551; Fig. 5.3c). The Cumulative Mass Development Function (CMDF) shows that the base of the productive zone (BPZ, 95% level), *i.e.* the depth level where shell growth ceases, of *G. glutinata* is found at a depth level of 74 m. This indicates that the non-spinose, symbiont-barren species *G. glutinata* calcifies over a narrow depth range in surface water and shell growth is, at least at this station, confined to the surface mixed layer. The Mass Development Density Function (CDDF) indicates that the highest amount of calcite (dM/dZ) is added in a depth of 46 m (Table 5.4). The hydrographic data from the tow station (Fig. 5.1) show that the chlorophyll maximum is well distributed over the upper 100 m. Since the $\delta^{18}O$ values of this species do not show any further change below the surface mixed layer, it may be expected that either *G. glutinata* growths and reproduces in the mixed layer, or if it sinks deeper for reproduction it does not precipitate any further calcite. A preference of *G. glutinata* to live and grow its shell in the surface mixed layer has also been observed by Fairbanks et al. (1982) in the Panama Basin. Consequently, we conclude that the $\delta^{18}O$ of *G. glutinata* records mixed layer temperature.

5.4.2.2 Globigerinoides ruber

The presence of species *Globigerinoides ruber* at the three stations allows to study its calcification pattern in different hydrographic conditions. At station M1-21, *G. ruber* shows an α of 0.6 and a β of 28 (Fig. 5.3b), while at stations EBC and M2-1153/1151 higher values were observed (α=2.5 β=140 and α=2.0 β=100, respectively) (Fig. 5.3a and c). However, our model estimates (CMDF) indicate that calcification of *G. ruber* ceases right beneath the thermocline (=BPZ, 95% level) at the three stations. At station M1-21, the BPZ refers to a depth of 166 m, while at stations EBC and M2-1153/1151, the BPZ is found in a water depth of 215 and 171 m, respectively. Our model estimates further implies that at stations M2-1153/1151 and M1-21 approximately 85% and 77% of the shell is build up in the surface mixed layer, respectively (MDDF). At station EBC, the amount of calcite precipitated in the mixed layer accounts for 54% (Table 5.4). The remaining amounts of calcite are precipitated below the surface mixed layer, *i.e.* in thermocline depths (126-180 m). The CDF indicates that *G. ruber* precipitates highest amounts of calcite at the sea surface at station M1-21, while at station EBC the depth level of highest growth rate is found at the base of mixed layer. This is in accordance with a study by Field (2004) in the California Current, where *G. ruber* was found

in moderate abundance at the base of the mixed layer or within the thermocline. It appears that spinose, symbiont-bearing species *G. ruber* commonly calcifies in the photic zone, which is consistent with earlier observations (Bé, 1977; Fairbanks et al., 1982). However, in contrast to *G. glutinata*, its calcite precipitated in the thermocline might be associated with gametogenesis and precipitation of gametogenic calcite, which considered to take place in deeper and colder waters below the euphotic zone (e.g. Duplessy and Bé, 1981). Thus, the $\delta^{18}O$ signal of this species represents a mixture of 'mixed layer calcite' and 'thermocline calcite'. The observations of *G. ruber* at three stations allows to address the variability of the alpha and beta parameter in response to variations in hydrographic structure. When stratification is higher, as at station M1-21, *G. ruber* calcifies largest amounts in the mixed layer. Calcification at the base of the mixed layer or within the thermocline, however, indicates that the $\delta^{18}O$ *G. ruber* is only partially indicative for sea surface water conditions.

5.4.2.3 Globigerinoides trilobus

Figure 2b shows that the species *G. trilobus* (=*G. sacculifer* without sac-like chamber) calcifies exclusively (100%) in the upper mixed layer at station M1-21 (α=1.8, β=14) (Fig. 5.3b, Table 5.4b). Our model indicates that calcification ceases at 26 m (=BPZ), thus 100% of the shell mass is built up in the mixed layer. Our observation agree well with results of Niebler et al. (1999), who suggest a similar calcification depth range for *G. trilobus* between 0-30 m. This spinose, symbiont-bearing species is generally considered to prefer the warm temperature of the surface mixed layer (e.g. Bé, 1977; Kemle-von Mücke and Oberhänsli, 1999). However, we assume that morphotypes, containing a sac-like chamber, a deeper calcification depth is very likely. Therefore, we assume that the slightly deeper habitat found for this species by other authors (Hemleben and Spindler, 1983; Bijma and Hemleben, 1994), maybe associated with gametogenetic calcification in deeper and colder waters below the euphotic zone (Duplessy and Bé, 1981). We therefore stress that the calcification pattern found here is valid for the morphotype without sac-like last chamber.

5.4.2.4 Neogloboquadrina dutertrei

The non-spinose, symbiont-barren species *Neogloboquadrina dutertrei* is characterized by a α value of 0.7 and a β value of 29 at station M1-21 (Fig. 5.3b). Our model (MDDF) suggests that the depth level of highest growth rate of *N. dutertrei* is found at the sea surface, while calcite precipitation ceases in 135 m (BPZ=95% level) (Table 5.4, Fig. 5.3b). Thus, *N. dutertrei* records an integrated $\delta^{18}O$ signal of the mixed layer and the thermocline, while 78% of the

shell calcite is precipitated in the mixed layer. This in agreement to findings of Bé (1977) and Niebler et al. (1999) who suggested that *N. dutertrei* calcifies between 0 and 100 m, while Fairbanks and Wiebe (1980), Fairbanks et al. (1982) and Kemle-von Mücke (1994) reported that *N. dutertrei* prefers thermocline water. Our modelled calcification pattern indicates that the assumption of *N. dutertrei* to reflect pure thermocline conditions is not true at this station.

Under laboratory conditions it was observed that *N. dutertrei* starts to growth a calcite crust at 15°C (Hemleben et al., 1989). Therefore we hypothesize that *N. dutertrei* adds the remaining 21% calcite below the mixed layer, *i.e.* between 76 m and 133 m, where temperatures of 15.0 to 12.4°C are found. The isotope composition of the calcite precipitated in deeper colder waters will have an effect on the total isotope composition of the test. Hence, our data indicate that the isotopic signal recorded by *N. dutertrei* is not indicative for pure thermocline conditions in this case. However, more model fits to field data are required to fully understand the calcification pattern of *N. dutertrei* and its variability in response to different hydrographic situations.

5.4.2.5 Globigerinella aequilateralis

At station M2-1153/1151 the model fir to the data indicates that the BPZ of the symbiont-bearing species *G. aequilateralis* is found at a depth of 266 m (CMDF). As a result, shell growth is mainly related to waters below the mixed layer (Fig. 5.3c). This is clearly indicated by the relatively high α and β values of 3.2 and 190 (Table 5.4c). Although the chlorophyll maximum at station M2-1153/1551 was associated with the surface mixed layer, *G. aequilateralis* built only 30% of its total shell mass in the surface mixed layer. Due to the fact that *G. aequilateralis* build the largest portion of its shell mass (MDDF) at intermediate depth (169 m) it can be assumed that the thermal information recorded in the isotopic composition of the calcite shell mirror thermocline and sub-thermocline conditions. This confirmes previous findings (Peeters, 2000) for the Arabian Sea region, where *G. aequilateralis* showed subsurface maxima in the shell concentration profiles, thus reflecting waters from slightly below the thermocline. This contradicts the observations of other studies (Berger, 1969; Deuser et al., 1981; Ottens, 1992; Niebler et al., 1999), who placed *G. aequilateralis* within the upper 100 m of the water column.

5.4.2.6 Pulleniatina obliquiloculata

Observations at station EBC indicate that the species *Pulleniatina obliquiloculata* (α=1.8; β= 206) has a relatively wide calcification range. The model suggests that highest amounts of calcite are precipitated within the thermocline (134 m) (Fig. 5.3a). Furthermore, we estimate that 35% of the total shell mass is formed in the mixed layer, while *P. obliquiloculata* adds the remaining 65% of its shell mass below the mixed layer. The CMDF shows that calcification ceases in a water depth of 344 m (=BPZ, 95% level). Thus, *P. obliquiloculata* shows a calcification depth range that comprises the surface mixed layer, the thermocline and sub-thermocline waters. Based on the oxygen isotopic composition from sediment surface samples, Niebler et al. (1999) suggested that *P. obliquiloculata* calcifies in a water depth between 0 and 100 m. This confirms observations by Bé (1977) who found maximum occurrences of *P. obliquiloculata* between 50 and 100 m. However, we observed highest shell concentration of this species at the sea surface at station EBC (Wilke et al., submitted), this exclude not further calcification in deeper waters. Since the species is known to form, on top of its calcite test, a thin amorphous layer on top of its calcite test (Hemleben et al., 1989) we suugest that this layer is formed while descending to deeper colder thermocline and sub-thermocline waters.

5.4.2.7 Globigerina calida

The calcification pattern of *Globigerina calida* at station M2-1153/1151 shows a relatively narrow interval of calcification in deeper water depth (α= 3.2, β= 233). The BPZ was located in a depth of 324 m, and *G. calida* shows highest increase in shell mass in a water depth of 208 m water depth, *i.e.* below the thermocline (Fig. 5.3c, Table 5.4c). Our model indicates that only 17% of the shell mass of *G. calida* is built up in the mixed layer. As a result, the shell isotope chemistry of this species reflects predominantly sub-thermocline conditions, supporting previous findings (Peeters, 2000). Fairbanks et al. (1982) and Niebler (1999) found a slightly shallower calcification depth range for *G. calida* (0 and 250 m) compared to our findings.

5.4.2.8 Globorotalia inflata

We compare the calcification pattern of *G. inflata* at two stations, M1-21 and station M2-1153/1151. At both stations the BPZ for *G. inflata* was found in similar water depth: in 356 m at station M2-1153/1151 (α= 1.2, β= 141) and slightly deeper in 426 m at station M1-21 (α= 1.2, β= 180) (Fig. 5.3b and c, Table 5.4b and c). At station M1-21, *G. inflata* precipitate highest amounts of calcite at the base of the mixed layer (53 m). At station M2-1153/1151 the

level of highest growth rate is found slightly shallower in 24 m. At both stations the level of highest growth rate is associated with the stations chlorophyll maximum. Model fit results indicates that at station M1-21 *G. inflata* precipitates 20% of its total shell mass in the mixed layer, while at station M2-1153/1151, where the mixed layer is deeper (0-138 m), the amount of calcite precipitated in the surface mixed layer accounts for 64%. Apparently, the shell growth pattern depends on the stratification structure of the water column. Under relatively stratified conditions and subsurface chlorophyll maximum (station M1-21), the maximum in the CDDF of *G. inflata* is shifted to deeper water depths and only 20% of the final shell mass was built in the mixed layer. In general, our results corroborate previous results about (Fairbanks et al., 1980; Hemleben et al., 1989; Niebler et al., 1999; Mortyn and Charles, 2003) and support the idea that *G. inflata* inhabits intermediate-deep water depths.

5.4.2.9 Turborotalita humilis

We observe that the spinose species *T. humilis* calcifies over a wide depth range (α= 3.3, β= 475) at station EBC (Fig. 5.3a). A high α and β combination, as observed here, indicate that a large fraction shell mass is added at deeper water depths: The base of the productive zone (BPZ) is found in 654 m, and highest amounts of calcite are precipitated in a water depth of 425 m (Table 5.4a). Based on a seasonal plankton tow study (Wilke et al., submitted) it is evident that this species shows highest concentrations in the nutrient-rich surface mixed layer at station EBC during winter, while it was found in deeper water depth during other seasons. For that reason, *T. humilis* is a good example of a species that seems to change its depth habitat and preferences during its ontogeny, *i.e.* from shallow surface water to deeper cooler water (Hemleben et al., 1989; Wilke et al., submitted). Our model results show that in the mixed layer only 1% of the total shell mass is built up.

5.4.2.10 Globorotalia truncatulinoides

This species shows a calcification depth range of *G. truncatulinoides* clearly exceeding the surface mixed layer and the thermocline depths. The α and β values were high at both stations EBC and M2-1153/1151, (α=2.0, β=414 and α=3.3, β=259, respectively). Similar to *T. humilis*, this indicates a deep calcification depth range. However, this does not inevitable mean that *G. truncatulinoides* calcifies exclusively in deeper waters, as mixed layer calcite accounts for approximately 10% of the total shell mass (Table 5.4a and c). Consequently, the calcite precipitated below the mixed layer, probably in form of a secondary crust (Lohmann and Schweitzer, 1990; Lohmann, 1995), accounts for ~90% of the total shell mass. The species is

considered to have an annual reproduction cycle (Hemleben et al., 1989), and it therefore seems likely that the growth of a calcite crust might take place over a longer time period and a larger depth range. Several studies (Lohmann and Schweitzer, 1990; LeGrande et al., 2004) differentiate between primary and secondary calcite and have explained the $\delta^{18}O$ using a so called two-depth approximation mass balance for *G. truncatulinoides*. Mulitza et al. (1997) observed lower $\delta^{18}O$ values of *G. truncatulinoides* in the subtropics, which they explained by calcification in shallower depth in subtropical environments, whereas in well stratified tropical surface waters *G. truncatulinoides* starts to calcify below the strong pycnocline. Unfortunately, no data from the tropics were used in this study.

Based on our model fits, the final $\delta^{18}O$ of *G. truncatulinoides* (dex.) is considered to reflect an integrated signal over the upper 710 m, while the final $\delta^{18}O$ of *G. truncatulinoides* (sin.) reflects an integrated signal over the upper 357 m (=BPZ) of the water column. Our results indicate that both, sinistral and dextral *G. truncatulinoides* are excellent indicators for deeper water.

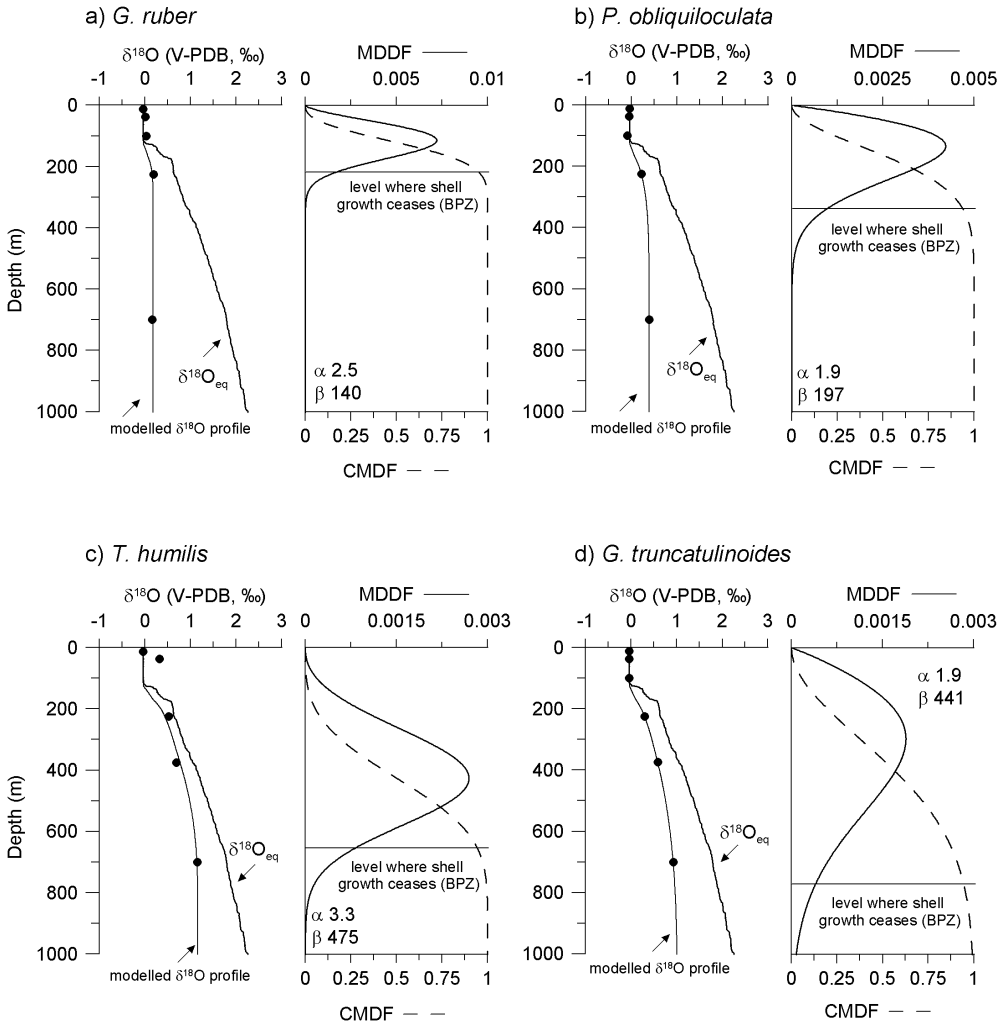

Figure 5.3a. Calcification pattern of four different species at station EBC north of the Canary Islands region off NW-Africa: a) *Globigerinoides ruber*, b) *Pulleniatina obliquiloculata*, c) *Turborotalita humilis* and d) *Globorotalia truncatulinoides*. The left graph shows the increase of the VE-corrected oxygen isotope composition ($\delta^{18}O$) (black dots) with increasing depth in the water column and *in situ* equilibrium ($\delta^{18}O_{eq}$) values calculated after Kim and O`Neil (1997) (thick black line). Further, the modelled $\delta^{18}O$ composition is shown for each species (thin black line). In the right graphs the species-specific cumulative mass development function (CMDF) (dashed line) describes the increase of shell mass with increasing depth characterized by two parameters alpha and beta. Further the species-specific 'growth pattern' is given by the mass development density function (MDDF) ('growth pattern') (black line). The MDDF gives information e.g. about the depth level of highest growths rate. The base of the productive zone (BPZ) indicates the depth level at which species have build up 95% of their shell mass.

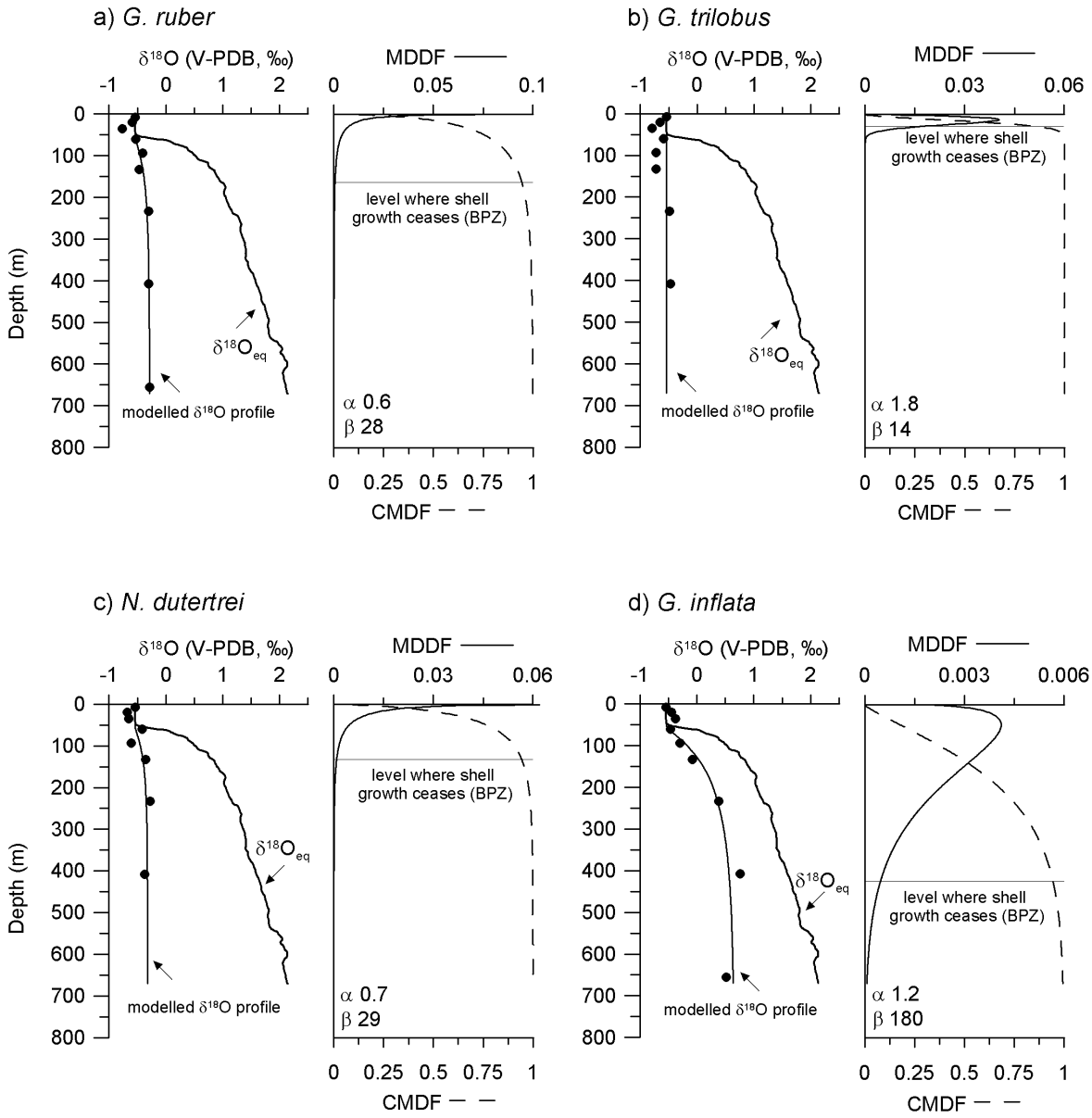

Figure 5.3b. Calcification pattern of four different species: a) *Globigerinoides ruber*, b) *Globigerinoides trilobus* c) *Neogloboquadrina dutertrei* and d) *Globorotalia inflata* at station M1-21 located in the southeastern Atlantic Ocean (Cape Basin). For more information see Figure caption 5.3a.

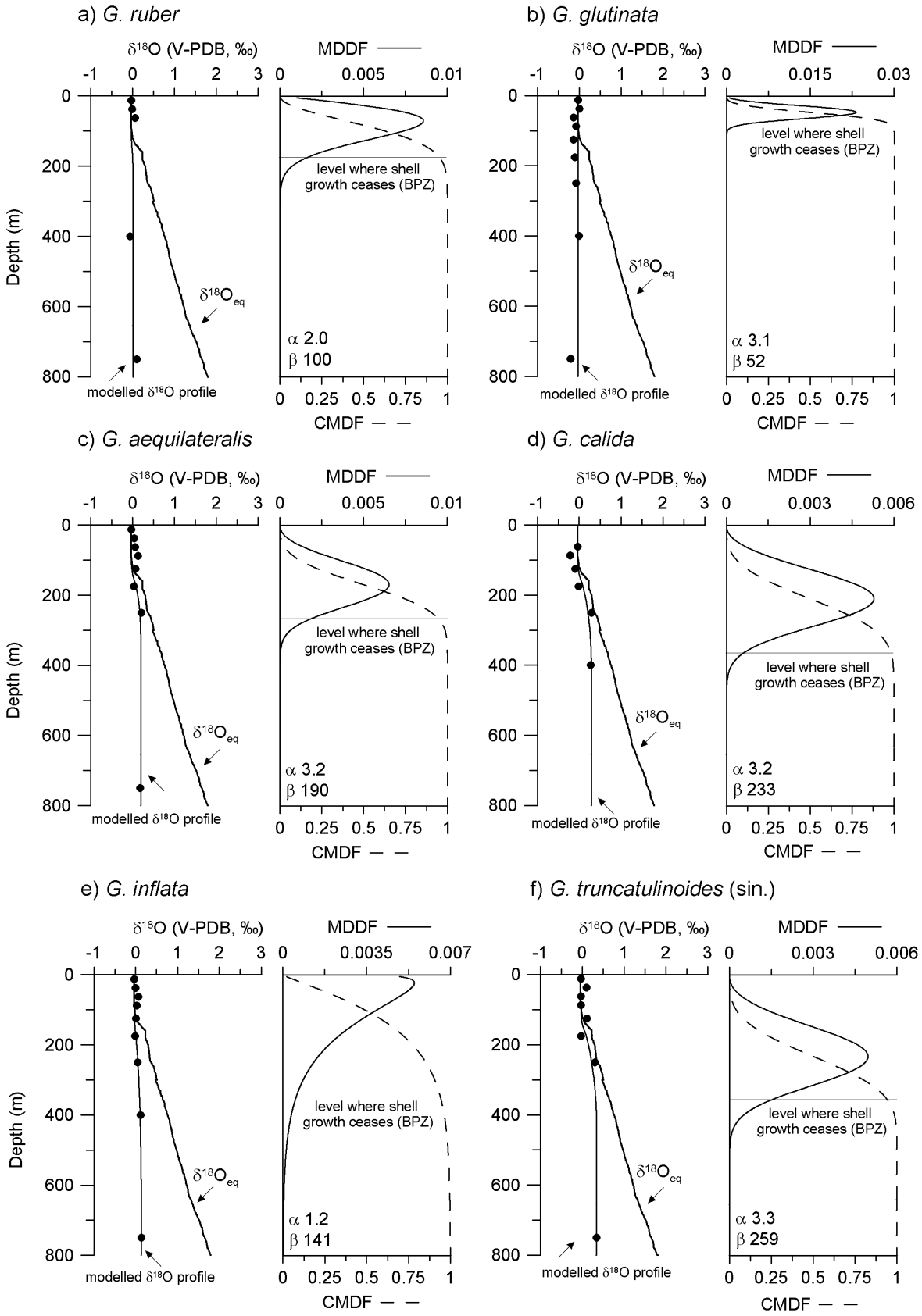

Figure 5.3c. Calcification pattern for six different species: a) *Globigerinoides ruber*, b) *Globigerinita glutinata*, c) *Globigerinella aequilateralis*, d) *Globigerina calida*, e) *Globorotalia inflata* and f) *Globorotalia truncatulinoides* (sin.) at station M2-1153/1151 located in the southeastern Atlantic Ocean (Cape Basin). For more information see Figure caption 5.3a.

Table 5.4. Summarized information on species-specific calcification pattern

a) Station EBC, MLD 126 m

Species	Station	$Depth_{max}$ (m)	alpha	beta	Depth (m) level of		% of $Calcite_{ML}$
					BPZ ($95\%_{shell\ mass}$)	highest growth rate	
G. ruber	EBC	0-25	2.5	140	215	114	54
P. obliquiloculata	EBC	0-25	1.9	197	344	133	35
T. humilis	EBC	0-25	3.3	475	654	425	1
G. truncatulinoides (dex.)	EBC	0-25	1.9	441	774	297	9

$Depth_{max}$ is the depth interval where the species occur in highest concentrations (Wilke et al., submitted)
$Calcite_{ML}$ = Amount of calcite precipitated in the mixed layer

b) Station M1-21, MLD 53 m

Species	Station	$Depth_{max}$ (m)	alpha	beta	Depth (m) level of		% of $Calcite_{ML}$
					BPZ ($95\%_{shell\ mass}$)	highest growth rate	
G. ruber	M1-21	0-15	0.6	28	166	sea surface	77
G. trilobus	M1-21	0-15	1.8	14	26	9	100
N. dutertrei	M1-21	0-15	0.7	29	135	sea surface	78
G. inflata	M1-21	0-15	1.2	180	426	53	20

$Calcite_{ML}$ = Amount of calcite precipitated in the mixed layer

c) Station M2-1153/1151, MLD 138 m

Species	Station	$Depth_{max}$ (m)	alpha	beta	Depth (m) level of		% of $Calcite_{ML}$
					BPZ ($95\%_{shell\ mass}$)	highest growth rate	
G. ruber	M2-1153/1151	25-50	2.0	100	171	71	85
G. glutinata	M2-1153/1151	25-50	3.1	52	74	46	100
G. aequilateralis	M2-1153/1151	75-100	3.2	190	266	169	30
G. calida	M2-1153/1151	100-150	3.2	233	324	208	17
G. inflata	M2-1153/1151	25-50	1.2	141	358	24	62
G. truncatulinoides (sin.)	M2-1153/1151	75-100	3.3	259	357	233	12

$Calcite_{ML}$ = Amount of calcite precipitated in the mixed layer

5.4.3 Sensitivity of alpha and beta to tow interval

For the approximation of the MDF ($\delta^{18}O^{*}_{shell}$) to the observed $\delta^{18}O_{shell}$ values, as shown in the examples above, we used the midpoint of the plankton tow intervals (see column 'G' in Figure 5.2). By doing so we received certain values for alpha and beta. For investigating the sensitivity of alpha and beta to the choice of depth level within the tow interval at which we approximate the observed $\delta^{18}O_{shell}$ values, we used the start and end depth instead of the midpoint of the tow interval.

Using the start depth of the tow interval leads in general to a deeper BPZ (lower alpha values), while using the end depth results in a shallower BPZ (larger alpha values). For instance, for shallow-living species *G. rub*er at station M1-21 (Table 5.4b), we found α and β values of 0.6 and 28 (for midpoint), respectively. This corresponds to a BPZ of 166 m. When using the start depth the BPZ is shifted to 215 m, while it is found at 131 m when the end depth of the tow interval is used. This leads to an uncertainty for the BPZ of approximately 80

m. In terms of mixed layer calcification we found comparable amounts of 73 to 79%. Independent of the chosen depth level, the MDDF showed highest calcification rates for *G. ruber* at the sea surface. Hence, we conclude that in case of shallow-living species, such as *G. ruber* at station M11-21, the choice of the depth level for approximating the data has no significant influence on the interpretation of the calcification pattern of this species. This is also true for species showing a deep calcification depth range and a highest growth rate well below the mixed layer, e.g. as *G. truncatulinoides*.

Caution must be taken when using species that show a large calcification depth range and a relatively shallow depth of maximal growth rate, such as *G. inflata* at station M1-21. Here, under relatively stratified conditions, a shift of the depth of maximal growth rate to a deeper water depth, when using the end depth of the tow interval, can have a significantly different impact on the interpretation. Due to the shallower mixed layer depth at station M1-21 the depth level of highest growth rate can shift from the base of the mixed layer (53 m) to a depth of 105 m, which is well below the mixed layer depth (Table 5.4b).

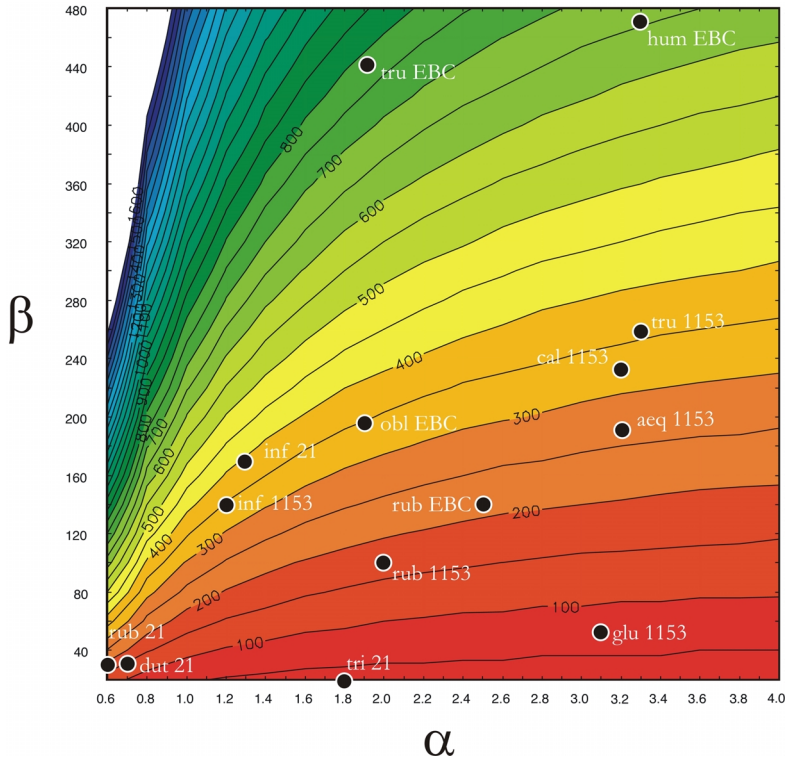

Figure 5.4. Contours showing the depth of the base of the productive zone as a function of the model parameters α and β. Deep living species, e.g. as *G. truncatulinoides, T. humilis* and *G. calida* have larger β-values and show deeper BPZ compare to shallow living species, such as *G. ruber, G. trilobus* and *G. glutinata*. It becomes evident that the same species can be characterized by a different α- and β- combination when found under different hydrographic conditions (e.g. *G. ruber*).

5.5 Conclusion

In this study we tested the use of a mass balance model for the oxygen isotope composition for foraminiferal species. We obtained results that indicate the model is well describing the oxygen isotopic composition of planktic foraminiferal calcite shells as a function of depth in the water column. We used a mass development function to model the increase of shell mass and thus $\delta^{18}O_{shell}$ with depth in the water column. The calcification patterns of ten different species at different stations (Canary Islands region and Cape Basin) are well described by the two parameters alpha and beta of our model. The model results appear useful to quantify the species-specific calcification pattern and providing direct information on the rate of shell mass increase with depth as well as the depth at which shell growth ceases. Although additional model fits to field data are needed to estimate the range of variability of potentially species-specific model parameters alpha and beta, our results thus far suggest that the calcification pattern of a given species may depend on the vertical stratification and level of food availability (e.g. mixed layer depth and deep chlorophyll max.), as also indicated in previous studies.

At the stations investigated here, the species *Globigerinita glutinata* and *Globigerinoides trilobus* calcified exclusively in the mixed layer, while *Globigerinoides ruber* represented a mixed sea surface (~75%) and upper thermocline (~25%) signal. Although at the investigated stations *G. glutinata* and *G. trilobus* preserve a pure mixed layer signal, most other species calcify over wider depth ranges. Our model further indicates that the information recorded in the isotopic composition of *P. obliquiloculata* and *G. aequilateralis* mirror thermocline to sub-thermocline conditions, although both species build up ~30% of their total shell mass in the mixed layer. The species *Globorotalia inflata* precipitates highest amounts of calcite near with the depth of the chlorophyll maximum, and continuous shell growth in relatively deep waters down to ~400 m. Under stratified conditions and subsurface chlorophyll maximum the depth of maximal precipitation of *G. inflata* is shifted to deeper water depths and only 20% of it final shell mass is built in the mixed layer. At the investigated stations, the calcification depth range of *Globigerina calida* is comparable to *G. inflata,* whereby the depth level of highest growth rate of *G. calida* is found deeper, *i.e.* below the thermocline, and only 17% of its calcite is built up in the mixed layer. Based on our model, the species *Globorotalia truncatulinoides* and *Turborotalia humilis* show the deepest calcification depth ranges. Calcification of *G. truncatulinoides* (dex.) ceases in ~770 m, while less than 10% of shell mass is added in the mixed layer. Highest amounts of calcite are added below 300 m, probably in form of a secondary crust which accounts for ~80-90%.

The results of this study provide a new basis for reconstructing the thermal structure of the water column using multiple species of planktic foraminifers and give therefore greater insights into the mechanism of climatic changes.

References

Bé, A.W.H., 1977. An ecological, zoogeographic and taxonomic review of recent planktonic foraminifera. In: Ramsay, A.T.S. (Editor), Oceanic Micropaleontology, Vol. 1, London, pp. 1-100.

Berger, W.H., 1969. Ecologic patterns of living planktonic Foraminifera. Deep-Sea Research I 16, 1-24.

Bijma, J., Faber, W.W. and Hemleben, C., 1990b. Temperature and salinity limits for growth and survival of some planktonic foraminifers in laboratory cultures. Journal of Foraminiferal Research 20, 95-116.

Bijma, J. and Hemleben, C., 1994. Population dynamics of the planktic foraminifer *Globigerinoides sacculifer* (Brady) from the central Red Sea. Deep Sea Research I 41(3), 485-510.

Deuser, W.G., Hemleben, C. and Spindler, M., 1981. Seasonal changes in species composition, numbers, mass, size, and isotopic composition of planktonic foraminifera settling into the deep Sargasso Sea. Palaeogeogr., Palaeoclim., Palaeoecol. 33, 103-127.

Duplessy, J.C. and Bé, A.W.H., 1981. Oxygen-18 enrichment of planktonic foraminifera due to gametogenic calcification below the euphotic zone. Science 213, 1247-1250.

Fairbanks, R.G., Sverdlove, M., Free, R., Wiebe, P.H. and Be, A.W.H., 1982. Vertical distribution and isotopic fractionation of living planktonic foraminifera from the Panama Basin. Nature 298, 841-844.

Fairbanks, R.G. and Wiebe, P.H., 1980. Foraminifera and chlorophyll maximum: vertical distribution, seasonal succession, and paleoceanographic significance. Science 209, 1524-1526.

Fairbanks, R.G., Wiebe, P.H. and Be, A.W.H., 1980. Vertical distribution and isotopic composition of living planktonic foraminifera in the western North Atlantic. Science 207, 61-64.

Field, D.B., 2004. Variability in vertical distribution of planktonic foraminifera in the California Current: Relationships to vertical ocean structure. Paleoceanography 19.

Hemleben, C. and Spindler, M., 1983. Recent advances in reasearch on living planktonic foraminifera. Utrecht Micropaleontol Bull 30, 141-170.

Hemleben, C., Spindler, M. and Anderson, O.R., 1989. Modern Planktonic Foraminifera. Springer Verlag, New York, 363 pp.

Kemle-von Mücke, S. and Oberhänsli, H., 1999. The distribution of living planktic foraminifera in relation to southeast Atlantic oceanography. In: Fischer, G. and Wefer, G. (Eds.), Use of proxies in paleoceanography: Examples from the South Atlantic. Springer, Berlin, pp. 91-115.

Kim, S.-T. and O`Neil, J.R., 1997. Equilibrium and non-equilibrium oxygen isotope effects in synthetic carbonates. Geochimica et Cosmochimica Acta 61, 3461-3475.

LeGrande, A.N., Lynch-Stieglitz, J. and Farmer, E., 2004. Oxygen isotopic composition of *Globorotalia truncatulinoides* as a proxy for intermediate depth density. Paleoceanography 19.

Lohmann, G.P., 1995. A model for variation in the chemistry of planktonic foraminifera due to secondary calcification and selective dissolution. Paleoceanography 10, 445-457.

Lohmann, G.P. and Schweitzer, P.N., 1990. *Globorotalia truncatulinoides*: Growth and chemistry as probes of the past thermocline: 1. shell size. Paleoceanography 5, 55-75.

Mortyn, G.P. and Charles, C.D., 2003. Planktonic foraminiferal depth habitat and delta ^{18}O calibrations: Plankton tow results from the Atlantic sector of the Southern Ocean. Paleoceanography 18.

Mulitza, S., Dürkoop, A., Hale, W., Wefer, G. and Niebler, H.S., 1997. Planktonic foraminifera as recorders of past surface-water stratification. Geology 25(4), 335-338.

Niebler, H.S., Hubberten, H.W. and Gersonde, R., 1999. Oxygen Isotope Values of Planktic Foraminifera. In: Fischer, G. and Wefer, G. (Eds.), Use of proxies in paleoceanography: Examples from the South Atlantic. Springer, Berlin, pp. 165-189.

Ortiz, J.D., Mix, A.C. and Collier, R.W., 1995. Environmental control of living symbiotic and asymbiotic foraminifera of California Current. Paleoceanography 10, 987-1009.

Ortiz, J.D., Mix, A.C., Rugh, W., Watkins, J.M. and Collier, R.W., 1996. Deep-dwelling planktonic foraminifera of the northeastern Pacific Ocean reveal environmental control of oxygen and carbon isotope disequilibria. Geochim. Cosmochim. Acta 60(22), 4509-4523.

Ottens, J.J., 1992. Planktic Foraminifera as indicators of ocean environments in the Northeast Atlantic. Ph.D.-thesis, 189 pp.

Peeters, F.J.C., 2000. The distribution and stable isotope composition of living planktic foraminifera in relation to seasonal changes in the Arabian Sea. Ph.D. Thesis. Free University, Amsterdam, The Netherlands, 184 pp.

Peeters, F.J.C., Brummer, G.-J. and Ganssen, G., 2002. The effect of upwelling on the distribution and stable isotope composition of *Globigerina bulloides* and *Globigerinoides ruber* (planktic foraminifera) in modern surface waters of the NW Arabian Sea. Global and Planetary Change 34, 269-291.

Peeters, F.J.C. and Wilke, I., in prep. Depth integrated growth of planktic foraminiferal shells Part 1. The theory of an oxygen isotope mass balance model.

Sautter, L.R. and Thunell, R.C., 1991a. Planktonic foraminiferal response to upwelling and seasonal hydrographic conditions: Sediment trap results from San Pedro Basin, Southern California Bight. Journal of Foraminiferal Research 21(4), 347-363.

Spero, H.J., Bijma, J., Lea, D.W. and Bemis, B., 1997. Effect of seawater carbonate concentration on foraminiferal carbon and oxygen isotopes. Nature 390, 497-500.

Watkins, J.M. and Mix, A., 1998. Testing the effects of tropical temperature, productivity, and mixed-layer depth on foraminiferal transfer functions. Paleoceanography 13, 196-205.

Watkins, J.M., Mix, A. and Wilson, J., 1996. Living planktic foraminifera: tracers of circulation and productivity regimes in the central equatorial Pacific. Deep Sea Research II 4-6, 1257-1282.

Wilke, I., Meggers, H. and Bickert, T., submitted. Seasonal distribution and stable oxygen isotope composition of planktic foraminifera off NW-Africa: from production to preservation.

CHAPTER 6*

THE INFLUENCE OF SEAWATER CARBONATE ION CONCENTRTATION [CO_3^{2-}] ON THE STABLE CARBON ISOTOPE COMPOSITION OF PLANKTIC FORAMINIFERA SPECIES *GLOBOROTALIA INFLATA*

Iris Wilke and Torsten Bickert

Fachbereich Geowissenschaften/MARUM, Universität Bremen, Leobenerstrasse, 28359 Bremen, Germany

*This chapter is submitted for publication
to *Marine Micropaleontology*

6.1 Abstract

We sampled the upper water column for living planktic foraminifera along the SW-African continental margin. The species *Globorotalia inflata* strongly dominates the foraminiferal assemblages with an overall relative proportion of up to 90%. The shell $\delta^{18}O$ and $\delta^{13}C$ values of *G. inflata* were measured and compared to predicted $\delta^{18}O_{calcite}$ values and to $\delta^{13}C_{DIC}$ of the dissolved inorganic carbon of seawater. The $\delta^{18}O$ of *G. inflata* reflects the general gradient observed in the predicted $\delta^{18}O_{calcite}$ profile, while the $\delta^{13}C$ of *G. inflata* shows almost no variation with depth and the reflection of the $\delta^{13}C_{DIC}$ in the foraminiferal shell seems to be covered by other effects.

The oxygen isotope composition were used to calculate in which proportion *G. inflata* takes up its isotopic signal in the different depth intervals of the upper 500 m of the water column. The mass-weighted $\Delta\delta^{13}C_{shell\text{-}DIC}$ signal correlates negatively with the $[CO_3^{2-}]$ of the water column. We found similar $\Delta\delta^{13}C_{shell\text{-}DIC}/ [CO_3^{2-}]$ slopes for *G. inflata* in the large size fraction (250-355 μm) and for the smaller specimens (150-250 μm) of -0.012 to 0.015 and –0.012 to -0.014‰ $(\mu mol*kg^{-1})^{-1}$, respectively. These slopes are in the range of those found for other non-symbiotic species, such as *Globigerina bulloides*, from laboratory culture experiments. Since the $\Delta\delta^{13}C_{shell\text{-}DIC}/ [CO_3^{2-}]$ slopes from our field data are nearly identical to the slopes established from laboratory culture experiments we assume that the influence of other effects on the $\delta^{13}C_{shell\text{-}DIC}$, such as temperature, are negligible small. If we correct the $\delta^{13}C$ values of *G. inflata* for a carbonate ion effect, the $\delta^{13}C_{shell}$ and $\delta^{13}C_{DIC}$ are correlated with an average offset of ~1.55‰.

6.2 Introduction

Planktic foraminifera usually use the dissolved inorganic carbon (DIC) of the surrounding seawater to build their calcitic shells. Hence, they are an excellent tool for the reconstruction of the $\delta^{13}C_{DIC}$ of past ocean waters, assuming equilibrium fractionation during calcification. Once this requirement is fulfilled or disequilibrium effects have been quantified, $\delta^{13}C_{DIC}$ can be used as a proxy for past oceanic circulation and variations of the carbonate system, biological productivity and nutrient cycling in surface waters (Kahn and Williams, 1981; Broecker and Peng, 1982; Bouvier-Soumagnac and Duplessy, 1985; Kroon and Ganssen, 1989). The $\delta^{13}C_{DIC}$ itself is mainly controlled by a kinetic fractionation during the photosynthesis-respiration cycle, and by a thermodynamic fractionation during the exchange of CO_2 between the atmosphere and the ocean (Broecker and Maier-Reimer, 1992; Charles et al., 1993; Lynch-Stieglitz et al., 1995).

Many studies have shown that the $\delta^{13}C$ of planktic foraminifera calcite often deviates from the $\delta^{13}C_{DIC}$. Ontogenetic and metabolic effects, kinetic fractionation effects and the effect of photosynthetic utilization by symbionts have been discussed (e.g. Shackleton and Vincent, 1978; Wefer and Berger, 1991; Ravelo and Fairbanks, 1995; Spero and Lea, 1996; Mulitza et al., 1999; Peeters et al., 2002). Furthermore, the carbonate ion concentration $[CO_3^{2-}]$ of seawater appears to be a major feature influencing the $\delta^{13}C$ of the shell carbonate (Spero et al., 1997). These authors demonstrated that the $\delta^{13}C$ of planktic foraminifera decreases with increasing $[CO_3^{2-}]$ of the culture medium since the HCO_3^- is isotopically heavier than the CO_3^{2-}

Since ice core records indicate lower atmospheric CO_2 concentrations during glacial times (Jouzel et al., 1993), different hypotheses arose to explain this lower atmospheric CO_2 content. Archer and Maier-Reimer (1994) put forward the hypothesis of an increased ocean alkalinity, i.e. a higher $[CO_3^{2-}]$ during glacial times. This was also suggested by Sanyal et al. (1995) using boron isotopes ($\delta^{11}B$) measurements for seawater pH reconstructions. An elevated seawater pH during glacial times might explain the more negative $\delta^{13}C$ values of planktic foraminifera calcite found in glacial sediments without altering mean ocean $\delta^{13}C_{DIC}$ (Lea et al., 1999).

This paper is a contribution to the field investigations of the carbonate ion effect on the $\delta^{13}C$ of planktic foraminifera (Russell and Spero, 2000; Itou et al., 2001; Bauch et al., 2002). For this purpose the non-symbiotic species *Globorotalia inflata* were chosen, sampled by stratified plankton tows at four stations in the southeast Atlantic Ocean (Fig. 6.1).

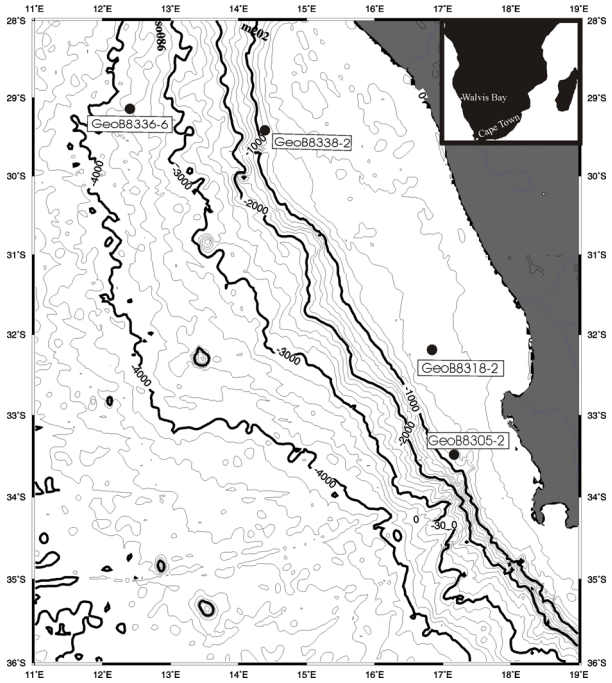

Figure 6.1. Map of the study area in the eastern South Atlantic (Cape Basin). Closed circles indicate location of plankton tow casts taken during M57/1 in January/ February 2003: GeoB 8336, 8338, 8318 and 8305.

6.3 Material and analysis

Plankton tow samples and samples of the ambient seawater investigated in this study were collected during Meteor cruise M57/1 in January/February 2003 in the southeastern Atlantic Ocean (Cape Basin) (Fig. 6.1, Table 6.1) (Schneider et al. 2003). Planktic foraminifer samples were collected with a Multiple Opening-Closing Net (multinet). The nets of 63 µm mesh size were towed vertically with maximum winch speed of 0.5 ms^{-1} at 20 m depth intervals for a shallow (0-20, 20-40, 40-60, 60-80 and 80-100 m) and a deep cast (100-200, 200-300 and 300-500 m). On board all samples were conserved with a saturated $HgCl_2$ solution and stored at 4°C. Planktic foraminifera species were picked out by pipette from the wet sample. All species >150 µm were counted and identified using the taxonomy of Bé (1977) and Hemleben et al. (1989).

Table 6.1. Station location and general hydrographic information

GeoB-Station	*Date*	Longitude (E)	Latitude (S)	Water depth (m)	SST (°C)	MLD (m)[2]	$Depth_{max}$ (m) *G. inflata*
8305	23.01.03	17°10.17	33°28.55	712	21.10	47	0-20/ 60-80
8318	28.01.03	16°48.47	32°09.16	307	18.05	12	40-60/ 80-100
8336	02.02.03	12°20.14	29°12.14	3626	21.00	37	20-40
8338	03.02.03	14°19.42	29°29.94	915	20.67	21	20-40/ 60-80

[1]SST = Sea Surface Temperature
[2]MLD = Mixed layer depth. The depth of the mixed layer is defines at that depth at which the water temperature is 0.5 °C less than the SST

Stable isotope determinations of *G. inflata* in two size classes (150-250 µm and 250-355 µm) were conducted at the University of Bremen using a Finnigan Mat 252 mass spectrometer equipped with an automatic carbonate preparation device. Isotope composition is given in the usual δ-notation and is calibrated to Vienna Pee Dee Belemnite (V-PDB) standard. Precision based on replicates of an internal standard (Solnhofer limestone) was better than 0.05‰.

Water samples were collected right before the plankton sampling procedure using a Rosette equipped with 18 water samplers (each 10 liters volume). Each station was accompanied by a CTD cast providing information on the vertical structure of the water column including temperature, salinity and fluorescence. Water from each sampler was filled into glass bottles, carefully avoiding air bubbles in the filling tube and in the bottle to minimize the exchange of CO_2 between water and air. Samples for $\delta^{13}C$ of the total dissolved inorganic carbon (DIC) were conserved with a saturated $HgCl_2$ solution and all samples were sealed airtight with molten paraffin. The DIC was extracted from seawater by reacting with 100 % H_3PO_4 at 25 °C applying a fully automatic extraction line using the Gas Bench II system (Finnigan MAT). The $\delta^{13}C$ of $\sum CO_2$ was measured with a Finnigan MAT Delta Plus mass spectrometer directly coupled to the Gas Bench via an open split. All $\delta^{13}C$ measurements were run triplicate. The external reproducibility was better than 0.06‰.

Since water sampled for oxygen isotope determination of seawater ($\delta^{18}O_w$) were not available, we calculated the $\delta^{18}O$ of the seawater using the equation for Southern Ocean surface water relationship between $\delta^{18}O_w$ and salinity as reported by Duplessy et al. (1991):

$$\delta^{18}O_w = -18.791 + 0.546 * S \qquad [1]$$

where S denoted the salinity. The oxygen "equilibrium calcite values", $\delta^{18}O_{calcite}$, are calculated using the calculated oxygen isotope composition of seawater ($\delta^{18}O_w$) and in situ temperature (T). We choose the equation of Kim and O`Neil (1997) because it is based on inorganic calcite without any species-specific biological influence. The oxygen isotope equilibrium value for inorganic (synthetic) calcium carbonate precipitated at low temperatures (10-40°C) follows the relationship:

$$\delta^{18}O_{calcite} = 25.778 - 3.333 * (43.704 + T)^{0.5} + \delta^{18}O_w \qquad [2]$$

Water samples for Total Alkalinity (TA) and total dissolved inorganic carbon (DIC) were filtered onboard and treated similar as the samples for $\delta^{13}C$. TA and DIC measurements were later conducted at the Alfred-Wegener Institute for Polar and Marine Research in Bremerhaven, Germany by titration and continous flow analysis (Stoll et al., 2001), respectively. The carbonate ion concentration [CO_3^{2-}] were calculated from DIC and TA using the software program CO2SYS (version 5.1) of Lewis and Wallace (1998). We used the constants of Weiss (1974) for k_o (the solubility of CO_2 in seawater), Roy et al. (1993) for k_1 (2s=2%) and k_2 (2s=1.5%), the equilibrium constants that define the speciation of CO_2 in seawater, and Dickson (1990) for k_B (dissociation constant of borate). The effects of pressure on k_1 and k_2 are from Millero (1995) and on k_B from Millero (1979).

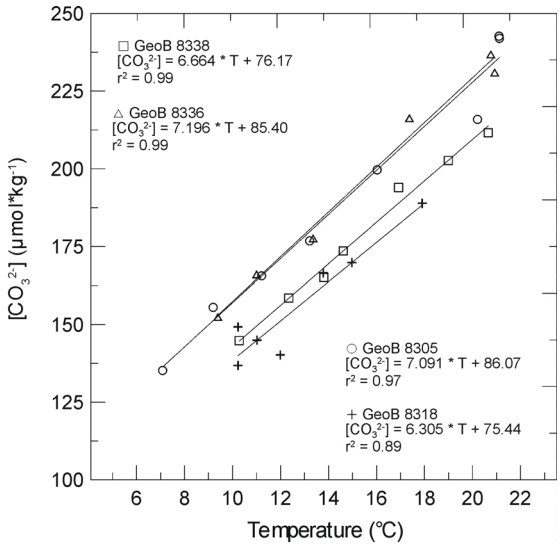

Figure 6.2. Seawater temperature versus carbonate ion concentration ([CO_3^{2-}]) of the upper 500 m of the water column at stations GeoB 8336, 8338, 8318 and 8305.

6.4 Hydrography of the Cape Basin

The Benguela Current Upwelling regime is one of the four major eastern ocean boundary currents of the world. Although upwelling occurs all along the African west coast, several regions of recurring patches of intense upwelling have been identified. The largest and most persistent cell is the Lüderitz upwelling cell, which effectively divides the Benguela upwelling system into a northern and southern regime. The upwelling cells are generally located in regions where there is a change in orientation of the coastline (Shannon and Nelson, 1996). In general, the wind dominated upwelling system brings cold nutrient-rich water to the surface.

Figure 6.3 shows temperature-salinity plots for station GeoB 8336 (3000 m water depth, open ocean) and GeoB 8318 (250 m water depth, shelf). Four water masses could be identified: South Atlantic Surface Water (SASW), South Atlantic Central Water (SACW), Antarctic Intermediate Water (AAIW) and North Atlantic Deep Water (NADW). Table 6.2 lists the physical characteristics of each water mass and the depth at which it was identified at this particular site. It is the SACW water that upwells to the surface along the coast between 18°S and 34°S. It is found throughout the SE Atlantic between surface waters and Antarctic Intermediate (AAIW) waters or it extends to the bottom on the continental shelf. It is formed at the Subtropical Convergence (STC) by sinking and northward spreading of mixed subtropical and subantarctic water masses. Its characteristic temperatures and salinities are 6.1°C-15.2°C and 34.4-35.4 psu, respectively. At stations GeoB 8318 and 8338 the influence of upwelling waters becomes clearly visible by a shallower mixed layer and a stronger gradient of temperature, $\delta^{13}C$ and $[CO_3^{2-}]$ in the upper 50 m (Fig. 6.4 and 6.5). Upwelling causes also changes in surface water carbonate chemistry. For example, at station GeoB 8318 upwelling leads to lower carbonate ion concentration in surface waters by ~60 μmol*kg^{-1}. Since temperature and $[CO_3^{2-}]$ are linear correlated in the ocean (Fig. 6.2), we used the linear regression between the two parameters ($[CO_3^{2-}] = 7.32*T + 73.62$) to calculate $[CO_3^{2-}]$ concentrations for depths were no samples were available to complete the CO_3^{2-}-profile.

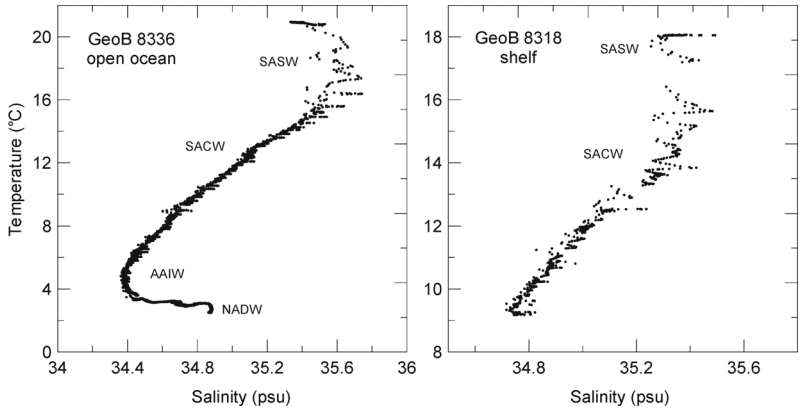

Figure 6.3. Temperature-salinity plot for station GeoB 8336 (~3000 m, open ocean) and 8318 (~250 m, shelf). In total four different water masses could be identified: South Atlantic Surface Water (SASW), South Atlantic Central Water (SACW), Antarctic Intermediate Water (AAIW) and North Atlantic Deep Water (NADW). For further information see Table 6.2.

Table 6.2. Physical characteristics of water masses encountered at CTD station GeoB8336

Water Mass	Temp. range (°C)	Salinity range (psu)	Depth range (m)	Density (sigma-t)
SASW	15.5- 21.3	35.3- 35.7	0- 60	25.0- 26.0
SACW	6.1- 15.2	34.4- 35.4	60- 600	26.3- 27.3
AAIW	4.0-6.0	34.3- 34.5	780 (core)	27.3- 27.5
NADW	< 3.0	> 34.5	1100 (core)	27.8- 28.0

6.5 Results

6.5.1 Planktic foraminifera abundance

The species *Globorotalia inflata* strongly dominates the faunal assemblage at all stations with an overall relative proportion of 68-89%. The absolute abundance of *G. inflata* (ind./m^3) individuals >150 μm in the upper 500 m (300 m at GeoB 8318) is highest at station GeoB 8338 with 444 ind/m^3 and lowest on the shelf at GeoB 8318, where only ~50 ind./m^3 occur (Fig. 6.4). Maximal shell concentration of *G. inflata* are found within the mixed layer and the thermocline, coincident to highest chlorophyll-a values indicating the high primary production zone and depth of maximum food supply. In general the shell concentration decreases with depth in the water column.

Beside *G. inflata*, the deep dwelling species *Globorotalia scitula* was abundant in relatively high concentrations below 100 m water depth, thus below the thermocline. The nearcoast station GeoB 8338 (915 m) shows elevated numbers of *Globigerina bulloides,* a species known to occur also in nutrient-rich upwelling waters (Thiede, 1975). At GeoB 8318, located on the shelf, we found increased numbers of the polar species *Neogloboquadrina pachyderma* (sin.). In contrast, the southern most station GeoB 8305 is characterized by increased numbers of tropical and subtropical species such as *Orbulina universa, Globigerinoides ruber* white and *Globorotalia menardii*, indicating probably a warm water influence by Indian Ocean waters via Agulhas leakage.

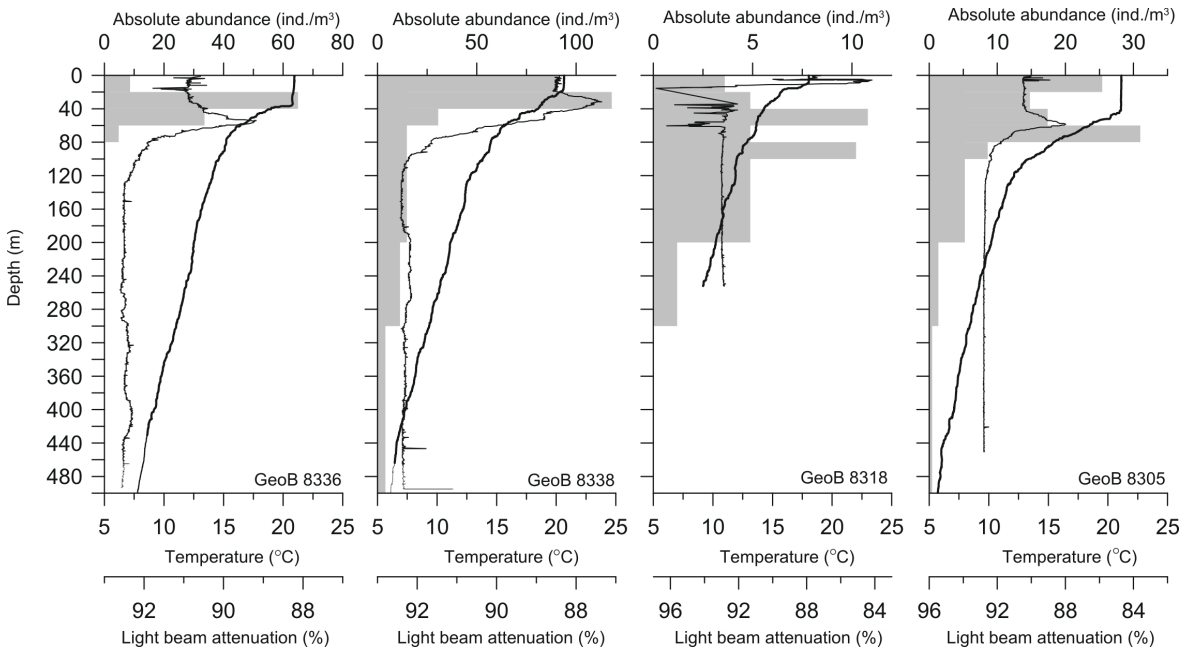

Figure 6.4. Graphs showing hydrographic conditions (temperature, light beam attenuation) and absolute abundances (ind./m³) of *G. inflata* (>150 μm) as standing stock in the upper water column at stations GeoB 8336, 8338, 8318 and 8305 collected in seven depth intervals. The widths of the gray bars cover the depth range of each sampling interval. Note different scales.

6.5.2 Stable isotopes

The vertical profiles of calculated $\delta^{18}O$ equilibrium calcite ($\delta^{18}O_{calcite}$) show a strong increase with depth (Fig. 6.5a) according to the observed decreasing temperature (e.g. Kim and O`Neil, 1997). The stable oxygen isotope depth profiles of *G. inflata* ($\delta^{18}O_{G.\ inflata}$) show also a strong increase with depth reflecting the general gradient seen in the $\delta^{18}O_{calcite}$ profiles. However, in the upper mixed layer $\delta^{18}O$ values of *G. inflata* (250-355 μm) are slightly higher (0.11‰ (±0.14‰)) than $\delta^{18}O_{calcite}$ equilibrium values (except at station GeoB 8318). Below the mixed layer, the $\delta^{18}O$ values are generally lower than the equilibrium values by about 0.5 to 1.1‰ (Table 6.3).

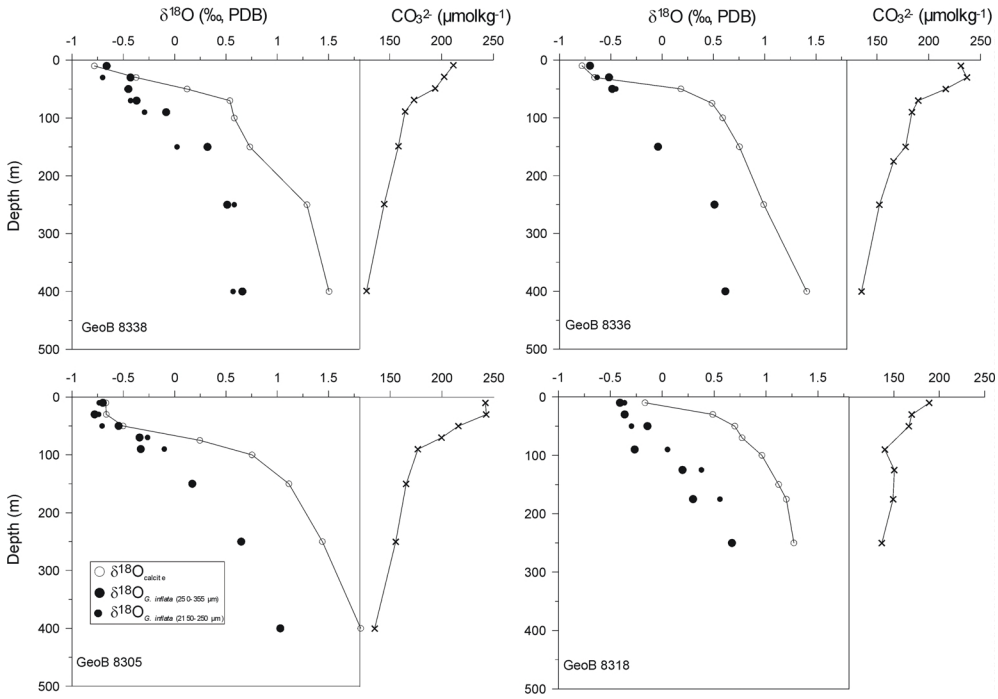

Figure 6.5a. The $\delta^{18}O$ composition of *G. inflata* (150-250(small filled dots) and 250-355 µm(large filled dots)) in the upper water column in the Cape Basin. The foraminiferal values are directly compared to equilibrium $\delta^{18}O_{calcite}$ values (open dots). For each station the decrease of the $[CO_3^{2-}]$ with depth in the water column are shown.

At all stations the $\delta^{13}C_{DIC}$ is highest at the sea surface and shows in general a sharp decrease below the mixed layer. Minimum $\delta^{13}C_{DIC}$ values occur at approximately 100 m and remain nearly constant below this depth. The carbon isotope values of *G. inflata* do not reflect the sharp decrease with depth observed in the $\delta^{13}C_{DIC}$. While showing some scatter in the upper mixed layer, *G. inflata* shows even a slight increase to heavier $\delta^{13}C$ values with depth (Fig. 6.5b, Table 6.3). The $\delta^{13}C$ of *G. inflata* range between +0.21 and +0.69‰ in the 150-250 µm size class, and between +0.38 and +0.88‰ in the larger size class 250-355 µm. In contrast to $\delta^{18}O$ values, the $\delta^{13}C$ values of *G. inflata* show a clear size dependence. Smaller individuals are on average 0.23‰ (±0.11‰, n=20) lighter compared to the individuals of the larger size fraction.

Specimens of *G. inflata* in the 250-355 µm size fraction are on average about 0.50‰ lighter than the $\delta^{13}C_{DIC}$ regarding the upper 500 m of the water column. Smaller specimens (150-250 µm) show even an average offset of –0.87‰. In the upper most depth interval (0-20 m) the deviations from $\delta^{13}C_{DIC}$ were usually highest: -0.95‰ in the larger size class and –1.21‰ in the smaller size class, respectively.

Table 6.3. Stable oxygen and carbon isotopic composition of *G. inflata* in two size fractions (150-250 and 250-355 μm) from plankton samples, and hydrographic data ($\delta^{13}C_{DIC}$, $\delta^{18}O_{calcite}$, carbonate ion concentration ($[CO_3^{2-}]$) and temperature at stations GeoB 8305, 8318, 8336 and 8338.

GeoB-Station	*Depth (m)*	$\delta^{18}O$ (‰, PDB)		$\delta^{13}C$ (‰, PDB)		$\delta^{13}C_{DIC}$ (‰, PDB)	$\delta^{18}O_{calcite}$ (‰, PDB)	$[CO_3^{2-}]$ (μmolkg^{-1})	T (°C)
		150-250 μm	250-355 μm	150-250 μm	250-355 μm				
8305	0-20	-0.74	-0.32	0.26	0.59	1.320	-0.670	242.0	21.12
	20-40	-0.74	-0.78	0.30	0.47	1.297	-0.666	242.7	21.10
	40-60	-0.71	-0.55	0.15	0.57	1.290	-0.502	215.9	20.20
	60-80	-0.26	-0.34	0.31	0.60	0.860	0.246		16.02
	80-100	-0.10	-0.33	0.24	0.55	0.630	0.754	176.8	13.21
	100-200	0.18	0.17	0.37	0.61	0.770	1.114		11.21
	200-300		0.65		0.69	0.848	1.440	155.5	9.19
	300-500		1.03		0.88	0.781	1.813	135.2	7.08
8318	0-20	-0.36	-0.41	0.21	0.60	1.712	-0.166	188.90	17.90
	20-40		-0.36		0.52	0.936	0.487		14.97
	40-60	-0.30	-0.14	0.27	0.54	1.035	0.699	166.5	13.78
	60-80					1.203	0.769		
	80-100	0.05	-0.27	0.35	0.55	1.176	0.961	140.2	11.99
	100-150	0.38	0.19	0.44	0.48	1.122	1.122	150.47	11.90
	150-200	0.56	0.14	0.47	0.57	1.047	1.196		10.23
	200-300		0.94		0.76	0.925	1.268	136.8	10.23
8336	0-20		-0.70		0.52	1.528	-0.781	231.0	20.92
	20-40	-0.63	-0.52	0.38	0.63	1.577	-0.658		20.76
	40-60	-0.45	-0.49	0.41	0.45	1.653	0.183	216.3	17.37
	60-80					1.098	0.486		15.27
	80-100					0.858	0.590	183.8	14.60
	100-200		-0.64		0.61	1.000	0.754	177.6	13.36
	200-300		0.51		0.77	1.081	0.990	152.4	12.51
	300-500		0.62		0.75	1.001	1.410	135.2	11.00
8338	0-20	-0.65	-0.66	0.52	0.83	1.669	-0.782	211.6	20.65
	20-40	-0.70	-0.43	0.69	0.82	1.502	-0.375		18.99
	40-60	-0.46	-0.45	0.55	0.72	1.070	0.121	194.0	16.92
	60-80	-0.43	-0.37	0.53	0.86	0.978	0.539		14.61
	80-100	-0.29	-0.08	0.33	0.49	0.941	0.581	165.0	13.80
	100-200	0.02	0.32	0.30	0.60	0.855	0.733		12.34
	200-300	0.58	0.51	0.40	0.61	0.790	1.289	144.8	10.28
	300-500	0.57	0.66	0.32	0.80	1.007	1.505		7.71

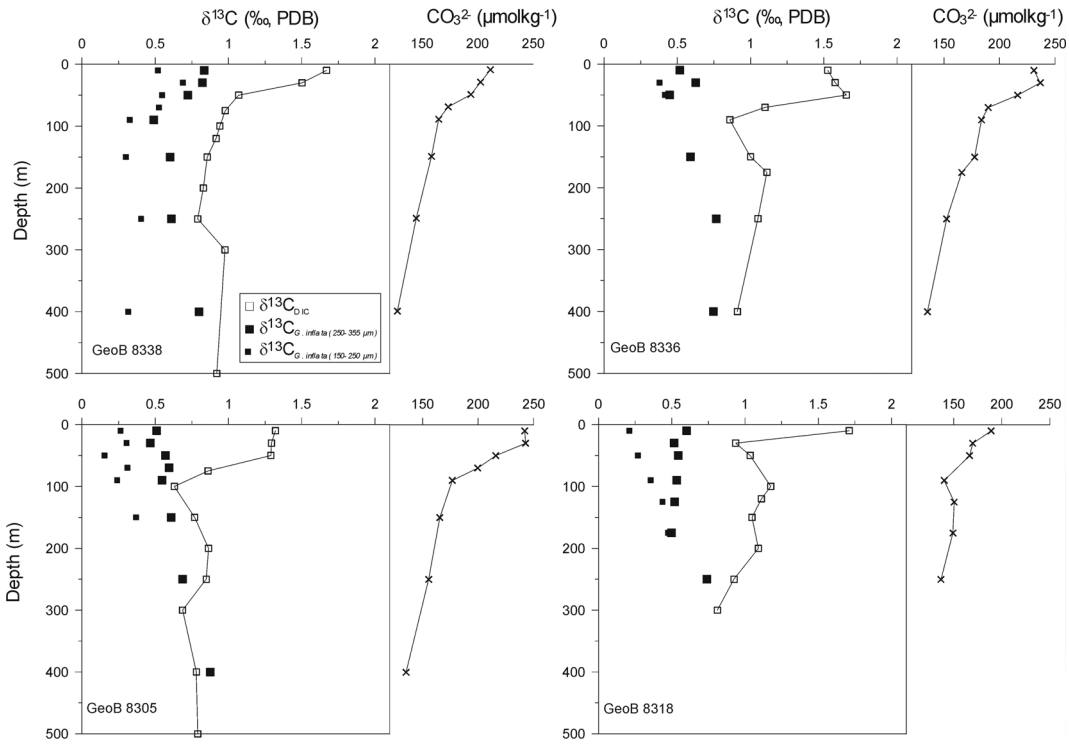

Figure 6.5b. The $\delta^{13}C$ composition of *G. inflata* (150-250 (small filled squares) and 250-355 µm (large filled squares)) in the upper water column in the Cape Basin. The foraminiferal values are directly compared to in situ $\delta^{13}C_{DIC}$ values (large open squares). For each station the decrease of the $[CO_3^{2-}]$ with depth in the water column are shown.

6.6 Discussion

6.6.1 Habitat depth and integrated calcification

Globorotalia inflata is known to be a species inhabiting transitional to subpolar oceanic regions (Bé and Hutson, 1977; Hemleben et al., 1989). In agreement with Fairbanks et al. (1982) we found maximum concentrations of *G. inflata* within the thermocline. Along the SW-African continental margin this corresponds to an average depth of 20-80 m depending on the varying depth of the thermocline between the different stations. However, we cannot assume that *G. inflata* calcifies exclusively at the depth where they were collected in highest numbers. Since the oxygen isotopic composition of *G. inflata* increases with increasing depth in the water column, it is evident that the shell growth occurs over a certain depth range. To quantify the exact amount of calcite precipitated in a distinct depth interval, we used an oxygen isotope mass balance model after Peeters and Wilke (in prep., Chapter 4), that describes the foraminiferal shell growth, *i.e.* the increase of shell mass, and the concomitant change in $\delta^{18}O$ with increasing depth in the water column. This model allows to quantify the amount of calcite precipitated within each depth interval, assuming shell growth starts at the sea surface.

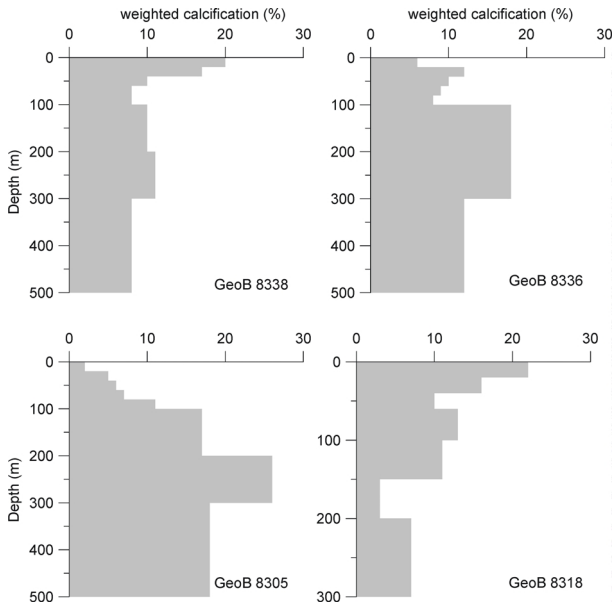

Figure 6.6. Graphs showing in which proportion *G. inflata* precipitated calcite in the depth intervals sampled the upper 500 m of the water column.

Figure 6.6 shows in which proportions *G. inflata* takes up its $\delta^{18}O$ signal at each depth interval in the upper 500 m of the water column (Table 6.4). At stations GeoB 8305 and 8336, where the thermocline was deeper, *G. inflata* precipitates highest amounts of calcite in deeper waters between 100 and 300 m. In contrast, at stations GeoB 8318 and 8338, which were influenced by upwelling, *G. inflata* tends to precipitate highest amounts at the sea surface. Thus, for GeoB 8305 and 8336 the depth of highest calcification tends to lie deeper than the vertical shell concentrations let assume. Hence, we conclude that *G. inflata* does not show an uniform calcification pattern at all stations but is rather guided by the local hydrographic differences between the open ocean and the upwelling influenced nearcoast stations. In the following we will use this knowledge about the integrated calcification of *G. inflata* within the upper water column for the interpretation of the relationship between $\Delta\delta^{13}_{\text{shell-DIC}}$ and $[CO_3^{2-}]$.

Table 6.4. The calculated weighted calcification indicates in which proportion *G. inflata* takes up its shell mass and isotopic composition in the different depth interval of upper 500 m of the water column. At GeoB 8318 and 8338, which are more influenced by upwelling, *G. inflata* calcifies high amounts in surface waters, while in the open ocean the depth of highest growth rate is shifted to deeper waters.

Depth interval	Weighted calcification (%)			
	GeoB 8338	GeoB 8336	GeoB 8305	GeoB 8318
0-20	20	2	1	35
20-40	17	8	4	22
40-60	10	11	7	11
60-80	8	11	9	
80-100	8	11	14	12
100-200	10	27	24	11
200-300	11	22	30	4
300-500	8	6	10	

6.6.2 Comparing $\delta^{13}C_{G.\ inflata}$ and $\delta^{13}C_{DIC}$

The $\delta^{13}C_{DIC}$ is usually enriched at the sea surface because of the preferentially consumption of the lighter isotope ^{12}C during photosynthesis, while in deeper waters $\delta^{13}C_{DIC}$ is depleted due to the remineralisation of organic matter (Broecker and Peng, 1982). It has been shown that the $\delta^{13}C$ of a foraminiferal shell is a function of the $\delta^{13}C_{DIC}$ (Spero, 1992). Thus one would expect that the decrease of $\delta^{13}C_{DIC}$ with increasing depth in the water column becomes also visible in the $\delta^{13}C$ of *G. inflata*. As our results indicate this is apparently not the case in this data set. At all stations $\delta^{13}C$ of *G. inflata* is lower compared to $\delta^{13}C_{DIC}$ and does not reflect the decrease with depth seen in the $\delta^{13}C_{DIC}$. Quite the reverse, *G. inflata* shows a slight increase with increasing depth in the water column.

Figure 6.8a illustrates that no relation exists when $\delta^{13}C_{G.\ inflata}$ (250-355 μm) is plotted versus $\delta^{13}C_{DIC}$. Why does the $\delta^{13}C$ of *G. inflata* not reflect the gradient seen in the $\delta^{13}C_{DIC}$ profile?

Laboratory culture experiments revealed that the seawater $[CO_3^{2-}]$ is an important factor affecting the incorporation of $\delta^{13}C$ in planktic foraminifera calcite shells. An increase in the $[CO_3^{2-}]$ results in a decrease in the carbon isotope values in the shells of foraminiferal species (Spero et al., 1997).

In the Cape Basin the $[CO_3^{2-}]$ shows a decrease in the upper 500 m of the water column from 250 μmol*kg^{-1} at the sea surface and 130 μmol*kg^{-1} at 500 m water depth. This allows to evaluate the carbonate ion effect on $\delta^{13}C$ of *G. inflata*. As shown before, *G. inflata* builds its shell at different depths in the water column. Hence, we cannot directly compare the measured ("raw") $\delta^{13}C$ data of *G. inflata* to the $[CO_3^{2-}]$ found at the same water depth. Instead

we applied the estimated portions of precipitated calcite in each depth level to calculate a mass-weighted $\delta^{13}C_{shell}$ and compared the obtained $\Delta\delta^{13}C_{shell\text{-}DIC}$ to the $[CO_3^{2-}]$ that was present in this water depth interval.

Figure 6.7 shows that the $\Delta\delta^{13}C_{shell\text{-}DIC}$ correlates well with $[CO_3^{2-}]$ at all four stations. At stations GeoB 8305 and 8336 we find slopes of –0.012‰ (µmol*kg^{-1})$^{-1}$ for both, the small and the large size fractions. At the upwelling-influenced stations GeoB 8338 and 8318 the $\Delta\delta^{13}C_{shell\text{-}DIC}$ versus $[CO_3^{2-}]$ yields slopes of –0.012 to 0.014‰ and–0.015‰ (µmol*kg^{-1})$^{-1}$ for specimens in the 150-250 and 250-355 µm size fraction, respectively. Model results by Zeebe et al. (1999) suggest that the magnitude of the carbonate ion effect is species-specific. The $\delta^{13}C/[CO_3^{2}]$ slope observed in laboratory experiments for other non-symbiotic species, such as *G. bulloides* (-0.013‰ (µmol*kg^{-1})$^{-1}$) was about twice the slope of symbiotic species *Orbulina universa* (-0.006‰ (µmol*kg^{-1})$^{-1}$) or *Globigerinoides sacculifer* (-0.005‰ (µmol*kg^{-1})$^{-1}$ (Bijma et al., 1998). If we assume that in general the non-symbiotic species respond stronger to changes of the $[CO_3^{2-}]$ it is likely that the slope of *G. inflata* is similar to the slope of non-symbiotic *G. bulloides*, as evident from our measurements.

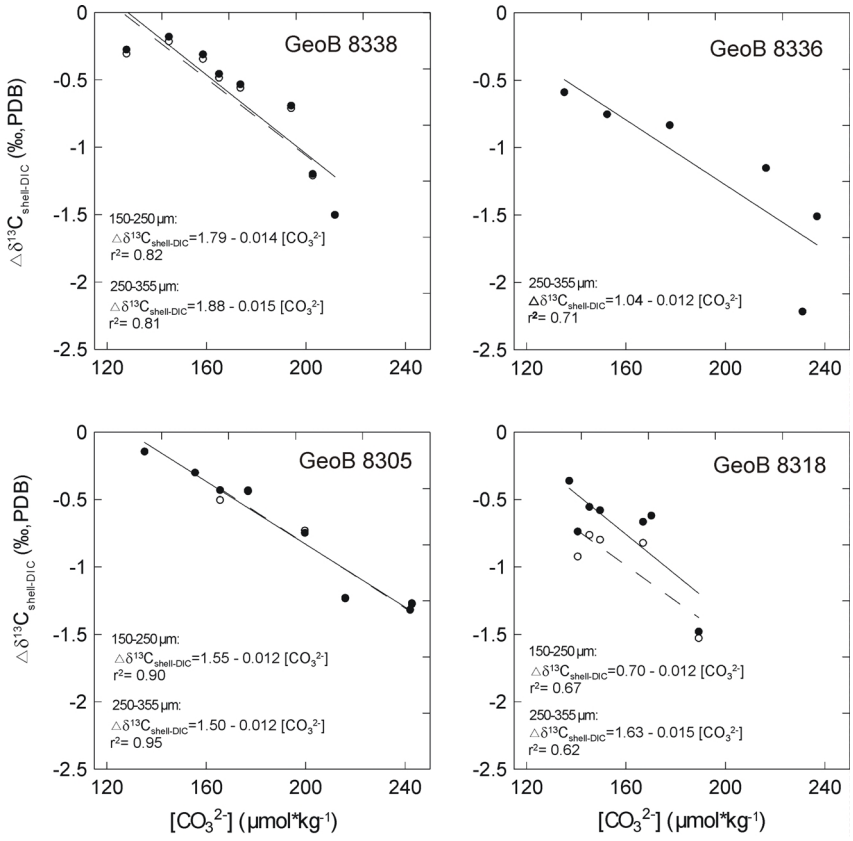

Figure 6.7. $\delta^{13}C_{DIC}$ corrected $\delta^{13}C_{shell}$ values for *G. inflata* (weighted $\Delta\delta^{13}C_{shell\text{-}DIC}$) versus the carbonate ion concentration ($[CO_3^{2-}]$) of the ambient sea water at stations GeoB 8336, 8338, 8318 and 8305.

However, the $[CO_3^{2-}]$ is not the only factor that varies with depth in the water column. Because temperature and $[CO_3^{2-}]$ in seawater are correlated with one another (Fig. 6.2) and show a similar vertical gradient within the water column, one can expect that the changes in the $\Delta\delta^{13}C_{shell\text{-}DIC}$ also correlate well with temperature. It is known that no temperature dependent fractionation occurs during the process of inorganic calcite precipitation (Romanek et al., 1992), but temperature may have an influence on the foraminiferal metabolic rate (Ortiz et al., 1996; Bemis et al., 2000). However, since the $\Delta\delta^{13}C_{shell\text{-}DIC}/[CO_3^{2-}]$ slopes from our field data are nearly identical to the slopes established from laboratory culture experiments we assume that the influence of temperature on the $\delta^{13}C_{shell\text{-}DIC}$ is negligible. Therefore, it can be concluded that the incorporation of $\delta^{13}C$ in *G. inflata* is mainly controlled by the $\delta^{13}C_{DIC}$ of the seawater, modified by the $[CO_3^{2}]$ of seawater.

These results have significant implications for paleoceanographic studies. Lea et al. (1999) calculated that an increased alkalinity during glacial times can account for nearly all of the observed reduced $\delta^{13}C$ values in planktic foraminifera. This offers an alternative to the generally assumed terrestrial biosphere-to-ocean transfer of carbon to explain lower glacial ocean $\delta^{13}C_{DIC}$ (Shackleton, 1977).

Figure 6.8b shows the correlation between the carbonate ion effect-corrected $\delta^{13}C$ of *G. inflata* and $[CO_3^{2-}]$ using the determined slopes. This suggests that $\delta^{13}C_{DIC}$ can be derived from $\delta^{13}C_{G.\ inflata}$ by correcting to a $[CO_3^{2-}]$ of 0 μmol*kg^{-1} and adding 1.55‰.

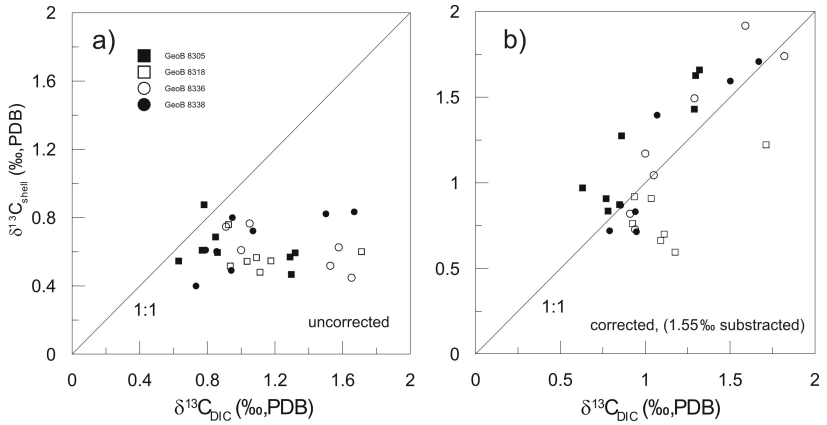

Figure 6.8. a) Uncorrected $\delta^{13}C_{DIC}$ versus $\delta^{13}C_{shell}$ values for *G. inflata* (250-355 μm) in the upper water column. The $\delta^{13}C$ values of *G. inflata* are nearly constant with varying $\delta^{13}C_{DIC.}$ b) Carbonate ion effect corrected $\delta^{13}C_{DIC}$ versus $\delta^{13}C_{shell}$ values for *G. inflata* (250-355 μm) in the upper water column. The $\delta^{13}C$ values of *G. inflata* responds to $\delta^{13}C_{DIC}$ variations, as expected from laboratory culture experiments. For the correction to a carbonate ion concentration of 0 μmol*kg^{-1}, we used the slopes derived for *G. inflata* via weighted $\Delta\delta^{13}C_{shell\text{-}DIC}/[CO_3^{2-}]$ correlation. From the 1:1 slope the correlation shows an average offset of about 1.55‰.

6.6.3 Shell sizes

Another issue to be considered for the interpretation of the stable carbon isotope fractionation is the effect of shell size. In general, the size of a planktic foraminifer increases with ontogeny, but also size variations due to temperature changes have been observed (Bijma et al., 1990b).

In the upper most interval (0-20 m) of the water column we found *G. inflata* in a wide range of shell sizes under constant hydrographic conditions. As an example Figure 6.9 shows the relationship between shell size (µm) and $\delta^{13}C_{shell}$ and further the relationship between shell size (µm) and shell mass (µg) of *G. inflata* in the shallowest depth interval (0-20 m) at station GeoB 8338. The shell size correlates positively with shell mass, i.e. larger individuals are indeed heavier in weight. At the same time the stable carbon isotope composition increases in general with shell size and shell mass, which was already shown for other species (e.g. Berger et al., 1978; Spero and Lea, 1996; Bemis et al., 2000). Over a certain size on (~300 µm) the $\delta^{13}C$ values are statistically identical. What causes the differences in $\delta^{13}C$ between different sizes?

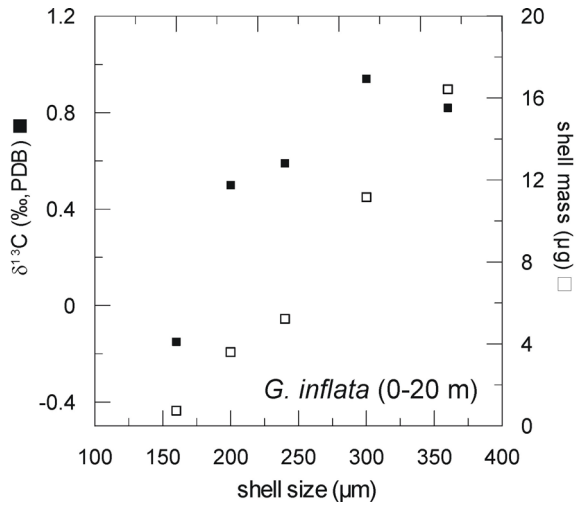

Figure 6.9. Relationship between shell size (µm) and $\delta^{13}C$ (‰, PDB) and shell mass (µg) of *G. inflata* collected in the upper most depth interval (0-20 m). Both, the $\delta^{13}C$ and the shell mass increases with increasing shell size.

The increase in $\delta^{13}C$ with increasing shell size may be attributed to 1) ontogenetic/metabolic effect (temperature controlled?) and/or 2) the effect of symbionts or symbiont activity. Because *G. inflata* is a species which lives without symbionts the symbiont effect can be neglected in this case. In early ontogenetic life stages individuals calcify faster and respire at higher rates (Berger et al., 1978; Hemleben et al., 1989). Thus, if high amounts

of respired $^{12}CO_2$ are used during calcification it is not surprising that smaller individuals of *G. inflata* show lower $\delta^{13}C$ compared to larger specimens.

6.7 Conclusion

We investigated the incorporation of stable carbon isotopes in calcite shells of planktic foraminifera species *Globorotalia inflata*. Thereby we concentrated in particular on the influence of the seawater carbonate ion concentration on the shell $\delta^{13}C$.

G. inflata clearly dominates the assemblage in the upper 500 m of the water column along the SW-African continental margin.

While the oxygen isotopic composition of *G. inflata* reflects the gradient observed in the predicted $\delta^{18}O$ equilibrium calcite profile with depth in the water column, the $\delta^{13}C$ of *G. inflata* do not mirror the depth gradient seen in the $\delta^{13}C_{DIC}$ profile.

Since the increase of the oxygen isotopic composition with depth indicates integrated shell growth of *G. inflata* over a certain depth range, we used an oxygen isotope mass balance model to quantify in which proportion *G. inflata* takes up its isotopic signal within the upper 500 m of the water column. Based on this knowledge, we were able to investigate the weighted $\Delta\delta^{13}C_{shell\text{-}DIC}$ changes as a function of the carbonate ion concentration with increasing depth in the water column.

We find $\Delta\delta^{13}C_{shell\text{-}DIC}/[CO_3^{2-}]$ slopes for *G. inflata* of -0.012 to –0.014‰ and -0.012 to -0.015‰ μmol*kg^{-1} for specimens in the 150-250 and 250-355 μm size fraction, respectively. These slopes are very similar to the ones established for other non-symbiotic species like *G. bulloides* from laboratory experiments. Hence, this suggests that the carbonate chemistry of surface waters is the significant mechanism controlling the carbon isotope composition of *G. inflata*. This is important for paleoceanographic studies since changes of the carbonate system between glacial and interglacial times has been established.

In addition to the carbonate ion effect, the $\delta^{13}C$ of *G. inflata* is influenced by a size-related ontogenetic/metabolic effect. Although found under same conditions (0-20 m), the stable carbon isotope composition of *G. inflata* increases in general with shell size and shell mass, *i.e.* and shell size and shell mass are linearly correlated.

Acknowledgments: We thank captains and crews of Meteor 57/1. We further thank M. Segl, B. Meyer-Schack for help with isotope analysis. Sylvia Kemle von Mücke helped in selecting and counting planktic foraminifera. Many thanks to Anja Terbrüggen from the Alfred-Wegener Institute in Bremerhaven who helped to measure the total alkalinity titration and the DIC. This study was funded by the Deutsche Forschungsgemeinschaft (International Graduate College "Proxies in Earth History", University Bremen).

References

Archer, D. and Maier-Reimer, E., 1994. Effect of deep-sea sedimentary calcite preservation on atmospheric CO_2 concentration. Nature 367, 260-263.

Bauch, D., Erlenkeuser, H., Winckler, C., Pavlova, G. and Thiede, J., 2002. Carbon isotopes and habitat of polar planktic foraminifera in the Okhotsk Sea: the "carbonate ion effect" under natural conditions. Mar. Micropaleontol. 871, 1-17.

Bé, A.W.H., Hembleben, C., Anderson, O.R., Spindler, M., Hacunda, J. and Tuntivate-Choy, S., 1977. Laboratory and field observations of living planktonic foraminifera. Micropaleontology 23, 155-179.

Bé, A.W.H. and Hutson, W.H., 1977. Ecology of planktonic foraminifera and biogeographic patterns of life and fossil assemblages in the Indian ocean. Micropaleontology 23, 369-414.

Bemis, B., Spero, H.J., Lea, D.W. and Bijma, J., 2000. Temperature influence on the carbon isotopic composition of *Orbulina universa* and *Globigerina bulloides* (planktic foraminifera). Mar. Micropalentol. 38, 213-228.

Berger, W.H., Killingley, J.S. and Vincent, E., 1978. Stable isotopes in deep-sea carbonates: Box Core ERDS-92 west equatorial Pacific. Oceanol. Acta 1, 203-216.

Bijma, J., Faber, W.W. and Hemleben, C., 1990b. Temperature and salinity limits for growth and survival of some planktonic foraminifers in laboratory cultures. Journal of Foraminiferal Research 20, 95-116.

Bijma, J., Spero, H.J. and Lea, D.W., 1998. Oceanic carbonate chemistry and foraminiferal isotopes: new laboratory results paper presented at the Sixth International Conference on Paleoceanography, Lisbon, 1998.

Bouvier-Soumagnac, Y. and Duplessy, J.-C., 1985. Carbon and oxygen isotopic composition of planktonic foraminifera from laboratory culture, plankton tows and recent sediment: implication for the reconstruction of paleoclimatic conditions and of the global carbon cycle. Journal of Foraminiferal Research 15, 302-320.

Broecker, W.S. and Maier-Reimer, E., 1992. The influence of air and sea exchange on the carbon isotope distribution in the sea. Global Biogeochemical Cycles 6, 315-320.

Broecker, W.S. and Peng, T.-H., 1982. Tracers in the sea. Lamont-Doherty geological observatory. University of Columbia, Palisades, New York 10964, 690 pp.

Charles, C.D., Wright, J.D. and Fairbanks, R.G., 1993. Thermodynamic influences on the marine carbon isotope record. Paleoceanography 8, 691-697.

Duplessy, J.-C., Labeyrie, L.D., Juillet-Leclerc, A., Maitre, F., Duprat, J. and Sarnthein, M., 1991. Surface salinity reconstruction of the North Atlantic Ocean during the last glacial maximum. Oceanol. Acta 14(4), 311-324.

Fairbanks, R.G., Sverdlove, M., Free, R., Wiebe, P.H. and Be, A.W.H., 1982. Vertical distribution and isotopic fractionation of living planktonic foraminifera from the Panama Basin. Nature 298, 841-844.

Hemleben, C., Spindler, M. and Anderson, O.R., 1989. Modern Planktonic Foraminifera. Springer Verlag, New York, 363 pp.

Itou, M., Ono, T., Oba, T. and Noriki, S., 2001. Isotopic composition and morphology of living *Globorotalia scitula*: a new peoxy of sub-intermediate ocean carbonate chemistry? Mar. Micropalentol. 42, 189-210.

Jouzel, J., Barkov, N.I., Barnola, J.M., Bender, M., Chappellaz, J., Genthon, C., Kotlyakov, V.M., Lipenkov, V., Lorius, C., Petit, J.R., Raynaud, D., Raisbeck, G., Ritz, C., Sowers, T., Stievenard, M., Yiou, F. and Yiou, P., 1993. Extending the Vostok ice-core record of palaeoclimate to the penultimate glacial period. Nature 364, 407-412.

Kahn, M.I. and Williams, D.F., 1981. Oxygen and carbon isotopic composition of living planktonic foraminifera from the northeast Pacific Ocean. Palaeogeogr., Palaeoclim., Palaeoecol. 33, 47-69.

Kim, S.-T. and O`Neil, J.R., 1997. Equilibrium and non-equilibrium oxygen isotope effects in synthetic carbonates. Geochimica et Cosmochimica Acta 61, 3461-3475.

Kroon, D. and Ganssen, G., 1989. Northern Indian Ocean upwelling cells and the stable isotope composition of living planktonic foraminifers. Deep Sea Research 36, 1219-1236.

Lea, D.W., Bijma, J., Spero, H.J. and Archer, D., 1999. Implications of a carbonate ion effect on shell carbon and oxygen isotopes for glacial ocean conditions. In: Fischer, G. and Wefer, G. (Eds.), Use of proxies in paleoceanography: Examples from the South Atlantic. Springer, Berlin, pp. 513-522.

Lewis, E. and Wallace, D.W.R., 1998. Program Developed for CO_2 System Calculations. ORNL/CDIAC-105. Carbon Dioxide Information Analysis Center, Oak Ridge National Laboratory, U.S. Department of Energy, Oak Ridge, Tennessee.

Lynch-Stieglitz, J., Stocker, T.F., Broecker, W.S. and Fairbanks, R.G., 1995. The influence of air-sea gas exchange on the isotopic composition of oceanic carbon: observations and modelling. Global Biogeochemical Cycles 9, 653-665.

Mulitza, S., Arz, H., Kemle-von Mücke, S., Moos, C., Niebler, H.S., Pätzold, J. and Segl, M., 1999. The South Atlantic carbon isotope record of planktic foraminifera. In: Fischer, G. and Wefer, G. (Eds.), Use of proxies in paleoceanography: Examples from the South Atlantic. Springer, Berlin, pp. 427-445.

Ortiz, J.D., Mix, A.C., Rugh, W., Watkins, J.M. and Collier, R.W., 1996. Deep-dwelling planktonic foraminifera of the northeastern Pacific Ocean reveal environmental control of oxygen and carbon isotope disequilibria. Geochim. Cosmochim. Acta 60(22), 4509-4523.

Peeters, F.J.C., Brummer, G.-J. and Ganssen, G., 2002. The effect of upwelling on the distribution and stable isotope composition of *Globigerina bulloides* and *Globigerinoides ruber* (planktic foraminifera) in modern surface waters of the NW Arabian Sea. Global and Planetary Change 34, 269-291.

Peeters, F.J.C. and Wilke, I., in prep. Depth integrated growth of planktic foraminiferal shells Part 1. The theory of an oxygen isotope mass balance model.

Ravelo, A.C. and Fairbanks, R.G., 1995. Carbon isotopic fractionation in multiple species of planktonic foraminifera from core-tops in the tropical Atlantic. Journal of Foraminiferal Research 25, 53-74.

Romanek, C.S., Grossman, E.L. and Morse, J.W., 1992. Carbon isotopic fractionation in synthetic aragonite and calcite: effects of temperature and precipitation rate. Geochimica et Cosmochimica Acta 56, 419-430.

Russell, A.D. and Spero, H.J., 2000. Field examination of the oceanic carbonate ion effect on stable isotopes in planktonic foraminifera. Paleoceanography 15, 43-52.

Sanyal, A., Hemming, N.G., Hanson, G.N. and Broecker, W.S., 1995. Evidence for a higher pH in the glacial ocean from boron isotopes in foraminifera. Nature 373, 234-236.

Schneider, R. and participants, 2003. Report and Preliminary Results of Meteor Cruise M57/1, Cape Town-Walvis Bay, 20.01. - 08.02.2003. Berichte Fachbereich Geowissenschaften, Universität Bremen 90, 216, 123 pp.

Shackleton, N.J., 1977. ^{13}C in *Uvigerina*: Tropical rainforest history and the equatorial Pacific carbonate dissolution cycles. In: Anderson, N. and Malahof, A. (Eds.), Fate of Fossil Fuel CO_2 in the Oceans. Plenum, New York, pp. 401-427.

Shackleton, N.J. and Vincent, E., 1978. Oxygen and carbon isotope studies in recent foraminifera from the southwest Indian Ocean. Mar. Micropalentol. 19, 275-285.

Spero, H.J., 1992. Do planktic foraminifera accurately record shifts in the carbon isotopic composition of sea water SCO_2? Mar. Micropalentol. 19, 275-285.

Spero, H.J., Bijma, J., Lea, D.W. and Bemis, B., 1997. Effect of seawater carbonate concentration on foraminiferal carbon and oxygen isotopes. Nature 390, 497-500.

Spero, H.J. and Lea, D.W., 1996. Experimental determination of stable isotope variability in *Globigerina bulloides*: Implications for paleoceanographic reconstruction. Mar. Micropalentol. 28, 231-246.

Stoll, M.H.C., Bakker, K., Nobbe, G.H. and Haese, R.R., 2001. Continous-Flow analysis of dissolved inorganic carbon content in seawater. Anal. Chem. 73, 4111-4116.

Thiede, J., 1975. Distribution of foraminifera in surface waters of a coastal upwelling area. Nature 253, 712-714.

Wefer, G. and Berger, W.H., 1991. Isotope paleontology: growth and composition of extant calcareous species. Marine Geology 100, 207-248.

CONCLUSION AND OUTLOOK

In this thesis a combined ecological and geochemical approach was used to improve the application of stable carbon and oxygen isotopes in planktic foraminifers as paleoceanographic proxies.

Two first steps are necessary before stable oxygen and carbon isotopes of planktic foraminifers can be used for paleoceanographic interpretations: 1) the determination of the seasonal distribution pattern of different foraminiferal species, and 2) the quantification of the depth integrated shell growth process in the water column in dependence on the hydrographic structure, *i.e.* information on the species-specific calcification depth range as well as on the shell growth pattern, e.g. in which depth calcite precipitation is maximal.

However, the effects of seasonal abundance and temperature characteristics of selected species in a specific region should be transferred carefully on fossil assemblages originating from other oceanic regions, since seasonality and depth preferences show a strong hydrographical component. The habitat within the annual cycle and the water depth occupied by a foraminiferal species depend on several controlling factors like temperature, food availability and light conditions. Therefore further recent calibration of species used for paleoceanographic purpose are indispensable.

In future studies, the quantification method of depth integrated shell growth, introduced in Chapter 4 and 5, could be used to unravel the thermal structure of the water column at a given station by combining the oxygen isotopic composition of different species that show different calcification patterns. Since foraminiferal species show clearly differences in the extend to which calcification occurs throughout the water column, in a paleoceanographic context, the use of multiple species is advantageous over a single species approach since this allows to distinguish between isotopic signatures caused by temporarily shifts in depth habitat or lower water temperatures, because different species show different responses to changes in hydrographic structure (Field, 2004). Especially at depths where the temperature gradient is small, shifts in habitat depth may considerably affect the oxygen and carbon isotopic records. Therefore, the test of the model to more species from other oceanic regions is further necessary in order to determine their model calcification parameters and to further estimate the variability of these parameters for each species due to different hydrographic structures. The results of this study provide a new basis for reconstructing the thermal structure of the water column using multiple species of planktic foraminifers and give therefore greater insights into the mechanism of climatic changes.

The possibility to determine where foraminifers exactly form their calcite shell in the water column, in other words in which proportion a species take up the isotopic signal in the

chosen depth intervals, allowed to investigate the effect of the seawater carbonate ion concentration ($[CO_3^{2-}]$) on the incorporation of stable carbon isotopes in the species *G. inflata* during its depth integrated shell growth process vertically throughout the water column. The identification of the so-called carbonate ion effect under natural conditions is a further important outcome of this thesis. The results validate the experimental carbonate ion effect, determined for planktic foraminifers and indicate that the incorporation of stable carbon isotopes in planktic foraminiferal shells is strongly controlled by the seawater carbonate system. For paleoceanographic studies this suggests that a portion of the glacial-interglacial difference in foraminiferal stable carbon isotopic composition may have been related to increased alkalinity of glacial surface waters. For a correct interpretation of the fossil record, future field studies on modern samples should therefore include the determination of seawater carbonate system parameters, such as total alkalinity and total dissolved inorganic carbon, which enables to calculate all other carbonate system parameters (*e.g.* $[CO_3^{2-}]$). More tests are necessary to investigate if this effect is also found for other living species under natural conditions, especially for species which have been studied under controlled conditions allowing a comparison with culture derived slopes. The same holds true for stable oxygen isotopes because culture experiments reveal that the effect is also present in the oxygen isotope composition. The fact that the oxygen isotope composition may be determined by other factors, in addition to *in-situ* temperature and $\delta^{18}O_w$, shows that temperature equations should no longer be used without correcting for carbonate system and/or ontogenetic effects. To investigate potential ontogenetic influences on the stable isotopic composition of foraminiferal species, isotopic measurements should be performed on several size-classes routinely. However, to achieve best possible results on stable isotope ratios, measurements should be ideally carried out on single specimens.

An interesting next step might also be the determination of the weight of living planktic foraminiferal species, because it has been suggested that glacial-interglacial changes in foraminiferal shell weight are related to changes in ambient $[CO_3^{2-}]$ through time in response to changing atmospheric pCO_2 (Barker and Elderfield, 2002). These authors show that foraminiferal shell weights are highest during the Last Glacial Maximum and show a large decrease into the early Holocene, which indicates that the controlling factor on shell weight must be carbonate ion and not calcification temperature. Culture experiments have also shown that the shell weights in similar-sized individuals increase with increasing carbonate ion concentration in the research vessel, interpreted as a consequence of thicker walls due to higher calcification rates at higher $[CO_3^{2-}]$ (Bijma et al., 1999). The observations of this

correlation should be tested and calibrate in future field studies by using plankton tow and sediment trap collected foraminifers.

References

Barker, S. and Elderfield, H., 2002. Foraminiferal calcification response to glacial-interglacial changes in atmospheric CO_2. Science 297, 833-836.

Bijma, J., Spero, H.J. and Lea, D.W., 1999. Reassessing foraminiferal stable isotope geochemistry: impact of the oceanic carbonate system (experimental results). In: Fischer, G. and Wefer, G. (Eds.), Use of proxies in paleoceanography: Examples from the South Atlantic. Springer, Berlin, pp. 489-512.

Field, D.B., 2004. Variability in vertical distribution of planktonic foraminifera in the California Current: Relationships to vertical ocean structure. Paleoceanography 19.

APPENDIX

Appendix 2A

Seasonal hydrographic data (T, S, chlorophyll a and $\delta^{18}O_w$) at EBC, ESTOC and LP, during plankton tows collection

Season/ Cruise	Station	Depth (m)	T (°C)	S (psu)	$\delta^{18}O_w$ (‰ SMOW)
Spring 1998	GeoB 5321-1	0	19.239	36.724	0.940
(Pos 237)	(EBC)	25	19.249	36.714	0.912
		50	19.233	36.710	0.887
		150	16.451	36.311	0.837
		300	13.828	35.924	0.731
		500	11.050	35.537	0.455
	GeoB 5323-1	0	19.726	36.792	1.030
	(ESTOC)	25	19.776	36.853	1.019
		50	19.754	36.849	0.946
		150	16.612	36.339	0.843
		300	14.037	35.948	0.736
		500	12.006	35.657	0.616
	GeoB 5325-1	0	20.157	36.931	1.087
	(LP)	25	20.157	36.973	0.956
		50	20.109	36.959	1.026
		150	17.478	36.456	0.910
		300	14.640	36.041	0.636
		500	12.081	35.667	0.542
Summer 1998	GeoB 5422-1	0	20.783	36.407	0.956
(M42/2)	(EBC)	25	20.584	36.458	0.614
		50	20.429	36.498	0.620
		150	16.407	36.286	0.619
		300	13.888	35.925	0.632
		500	11.703	35.617	0.631
	GeoB 5425-1	0	21.309	36.760	
	(ESTOC)	25	21.158	36.787	0.609
		50	20.781	36.728	0.439
		150	17.765	36.531	0.697
		300	14.322	35.968	0.650
		500	12.025	35.669	0.566
	GeoB 5327-1	0	22.070	36.999	1.150
	(LP)	25	21.984	37.018	0.816
		50	21.724	37.007	0.659
		150	17.770	36.512	1.054
		300	14.731	36.058	1.034
		500	12.136	35.650	1.071
Fall 1995	GeoB 3513-1	0	21.50	36.65	0.970
(Pos 212)	(EBC)	25	21.50	36.65	0.969
		50	20.43	36.49	0.925
		100	17.95	36.57	0.892
		150	16.90	36.48	

		200	16.03	36.34	0.746
		300	14.55	36.08	0.453
		500	11.97	35.67	0.664
	GeoB 3508-1	0	23.050	36.810	
	(ESTOC)	50	22.978	36.839	0.988
		150	17.395	36.569	0.954
		300	14.320	36.025	0.762
		500	11.930	35.655	0.548
	GeoB 3503-1	0	24.010	37.120	
	(LP)	50	23.876	37.030	1.167
		150	16.729	36.415	0.961
		300	14.583	36.061	0.863
		500	11.879	35.644	0.541
Winter 1997	GeoB 4003-1	0	19.441	36.807	0.970
VH 96/1	(EBC)	25	19.429	36.803	0.927
		50	19.421	36.802	0.860
		150	17.599	36.528	0.960
		300	14.634	36.090	0.802
		440	12.541	35.743	0.614
	GeoB 4001-1	0	19.750	36.816	1.056
	(ESTOC)	25	19.743	36.814	1.081
		50	19.746	36.813	1.067
		150	17.437	36.497	0.998
		300	14.687	36.065	0.807
		440	12.868	35.776	0.723
	GeoB 4010-1	0	19.507	36.875	1.023
	(LP)	25	19.419	36.870	1.007
		50	19.314	36.857	0.995
		150	17.460	36.548	0.924
		300	14.566	36.133	0.660
		440	12.737	35.855	0.530

Appendix 2B

The $\delta^{18}O$ composition of planktic foraminifera from plankton tows, sediment traps and surface sediments at EBC, ESTOC and LP during winter

Station	Depth interval (m)	*G. ruber* white		*G. ruber* pink	*P. obliquiloculata*			*G. truncatulinoides*			*T. humilis*	Equil. Calcite[a] $\delta^{18}O_{calcite}$
		150-250	250-350	250-350	<280	280-380	>380	<280	280-440	>440	150-250	
GeoB 4003	0-25	-0.30				0.08		-0.25	-0.01		-0.65	-0.027
EBC	25-50	-0.25				0.07			-0.05		-0.29	-0.081
	50-150	-0.23				0.14		-0.22	-0.03			0.019
	150-300	-0.07				0.34			0.26		-0.09	0.705
	300-440								0.67		0.08	1.006
	700	-0.10	-0.18			0.45	0.38		0.95	1.22	0.55	1.485
	1360	-0.07	-0.21			0.57	0.53		0.99	1.19	0.54	
GeoB 4001	0-25	-0.55	-0.75		-0.03	0.08	0.09	-0.24	-0.06		-0.46	-0.080
ESTOC	25-50				-0.10	0.02	0.15	-0.39	-0.09		-0.32	-0.072
	50-150	-0.63			-0.25	0.03	0.18	-0.40	-0.13	0.03		0.050
	150-300					0.36			0.26		-0.28	0.615
	300-440											0.936
	500	-0.20	-0.34	-0.18	0.36	0.45	0.52	0.65	0.89	1.00	0.38	1.089
	3000	-0.19	-0.13	-0.05		0.48	0.52		0.84	1.07	0.36	
	3610	-0.21	-0.24	-0.69		0.60	0.46		1.10	1.11		
GeoB 4010	0-25								-0.07			0.033
LP	25-50											0.039
	50-150							-0.33	0.03		-0.49	0.205
	150-300							0.20	0.31			0.546
	300-440										0.16	0.861
	900	-01.0				0.33	0.20		0.94	0.98	0.13	
	3700	-0.12	-0.15			0.56	0.51		1.01		0.30	
	4327	-0.11	-0.24			0.55	0.69		1.06	1.15		

[a]Equilibrium calcite values ($\delta^{18}O_{calcite}$) were calculated using measured temperatures and measured oxygen isotope values of the sea water ($\delta^{18}O_w$).

Appendix 2C

$\delta^{18}O$ composition of planktic foraminifera from plankton tows, sediment traps and surface sediments at EBC, ESTOC and LP during fall.

Station	Depth interval (m)	*G. ruber* white		*G. ruber* pink	*G. bulloides*		Equil. Calcite[a] $\delta^{18}O_{calcite}$
		150-250	250-350	250-350	150-250	250-355	
GeoB 3513	0-25						-0.438
EBC	25-50		-1.30	-0.97		-1.10	-0.392
	50-100		-0.95	-1.15		-0.66	0.023
	100-200			-1.10		-0.45	0.369
	200-275		-0.72				0.485
	700		-0.69		-0.81	-0.06	
	1360	-0.07	-0.21	-0.58	-0.36	-0.11	
GeoB 3508	0-50			-1.26			-0.736
ESTOC	50-150		-0.87	-1.08			0.057
	150-300		-0.93	-1.08			0.671
	300-500						1.034
	500-800						1.423
	500	-0.52	-0.65	-0.87			
	3000	-0.42	-0.79	-0.82			
	3610	-0.21	-0.24	-0.69			

[a]Equilibrium calcite values ($\delta^{18}O_{calcite}$) were calculated using measured temperatures and measured oxygen isotope values of the sea water ($\delta^{18}O_w$).

Appendix 3A

List of 29 planktic foraminifera species found in the sediment trap MST-15 between August 2000 and February 2001. Average flux m^{-2} day^{-1} and average relative abundance are calculated

Species	Average flux m^{-2} day^{-1}	Average %
Globorotalia inflata	499.9	45.9
Globigerina bulloides	100.5	10.3
Globigerina falconensis	62.2	6.5
Turborotalita quinqueloba	4.4	0.5
Turborotalia humilis	0.1	<0.1
Globigerinella calida	23.5	2.3
Globigerinella aequilateralis	28.1	2.9
Globigerinella digitata	6.4	0.6
Globigerinoides ruber	31.9	3.1
Globigerinoides sacculifer	9.4	1.0
Orbulina universa	7.8	0.9
Neogloboquadrina dutertrei	27.0	2.8
Neogloboquadrina pachyderma (sin.)	14.1	1.3
Neogloboquadrina pachyderma (dex.)	69.2	6.3
Pulleniatina obliquiloculata	1.6	0.2
Globigerinata glutinata	111.0	10.0
Globorotalia menardii	2.6	0.2
Globorotalia hirsuta	15.1	1.5
Globorotalia truncatulinoides (sin.)	5.6	0.6
Globorotalia truncatulinoides (dex.)	0.8	0.1
Globorotalia anfracta	0.4	0.03
Globorotalia theyeri/ G. scitula cpx.	27.8	2.5
Globorotalia crassaformis	<0.1	
Globigerinoides tenellus	3.1	0.3
Hastigerina pelagia	0.1	<0.1
Globoturborotalita rubescens	0.4	<0.1
Globigerinodes conglobatus	<0.1	<0.1
Globigerinita iota	0.1	<0.1
Globorotalia tumida	0.3	0.1

Appendix 3B

The $\delta^{18}O$ and $\delta^{13}C$ composition (‰, PDB) of planktic foraminifera collected in sediment trap MST-15

Trap cup	Date (end)	*G. ruber* (150-250 μm)		*N. pachyderma (dex.)* (150-250 μm)		*G. inflata* (250-355 μm)		*G. glutinata* (150-250 μm)		*G. aequilateralis* (250-355 μm)		*N. dutertrei* (250-355 μm)		*G. theyeri/G. scitula cpx.* (150-250 μm)		*G. bulloides* (150-250 μm)	
		$\delta^{18}O$	$\delta^{13}C$	$\delta^{18}O$	$\delta^{13}C$	$\delta^{18}O$	$\delta^{13}C$	$\delta^{18}O$	$\delta^{13}C$	$\delta^{18}O$	$\delta^{13}C$	$\delta^{18}O$	$\delta^{13}C$	$\delta^{18}O$	$\delta^{13}C$	$\delta^{18}O$	$\delta^{13}C$
1	09/08/00	-0.69	-0.15			0.57	0.21			-0.15	-0.32	-0.01	0.18			-0.24	-2.21
2	17/08/00	-0.66	-0.44			0.26	-0.30	-0.69	-1.38	-0.26	-0.44					-0.46	-2.23
3	25/08/00	-0.33	-0.63			0.25	-0.33	-0.551	-1.31	-0.03	-0.35					-0.25	-2.25
4	02/09/00																
5	10/09/00					0.43	-0.32	-0.63	-0.90	0.05	-0.38	0.11	-0.06			-0.04	-2.21
6	18/09/00					0.38	-0.16	-0.35	-1.02			0.12	-0.25			0.18	-1.54
7	26/09/00			0.10	-1.07	0.53	-0.21	-0.34	-0.78			0.07	-0.46	0.90	-0.57	0.13	-2.00
8	04/10/00			0.17	-0.77	0.66	0.04	-0.17	-1.33			0.08	-0.66	0.96	-0.58	0.25	-1.84
9	12/10/00	-0.77	-0.53	0.42	-0.51	0.90	0.20	0.04	-0.98			-0.17	0.05			0.79	-0.66
10	20/10/00	-0.66	-0.30	0.29	-0.31	0.94	0.41	-0.62	-1.58	-0.41	-0.26	0.00	0.19			0.54	-1.28
11	28/10/00																
12	05/11/00	-0.66	-0.64			0.74	0.25	-0.84	-1.85	-0.01	-1.28	-0.38	-0.20			-0.34	-1.99
13	13/11/00	-0.73	-0.47	-0.15	-0.70	0.60	-0.03	-0.67	-1.73	-0.35	-1.20	-0.02	0.35				
14	21/11/00	-0.80	-0.60			0.51	0.06	-0.82	-1.76	0.17	-0.05	-0.38	-0.03	1.28	-0.24		
15	29/11/00	-0.84	-0.29			0.51	-0.14	-0.96	-2.16			-0.07	0.16	0.68	-0.68	-0.66	-2.22
16	07/12/00	-0.89	-0.30	-0.10	-0.73	0.41	-0.10	-0.67	-1.52	0.32	-0.55	-0.33	0.16	1.91	-0.38	-0.91	2.35
17	15/12/00	-0.74	-0.50	-0.14	-0.46	0.32	-0.16	-0.72	-1.73	0.12	-1.01	-0.31	-0.47	2.20	-0.27	-0.85	-2.41
18	23/12/00	-0.78	-0.42	-0.21	-0.90	0.22	-0.22	-0.84	-1.67	-0.29	-0.56	-0.21	-0.12	0.93	-0.54	-0.54	-2.34
19	31/12/00	-0.76	-0.29	-0.10	-0.99	0.50	-0.05	-0.59	-1.48	-0.01	-0.50	-0.10	-0.20	2.05	-0.28	-0.34	-2.30
20	08/01/01	-0.69	-0.80	-0.22	-1.07	0.45	-0.08	-0.78	-1.59	-0.05	-0.02	-0.13	-0.61	1.27	-0.28	-0.27	-2.12
21	16/01/01	-0.90	-0.40	0.11	-0.65	0.39	-0.03	-0.48	-1.36	-0.15	-0.29			0.99	-0.66	-0.13	-1.98
22	24/01/01	-0.62	0.19	0.33	-0.55	0.70	0.23	0.40	-0.70	-0.06	-0.39			1.81	-0.13	-0.06	-1.81
23	01/02/01			0.35	-0.74	0.64	0.55	0.29	-0.67					1.25	-0.28	-0.01	-1.62
24	09/02/01			0.35	-0.64	0.60	0.19	0.49	-0.65	-0.39	-0.55			1.05	-0.39	0.06	-1.76

Appendix 5A

The oxygen isotopic composition of planktic foraminifera species ($\delta^{18}O_{shell}$) and the predicted values ($\delta^{18}O_{eq}$)

Station EBC

Interval mid-depth	$\delta^{18}O_{eq}$	*G. ruber* white (150-250 μm)	*P. obliquiloculata* (280-380 μm)	*T. humilis* (150-250 μm)	*G. truncatulinoides* (280-440 μm)
(m)	(‰, PDB)	(‰, PDB)	(‰, PDB)	(‰, PDB)	(‰, PDB)
13	-0.027	-0.30	0.08	-0.65	-0.01
38	-0.081	-0.25	0.07	-0.29	-0.05
100	0.019	-0.23	0.14		-0.03
225	0.705	-0.07	0.34	-0.09	0.26
375	1.006			0.08	0.67
700*	1.485	-0.10	0.45	0.55	0.95

* samples in this depth were collected by a sediment trap at station EBC

Station M1-21

Interval mid-depth	$\delta^{18}O_{eq}$	*G. ruber*$_{conc.\text{-}weighted}$	*G. trilobus*$_{conc.\text{-}weighted}$[1]	*N. dutertrei*$_{conc.\text{-}weighted}$[1]	*G. inflata*$_{conc.size\ weighted}$[1]
(m)	(‰, PDB)	(‰, PDB)	(‰, PDB)	(‰, PDB)	(‰, PDB)
8	-0.54	-1.15	-0.97	-0.54	-0.76
20	-0.54	-1.21	-1.08	-0.68	-0.66
35	-0.54	-1.38	-1.22	-0.65	-0.59
61	-0.10	-1.14	-1.02	-0.42	-0.68
94	0.48	-1.02	-1.15	-0.61	-0.51
133	0.83	-1.08	-1.14	-0.35	-0.29
234	1.12	-0.92	-0.92	-0.28	0.16
408	1.59	-0.91	-0.90	-0.37	0.54
656	2.11	-0.90			0.30

[1] $\delta^{18}O_{shell} = ((\delta^{18}O_{small} * \text{shell conc.}_{small}) + (\delta^{18}O_{large} * \text{shell conc.}_{large}))/(\text{shell conc.}_{small} + \text{shell conc.}_{large})$

Station M2-1153/1151

Interval mid-depth	$\delta^{18}O_{eq}$	*G. ruber* white (150-250 μm)	*G. glutinata* (150-250 μm)	*G. aequilateralis* (250-500 μm)	*G. calida* (150-500 μm)	*G. inflata*$_{conc.\text{-}weighted}$[1]	*G. truncatulinoides* (250-500 μm)
(m)	(‰, PDB)	(‰, PDB)	(‰, PDB)	(‰, PDB)	(‰, PDB)	(‰, PDB)	(‰, PDB)
13	-0.033	-0.52	-0.61	-0.38	-0.74	-0.11	-0.28
38	-0.034	-0.50	-0.57	-0.30	-0.73	-0.07	-0.15
63	-0.035	-0.43	-0.72	-0.28	-0.68	-0.01	-0.27
88	-0.033		-0.66	-0.22	-0.78	-0.05	-0.27
125	0.023		-0.72	-0.27	-0.69	-0.07	-0.13
175	0.237		-0.69	-0.32	-0.55	-0.09	-0.28
250	0.366		-0.66	-0.14	-0.37	-0.03	0.06
400	0.763	-0.55	-0.59			0.05	
750	1.652	-0.38	-0.79	-0.16	-0.27	0.06	0.09

[1] $\delta^{18}O_{shell} = ((\delta^{18}O_{small} * \text{shell conc.}_{small}) + (\delta^{18}O_{large} * \text{shell conc.}_{large}))/(\text{shell conc.}_{small} + \text{shell conc.}_{large})$